INTEGRATION OF DESALINATION AND PURIFICATION PROCESSES FOR THE TREATMENT AND VALORISATION OF INDUSTRIAL BRINES

A thesis accepted by the faculty of Energy-, Process- and Bio-Engineering of the University of Stuttgart

In partial fulfilment of the requirements for the degree of
DOCTOR OF ENGINEERING SCIENCE (Dr.-Ing.)

by

Marina Micari

born in Palermo, Italy

1. Examiner	Prof. Dr. Valentin Bertsch
2. Examiner	Prof. Dr. Ulrich Nieken
3. Examiner	Prof. Dr. Giorgio Micale
Date of defence	28.07.2020

Institute for Building Energetics, Thermotechnology and Energy Storage (IGTE), University of Stuttgart

2020

University of Stuttgart
Germany

Erklärung über die Eigenständigkeit der Dissertation

Ich versichere, dass ich die vorliegende Arbeit mit dem Titel

INTEGRATION OF DESALINATION AND PURIFICATION PROCESSES FOR THE TREATMENT AND VALORISATION OF INDUSTRIAL BRINES

selbständig verfasst und keine anderen als die angegebenen Quellen und Hilfsmittel benutzt habe; aus fremden Quellen entnommene Passagen und Gedanken sind als solche kenntlich gemacht.

Declaration of Authorship

I hereby certify that the dissertation entitled

INTEGRATION OF DESALINATION AND PURIFICATION PROCESSES FOR THE TREATMENT AND VALORISATION OF INDUSTRIAL BRINES

is entirely my own work except where otherwise indicated. Passages and ideas from other sources have been clearly quoted.

Name/Name: MARINA MICARI

Unterschrift/Signed: 

Datum/Date: 08.09.2020

Table of Contents

Papers included in the dissertation

1) **M. Micari**, M. Moser, A. Cipollina, B. Fuchs, B. Ortega-Delgado, A. Tamburini, G. Micale, "*Techno-economic assessment of multi-effect distillation process for the treatment and recycling of ion exchange resin spent brines*", Desalination, 2019, vol. 456, p- 38-52, https://doi.org/10.1016/j.desal.2019.01.011
2) **M. Micari**, A. Cipollina, A. Tamburini, M. Moser, V. Bertsch, G. Micale, "*Combined Membrane and Thermal Desalination Processes for the Treatment of Ion Exchange Resins Spent Brine*", Applied Energy, 2019, Article number 113699, https://doi.org/10.1016/j.apenergy.2019.113699
3) **M. Micari**, M. Moser, A. Cipollina, A. Tamburini, V. Bertsch, G. Micale, "*Towards the Implementation of Circular Economy in the Water Softening Industry: A Technical, Economic and Environmental Analysis*", Journal of Cleaner Production, 2020, Article number 120291, https://doi.org/10.1016/j.jclepro.2020.120291.
4) **M. Micari**, D. Diamantidou, B. Heijman, M. Moser, A. Haidari, H. Spanjers, V. Bertsch, *"Experimental and Theoretical Characterization of Commercial Nanofiltration Membranes for the Treatment of Ion Exchange Resins Spent Brine"*, Journal of Membrane Science, 2020, Article number 118117, https://doi.org/10.1016/j.memsci.2020.118117
5) **M. Micari**, A. Cipollina, A. Tamburini, M. Moser, G. Micale, V. Bertsch, *"Techno-economic Analysis of Integrated Treatment Chains for the Valorisation of Neutral Coal Mine Effluents",* Journal of Cleaner Production, 2020, Article number 122472, https://doi.org/10.1016/j.jclepro.2020.122472

Other papers

1) **M. Micari**, M. Bevacqua, A. Cipollina, A. Tamburini, W. Van Baak, T. Putts, G. Micale, "*Effect of different aqueous solutions of pure salts and salt mixtures in reverse electrodyalisis systems for closed-loop application*", Journal of Membrane Science, 2018, vol. 551, p. 315-325, https://doi.org/10.1016/j.memsci.2018.01.036
2) P. Palenzuela, **M. Micari**, B. Ortega-Delgado, F. Giacalone, G. Zaragoza, D. Alarcon-Padilla, A. Cipollina, A. Tamburini, G. Micale, "*Performance Analysis of a RED-MED Salinity Gradient Heat Engine*", Energies, 2018, vol. 11, 3385; https://doi.org/10.3390/en11123385
3) **M. Micari**, A. Cipollina, F. Giacalone, G. Kosmadakis, M. Papapetrou, G. Zaragoza, G. Micale, A. Tamburini, "*Towards the first proof of the concept of a Reverse ElectroDialysis-Membrane Distillation Heat Engine*", Desalination, 2019, vol. 453, p.77-88, https://doi.org/10.1016/j.desal.2018.11.022

Abstract

The industrial sector should shift more towards sustainability. The industrial production is continuously growing driven by the increasing demand, which leads to heavy consumption of raw materials and to the release of significant amounts of highly-concentrated wastewater streams into the environment. To achieve a more sustainable development, it is fundamental to decouple these phenomena by introducing circular economy models. These would allow for reducing the environmental impact of the industrial process by recovering energy and materials and recycling pre-treated effluents. However, so far, very few studies have dealt with the technical implementation of circular economy at the industrial scale and have performed economic analysis of large-scale plants.

To fill this gap, the activities performed during my Ph.D. project were based on three research questions, which concerned (i) the selection of treatment processes to purify industrial effluents and to recover raw materials; (ii) the development of economically feasible treatment chains; (iii) the estimation of the energy demand of the treatment chains and the possibility to couple the chains with more environmentally friendly energy supply systems.

Such questions may be applied to any industrial sector producing industrial wastewater and to answer them, I developed a novel multi-step method able to simulate and analyse integrated processes (chains) for the treatment of industrial effluents. The proposed method is given by four steps: (a) implementation of techno-economic models for pre-treatment and concentration technologies; (b) definition of suitable inputs and parameters and of representative outputs for each model; (c) development of integrated platforms simulating the treatment chains by interconnecting the models of single technologies; (d) definition of global assessment criteria informative about the performances of the entire chain.

Concerning the last point, the technical performances are assessed by estimating the total electric and thermal energy demand; the economic feasibility is based on the calculation of the levelised cost of the target product of the chain and the environmental impact is evaluated via the specific CO_2 emissions connected to the energy requirements. In this regard, I included different thermal and electric energy supply systems in the scenarios analysed in the thesis by giving suitable costs and CO_2 emission factors.

The developed method is flexible and able to simulate treatment chains for different wastewater effluents. The thesis presents the results obtained by applying the novel method to two case studies: water softening industry and coal mines. In the first case, I developed treatment strategies to purify the wastewater and recover a target NaCl-water solution reusable as a reactant. Conversely, for the coal mine effluent, the treatment chains were designed to produce NaCl crystals competitive with the market.

For each case, I identified the most economically feasible and the least energy intensive chain among various alternatives. The environmental impact of the industrial process decreased because the treatment strategies allowed for minimising the discharge of polluted effluent into the environment and for reducing the demand for raw materials. In addition, for the softening industry case, the specific CO_2 emissions connected to the energy requirements of the treatment systems resulted to be lower than those due to the production of the fresh regenerant, both with grid supply and with a photovoltaic-battery system. The chains turned out to be beneficial also from the economic point of view. In fact, the levelised cost of the

brine produced by treating the wastewater of the softening industry was 40 to 50% lower than the current cost of the regenerant. In the case of the coal mine effluent, I found that the most feasible levelised cost of salt was comparable with the lower bound of the market price range of high purity sodium chloride.

Overall, the method developed and presented in this thesis is a powerful tool that can be used for decision support by the industries to minimise the environmental impact of the processes, by introducing economically feasible treatment and recycling strategies.

Zusammenfassung

Die industrielle Produktion wächst ständig, angetrieben durch die steigende Nachfrage, die zu einem hohen Verbrauch von Rohstoffen und zur Freisetzung erheblicher Mengen hochkonzentrierter Abwasserströme in die Umwelt führt. Die Einführung von Kreislaufwirtschaftsmodellen würde es ermöglichen, die Umweltauswirkungen der Industrieprozesse durch Rückgewinnung von Energie und Materialien und durch Recycling von vorbehandeltem Abwasser zu reduzieren. Bislang haben sich jedoch nur sehr wenige Studien mit der technischen Umsetzung der Kreislaufwirtschaft im industriellen Maßstab befasst und wirtschaftliche Analysen von Großanlagen durchgeführt.

Um diese Lücke zu schließen, basierten die während meines Promotionsprojekts durchgeführten Aktivitäten auf drei Forschungsfragen, die (i) die Auswahl von Behandlungsverfahren zur Reinigung von Industrieabwässern und zur Rückgewinnung von Rohstoffen, (ii) den Aufbau wirtschaftlich tragfähiger Behandlungsketten, (iii) die Abschätzung des Energiebedarfs der Behandlungsketten und die Möglichkeit der Kopplung der Ketten mit umweltfreundlicheren Energieversorgungssystemen betrafen.

Solche Fragen können auf jeden Industriesektor angewendet werden, der Industrieabwässer produziert, und um sie zu beantworten, habe ich eine neuartige mehrstufige Methode entwickelt, die in der Lage ist, integrierte Prozesse (Ketten) für die Behandlung von Industrieabwässern zu simulieren und zu analysieren. Die vorgeschlagene Methode besteht aus vier Schritten: (a) Implementierung von technisch-ökonomischen Modellen für Vorbehandlungs- und Konzentrationstechnologien; (b) Definition geeigneter Inputs und Parameter und repräsentativer Outputs für jedes Modell; (c) Entwicklung integrierter Plattformen zur Simulation der Behandlungsketten durch die Verbindung der Modelle einzelner Technologien; (d) Definition globaler Bewertungskriterien, die über die Leistungen der gesamten Kette Auskunft geben.

Was den letzten Punkt betrifft, werden die technischen Leistungen durch die Schätzung des gesamten elektrischen und thermischen Energiebedarfs bewertet; die wirtschaftliche Durchführbarkeit basiert auf der Berechnung der spezifischen Kosten des Zielprodukts der Kette und die Umweltauswirkungen werden über die spezifischen CO2-Emissionen in Verbindung mit dem Energiebedarf bewertet. In diesem Zusammenhang habe ich verschiedene thermische und elektrische Energieversorgungssysteme in die in der Dissertation analysierten Szenarien einbezogen, indem ich geeignete Kosten und CO2-Emissionsfaktoren angegeben habe.

Die entwickelte Methode ist flexibel und in der Lage, Behandlungsketten für unterschiedliche Abwasserströme zu simulieren. Die Arbeit stellt die Ergebnisse vor, die durch die Anwendung der neuartigen Methode auf zwei Fallstudien erzielt wurden: Wasserenthärtungsindustrie und Kohlebergwerke. Im ersten Fall entwickelte ich Behandlungsstrategien zur Reinigung des Abwassers und zur Rückgewinnung einer als Reaktionsmittel wiederverwendbaren NaCl-Wasserlösung. Umgekehrt wurden die Behandlungsketten für das Abflussrohr des Kohlebergwerks so ausgelegt, dass NaCl-Kristalle produziert werden, die mit dem Markt konkurrieren können.

Für jeden der betrachteten Fälle habe ich die wirtschaftlich effizienteste und am wenigsten energieintensive Kette unter den verschiedenen Alternativen ermittelt. Die Umweltauswirkungen des Industrieprozesses wurden reduziert, da die Behandlungsstrategien es ermöglichten, die Einleitung von verschmutztem Abwasser in die Umwelt zu minimieren und die Nachfrage nach Rohstoffen zu verringern. Darüber hinaus fielen im Fall der Enthärtungsindustrie die spezifischen CO2-Emissionen, die mit dem Energiebedarf der Aufbereitungsanlagen verbunden sind, niedriger aus als diejenigen, die durch die Produktion des frischen Regeneriermittels entstehen, sowohl bei der Netzversorgung als auch bei einer Photovoltaik-Batterieanlage. Die Ketten erwiesen sich auch unter wirtschaftlichen Gesichtspunkten als vorteilhaft. Tatsächlich waren die Kosten für die durch die Behandlung des Abwassers der Enthärtungsindustrie erzeugte Sole 40 bis 50% niedriger als die derzeitigen Kosten des Regeneriermittels. Im Falle des Abflusses aus dem Kohlebergwerk stellte ich fest, dass die Kosten für die Einebnung des Salzes am besten mit der unteren Grenze der Marktpreisspanne für hochreines Natriumchlorid vergleichbar waren.

Insgesamt ist die in dieser Arbeit entwickelte und vorgestellte Methode ein leistungsstarkes Werkzeug, das zur Entscheidungshilfe für die Industrie eingesetzt werden kann, um die Umweltauswirkungen der Prozesse durch die Einführung wirtschaftlich durchführbarer Behandlungs- und Recyclingstrategien zu minimieren.

1. Introduction

The release of continuously growing amounts of polluted and highly concentrated wastewater effluents produced by the industrial sector has become a severe issue. The adverse environmental effects due to the discharge of effluents have been widely reported in the literature. To solve this issue, many treatment strategies have been proposed, mainly to purify the effluent before discharge. However, to make an industrial process more sustainable, circular and more comprehensive strategies, including the recovery of reactants and the reuse of low-grade waste heat, should be proposed and analysed at the full-plant scale. In the following, I reported an overview about the environmental impact of the discharge of wastewater effluents. Then, the second paragraph (1.2) presents a detailed literature review on the circular strategies proposed so far for the most relevant industrial sectors, whereas the third paragraph (1.3) summarises the few works where a techno-economic assessment of treatment systems was performed. The literature review allows for highlighting the literature gaps that I collected in paragraph 1.4 together with the main research questions of this thesis.

1.1 Environmental impact of industrial wastewater effluents

One of the most **adverse environmental effects** of many industrial sectors consists in the discharge of wastewater effluents, whose impact strongly depends on the industrial process [1]. In most cases, the effluents present chemicals which are used for pre-treatment in the industrial process, organic compounds, heavy metals and salts. Various industrial sectors consume high volumes of water and, consequently, contribute to producing wastewater effluents, with high concentrations of salt (brines). Five industrial processes have been identified as the major potential responsible for damaging the natural environment, since they produce highly toxic effluents, presenting severe mutagenic risks [1]. These are pulp and paper, coal mine, textile, pharmaceutical and petrochemical industry. The wastewater produced by the **pulp and paper industry** typically contains micro-pollutants, such as organics and heavy metals, and has a high Chemical Oxygen Demand (COD) and Total Organic Carbon (TOC) [2]. The discharge of this effluent would generate serious problems to the marine ecosystem, by disrupting the carbohydrate metabolism and causing biotransformation activity of the enzymes. Concerning the **coal mine industry**, the effluents can have various compositions depending on the hydrogeology and they can vary from acid to basic drainage [3]. The acid mine drainage constitutes the main threat to the environment and to human health, as it presents high concentration of H^+, SO_4^{2-} and Fe(II), together with heavy metals (as Cu, Ni, Zn and Co) and alkaline earth metals (as Mg and Ca). The release of the acid mine effluent into the sea would cause a deterioration of the quality of water and a pH variation, which would lead to the destruction of the natural bicarbonate buffer of water and would affect the physiological functions of the organisms [4]. In addition, the precipitation of ferric hydroxides and other components creates a yellow or orange coating in the water channels, which reduces the oxygen concentration and prevents the penetration of the light, endangering the entire ecosystem [5]. Another threat to the environment is the wastewater effluent produced by the **textile industry**. The most polluted effluent is the spent dyeing solution, which contains high amount of colour, organic compounds and salts [6]. Several problems are connected to the discharge of the dyeing into the environment. Firstly, the

colour would cause a significant aesthetic pollution, together with eutrophication and variation of the aquatic ecosystem. Secondly, the effluent typically contains chemicals used during the pre-treatment, which are toxic, mutagenic and carcinogenic to various fish species. Thirdly, the dye absorbs light of wavelengths within the visible region and this is problematic to the photosynthetic aquatic plants and algae [7]. Furthermore, the **pharmaceutical industry** produces a growing amount of toxic wastewater, with high level of Chemical Oxygen Demand and salinity. In addition, it presents organic pollutants which are resistant to the conventional wastewater treatment processes and which require advanced treatment systems [8]. Finally, the **petrochemical wastewater** effluent is contaminated by coke particles [9], presents high amount of organic compounds and constitutes a serious risk to human health and to the marine ecosystem for its high toxicity and ability to create mutagenicity [10].

Other industrial wastewater effluents characterised by high salinity and/or concentration of organic compounds are the ones generated by desalination plants and by **ion exchange resins** used for water purification, and the **ballast water**, which typically presents a variety of micro-organisms that can be harmful to the marine ecosystem [11]. There is an extensive literature about the environmental impact of **desalination plants** [12]. Five adverse effects have been identified: the land use, the effect of the aquifer due to pipes leakage, the energy consumption, the noise due to the employment of high-pressure pumps and turbines and the brine discharge into the marine environment [13]. The brine discharge has a physicochemical impact, since the brine produced by desalination plants may cause a variation of the salinity and the temperature of the environment where it is released, and an ecological impact, as the seagrass habitat, the invertebrates and the fish community can be seriously damaged [14]. With this regard, the brine produced by reverse osmosis plants (RO brines) have been found to be a threat to the marine ecosystems and to some specific species as *Posidonia Oceanica* [15]. In fact, the RO brines present residuals of the chemical pre-treatments and heavy metals due to the pipes corrosion. Thus, they constitute a serious risk for the environment, as they may cause pH fluctuation, eutrophication and proliferation of heavy metals in natural environment [16]. Concerning the spent regenerant produced by the ion exchange resins, this presents multivalent ions and organic components, depending on the application of the ion exchange resins. Therefore, these can be used for various applications, e.g. for water purification from perchlorate and nitrate [17], in sugar decolourisation industries [18] and for the removal of natural organic matter to produce potable water [19]. The main problem of the ion exchange technology concerns the production of significant volumes of spent regenerant that can be highly polluted, since it is enriched of the components removed by the resins during the operation.

Finally, the **food industry** produces a significant amount of waste during all the food life cycle, starting from the agricultural phase to the food processing, distribution and sale [20]. The wastewater produced by the fruit and vegetables processing presents pesticides, herbicides and chemicals used for cleaning. Also, the olive industry generates effluents rich of organic compounds and the dairy wastewater contains significant amount of proteins, fatty residuals, lactose and chemicals for cleaning [21].

1.2 Literature review on circular strategies for water treatment and recycling

Due to their critical environmental impact, certain limitations have been imposed on the discharge of polluted brines, depending on the volumes produced and the composition. In most cases, it is mandatory to implement brine management strategies, which can provide minimisation, pre-treatment and disposal or reuse [16]. In addition, the effluents often contain materials and products, which can be very valuable. Therefore, the recycle of the treated effluent and the **recovery of secondary raw materials** can be of great importance to deal with the net increase of demand for fresh water, energy and raw materials, due to the intensification of several industrial sectors. As a matter of fact, a smart treatment of industrial effluents can lead to a double benefit, as it would reduce the volumes of wastewater discharged into the environment and it would allow for recovering valuable materials from waste. Several applications of this concept to real case studies are reported in the literature, such as the extraction of sodium carbonate from the effluents of the ceramic industry [22], the recovery of water and detergent from the effluents of the laundering industry [23], the production of carbon adsorbents from paper mill wastewater [24] and the recovery of hydrochloric acid from waste pickling solutions [25].

The treatment of waste streams and the recovery of industrial streams and/or secondary raw materials are waste management strategies that can be located within the wide framework of the **circular economy** (CE). CE is defined as "*an industrial economy that is restorative and regenerative by intention and design*" [26]. Circular economy consists in innovative business models, aimed at a more sustainable management of resources, whose consumption has to be decoupled from the economic growth [27]. The main principles, which constitute the ways in which CE is practically realised, are reduction, reuse and recycle [28]. Reduction concerns all the actions to improve the efficiency of the industrial process and to limit the demand of energy, utilities and raw materials [29]. Reuse is realised when a stream or a component of the industrial process, which does not constitute a waste, is used again for the same initial purpose [30]. Recycle refers to any operation aimed at treating waste materials, to convert them into reusable products, which can be employed for their initial or for a different purpose [31]. Many works in literature focused on the implementation of such strategies at various levels and three main circles have been defined [32]. The first circle, the micro-level, consists in single industrial plants, where CE strategies can be applied to minimise the waste production or to improve the energy efficiency of the process. In this context, a strategy that is worth mentioning is the cleaner production strategy, which is based on three principles: pollution prevention, reduction of the use of toxic substances and design for environment. The design of the plant is a crucial part, since it can affect strongly the sustainability of the operation and of the products [33]. The second cycle, the meso-level, corresponds to the inter-firm level and the eco-industrial parks, where more firms are part of an eco-industrial network and share material, energy and water management systems [34]. Finally, the macro-level is the third cycle and includes cities, provinces and regions. At this level, the implementation of CE strategies consists in redesigning the industrial, infrastructure, cultural and social system. Initiatives connected to the implementation of CE at the macro-level include the establishment of eco-cities, where ambitious recycling legislation and significant technological improvements are put into place to reduce the environmental impact [35].

Many works in literature focus on the development of waste management strategies in various industrial sectors to reduce or prevent the environmental damage and to recover valuable resources, thus these works constitute examples of implementation of the **circularity concept at the individual firm level**.
In the following, I will report a literature review of brine management and recycling strategies providing secondary raw materials recovery, developed for industrial sectors producing polluted and highly concentrated wastewater effluents.
An overview of the most relevant treatment processes described in literature applied to four industrial sectors is shown in Figure 1.

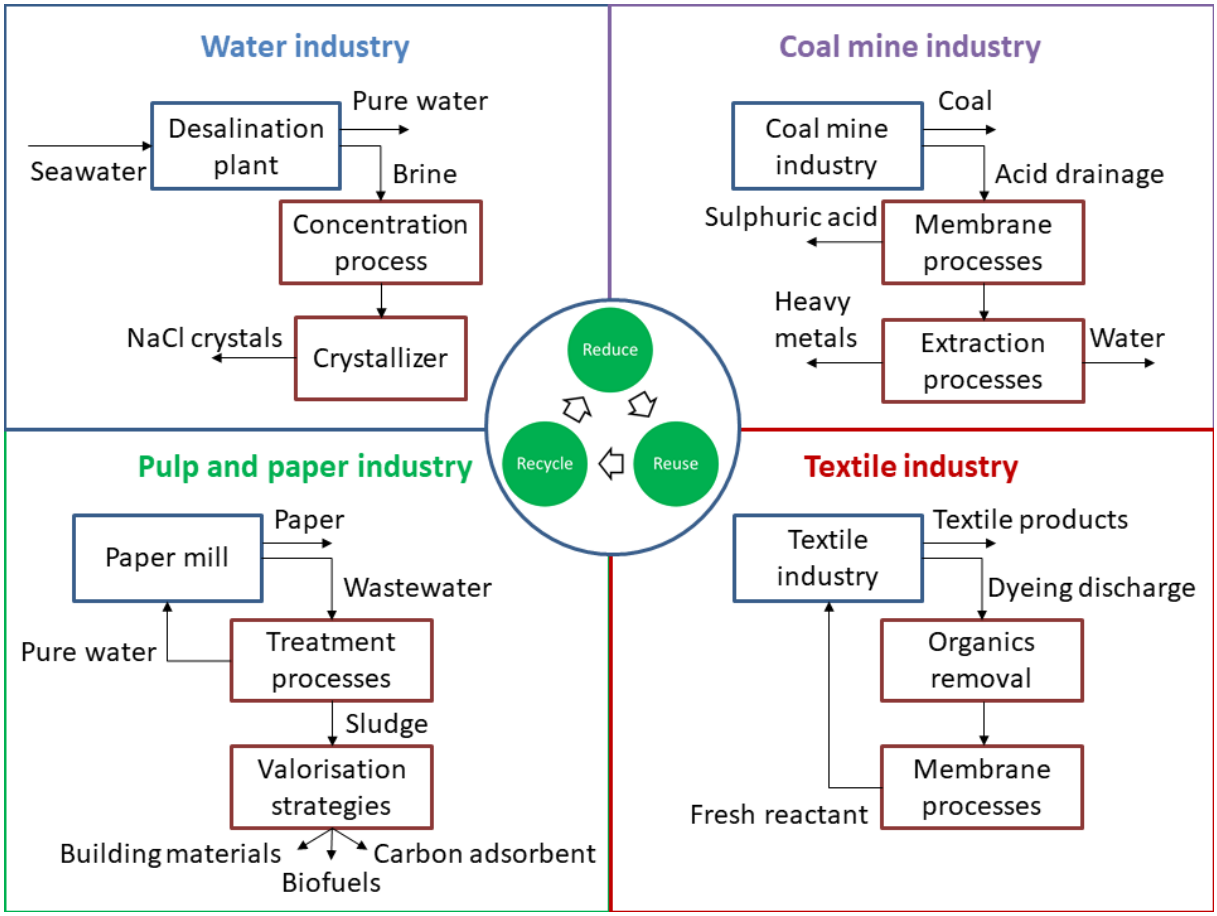

Figure 1. Overview of treatment processes reported in literature for four industrial sectors.

Water industry

Concerning the water industry, two highly-concentrated wastewater effluents are worth mentioning: the brine produced by desalination plants and the spent water solution given by the regeneration of ion-exchange resins.

Desalination brines

Various strategies and technological solutions have been proposed to treat the **desalination brines** and to recover salts and chemicals, in order to ensure a decrease of the desalination costs and to obtain a lower levelised cost of water [16]. Emerging technologies have been considered for salt production, such as membrane distillation coupled with crystallization,

electrodialysis and forward osmosis [36]. These technologies were proven to allow for recovering the major components of seawater, i.e. sodium chloride, magnesium and calcium minerals, acid and basic solutions [15]. In particular, integrated membrane systems, composed of filtration units as microfiltration and nanofiltration, reverse osmosis and membrane crystallization have been investigated to produce simultaneously fresh water, salts and minerals [37]. The authors showed that the production of salt crystals sellable as raw material may allow for decreasing the total desalination cost [38]. Other authors proposed to combine thermal and membrane purification processes to treat seawater and produce salt and pure water: cost estimations showed that the cost of water produced in such dual-purpose plant may be competitive with the current cost of potable water produced in traditional thermal or reverse osmosis plants [39]. Moreover, the technical feasibility of using the NaCl salt produced by concentrating desalination brines as a reactant in the chlor-alkali industry has been investigated. In particular, an electrodialysis unit was used to concentrate the SWRO brine up to saturation [40]. Other works focused on the recovery of calcium and magnesium minerals, as calcium carbonate and magnesium sulphate [41, 42]. Furthermore, highly-concentrated NaCl solutions were treated in an electrodialysis unit with bipolar membranes, to produce strong acid and basic solutions, i.e. sodium hydroxide and hydrochloric acid [43]. This technology turned out to be promising at the lab-scale, since it has lower energy consumption with respect to the traditional technology used to produce NaOH via the chlor-alkali process [44]. However, the economic feasibility of all these emerging technologies at the industrial scale has not been assessed yet. Other recovery strategies have been proposed, such as the production of minor compounds as caesium, rubidium and indium through ion-exchange resins, adsorption or liquid-liquid extraction [45]. Also for these cases, a positive market trend was predicted, but it is fundamental to develop and test technologies which are efficient and competitive at the industrial scale. Finally, in some cases, the brines were treated and concentrated up to a certain concentration, in order to be reused for other scopes than crystallization, as reactant solutions within the industrial process [46].

Ion exchange resins brines

The other effluent produced in large amounts in the water industry is the spent reactant solution used for the **regeneration of ion-exchange resins**. The ion-exchange resins are used for a wide range of application. Resins' operation is made of two phases: the purification, during which the pollutants are removed from the feed solution and exchanged with the charged groups of the resins, and the regeneration, during which the charged groups of the resins are re-established via the employment of a suitable regenerant solution. Therefore, this technology produces a significant amount of wastewater that is the spent regenerant solution enriched of the pollutants. Depending on the application, different resins can be employed, which require specific regenerant solutions and, consequently, produce wastewater with very diverse composition. In many cases, recycling strategies have been proposed to treat the effluent by removing the pollutants and to recycle the purified solution as fresh regenerant solution. For the case of ion-exchange resins employed to purify the groundwater and remove nitrate and perchlorate, the contaminated regenerant solution has been treated via advanced biological treatment [17] or via catalytic reduction [47] to enable its reuse for the following regeneration cycles. Moreover, various combinations of pressure (ultrafiltration and

nanofiltration) and electric (electrodialysis) driven technologies have been tested to remove the Natural Organic Matter (NOM) present in spent regenerant solutions, produced by ion-exchange resins employed for municipal wastewater purification [19]. Finally, an important application of the resins consists in water softening, i.e. the removal of hardness (magnesium and calcium ions) from the water, to prevent scaling. Also in this case, it is necessary to treat the effluent to be able to recycle it to the following regeneration process; otherwise the hardness would accumulate and reach critical levels. Brine recycling systems were firstly proposed by Flodman and Dvorak. They found that the inclusion of a single or double tank allowing for the partial recycling of the regenerant solution reduced significantly the salt consumption and the waste discharge, without increasing the hardness leakage [48]. Other authors proposed the combination of membrane processes to recover the regenerant solution, and in particular a system composed of dia-nanofiltration, nanofiltration and reverse osmosis, which was used for either a KCl or a NaCl regenerant solution [49]. When weak ion-exchange resins are employed for water softening, the charged group of the resins are H^+ ions that are released to the water solution during the softening phase. The regeneration is performed via an acid solution and its effluent can be treated via an electrodialysis unit with bipolar membranes and a crystallizer. This combination allowed for restoring the acid and basic solutions and producing the crystals of the hardness minerals [50].
Also for these effluents, a detailed economic analysis concerning industrial-scale treatment plants is missing and it constitutes a crucial point for the practical realisation of these systems.

Pulp and paper industry

The circularity approaches applied in the **pulp and paper industry** mostly concern the sludge generated by the wastewater treatment processes. Therefore, as already mentioned, the wastewater produced by this industrial sector is highly polluted and needs to be treated to remove the contaminants. The treatment includes physicochemical processes, as sedimentation, ultra-filtration, flocculation, coagulation, ozonation and electrolysis, and biological processes, both aerobic and anaerobic, to remove the organics [51]. The purified water can be recycled to the industrial process or can be discharged into the environment, if it meets the legislation requirements [2]. However, a crucial product of the wastewater treatment is the biological sludge, which represents a major environmental concern. Therefore, various valorisation strategies have been proposed to convert the sludge into secondary materials and to avoid the landfill disposal [24]. The sludge can be used as a building material, and in particular to produce clinkers/cements [52] or as a reinforcement filler [53]. Moreover, the sludge has found a wide application to produce carbon adsorbents, given its carbonaceous nature [24]. In particular, the so-obtained carbon adsorbents have been used for phenol removal [54, 55] and for sorption of heavy metals, such as cadmium and lead [56]. Finally, the anaerobic digestion of the sludge can be a promising option to produce biofuels and in particular methane gas [53]. Overall, it has been demonstrated that these processes allow for reducing the environmental impact of the sludge disposal, but an accurate cost assessment is still needed to evaluate their cost-effectiveness [24].

Coal mine industry

Another industrial effluent representing a severe environmental issue is the **coal mine effluent**, whose composition and pH strongly depends on the hydrogeological characteristics of the mine where it is produced. As already mentioned, neutral, acid or basic drainages can be generated. Concerning the neutral effluents, these typically present a very high concentration of salt. Therefore, various combinations of treatment processes have been evaluated in the literature to recover the NaCl salt. These included membrane and thermal processes, such as nanofiltration, evaporation and crystallization [57] or electrodialysis, evaporation and crystallization [58] to recover the salt crystals. A more comprehensive utilisation of the effluent was also performed to meet the Zero Liquid Discharge (ZLD) target [59]. Another study proposed to use vacuum-enhanced membrane distillation (VMD) to reduce the salinity and make the treated water usable as potable water, after a mineralisation step [60]. A more extensive research has been carried out about the treatment of acid mine drainage (AMD) and the recovery of water, acids and dissolved metals. AMD are typically treated with neutralisation reagents, but this leads to the production of sludge, which has to be further treated and disposed. Therefore, more sustainable strategies for AMD treatment and materials recovery have been proposed in the literature [61]. The recovery of the dissolved metals can be performed through a number of technologies, such as selective precipitation, ion exchange, adsorption and membrane filtration [62]. Among these processes, ion exchange has been used to remove copper, nickel and vanadium as well as lead and cadmium [63] and nanofiltration membranes have been tested to remove copper [64]. However, the preferred method for heavy metal recovery appears to be the adsorption, which is in continuous development thanks to the introduction of new nanomaterials with high surface area and low diffusion resistance [4]. With this regard, nanoparticles of maghemite have been employed to remove chromium, copper and nickel [65] and carbon nanotubes to adsorb lead and cadmium [66]. The recovery of water has been performed via membrane technology, as membrane distillation and electrodialysis [4] or in combination with recovery of other products, as gypsum and limestone, by adding magnesite nanosheets, lime and CO_2 bubbles [3]. Another component, whose recovery may be also economically beneficial, is the sulfuric acid, which can be produced via membrane processes, ion exchange, solvent extraction, rectification and crystallization [67]. Among the membrane processes, previous works demonstrated the feasibility to employ electrodialysis [68] and nanofiltration technologies [69] to recover the sulfuric acid from AMD. Moreover, Kesieme et al. proposed integrated schemes based on solvent extraction technologies to produce water, sulfuric acid and metals [70]. Finally, other effluent management strategies include the recovery of rare earth elements via nanofiltration [71] and the conversion of the coal mine drainage ochre into water treatment reagent. The ochre is a sludge rich of hydrous ferric oxides. From the sludge, it is possible to recover Fe-based reagents that can be reused for various water treatment applications, such as for the removal of phosphorus and zinc [72].

Overall, these management strategies were proposed once the constituents of the AMD were finally considered as valuable products to recycle. As a matter of fact, the recovery of these resources may offset the costs required for the treatment and may make the whole plant profitable. However, only a few works reported an economic analysis of the processes

required for materials recovery and some of them showed that more efficient separation and purification technologies as well as a proper design and optimisation of such systems is required to get economic benefits [4, 67].

Textile industry

Textile industry is another industrial sector producing significant amounts of highly polluted wastewater. An extensive research has been conducted to treat the wastewater via physical, oxidative and biological methods to abate the contaminants before disposal [6]. However, the environmental policies together with the increasing water cost and the issue of water shortage have led to the development of more sustainable solutions, which provide the treatment and recycle of water and reactants [73]. As a matter of fact, different effluent streams are produced, with various pollution levels. Therefore, diverse treatment systems can be devised to remove the contaminants and recover water and salt. A high percentage of the total water demand, between 60 and 90%, is used for washing and rinsing and the corresponding effluent would require a less intensive treatment or even no treatment before being reused [74]. Conversely, the most contaminated effluent is the dyeing discharge, which is very challenging to treat, as it contains both organics and salt. To reduce the environmental damage due to its release and the demand for raw materials, various strategies have been proposed to purify the dyeing and to reuse it as a fresh reactant solution [75]. Firstly, advanced oxidation processes have been tested to decompose the organic compounds: it was found that ozonation is the most suitable process for decolourisation purposes, to enable the reuse of the dyeing solution [75]. Secondly, membrane processes have been widely used for colour removal: several studies focused on the assessment of nanofiltration (NF) performances to remove the dye from salty wastewater [76-78]. Novel positively charged NF membranes have been also developed to obtain high rejections of positive dyes [79]. Moreover, integrated membrane processes as ultrafiltration and NF have been proposed to improve the wastewater quality and allow for effluent reusing [80]. Reverse Osmosis (RO) has also been used in combination with biological treatments for water recovery and recycle [81]. However, the high energy demand of pressure-driven membrane processes as RO and NF has opened up a path to thermal processes as membrane distillation (MD) [82]. In this context, various studies demonstrated the feasibility of using MD for the treatment of textile effluents and showed high removal of organics and colour [83, 84]. However, the economic feasibility of such systems is only roughly assessed and it is strictly specific to the wastewater characteristics. Therefore, in general, it is still needed a more comprehensive techno-economic analysis of the membrane processes used for the treatment of textile wastewater, especially at the full industrial scale [85, 86].

Other methods to treat the effluent and enable its reuse are chemical processes, such as (i) electrochemical and chemical coagulation, used to remove colour, turbidity and organic compound and (ii) ion exchange to reduce conductivity, iron and hardness concentrations [87]. In addition, electrochemical oxidation enhanced with UV radiation has been tested for colour removal and it turned out to be a promising option, since it allowed for recovering around 70% of salt and water and the recovered solution showed good performances in the following dyeing operations [88].

Overall, a growing attention has been paid to the development of strategies to improve the sustainability of the textile industry, not only by treating the effluent before disposal, but also by reusing the purified reactants in the industrial process. These technologies have shown high separation efficiencies, since high values of colour removal and of salt and water recovery were achieved. However, most of the analyses have been performed at a small scale and very little information is available about long-term operations and economic feasibility at industrial scale.

Pharmaceutical industry

The wastewater effluents produced by **pharmaceutical industry** are heavily contaminated and their composition can vary significantly. Therefore, a big variety of treatment technologies has been developed, to take into account the different pharmaceutical waste that can originate from the industrial process. The treatment processes can be classified into biological (aerobic and anaerobic), advanced processes as membrane technologies and adsorption, advanced oxidation processes and hybrid technologies [89]. Among the advanced oxidation processes, Fenton oxidation and ozonation are suitable to abate the Chemical Oxygen Demand (COD) [1, 8]. Moreover, NF unit has been employed to concentrate antibiotics [90] and to recover amoxillicin from pharmaceutical wastewater [89]. Concerning the recovery strategies, given the high purity requirements of the products involved in the pharmaceutical industry, the possibility of reusing reactants is quite limited [89]. However, the purified water can be reused for various applications, as for irrigation or for industrial processes, and the technologies to employ depend on the requirements to meet for the specific case. Among the treatment systems aimed at water reuse, membrane filtration is used to remove microorganisms and natural organic matters, and nanotechnologies are employed for bioremediation and disinfection [91]. Moreover, pharmaceutical wastewaters can be utilised in microbial fuel cells to generate bioelectricity [92].

Petrochemical industry

The **petrochemical wastewater** has a high content of toxic and organic compounds. Thus, physicochemical and biological treatments have been devised to purify the water before releasing it into the environment [93]. Various valorisation strategies have been proposed in the literature, mainly concerning the potential of using such wastewater for renewable energy production [1]. Firstly, anaerobic digestion has been suggested as a promising treatment option for petrochemical wastewater to generate bio-methane. In this context, ultrasonic and microwave pre-treatments have been considered to enhance the methane generation to improve the energy efficiency [10]. Secondly, as an alternative to typical aerobic and anaerobic treatment methods, petrochemical wastewater has been treated in microbial fuel cells, with simultaneous generation of bio-electricity [94]. Furthermore, treatment processes have been also devised for the production of high quality water to be reused for industrial or agricultural applications. With this regard, MD has been accounted as a promising option, since a 100% rejection of salt and non-volatile compounds can be theoretically achieved and the required thermal energy can be supplied by low-cost sources [95]. However, the wastewater has to be treated before the membrane process to remove dissolved oils, such as

phenols. For this aim, a recent study proposed the combination of oil-water separation and photo-catalysis units to realise photo-degradation and removal of dissolved organics [96]. These pre-treatments were combined with a direct contact MD unit, which allowed for purifying the water to be reused. Finally, the removal and recovery of copper and chromium from petrochemical wastewater was realised by adding a calcium hydroxide solution and adjusting the wastewater pH [97].

Food industry

Food industry produces a significant amount of very diverse wastes. In order to improve the sustainability, various approaches have been promoted to reduce the waste generation and to recover materials or energy. Many sectors within the food industry produce wastewater that can be treated and reused. Among those sectors, beverage industry, sugar industry, olive mills and dairy industry are worth mentioning. Within the beverage industry, the production of orange juice is responsible for generating wastewater rich of phenolic compounds and organic acids. The physicochemical analysis of this effluent showed that it contains many components reusable in other food industrial sectors [98]. For example, it may be possible to use extracts rich of dietary fibre and antioxidants recovered from orange industry in meat and dairy products [20].

In the sugar industry, most of the valorisation strategies concern the use of a primary by-product, the bagasse, for pyrolysis to generate clean energy [99]. However, some studies focused on the wastewater produced by the regeneration of ion exchange resins employed for sugar decolourisation [100]. In particular, various treatment schemes including NF were proposed to remove the colourants and to recycle the regenerant solution for other regeneration cycles [18].

The wastewater produced in olive mills is rich of polyphenols, which are accounted as valuable components for their antioxidant properties. Therefore, recovery strategies have been devised to produce phenolic antioxidants usable for food cosmetic and pharmaceutical industries [101]. Other valorisation strategies include the production of enzymes via biotechnological methods and the generation of biogas through anaerobic digestion [102]. However, it was stated that the cost of the technologies to treat the wastewater and recover materials is still too high and technological developments are required to realise such strategies at the industrial scale [102].

Finally, the dairy wastewater typically contains diluted milk and chemicals used for cleaning. Water, proteins and lactose can be recovered from the wastewater by implementing suitable treatment and recycling schemes. In this context, some studies proposed integrated membrane systems composed of ultrafiltration and NF. The ultrafiltration unit aims at separating whey proteins, which can be supplied to algae cultivation to produce biofuels and biodiesel [103]. The NF process produces reusable water as a permeate, while lactose and chemicals are concentrated in the NF retentate and can be used to produce biogas via anaerobic digestion [104].

1.3 Literature review on techno-economic analysis of water treatment strategies

Notwithstanding the extensive research devoted to investigating innovative strategies for industrial wastewater treatment, only a few works focus on the economic feasibility of these systems and compare various layouts, by assessing the relevant costs and the ability to recover resources. Within the water industry, some research dealt with the comparison of integrated systems for seawater desalination and salt recovery from the brine [38]. These systems included thermal and membrane processes and provided pre-treatment units (ultrafiltration and nanofiltration), desalination units (reverse osmosis or multi-stage flash) and post-treatment for brine concentration and salt production (membrane distillation, electrodialysis and crystallization) [105]. This study estimated the amount of salt and minerals recovered and the total desalination costs, and then compared the specific cost of desalinated water accounting also for the revenues given by the by-products. However, they concluded that still much research is needed to find low-cost, low-energy and -chemicals consumption technologies.

Concerning the textile industry, the economic evaluation has a key role to identify the strategy to implement for the treatment and recycling of the spent dyeing solution. Dasgupta et al. reviewed the studies carried out in the literature to assess the economic feasibility of membrane processes within the textile industry [106]. In particular, some researchers performed a techno-economic evaluation of integrated membrane systems to achieve the zero liquid discharge target [107]. They compared different scenarios presenting combinations of membrane filtration units. Firstly, the raw wastewater produced by the textile industry was treated via membrane filtration. Secondly, the produced retentate was further concentrated in a MD unit and finally, the MD retentate was sent to the incinerator. Moreover, another study reported the economic evaluation of an evaporator for RO concentrate coming from the textile industry with or without an electrodialysis unit used as pre-treatment [108]. Generally speaking, these studies concluded that the employment of innovative membrane technologies may be of fundamental importance to improve the cost-effectiveness and the environmental-friendliness of the textile sector [106].

Within the coal mine industry, the economic feasibility of processes aimed at recovering sulphuric acid and metals from acid mine drainage has been investigated in a few works. Various methods for sulphuric acid recovery have been compared from the economic point of view and it turned out that, for some cases, the revenues due to the production of treated water and sulphuric acid were able to offset the cost of the treatment [67]. Moreover, concerning the metal recovery, the feasibility of the relevant processes depends on several factors: the market value of the metal; the metal importance, which is correlated to its impact on the market and the risk of its supply; the concentration of the metal in the effluent and the efficiency of removal [61]. So far, the high costs and the issues due to membrane fouling and lifespan constitute significant challenges for the full-scale implementation of treatment strategies to recover metals. Finally, Simate et al. presented integrated treatment processes which have been commercially developed to produce various final products, such as potable water, gypsum, calcium carbonate and metal hydroxides [4]. Although various integrated systems have been proposed, there is no cost-efficient commercial technology which is able to treat the acid mine drainage without generating new waste streams. As a matter of fact, all the

proposed systems produce vast amount of sludge whose treatment and disposal can be very expensive and the membrane performances are still a severe issue. Therefore, it is fundamental to couple more stages in a holistic manner to improve sustainability and cost-efficiency.
Other examples of techno-economic analysis of wastewater treatment processes concern the industrial laundry wastewater and the chemical cleaning water. For the first, researchers performed a techno-economic assessment of a full-scale membrane bioreactor to recover clean water [109]. For the second, combined and separate processes for pickling and alkaline cleaning effluent were compared from the economic point of view [110].

The studies mentioned so far proposed and analysed from the techno-economic perspective various strategies for wastewater treatment and resource recovery in specific industrial sectors. However, they are much focused on specific case studies and can be applied only to the accounted industrial effluent. A more general framework for industrial wastewater treatment was proposed by Sujak et al., who developed a superstructure composed of various potential treatment technologies and able to identify the optimal network by maximising the net present value (NPV) [111]. This work focused on the treatment of industrial wastewaters characterised by high organics content and the technologies were categorised into primary treatment, resource extraction and product recovery type. Finally, other studies applied a holistic approach for the design of optimal water networks within industrial sectors [112]. This approach allows minimising the water consumption of an industrial process by reducing the demand and by reusing water streams directly or after a regeneration step [113].

1.4 Literature gaps and aim of the doctoral thesis

Although an extensive research has been carried out in the last years about the treatment of industrial wastewater effluents, the study of the literature has highlighted some important gaps to fill. Firstly, the main focus of most studies is on the removal of contaminants for water purification before discharge rather than on the recovery of resources. In this regard, there is a net prevalence of works about the removal of organic compounds from municipal as well as industrial wastewater via biological, physical or chemical treatments. Thus, a first gap concerns the fact that in many industrial sectors, proper resource recovery strategies have not been proposed yet.
In addition, the literature mostly concerns experimental results of laboratory-scale technologies, whose implementation at the full-scale is still challenged by several factors: high costs, considerable amounts of waste produced, membrane fouling and membrane lifetime. Therefore, a second gap regards the scale of implementation of the treatment technologies, since most of the works do not consider full-scale implementations.
Moreover, only a few works report an economic evaluation of the treatment processes and, among these, some works focused only on the operational expenditures and others performed a rough estimation of the capital costs starting from lab-scale data and scaling them with the plant capacity. As a matter of fact, it was stated in several papers that, although the lab-scale results highlighted the potential of recovery strategies, much more research is needed to investigate real-scale plants and to assess their economic feasibility [4, 24, 67, 102]. Thus, an

important aspect that is often missing regards the assessment of the economic feasibility of the treatment processes.
Finally, the treatment strategies proposed in the literature so far and reviewed in paragraph 1.2 are very specific to particular industrial applications, whereas a comprehensive framework accounting for different types of wastewater is missing, especially for highly-concentrated effluents (industrial brines).

This doctoral thesis aims at covering these gaps, by introducing a novel multi-step methodological approach for the technical, economic and environmental assessment of integrated treatment processes (chains) devised for industrial brines. I developed a comprehensive method that bridges different levels of investigation, from the definition of transfer mechanisms within each single treatment unit to the economic analysis of whole integrated systems at the real plant size. More in detail, I developed and implemented in Python technical models for the design of various pre-treatment and concentration technologies and I built a general framework where the models could be integrated and interconnected to simulate the treatment chains. The novel framework allowed for simulating various combinations of treatment technologies and for analysing and comparing them through global technical, economic and environmental assessment criteria.
Such a comprehensive approach was designed to identify the most economically feasible and least energy-intensive treatment chains for the investigated effluents. In this regard, a particular attention was also devoted to devising treatment strategies able to increase the revenues given by secondary raw materials, in order to offset the costs of the treatment units.
Therefore, the aim of the thesis was to develop a novel method able to simulate and analyse various treatment chains and to find the most suitable one, economically feasible and able to reduce the environmental impact of the industrial process.
The three main research questions of this doctoral thesis, together with the fundamental objectives defined to answer each question, are reported in Table 1. The research questions are general and could be applied to any of the industrial sectors listed in paragraph 1.2. This thesis includes the results obtained in the context of two case studies, i.e. water softening industry and coal mines.

Table 1. Research questions and objectives of this doctoral thesis.

Research questions	Objectives
1. Which treatment processes can be used to purify industrial wastewater effluents and to recover raw materials?	1.1. Development and implementation of technical and economic models for water treatment processes. 1.2. Models simulation by giving as input the composition of real water effluents produced by industrial plants. 1.3. Sensitivity analyses to assess the most suitable operating conditions depending on the inputs and the targets.
2. How the treatment processes should be interconnected in integrated systems to be economically feasible?	2.1. Integration of the techno-economic models in a simulation platform (RCE). 2.2. Construction of treatment chains by interconnecting the models and implementing mass and energy balances. 2.3. Definition of global economic outputs including costs and revenues given by by-products to assess the economic feasibility.
3. How high is the energy demand of the treatment chains and which energy supply systems can be used to make the chain more environmentally friendly and economically feasible?	3.1. Calculation of the thermal and electric energy demand of each treatment process in the chains. 3.2. Inclusion of different energy supplies through economic and environmental (CO_2 emission factor) coefficients. 3.3. Estimation of global costs and global CO_2 emissions in presence of different energy supply systems to assess economic feasibility and environmental impact.

1.5 Outline of the thesis

The extensive literature review reported in this chapter highlighted the main literature gaps that this thesis aims at filling. For this scope, I identified three relevant research questions that have guided the activities performed during the Ph.D. The following chapters describe the methodology followed and introduce and discuss the papers included in this thesis.

In Chapter 2, the novel multi-step methodological approach developed and applied in the thesis is described in detail. Within the chapter, a wide section is devoted to presenting the techno-economic models that I implemented to simulate pre-treatment and concentration technologies. Furthermore, the simulation platform used to simulate integrated treatment processes by interconnecting the single models is graphically depicted and explained.

Chapter 3 concerns the aspects related to the energy supply and the energy demand. Energy has a central role in the thesis, because the water treatment plants can have very high energy requirements and this can constitute a limitation to their implementation, because of economic and environmental reasons. In the first part of Chapter 3 the electric and thermal energy supply systems that I used for the techno-economic analysis are described. The second part summarises the electricity and heat demands of the investigated pre-treatment and concentration technologies.

Chapter 4 presents a general overview of the papers produced within the doctoral thesis and shows how the papers are located within the framework of the research questions. Then, each paper is shortly introduced in a dedicated paragraph. The whole papers are attached to the appendix.

Finally, in Chapter 5, the main findings of the papers are discussed and the results are reported and commented in relation to the research questions. Possible applications of the proposed method, limitations and future outlooks are also considered and reviewed in the concluding chapter.

2. Methodological approach

In order to realise a general framework for the development and assessment of treatment schemes for industrial brines, it was necessary to develop a novel methodological approach able to bridge different levels of investigation and to provide a comprehensive analysis of the treatment schemes. The structure of the methodological approach developed in this doctoral thesis is depicted in Figure 2.

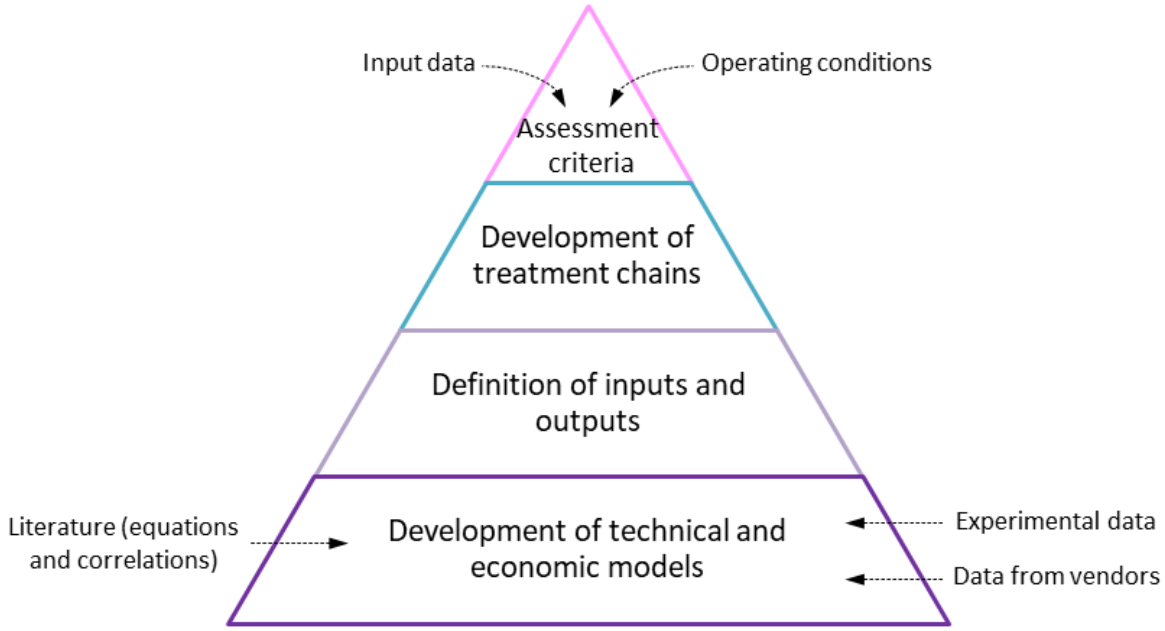

Figure 2. Pyramid diagram showing the methodological approach developed in this doctoral thesis.

The method presents a **multi-level structure**, which allows for integrating different aspects in the calculation of the global outputs. As a matter of fact, the outputs of the techno-economic models of the single processes (lower level) feed into the models of the whole treatment chains (higher level). In this way, it is possible to assess the role of some specific aspects, like the membrane properties or the energy consumption of a single process, on the global outputs of the treatment chain.

The foundation of the method consists in the development and implementation of detailed technical and economic models of each treatment process potentially involved in the chains. In this thesis, I focused on five treatment processes: two belong to the pre-treatment category, i.e. nanofiltration (NF) and crystallization, and three to the concentration category, i.e. multi-effect distillation (MED), reverse osmosis (RO) and membrane distillation (MD).

For each of these, firstly, I implemented a **technical model**, based on mass and energy balances and mass and energy transfer equations. The models include equations and correlations taken from the relevant literature and, in some cases, novel experimental data obtained within the doctoral project. The technical models themselves typically have a hierarchical structure that I developed for the first time to follow the structure of the corresponding real unit: for example, the models describing membrane processes presents a low-hierarchy model to describe the transfer mechanisms through the membrane, a medium-hierarchy model to describe the profiles of the variables along the unit and a high-hierarchy

model to design a full-scale plant and estimate its energy demand for a given separation. Also, all technical models are able to run in the *design* mode and in the *operation* mode: either the target recovery rate or the plant size is fixed. In the first case the suitable plant size is estimated, whereas in the second case the output mass and energy flows are characterised.
Secondly, I implemented the **economic models** for each technology and I coupled them with the relevant technical models. As a matter of fact, the technical and the economic models are strictly connected, since the outputs of the technical design model feed into the economic model to estimate the capital and the operating costs. The main inputs of the economic models produced by the corresponding technical models are the size of the plant (e.g. required area of the membranes or of heat exchangers) and the thermal and electric energy requirements. The economic models include cost correlations taken from the literature and data provided by the vendors for the estimation of the investment costs and the costs of utilities, such as energy and reactants.
Each process has inlet and outlet material and energy flows, which correspond to **inputs and outputs** of the corresponding technical models. The identification of the sets of significant inputs and parameters of each process is very important. A considerable part of this phase consists in performing sensitivity analyses to find the most suitable operating conditions and geometric parameters of the single technologies.
Once the techno-economic models are implemented and the inputs and output are identified, it is possible to build integrated models to simulate the **treatment chains**. Therefore, the treatment processes constitute the building blocks of the chains and the multi-level structure allows for devising and simulating various chains in a modular way. Depending on the case study, it is possible to explore different combinations of pre-treatment and concentration processes and to compare them to find the one able to reduce costs and environmental impact. The chains can be devised also with different scopes and different targets of products to obtain for recycling or selling purposes. In this context, the layouts can be compared taking into account the revenues due to the by-products produced in the different cases.
For the comparison of integrated systems, it is necessary to define **assessment criteria** that are representative of the overall performances. For this doctoral thesis, three criteria have been selected to quantify the technical, economic and environmental performances of the treatment chains. For the technical aspects, the heat and electricity demand of the whole chain are used as reference outputs. The economic performances are defined through global levelised costs, which represent the selling price that the main product of the chain would have to break-even. Thus, the global economic output depends on the capital and operating costs of the treatment units, on the revenues given by the by-products and on the productivity of the chain in terms of the selected main product. Finally, the environmental aspects are assessed through the operational CO_2 emissions, due to the energy requirement of the chain, per unit of main product produced.
Overall, the main novelty introduced by this doctoral thesis consists in developing a simulation platform where ad hoc implemented techno-economic models could be easily integrated and interconnected to simulate treatment chains. These were compared by estimating novel assessment outputs able to inform about the technical, economic and environmental performances of the whole system.

2.1 Technical and economic models

In this section, the technical and economic models developed and implemented for five treatment processes are described in detail. The treatment processes are categorised into pre-treatment and concentration processes. Nanofiltration and crystallization belong to the first group, whereas multi-effect distillation, reverse osmosis and membrane distillation belong to the second. The techno-economic models developed and implemented during the thesis have been schematically represented within the framework of the multi-level method in Figure 3.

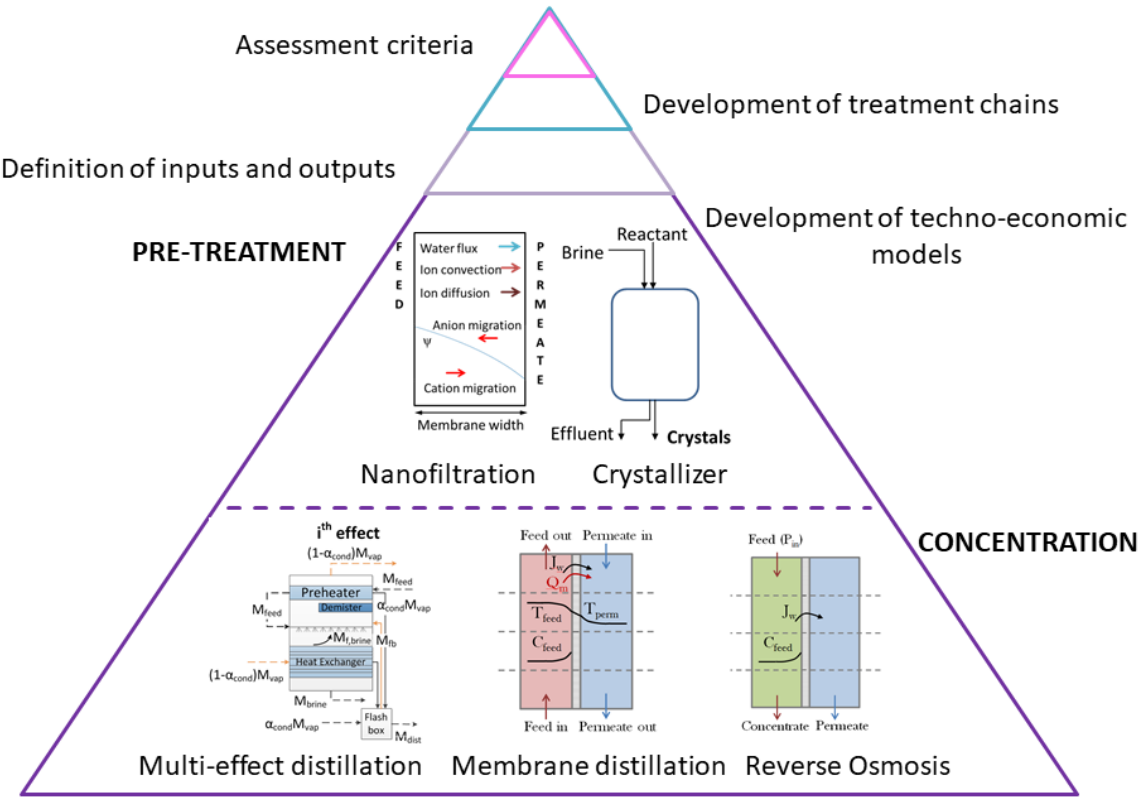

Figure 3. Representation of the multi-level methodological approach, with a focus on the techno-economic models developed and implemented for this thesis.

2.1.1 Nanofiltration (NF)

NF is a pressure-driven membrane process, which is widely used as a pre-treatment unit in industrial processes since it is very suitable to selectively separate bivalent and multivalent ions from water solutions.

2.1.1.1 Technical model

The technical model has a hierarchical structure and presents three levels of investigation. The low-hierarchy model concerns the transfer mechanisms within the membrane and is based on the resolution of the extended Nernst Planck equation. The medium-hierarchy model

describes the NF element and is composed of mass and energy balance equations. The high-hierarchy model regards the whole NF plant to be employed to achieve a certain recovery and is based on an iterative calculation for the design of the plant. The structure of the NF model is schematically shown in Figure 4.

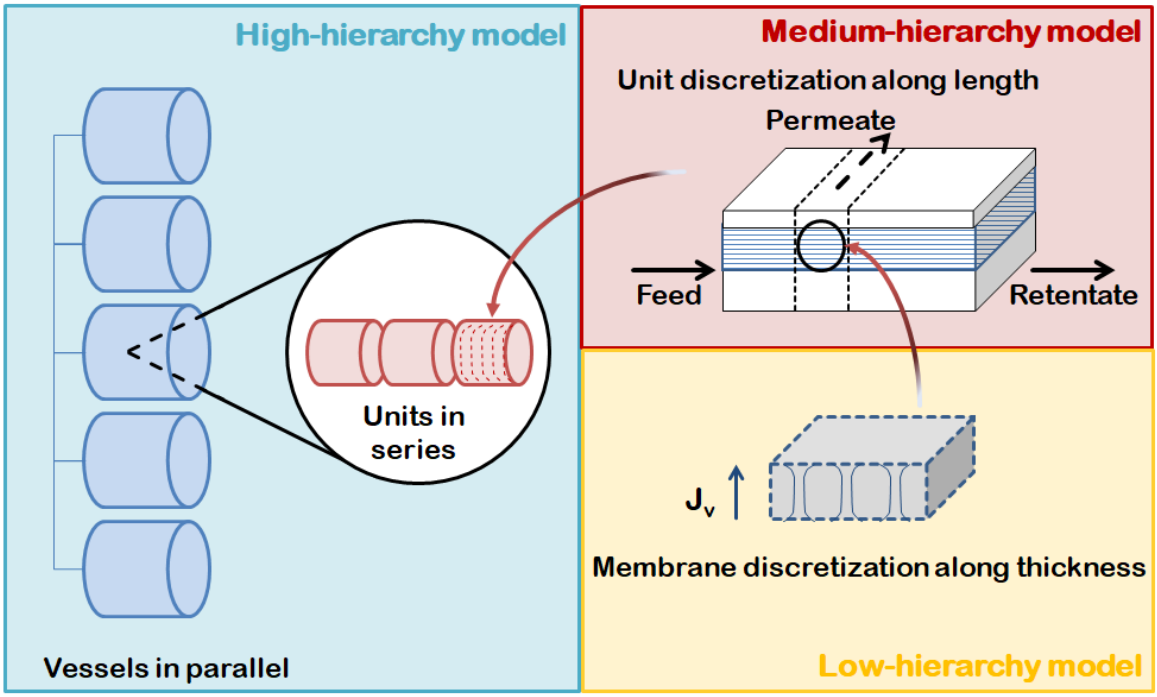

Figure 4. Schematic representation of the NF hierarchical model.

Low-hierarchy model

The mechanisms within the NF membranes are described via the Donnan Steric Pore Model with Dielectric Exclusion (DSPM-DE). This modelling approach, introduced by Bowen et al. [114] and widely used in the literature [115-117], allows for a full characterisation of the NF membranes when four membrane parameters are known: membrane pore radius (r_{pore} [nm]), active layer membrane thickness (δ_m [µm]), pore dielectric constant (ε_{pore} [-]) and membrane charge density (X_d [mol/m^3]).

Table 2 reports the main equations of the DSPM-DE concerning the mass transfer mechanisms through the NF membranes. The DSPM-DE is based on the extended Nernst Planck equation (equation 1). The flux of each ion through the membrane (j_i [mol/m^{2}s]), which is equal to the product of the water flux (J_v [m/s]) by the concentration of the ion in the permeate (C^p_i [mol/m^3]), is defined by the Nernst Planck equation as the sum of three terms: diffusive, electro-migrative and convective fluxes. The diffusive flux depends on the diffusivity of the ion within the pore ($D_{i,pore}$ [m^2/s]) and on the variation of concentration along the y axis, i.e. within the membrane (C^m_i [mol/m^3]). The electro-migrative flux is function of the ion valence (z_i [-]), the concentration within the membrane (C^m_i), the diffusivity of the ion within the pore ($D_{i,pore}$) and the variation of electrical potential (ψ [V]) along the y axis. The convective flux depends on the convective mass transfer coefficient ($k_{i,c}$ [-]), the concentration inside the membrane (C^m_i) and the water flux (J_v). The diffusion and

convection within the pores are hindered because of the pore size, thus suitable mass transfer coefficient ($k_{i,c}$ and $k_{i,d}$) are defined in equation 3 and 4 in function of the parameter λ_i [-], equal to the ratio between the ion Stokes radius and the pore radius.
Concerning the water transport, J_v is estimated using the Hagen-Poiseuille equation (equation 6), which defines the water flux as function of the net pressure difference (ΔP [Pa]), the pore radius (r_{pore}), the active layer membrane thickness (δ_m) and the solution dynamic viscosity (η [Pa s]). The net pressure difference is given by the difference of the applied pressures in the feed and the permeate channel minus the osmotic pressure difference $\Delta\Pi$, defined in equation 7.

Table 2. Equations of the DSPM-DE about the mass transfer mechanisms within the NF membrane.

$$j_i = J_v C^p{}_i = -D_{i,pore}\frac{dC^m{}_i}{dy} - z_i C^m{}_i D_{i,pore}\frac{F}{RT}\frac{d\psi}{dy} + k_{i,c} C^m{}_i J_v \quad (1)$$

$$\phi_i = (1-\lambda_i)^2 \quad (2)$$

$$k_{i,d} = \frac{1 + {}^9/_8\,\lambda_i \ln(\lambda_i) - 1.56034\,\lambda_i + 0.528155\,\lambda_i{}^2 + 1.91521\,\lambda_i{}^3 - 2.81903\,\lambda_i{}^4 + 0.270788\,\lambda_i{}^5 + 1.10115\,\lambda_i{}^6 - 0.435933\,\lambda_i{}^7}{\phi_i} \quad (3)$$

$$k_{i,c} = \frac{1 + 3.867\,\lambda_i - 1.907\,\lambda_i{}^2 - 0.834\,\lambda_i{}^3}{1 + 1.867\,\lambda_i - 0.741\,\lambda_i{}^2} \quad (4)$$

$$D_{i,pore} = k_{i,d} D_{i,\infty} \quad (5)$$

$$J_v = \frac{\Delta P\, r_{pore}{}^2}{8\,\eta\,\delta_m} \quad (6)$$

$$\Delta\Pi = RT \sum_i (C^{bm}{}_i - C^p{}_i) \quad (7)$$

Concerning the solution membrane interface, equation 8 defines the ratio between the ion activity just inside the membrane on the feed side ($\gamma^m{}_{i,1} C^m{}_{i,1}$) and the ion activity just outside the membrane in the solution ($\gamma^{bm}{}_i\ C^{bm}{}_i$). Equation 9 is the analogous ratio at the permeate-membrane interface. The activity coefficients are calculated via the Davies equations (equations 10-11). The three exclusion mechanisms, i.e. size, dielectric and Donnan exclusions, are defined through the steric coefficient ϕ_i [-] (equation 2), the Born solvation coefficient $\phi_{B,i}$ [-] (equation 12) and the Donnan term, respectively. The Born solvation coefficient is function of the solvation energy barrier ΔW_i [J], which depends on ε_{pore} (equation 13). The Donnan term depends on the Donnan potential at the solution-membrane interfaces $\Delta\psi_D$ [V].

Table 3. Equations of the DSPM-DE about the exclusion mechanisms in the NF membrane.

$$\frac{\gamma^{m}_{i,1} C^{m}_{i,1}}{\gamma^{bm}_{i} C^{bm}_{i}} = \phi_i \phi_{B_i} \exp\left(-\frac{z_i F}{RT} \Delta\psi_{D,feed}\right) \quad (8)$$

$$\frac{\gamma^{m}_{i,N} C^{m}_{i,N}}{\gamma^{p}_{i} C^{p}_{1}} = \phi_i \phi_{B_i} \exp\left(-\frac{z_i F}{RT} \Delta\psi_{D,perm}\right) \quad (9)$$

$$\log \gamma_i = -A\, {z_i}^2 \left(\frac{\sqrt{I}}{1+\sqrt{I}} - 0.3\, I\right) \quad (10)$$

$$A = \frac{{e_0}^3 \, {N_A}^{1/2}}{\ln(10)\, 4\pi \sqrt{2}\, (\varepsilon\, k_B T)^{3/2}} \quad (11)$$

$$\phi_{B_i} = \exp\left(-\frac{\Delta W_i}{k_B T}\right) \quad (12)$$

$$\Delta W_i = \frac{{z_i}^2 {e_0}^2}{8\pi\varepsilon_0 r_i}\left(\frac{1}{\varepsilon_{pore}} - \frac{1}{\varepsilon_{bulk}}\right) \quad (13)$$

The concentration of the ions just outside the membrane on the feed side (C^{bm}_i) is different from the concentration in the bulk (C^{b}_i) because of the concentration polarisation phenomenon. This occurs because the ions would have different rates in moving from the bulk to the membrane interface and in crossing the membrane. Therefore, C^{bm}_i is calculated by equating the fluxes as in equation 14, where the right-hand of the equation is the ionic flux from the bulk to the membrane. The mass transfer coefficient is calculated by using the expression for spiral wound membranes (equation 16) and by correcting it with the coefficient Ξ that represents the suction effect due to membrane permeation [118]. The mass transfer coefficient $k^{b}_{c,i}$ depends on some geometric properties, i.e. the mixing efficiency of the net (η_{mix} [-]), the mixing length of the spacer (L_{mix} [m]) and the height of the feed channel (h_f [m]), and on two a-dimensional numbers, i.e. Peclet (Pe, equation 17) and Schmidt (Sc, equation 18).

Table 4. Equations for the estimation of concentration polarisation in the DSPM-DE.

$$j_i = -k'^{b}_{c,i}\,(C^{bm}{}_i - C^{b}{}_i) + J_v C^{bm}{}_i - z_i C^{bm}{}_i D_{i,\infty} \frac{F}{RT}\xi \quad (14)$$

$$k'^{b}_{c,i} = k^{b}_{c,i}\,\Xi = k^{b}_{c,i}\left[\frac{J_v}{k^{b}_{c,i}} + \left(1 + 0.26\left(\frac{J_v}{k^{b}_{c,i}}\right)^{1.4}\right)^{-1.7}\right] \quad (15)$$

$$k^{b}_{c,i} = 0.753\left(\frac{\eta_{mix}}{2-\eta_{mix}}\right)^{1/2}\left(\frac{D_{i,\infty}}{h_f}\right) Sc^{-1/6}\left(\frac{Pe_i h_f}{L_{mix}}\right)^{1/2} \quad (16)$$

$$Pe = \frac{2\, h_f u_f}{D_{i,\infty}} \quad (17)$$

$$Sc = \frac{\eta_f}{\rho_f\, D_{i,\infty}} \quad (18)$$

In addition, the electro-neutrality conditions reported in Table 5 have to be fulfilled at the feed-membrane interface (equation 19), in the permeate solution (equation 20) and inside the membrane (equation 21).

Table 5. Electro-neutrality conditions in the DSPM-DE.

$\sum_i z_i C^{bm}{}_i = 0$	(19)
$\sum_i z_i C^{p}{}_i = 0$	(20)
$\sum_i z_i C^{m}{}_{i,j} + X_d = 0$	(21)

The system of equation reported so far is highly non-linear and very complex to solve. Geraldes et al. proposed an implementation consisting of an iterative resolution of a linearised system, whose coefficients are updated in each iteration [117]. I followed this approach and I implemented in Python the linearised system of equations, which is simultaneously solved via the *LAPACK routine_gesv*. In the first iteration, the coefficients contain guess values of ionic concentration and potential profiles. After the first iteration, the coefficients are updated with the results of the linear system and a new iteration starts. The procedure continues until suitably defined residuals are below 10^{-4} [117].

Medium-hierarchy model

The medium-hierarchy model describes a NF unit that is discretised in a certain number of discretisation elements along the feed stream-wise direction (x axis). The medium-hierarchy model calls the low-hierarchy model in each discretisation element and presents mass balances to estimate the outputs of each element and the inputs of the following one. Table 6 reports the equations used to estimate the profiles of permeate and retentate flow rates and concentrations and the pressure profile along the x axis. The permeate flow rate (M_p [m^3/s]) increases because of the water flux that crosses the membrane (J_v) and the retentate flow rate (M_{ret} [m^3/s]) decreases correspondingly (equation 22 and 23). At the same time, the ionic fluxes (j_i) through the membrane cause a variation in the concentration of the permeate (C^p_i [mol/m^3]) and the retentate (C^{ret}_i [mol/m^3]) solutions (equation 24 and 25). Once the outlet retentate concentration and flow rate are calculated in a discretisation element, these are used as inlet feed concentration and flow rate of the following element (equation 26 and 27). Finally, the pressure profile (P [Pa]) along the NF unit depends on the pressure losses, which are function of the friction factor (f [-]), defined in equation 29 [119].
As showed in the equations of Table 6, for each element the water and the ionic fluxes are calculated via the DSPM-DE (low-hierarchy model). For this aim, I set up an iterative calculation, because the value of the permeate concentration is required to calculate the osmotic pressure and the mass transfer coefficient in the membrane model.

Table 6. Equations to model a NF unit.

$$M_{p_x} = M_{p_{x-1}} + J_{v_x} \frac{A_{membr,elem}}{n_{discr,L}} \quad (22)$$

$$M_{ret_x} = M_{b_x} - J_{v_x} \frac{A_{membr,elem}}{n_{discr,L}} \quad (23)$$

$$C^p{}_{i_x} = \frac{C^p{}_{i_{x-1}} M_{p_{x-1}} + j_{i_x} \frac{A_{membr,elem}}{n_{discr,L}}}{M_{p_x}} \quad (24)$$

$$C^{ret}{}_{i_x} = \frac{C^b{}_{i_x} M_{b_x} - j_{i_x} \frac{A_{membr,elem}}{n_{discr,L}}}{M_{ret_x}} \quad (25)$$

$$M_{b_x} = M_{ret_{x-1}} \quad (26)$$

$$C^b{}_{i_x} = C^{ret}{}_{i_{x-1}} \quad (27)$$

$$P_x = P_{x-1} - \Delta P_{losses} = P_{x-1} - \frac{f}{2} \frac{l}{D_H} \varrho_f \, {u_f}^2 \quad (28)$$

$$f = \frac{6.23}{Re^{0.3}} \quad (29)$$

$$Re = \frac{\rho_f u_f D_H}{\eta_f} \quad (30)$$

High-hierarchy model

The high-hierarchy model is a design model able to estimate the size that the plant should have to achieve a certain recovery (given by the ratio between the total outlet permeate flow rate and the inlet feed flow rate). The NF plant is typically composed of a number of vessels in parallel and each vessel contains some units in series. The number of NF units inside each vessel is a parameter; whereas the number of vessels in parallel corresponds to the total membrane area required for a certain separation and it is the main output of the design model. The model presents an iterative procedure, represented in Figure 5. The iteration starts from a guess number of vessels in parallel, calculated from the ratio between the total permeate flow rate to be produced and a guess average water flux in the vessel. Then, the total feed flow rate is distributed among the vessels and each unit inside the vessel is solved by applying the medium-hierarchy and the low-hierarchy models. If the feed flow rate of each vessel is lower than the minimum design flow rate, the number of vessels has to decrease or the pressure has to increase. If the pressure cannot be increased, a two-stage NF plant has to be designed. Within each vessel, the outlet retentate flow rate and concentration of a unit correspond to the inlet feed flow rate and concentration of the following one. Conversely, the permeate streams produced by each unit are mixed and constitute the outlet permeate of the vessel. At the end of the first iteration, the total recovery is calculated and compared with the required recovery. If the obtained value is lower than the target, the number of vessels in parallel is recalculated on the basis of the calculated water flux. The iterative procedure stops as soon as the calculated recovery is equal or slightly higher than the required one (maximum difference of 5%).

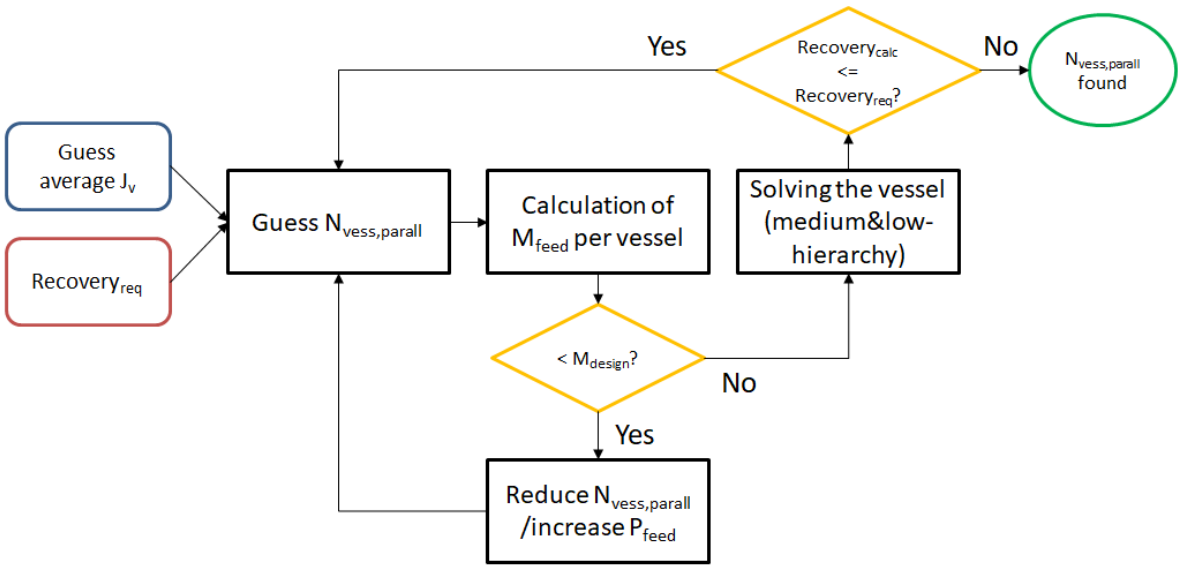

Figure 5. Representation of the iterative procedure implemented in the high-hierarchy model.

2.1.1.2 Economic model

To estimate the capital and the operating costs of the NF plant, the Verberne cost model was implemented [120]. The main equations for the calculation of the capital costs are reported in Table 7. These allow for estimating (i) the cost for the building housing the plant C_{civil} [$]; (ii) the costs for pumps, filters and piping system C_{mech} [$]; (iii) the cost for the energy supply system $C_{electro}$ [$]; and (iv) the cost for the membranes $C_{membrane}$ [$].
The main inputs to provide to the economic model are the total feed flow rate M_{feed} [m^3/h], the number of vessels in parallel n_{vessel} [-] and the feed pressure P_{feed} [bar]. Note that these equations make reference to vessels with a membrane area of 30 m^2. Thus, in the calculations, I considered that each vessel contains 6 units in series, each one composed of 5 NF membrane sheets wounded together with an area of 1 m^2.

Table 7. Equations to estimate the capital costs of a NF plant.

$C_{civil} = 1034.4\, M_{feed} + 1487\, n_{vessel}$	(31)
$C_{mech} = 4329.6\, {M_{feed}}^{0.85} + 1089.6\, n_{vessel}$	(32)
$C_{electro} = 1.68 * 10^6 + 64.8\, P_{feed}\ M_{feed}$	(33)
$C_{membrane} = 1200\, n_{vessel}$	(34)

The total costs in [$] are linearly depreciated by assuming different depreciation periods: 30 years for the civil investment, 15 years for the mechanical and the electric equipment and 5 years for the membranes [120]. An interest rate of 6% is used for the calculation of the total annualised capital costs (CAPEX [$/y]). The operating costs include the energy supply cost, the cost of chemicals, the maintenance cost and the quality control and daily operation costs. Each of the three last terms is estimated as 2%/y of the total investment cost in [$]. The cost

of chemicals is calculated in the range of 0.020-0.025 $/m^3 of permeate [121]. Finally, the energy costs include the cost for the pumping energy and an average consumption of the membrane modules of 40 Wh/m$^3_{feed}$ [120].

2.1.2 Crystallizer

The crystallizers considered in this doctoral thesis are reactive crystallizers where magnesium and calcium hydroxides are produced by adding an alkaline solution to the wastewater containing magnesium and calcium ions. Each crystallizer is followed by a disc and drum filter, used to separate the liquid phase from the solid crystals. The simplified scheme of the crystallization step is sketched in Figure 6.

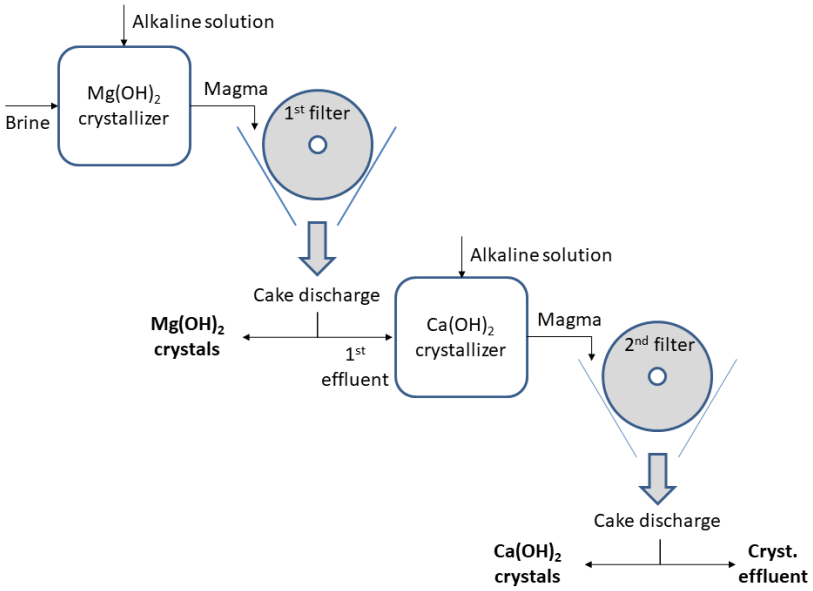

Figure 6. Illustration of the crystallization step to produce $Mg(OH)_2$ and $Ca(OH)_2$.

2.1.2.1 Technical model

Crystallization is typically modelled via population balance equations, which are able to describe the properties of the crystals in space and time. The population balance equation takes into account the different mechanisms occurring inside the crystallizer, i.e. nucleation, growth and aggregation, and it estimates the variation of the number density function n(L, t), according to the following expression [122]:

$$\frac{dn(L,t)}{dt} = -\frac{d[G(L)\,n(L,t)]}{dL} + B(L,t) - D(L,t) \qquad (35)$$

where L is the particle length, G(L) is the growth rate, B(L, t) is the birth rate due to the aggregation and D(L, t) is the death rate due to the aggregation. In this case, the breakage of the crystals is neglected.

The population balance equation can be solved following different approaches; one of the most widely used involves the conversion of the population balance into a moment balance. In particular, an attractive option is the quadrature method of moments (QMOM), which is robust and able to handle complex systems, including aggregation and breakage mechanisms [123]. This method is based on a quadrature approximation, which converts the integral in the moments' definition into a summation [124]:

$$m_k = \int_0^{+\infty} n(L) L^k dL \sim \sum_{i=1}^{N_q} w_i {L_i}^k \tag{36}$$

where N_q is the number of quadratures (N_q=3 was shown to be sufficient to describe the moments evolution accurately [123]), w_i are the weights and L_i are the abscissas. The calculation of weights and abscissas is performed via the product-difference algorithm that requires to know the first $2N_q$ moments [125]. Thus, if the first six orders moments m_k at t_0 are known, the moments at the following time-step (m_k at t_1) are calculated by applying the corresponding moment balance equations.

$$\frac{dm_k(t)}{dt} = (0)^k J(t) + \int_0^{\infty} k\, L^{k-1} G(L) n(L,t) + B_k(t) - D_k(t) \tag{37}$$

where J(t) is the nucleation rate and B_k and D_k are the moments relevant to birth and death for aggregation. The kinetics of growth, nucleation and agglomeration have been estimated experimentally for $Mg(OH)_2$ crystallization by Alamdari et al. [126].
For each time-step, once the moments are known, they are used to calculate the weights and the abscissas via the product-difference algorithm. Thus, the new weight and abscissas are employed for the calculation of the kinetics in the following time-step.
The population balance equations have been used during the doctoral thesis to investigate the evolution of the number and size of crystals of hydroxides with time. Experimental activities are still ongoing at University of Palermo to validate the modelling results.
However, for the techno-economic analyses performed during the doctoral thesis, I used a simplified model, based on mass balances under the assumption of a 100% conversion of the dissolved magnesium and calcium ions into the respective hydroxides [127]. Two separate crystallizers are considered for the production of the two hydroxides and each of the two units is followed by a filter to obtain the solid crystals. For each crystallization unit, an alkaline reactant (NaOH-water solution) is used. The main mass balance equations for the $Mg(OH)_2$ crystallizer are reported in Table 8, where Q^{mol} is the molar flow rate in [mol/h], n_{stoich} is the stoichiometric number, equal to 2 in this case, M is the mass flow rate in [kg/h] and C is the concentration in [ppm]. The equations are analogous for the $Ca(OH)_2$ crystallizer. The flow rate of alkaline solution required for the reaction is calculated assuming an excess of 10% with respect to the stoichiometric ratio (equation 38). The outlet molar flow rate of hydroxide is equal to the inlet molar flow rate of magnesium (equation 39), while the outlet mass flow rate of solution is calculated with the total mass balance including the inlet flow rates of the feed and the alkaline solution and the outlet flow rate of crystals (equation 40). Finally, the

outlet mass concentration of Na^+ is calculated considering the addition of sodium present in the alkaline solution (equation 41).

Table 8. Mass balance equations for the $Mg(OH)_2$ crystallizer

$$Q^{mol}{}_{NaOH,in} = 1.1 Q^{mol}{}_{Mg^{2+},in}\, n_{stoich} \quad (38)$$

$$Q^{mol}{}_{Mg(OH)_2,out} = Q^{mol}{}_{Mg^{2+},in} \quad (39)$$

$$M_{effluent,out} = M_{feed} + M_{NaOH,in} - M_{Mg(OH)_2,out} \quad (40)$$

$$C^{effl}{}_{Na^+} M_{effluent,out} = C^{feed}{}_{Na^+} M_{feed} + C^{alk}{}_{Na^+} M_{NaOH,in} \quad (41)$$

2.1.2.2 Economic model

The economic model estimates the capital and the operating costs of the crystallizers and the filters. The capital costs are calculated via the Module Costing Technique [128], by calculating the purchase cost of two crystallizers as a function of their volume V_{cryst} [m^3] and of two disc and drum filters as a function of the area A_{filter} [m^2]. The volume of the crystallizer is designed on the basis of the inlet total volume flow rate, the design fluid velocity within the reactor and a fixed length. The area of the filter depends linearly on the mass flow rate of the crystals produced. The purchase costs of the crystallizer and the filter are reported in equations 42 and 43 [128].

$$\log C_{p,0}{}^{cryst} = 4.5097 + 0.1731 \log V_{cryst} + 0.1344 \log V_{cryst}{}^2 \quad (42)$$

$$\log C_{p,0}{}^{filter} = 4.8123 + 0.2858 \log A_{filter} + 0.042 \log A_{filter}{}^2 \quad (43)$$

Then, the purchase costs are updated using the Chemical Engineering Plant Cost Index (CEPCI) and corrected with the bare module factor (F_{bm} [-]) that depends on the material used and the operating conditions. This is equal to 1.6 for the crystallizers and 1.65 for the filters.
The total capital cost is then linearly depreciated, using a depreciation time of 20 years and an interest rate of 6%.
The operating costs are given by the cost of the alkaline reactant and the cost of the energy required for pumping the feed in the crystallizer and for operating the filter. For the first term, I assume a pressure drop of 0.5 bar in each crystallization unit. For the filters, I assume that the consumption is linearly proportional to the inlet flow rate of the suspension produced by the crystallizer (magma) and a filter consuming 0.5 kW with a flow rate of 0.3 m^3/h is taken as a reference [129].

2.1.3 Multi-Effect Distillation

Multi-Effect Distillation (MED) is a thermal desalination technology, widely used for seawater desalination purposes. The MED plant consists of a certain number of stages (called effects), which can be arranged in different ways: typical arrangements are the forward feed and the parallel feed layouts [130]. In the first, the feed crosses all the stages disposed in

series; whereas, in the second, the feed is distributed among the stages disposed in parallel. I adopted a forward feed arrangement, as it is more suitable to the high concentrations and high temperatures that are expected in the treatment of concentrated brines [131]. Each effect presents an evaporator and a preheater. The evaporator is a horizontal tube-bundle where the feed solution partially evaporates on the external surface and the steam condensates inside the tubes. The preheater is a heat exchanger: the feed circulates inside the tubes and its temperature increases, because of the condensation of the vapour on the external surface of the tubes. In the forward feed arrangement, the brine generated by the partial evaporation of the feed in the evaporator is sent to the following stage as the feed solution; whereas, the vapour generated in the evaporator is used as the external heat source inside the tubes of the evaporator of the following effect.
The MED plant with a forward-feed arrangement is schematically represented in Figure 7.

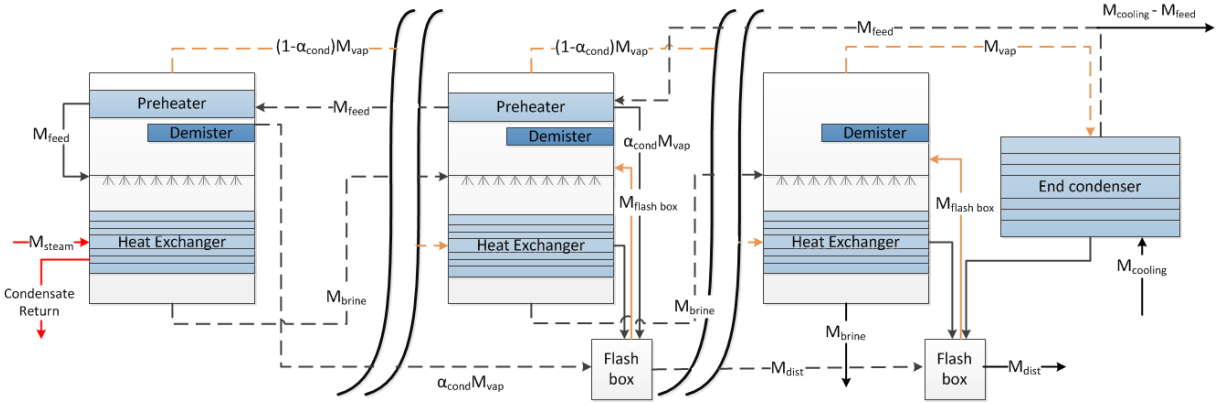

Figure 7. Schematic representation of the MED plant. The three stages represent the first, a generic intermediate and the last stage.

2.1.3.1 Technical model

The technical model is a design model able to estimate the size of the MED plant required for a certain separation, i.e. to reach a given concentration in the produced brine or to produce a fixed flow rate of distillate solution. With a given number of stages in series, the model is able to calculate the area of the evaporator and the preheater in each stage and the flow rate of steam to supply to the first effect. The technical model presents an iterative procedure with three minimisation loops, which is repeated until three conditions are simultaneously fulfilled: (i) the areas of the evaporators of all effects have to be equal; (ii) the areas of the preheaters of all effects have to be equal and (iii) the distillate flow rate produced has to be equal to the required one or has to satisfy the global mass balance (if the given condition concerns the brine salinity). The minimisation functions are solved by changing the values of the temperature change in the effects (ΔT_{effect} [°C]), the ones in the preheaters (ΔT_{preh} [°C]) and the mass flow rate of the external steam (M_s [kg/s]). The iterative procedure is reported in Figure 8.

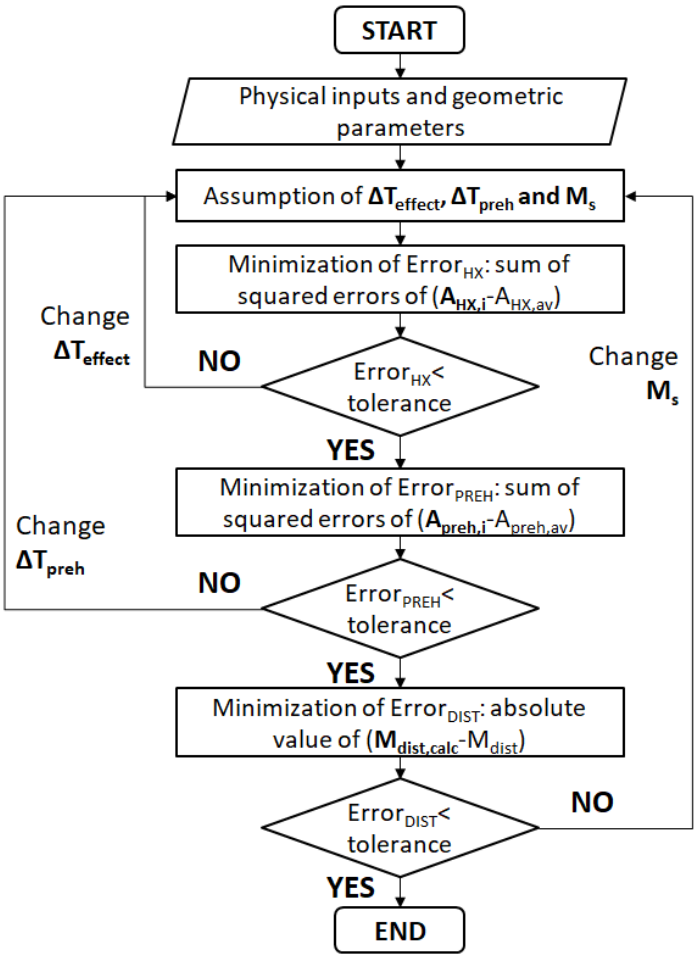

Figure 8. Solution algorithm of the MED technical model.

Once the inputs and the geometric parameters are given, the global mass balances are solved. The underlying assumption is that the distillate is pure water, so it is not included in the salt balance.

$$M_{feed} = M_{dist} + M_{brine} \tag{44}$$

$$M_{feed}\, X_{feed} = M_{brine}\, X_{brine} \tag{45}$$

where M_{feed}, M_{dist} and M_{brine} [kg/s] are the mass flow rates of the inlet feed solution and the outlet distillate and brine solutions, respectively and X_{feed} and X_{brine} [ppm] are the salt concentrations in the feed and in the brine, respectively.

Concerning the temperatures, six temperature values have to be evaluated for each effect: the temperature of the brine (T), the maximum feed temperature reached in the preheater (T_{preh}), the temperature of the saturated vapour generated (T_{vsat}), the temperature of the vapour after crossing the demister (T'_{vsat}), the temperature of the vapour after crossing the connecting lines (T'_c) and the condensation temperature of the vapour in the following effect (T_c).

These terms are inter-related: the temperature of the saturated vapour is lower than the temperature of the brine because of the boiling point elevation (BPE) and the temperature of

the vapour gradually decreases from one effect to the following because of pressure drops in the demister, in the connecting lines and in the evaporator. The relevant equations are reported in Table 9.

Table 9. Equations to define the temperature drops in the MED.

$T_{vsat} = T - BPE(T,\ X_{brine})$	(46)
$T'_{vsat} = T_{vsat} - \Delta T_{demister}$	(47)
$T'_c = T'_{vsat} - \Delta T_{lines}$	(48)
$T_c = T'_c - \Delta T_{grav} - \Delta T_{acc}$	(49)

The BPE is calculated according to the Pitzer model, which is valid in a wide range of salinity [132]. The other temperature drops are estimated on the basis of correlations reported in the literature [133, 134]. Concerning the equations to describe the effects, three different systems of equations are used for the first, the generic intermediate and the last effect. The first effect is the only effect receiving thermal energy from an external source, in the form of steam at a temperature typically between 70°C and 120°C (M_s). The total feed flow rate is sprayed on the external surface of the tube bundle, after having crossed all the preheaters, from the last to the first effect. The partial evaporation of the feed generates a vapour flow rate (M_d) and a brine flow rate (M_b) (equation 50). In the first effect, the vapour generated by evaporation of the feed is the only contribution to the total vapour generated in the effect (M_{vap}) (equation 52). The vapour crosses the demister to remove the remaining liquid particles and the first preheater, where it partially condenses to increase the temperature on the feed inside the tubes. The condensed fraction (α_{cond} M_{vap}) is a distillate liquid flow rate, whereas the remaining vapour flow rate is sent to the following effect as the heating steam. The equations to model the first effect are reported in Table 10.

Table 10. Mass and energy balance equations in the first effect.

$M_{feed} = M_D[0] + M_b[0]$	(50)
$M_{feed}\, X_{feed} = M_b[0]\, X_b[0]$	(51)
$M_{vap}[0] = M_D[0]$	(52)
$M_s\, \lambda(T_s) + M_{feed}\, h_{sw}(T_{preh}[1],\ X_{feed}) = M_b[1]\, h_{sw}(T[1],\ X_b[1]) + (1 - \alpha_{cond}[1])\, M_{vap}[1]\, h_{vap}(T'_{vsat}[1]) + \alpha_{cond}[1] M_{vap}[1]\, h_{liq}(T'_{vsat}[1])$	(53)

The mass and energy balance equations to model the generic intermediate effects are reported in Table 11. The first two equations are the global mass and salt balance equations on the effect. In each intermediate effect, the feed solution that is sprayed on the external surface of the tube bundle is the brine generated in the previous effect (M_b[i-1]). Since the pressure

decreases from one effect to the following, the brine entering the effect flashes and generates a vapour flow rate (M_{fbrine}) (energy balance in equation 59). In the evaporator, the partial evaporation gives rise to the vapour flow rate (M_d) and the brine flow rate (M_b), as in the first effect. Inside the tubes, the condensation of the vapour generates a distillate liquid flow rate, which is sent to a flash box. In fact, the flash box is included, in order to recover as much vapour as possible and to reduce the demand for external heat supply. In the flash box, part of the distillate flashes and an additional vapour flow rate (M_{fb}) is generated and mixed with M_d and M_{fbrine}. The remaining liquid flow rate in the flash box is the distillate produced in the effect (M_c). The mass balance on the vapour phase is reported in equation 56, whereas equations 57 and 58 are the mass and the energy balance on the flash box, respectively. Finally, the energy balances on the heat exchanger and on the preheater are reported in equations 60 and 61, respectively.

Table 11. Mass and energy balance equations in the generic intermediate effect.

$$M_b[i-1] = M_D[i] + M_{fbrine}[i] + M_b[i] \quad (54)$$

$$M_b[i-1]X_b[i-1] = M_b[i]\,X_b[i] \quad (55)$$

$$M_{vap}[i] = M_D[i] + M_{fbrine}[i] + M_{fb}[i] \quad (56)$$

$$M_c[i-1] + \alpha_{cond}[i]\,M_{vap}[i] + (1-\alpha_{cond}[i-1])M_{vap}[i-1] = M_{fb}[i] + M_c[i] \quad (57)$$

$$\begin{aligned} &M_c[i-1]\,h_{liq}\big(T'_{v,sat}[i-1]\big) + \alpha_{cond}[i]\,M_{vap}[i]\,h_{liq}(T'_{vsat}[i]) \\ &\quad + (1-\alpha_{cond}[i-1])M_{vap}[i-1]\,h_{liq}(T_c[i-1]) \\ &\quad = M_{fb}[i]h_{vap}(T'_{vsat}[i]) + M_c[i]h_{liq}(T'_{vsat}[i]) \end{aligned} \quad (58)$$

$$M_{fbrine}[i]\,\lambda\big(T_{brine,f}[i]\big) = M_{brine}[i-1]\,c_{P_{sw}}(T_{mean},\,X_b[i-1])\big(T[i-1] - T_{brine,f}[i]\big) \quad (59)$$

$$\begin{aligned} &(1-\alpha_{cond}[i-1])M_{vap}[i-1]\,\lambda(T_c[i-1]) \\ &\quad + M_{fbrine}[i]\Big(h_{sw}(T[i-1],X_b[i-1]) - h_{vap}(T'_{vsat}[i])\Big) \\ &\quad + M_b[i]\big(h_{sw}(T[i-1],X_b[i-1]) - h_{sw}(T[i],X_b[i])\big) \\ &\quad = M_d[i]\Big(h_{vap}(T'_{vsat}[i]) - h_{sw}(T[i-1],X_b[i-1])\Big) \end{aligned} \quad (60)$$

$$M_{feed}\,c_{P_{sw}}\big(T_{mean},\,X_f\big)\,\big(T_{preh}[i] - T_{preh}[i+1]\big) = \alpha_{cond}[i]\,M_{vap}[i]\,\lambda(T'_{vsat}[i]) \quad (61)$$

Finally, in the last effect, there is no preheater and the vapour generated is sent to the end condenser. The brine produced in the last effect is the final brine produced in the MED plant, while the vapour condenses in the end condenser and the produced liquid distillate is sent to the last flash box. The liquid flow rate produced in the last flash box is the outlet distillate flow rate of the plant. The relevant equations are reported in Table 12. The mass and salt balances are analogous to equations 54 and 55. The energy balance on the effect is reported in equation 62. The mass and energy balances on the flash box (equations 63 and 64) are slightly different than those for a generic flash box, because there is no vapour condensed in the preheater in the last effect, but all vapour is condensed in the end condenser (M_{vap}[N-1]).

Finally, equation 65 presents the energy balance in the end condenser, where M_{cw} is the total cooling water flow rate required to condensate the vapour.

Table 12. Mass and energy balance on the last effect and the end condenser.

$$(1-\alpha_{cond}[N-1])M_{vap}[N-1]\,\lambda(T_c[N-1]) + M_{fb}[N]\,h_{vap}(T'_{vsat}[N]) + M_b[N-1]\,h_{sw}(T[N-1],\,X_b[N-1]) = M_b[N]\,h_{sw}(T[N],\,X_b[N]) + M_{vap}[N]\,h_{vap}(T'_{vsat}[N]) \quad (62)$$

$$M_c[N-2] + M_{vap}[N-1] + (1-\alpha[N-2])M_{vap}[N-2] = M_{fb}[N-1] + M_c[N-1] \quad (63)$$

$$M_c[N-2]\,h_{wat,l}\left(T'_{v,sat}[N-2]\right) + M_{vap}[N-1]\,h_{wat,l}\left(T'_{v,sat}[N-1]\right) + (1-\alpha[N-2])M_{vap}[N-2]\,h_{wat,l}(T_c[N-2]) = M_{fb}[N-1]h_{wat,v}\left(T'_{v,sat}[N-1]\right) + M_c[N-1]h_{wat,l}\left(T'_{v,sat}[N-1]\right) \quad (64)$$

$$M_{cw}\,Cp_{SW}\left(\overline{T_{cw}}, X_{feed}\right)\left(T_{cw,out} - T_{cw,in}\right) = M_{vap}[N-1]\,\lambda(T'_c[N-1]) \quad (65)$$

For what concerns the design of the effects, the areas of the heat exchangers (A_{hx}), of the preheaters (A_{preh}) and of the end condenser (A_{cond}) are calculated according to the equations in Table 13. The $DTML_{preh}$ and $DTML_{cond}$ are the temperature logarithmic means in the preheater and the condenser, respectively. U_{evap} and U_{cond} are the heat transfer coefficients for the evaporator and the condenser, calculated according to correlations reported in the literature [135].

Table 13. Equations for the design of heat exchangers, preheaters and end condenser.

$$A_{hx}[0] = \frac{M_{feed}c_{P_{sw}}\left(T_{mean},\,X_f\right)\left(T[1] - T_{preh}[1]\right) + M_d[1]\,\lambda(T_{vsat}[1])}{U_{evap}(T[1])(T_{steam} - T[1])} \quad (66)$$

$$A_{hx}[i] = \frac{(1-\alpha_{cond}[i-1])M_{vap}[i-1]\,\lambda(T_c[i-1])}{U_{evap}(T[i])(T_c[i-1] - T[i])} \quad (67)$$

$$A_{preh}[i] = \frac{\alpha_{cond}[i]\,M_{vap}[i]\;\lambda(T'_{vsat}[i])}{U_{cond}(T'_{vsat}[i])\;DTML_{preh}} \quad (68)$$

$$A_{cond} = \frac{M_{cw}\,c_{P_{sw}}\left(\overline{T_{cw}}, X_{feed}\right)\left(T_{cw,out} - T_{cw,in}\right)}{U_{cond}(T'_c[N])\;DTML_{cond}} \quad (69)$$

2.1.3.2 Economic model

The economic model estimates the capital costs through the Module Costing Technique [128] and the purchase costs are calculated by representing each effect as the combination of two heat exchangers (evaporator and preheater) and a vessel (flash box). The equations to calculate the purchase costs are reported below.

$$\log {C_{p,0}}^{hx} = 4.3247 - 0.3030 \log A_{hx} + 0.1634 \log {A_{hx}}^2 \quad (70)$$

$$\log {C_{p,0}}^{vessel} = 3.5565 + 0.3776 \log V_{vessel} + 0.0905 \log {V_{vessel}}^2 \quad (71)$$

Then, the purchase costs are corrected considering the materials and the operating conditions, in particular the heat exchangers are supposed to have a carbon steel shell and tubes in a nickel-based alloy, to resist to high temperatures and to salty water [136]. These aspects are all included in the bare module factor (F_{bm} [-]) and the product of the purchase cost of the equipment and the bare module factor gives the bare module cost of the equipment. Thus, the investment cost is given by the sum of the costs of the effects and of the end-condenser, plus the contingency and fee that are assumed as 15% and 3% of the cost of the equipment [128]. Finally, the investment costs are updated through the CEPCI index and linearly depreciated, considering a discount rate of 6% and a depreciation period of 25 years.
The operating costs include the costs for maintenance, labour and personnel and the costs for chemicals, thermal and electric energy. The maintenance cost is calculated as 3%/y of the total investment cost. The personnel cost depends on the average cost of the workers and on the required number of workers, which is estimated as a function of the size of the plant. The labour cost for maintenance is defined as 20% of the personnel cost [137]. The chemicals costs include the costs for pre-treatments to apply to the feed, such as anti-scaling and anti-foaming, and to the cooling water, such as chlorination, and for post-treatments of the distillate. The electric energy cost is given by the product of the specific electric cost and the electric consumption. In this regard, the specific electric consumption has been assumed equal to 1.5 kWh_{el}/m^3_{dist} [138]. Finally, the thermal energy cost is given by the product of the specific cost of the thermal energy and the thermal consumption. The total thermal consumption is calculated by multiplying the external steam flow rate M_s by the latent heat of vapour at the inlet temperature.

2.1.4 Reverse Osmosis

Reverse Osmosis is a pressure-driven membrane process, widely used for seawater desalination to obtain potable water. However, it is effective in treating water at any salinity, from brackish water up to high salinity waters. The technology is commonly present at the industrial scale and several efforts have been made to produce highly performing membranes, with very high salt rejection (approx. 99%) and high water flux [139].

2.1.4.1 Technical model

The RO model implemented for this doctoral thesis can simulate a single- or a double-stage plant with concentrating staging. The choice of a single- or a double-stage RO plant depends on the total recovery, defined as the ratio between the permeate and the feed flow rate: for any recovery lower than 50% a single-stage plant is used, whereas for higher recoveries a double-stage plant is required. Moreover, the model has a hierarchical structure, which follows the structure of the real plant. Typically, the RO plant presents a certain number of vessels in parallel, each containing a fixed number of RO units in series. These units are composed of RO membrane sheets wounded in a spiral-wound geometry. Therefore, the low-hierarchy

model describes the transfer mechanisms within the membrane; the medium-hierarchy model estimates the flow rate, concentration and pressure profile along the RO unit and the high-hierarchy model designs the RO plant and calculates the required number of vessels in parallel for a certain separation. The RO plant structure and the corresponding modelling hierarchies are sketched in Figure 9.

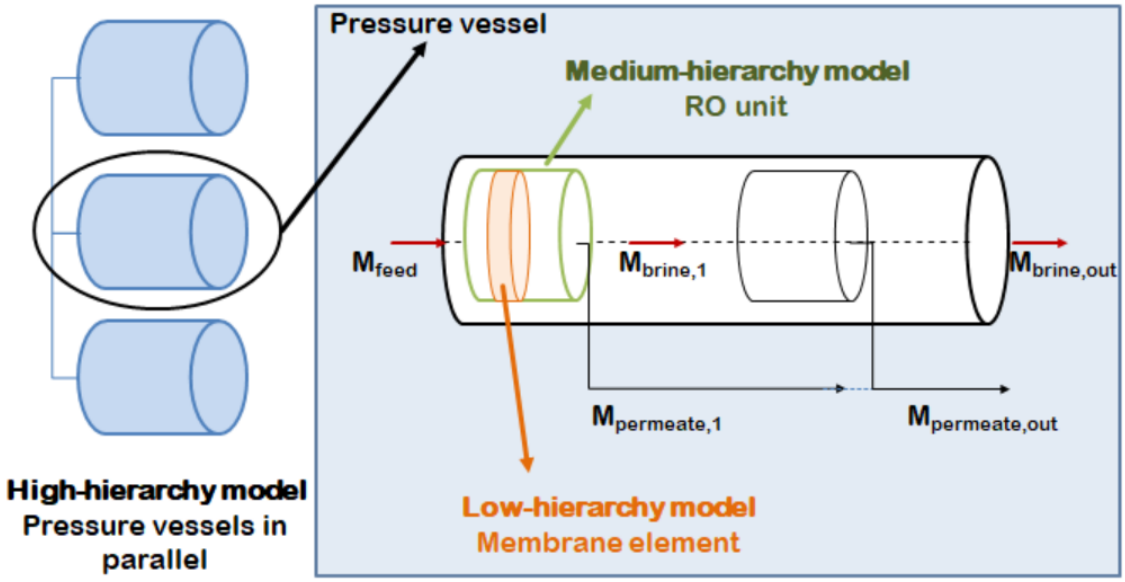

Figure 9. Representation of the RO plant and the corresponding model hierarchical structure.

Low-hierarchy model

The model to describe the transfer mechanisms through the RO membrane is a two-parameter solution-diffusion model. Both water and salt are supposed to diffuse through the membrane and their transfer is defined through two parameters: pure water permeability in the membrane (A_{membr} [kg/(s m^2 bar)]) and solute permeability in the membrane (B_{membr} [kg/(s m^2)]). The main equations of the low-hierarchy model are reported in Table 14. The flux of water F_w [kg/(m^{2}s)] depends on the water permeability A_{membr} and on the net pressure difference across the membrane (equation 72). The net pressure difference is given by the difference of the applied pressures at the two membrane interfaces ΔP minus the osmotic pressure difference $\Delta\Pi$ [bar], defined in equation 74. The flux of salt F_s [kg/(m^{2}s)] depends on the salt permeability B_{membr} and on the difference between the feed concentration at the feed-membrane interface $X_{f,w}$ [ppm] and the permeate concentration X_p [ppm]. $X_{f,w}$ depends on the concentration polarisation phenomenon, which has been quantified through the concentration polarisation factor (CPF [-]). The CPF is calculated as a function of the recovery of the element R_i [-], according to equation 78. The nominal membrane parameters $A_{membr,nom}$ and $B_{membr,nom}$ are calculated starting from test data, provided by the membrane producer. The real membrane properties A_{membr} and B_{membr} are found by correcting the nominal membrane parameters with the temperature correction factor (TCF [-]) and with the membrane ageing factors for the water (MAF_w [-]) and for the salt (MAF_s [-]) fluxes. The TCF is function of a membrane parameter depending on the barrier material (around 2,500-3,000 for polyamide

membranes [139]) and of the operating temperature T [K]. Concerning the ageing factor, age_{membr} is the average life time of the RO membranes (taken equal to 4 years) and $\Delta\Phi_w$ and $\Delta\Phi_s$ are measures of the relative water passage loss and of the relative solute passage increase with time (equal to 0.07 and 0.1 respectively) [140].

Table 14. Equations of the low-hierarchy RO model.

$F_w = A_{membr}\,(\Delta P - \Delta\Pi)$	(72)
$F_s = B_{membr}\,(X_{f,w} - X_p)\,10^{-6}$	(73)
$\Delta\Pi = \frac{2\,RT\,\rho}{M_{NaCl}}\,10^{-5}(X_{f,w} - X_p)10^{-6}$	(74)
$TCF = \frac{1}{e^{C_{membr}\left(\frac{1}{T}-\frac{1}{298}\right)}}$	(75)
$MAF_w = (1-\Delta\Phi_w)^{age_{membr}}$	(76)
$MAF_s = 1+\Delta\Phi_{s,coeff}\times age_{membr}$	(77)
$CPF = \frac{X_{f,w}}{X_f} = k_p e^{\left(\frac{2\,R_i}{2-R_i}\right)}$	(78)

Medium-hierarchy model

The medium-hierarchy model describes the RO unit. In the industrial plants, the RO units typically present a spiral-wound geometry. However, in the model, the membranes are described as unwounded, because the channel thickness is much smaller than the module radius and the configuration can be modelled as a plate and frame system with negligible errors [118]. Also, the variation of flow rate and concentration is neglected along the permeate flow direction and the membrane is discretised along the feed main flow direction [141]. For each discretisation element, the water and salt fluxes F_w and F_s are calculated using the low-hierarchy model and then, they are used in the mass balances in equations 79 and 80 to estimate the permeate flow rate (M_{perm} [kg/s]) and composition (X_{perm} [ppm]). The brine flow rate (M_{brine} [kg/s]) and composition (X_{brine} [ppm]) are calculated via mass balances on the element (equations 81-82) and they constitute the inlet feed flow rate (M_f [kg/s]) and composition (X_f [ppm]) of the following element (equations 83-84). Conversely, the permeates produced in all elements are collected and constitute the outlet permeate of the RO unit ($M_{perm,out\ unit}$ [kg/s]) (equations 85-86).

Table 15. Equations of the medium-hierarchy RO model.

$$M_{perm}[i] = (F_w[i] + F_s[i]) \frac{A_{elem}}{n_{discr}} \quad (79)$$

$$X_{perm}[i] = \frac{F_s[i]}{F_w[i]} 10^6 \quad (80)$$

$$M_{brine}[i] = M_f[i] - M_{perm}[i] \quad (81)$$

$$X_{brine}[i] = \frac{X_f[i] M_f[i] - X_{perm}[i] M_{perm}[i]}{M_{brine}[i]} \quad (82)$$

$$M_f[i+1] = M_{brine}[i] \quad (83)$$

$$X_f[i+1] = X_{brine}[i] \quad (84)$$

$$M_{perm,out\ unit} = \sum_i M_{perm}[i] \quad (85)$$

$$X_{perm,out\ unit} = \frac{\sum_i M_{perm}[i]\ X_{perm}[i]}{\sum_i M_{perm}[i]} \quad (86)$$

High-hierarchy model

Finally, the high-hierarchy model allows for designing an industrial-scale RO plant. The model used in the design mode calculates the number of vessels required in each stage to achieve a certain recovery rate (R_{plant} [%]), whereas the operational mode allows for estimating the recovery achieved with a fixed number of vessels and a certain feed pressure. Within each vessel, a number of RO units are arranged in series: the retentate produced by one unit is sent to the following unit as the feed solution, whereas the permeates are collected together and constitute the outlet permeate solution.

For design purposes, I implemented an optimisation procedure to find the feed pressure (P_{feed} [bar]) required to achieve the plant recovery, defined in equation 88. For each investigated pressure, the total membrane area A_{tot} [m^2] is estimated by considering an average value of water flux (equation 87). Then, the feed flow rate of each vessel in parallel is calculated and the composition ($X_{perm,out}$ [ppm]) and the total flow rate ($M_{perm,out}$ [kg/s]) of the outlet permeate solution are estimated by simulating the vessel. Finally, P_{feed} is found by minimising the squared error between the calculated and the required R_{plant}.

The electric power demand of the high pressure pump (P_{HP} [W]) is estimated via equation 90. Also, the possibility to couple the RO with energy recovery devices (ERD) has been considered: the pressure exchangers allow for recovering most of the pressure of the outlet brine, with an efficiency of 98% [136]. The remaining pressure increase is carried out in a booster pump and its power demand (P_{BP} [W]) is calculated via equation 91.

Table 16. Equations of the high-hierarchy RO model.

$$A_{tot} = \frac{R_{plant}\, M_{feed}}{F_w} \quad (87)$$

$$R_{plant} = \frac{M_{perm,out}}{M_{feed}} \times 100 \quad (88)$$

$$X_{perm,out} = \frac{\sum_{elem} M_{perm,out\ elem}\, X_{perm,out\ elem}}{M_{perm,out}} \quad (89)$$

$$P_{HP} = \frac{P_{feed}\, 10^5 M_{perm}}{\rho\, \eta_{pump}} \quad (90)$$

$$P_{BP} = \frac{(P_{feed} - P_{ERD,out})\, 10^5 M_{feed}}{\rho\, \eta_{pump}} \quad (91)$$

2.1.4.2 Economic model

The economic model estimates the capital and the operating costs of an industrial-scale RO plant. The capital costs include the costs for membrane units, pressure vessels, pumps, piping and intake. I took the costs for membrane units and pressure vessels reported in the literature [142, 143]. Also, I used different correlations to estimate the cost of the high pressure pump depending on the feed flow rate, as reported in Table 17. Equation 92 refers to pumps with flow rate (Q_{feed}) lower than 200 m^3/h; equation 93 is used for pumps with Q_{feed} between 200 and 450 m^3/h; equation 94 estimates the cost of pumps with Q_{feed} of 450 m^3/h. For higher flow rates, multiple pumps in parallel have to be installed and the costs are calculated combining the equations in Table 17.

Table 17. Equations to estimate the cost of high pressure pumps with different flow rates [142].

$$Cost_{HPP} = 52\, P_{feed} Q_{feed} \quad (92)$$

$$Cost_{HPP} = 81\, \left(P_{feed} Q_{feed}\right)^{0.96} \quad (93)$$

$$Cost_{HPP} = 393{,}000 + 10{,}710\, P_{feed} \quad (94)$$

The costs of the equipment are updated through the index CEPCI. The sum of the capital costs is the total investment cost, which is annualised by assuming a discount rate of 6% and a depreciation period of 25 years [144].

The operating costs include the cost for electricity, maintenance, labour, chemicals and membrane replacement. The maintenance costs are calculated as 3%/y of the total investment cost plus 20% of the labour cost [137]. The labour cost is estimated considering the number of workers required in the plant as linearly dependent on the total inlet feed flow rate, used as a measure of the size of the plant. The chemicals include the ones required for the pre-treatment of the feed, such as the anti-scaling agent, and for the post-treatment of the permeate. Finally, the membrane replacement cost is calculated by multiplying the cost of the membrane units, the total number of units and the replacement rate, which is equal to 15% per year [144].

2.1.5 Membrane distillation

Membrane Distillation (MD) is a hybrid membrane-thermal desalination process that makes use of a microporous hydrophobic membrane, permeable only to water vapour. The two interfaces of the membrane are kept at different temperatures: this temperature gradient corresponds to a vapour pressure difference, which generates a vapour flux through the membrane. Potentially, MD is a very advantageous desalination technology: it requires lower temperatures and smaller footprint than MED plants, it is very suitable in the case of low-grade waste heat availability and it works at much lower pressures than RO. Moreover, since the separation occurs by evaporation of water at the hot interface and by condensation of the vapour at the cold interface, the theoretical rejection to any solute is 100% [95]. However, the main issue of the MD process regards a non-ideality phenomenon, namely the temperature polarisation. In fact, the driving force for the vapour flux depends on the temperature difference at the two interfaces ($T_{membrane,hot} - T_{membrane,cold}$) and these temperatures are different from those in the bulk, because of the temperature polarisation phenomenon [145]. Another drawback of the MD process is that the water flux is relatively low, if compared with other technologies as RO, and the heat lost by conduction is significant, thus the thermal energy requirement is typically very high [146].
Various MD configurations have been proposed and employed: the most widely used configuration is the Direct Contact MD (DCMD), where both hot and cold fluids are in direct contact with the membrane on the two sides; other configurations present an air gap between the membrane and a cold condensing plate (AGMD) or a cold sweep gas which substitutes the cold permeate and provides the driving force (SGMD) or the vacuum applied on the permeate side to enhance the pressure difference (VMD). For this doctoral thesis, I chose to use the DCMD configuration, because of its operational simplicity and high fluxes and because it can operate both in the flat sheet and in the spiral-wound geometry [95].

2.1.5.1 Technical model

The technical model presents a hierarchical structure, which represents the real structure of the MD plant. The lower-hierarchy model is focused on the description of the heat and mass transfer through the membrane. The medium-hierarchy model contains mass and energy balances, to assess the profiles of temperature, flow-rates and concentrations along the feed stream-wise direction. The high-hierarchy model simulates a full-scale plant, in which MD units are arranged in series and in parallel to achieve a certain total recovery.
The structure of the MD plant is schematically reported in Figure 10.

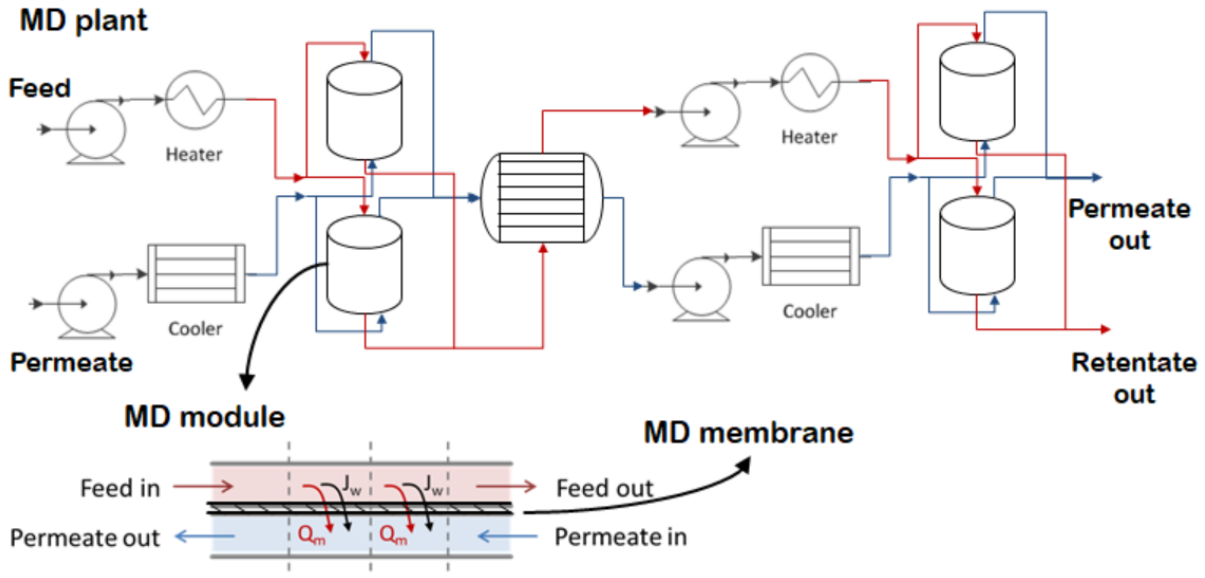

Figure 10. Scheme of the MD plant structure, with two branches in parallel, each composed of two modules in series.

Low-hierarchy model

The low-hierarchy model describes the heat and mass transfer mechanisms through the membrane. Table 18 includes the main equations regarding the heat transfer mechanisms. Three heat fluxes have to be defined: the convective flux from the bulk of the hot channel to the membrane ($Q_{conv,hot}$ [W/m^2]); the heat flux through the membrane (Q_m [W/m^2]) and the convective flux from the membrane to the bulk of the cold channel ($Q_{conv,cold}$ [W/m^2]). The convective flux on the bulk side is defined in equation 95 and depends on the heat transfer coefficient (h_f [W/(m^{2}K)]) and on the temperature difference between bulk ($T_{bulk,hot}$ [K]) and membrane interfaces ($T_{m,hot}$ [K]).

The heat flux through the membrane is reported in equation 96 and is given by the sum of the heat transferred by conduction ($Q_{cond,m}$ [W/m^2] defined in equation 97) and the latent heat associated to the vapour flux ($Q_{evap,m}$ [W/m^2] defined in equation 98).

The convective flux in the cold channel ($Q_{conv,cold}$ [W/m^2]) depends on the convective heat transfer coefficient on the permeate side (h_p [W/(m^{2}K)]) and the temperature difference between the membrane interface ($T_{m,cold}$ [K]) and the bulk of the permeate ($T_{bulk,cold}$ [K]), as shown in equation 99.

A very important aspect concerns the definition of the temperatures at the membrane interfaces, since their difference constitutes the driving force for the separation. $T_{m,hot}$ and $T_{m,cold}$ are defined in equations 100 and 101 that are obtained by equating $Q_{conv,hot}$ to Q_m and Q_m to $Q_{conv,cold}$, respectively [147]. For the estimation of these temperatures, the heat transfer coefficients have to be known. Within the membrane, the heat transfer coefficient h_m is given by the ratio between the conductivity of the membrane k_m [W/(m K)] and the thickness of the membrane δ_m [m]. The membrane conductivity is a combination of the conductivity of the polymeric structure ($k_{membr,pol}$ [W/(m K)]) and the conductivity of air (k_{air} [W/(m K)]). The weight of the two terms depends on the membrane porosity ε [-] (equation 102). The

convective coefficients h_f and h_p depend on the Nusselts number that is defined in equation 103 for laminar flows [148] and in equation 104 for turbulent flows [149].

Table 18. Equations about heat transfer mechanisms through MD membranes.

$$Q_{conv,hot} = h_f\left(T_{bulk,hot} - T_{m,hot}\right) \quad (95)$$

$$Q_m = Q_{cond,m} + Q_{evap,m} \quad (96)$$

$$Q_{cond,m} = h_m\left(T_{m,hot} - T_{m,cold}\right) \quad (97)$$

$$Q_{evap,m} = J_w \Delta H_{evap}\left[\frac{T_{m,hot} + T_{m,cold}}{2}\right] \quad (98)$$

$$Q_{conv,cold} = h_p\left(T_{m,cold} - T_{bulk,cold}\right) \quad (99)$$

$$T_{m,hot} = \frac{\frac{k_m}{\delta_m}\left(T_{b,cold} + \frac{h_f}{h_p} T_{b,hot}\right) + h_f T_{b,hot} - J_w \Delta H_{evap}}{\frac{k_m}{\delta_m} + h_f + k_m \frac{h_f}{h_p \delta_m}} \quad (100)$$

$$T_{m,cold} = \frac{\frac{k_m}{\delta_m}\left(T_{b,hot} + \frac{h_p}{h_f} T_{b,cold}\right) + h_p T_{b,cold} + J_w \Delta H_{evap}}{\frac{k_m}{\delta_m} + h_p + k_m \frac{h_p}{h_f \delta_m}} \quad (101)$$

$$k_m = \varepsilon\, k_{air} + (1 - \varepsilon)\, k_{membr,pol} \quad (102)$$

$$Nu = 0.13\, Re^{0.64} Pr^{0.38} \quad (103)$$

$$Nu = 0.22\, Re^{0.69} Pr_{bulk}^{\ 0.13} \left(\frac{Pr_{bulk}}{Pr_{membr}}\right)^{0.25} \quad (104)$$

Table 19 presents the main equations relevant to the mass transfer mechanisms through the membrane. The vapour flux J_w [kg/(m^{2}s)] is function of the vapour pressure difference between the two membrane interfaces and the mass transfer coefficient B_m [kg/(m^{2}s Pa)], as reported in equation 105. The mass transfer coefficient depends on the main transport mechanism through the membrane among (i) Knudsen diffusion, (ii) molecular diffusion or (iii) a combination of these two [145]. The main transport mechanism can be identified through the Knudsen coefficient (Kn [-]), defined as the ratio between the molecular mean free path λ [m] (equation 106) and the pore diameter r_{pore} [m]. If λ is higher than r_{pore} (Kn > 1), the Knudsen diffusion is the most representative transport mechanism. In fact, the collisions between the molecules and the wall are dominant with respect to the collisions molecules-molecules [145]. Conversely, if r_{pore} is higher than λ (Kn < 0.01), the predominant transport mechanism is the molecular diffusion. In most cases, the value of Kn is between 0.01 and 1, which means that the transport is given by the combination of the two mechanisms.

Thus, the definition of the mass transfer coefficient takes into account both transport terms, here represented by the coefficients $D_{w,k}$ (equation 107) and $D_{w,m}$ (equation 108). The first depends on r_{pore}, porosity ε, tortuosity τ [-], temperature T [K] and molecular weight of water ($M_{w,wat}$ [g/mol]). The second depends only on ε, τ and T. Both are included in the definition of the coefficient B_m, reported in equation 109.

Finally, as already mentioned for the temperature, also the concentration at the membrane interface is different than the one in the bulk of the feed solution, because of the concentration polarisation. The concentration at the bulk membrane interface $C_{m,hot}$ [ppm] is calculated

through equation 110, where $k_{f,mass}$ [m/s] is the mass transfer coefficient in the feed channel. The coefficient $k_{f,mass}$ is calculated from the Sherwood number (Sh [-]), which is defined in analogy with Nu definition (equations 103-104) as a function of Reynolds and Schmidt numbers.

Table 19. Equations about mass transfer mechanisms through MD membranes.

$$J_w = B_m\left(P_{m,hot} - P_{m,cold}\right) \quad (105)$$

$$\lambda = \frac{K_b T}{\sqrt{2}\,\pi P_{pore} {d_{wat}}^2} \quad (106)$$

$$D_{w,k} = \frac{2\, r_{pore}\, \varepsilon}{3\, \tau} \sqrt{\frac{8\, R\, T}{\pi\, M_{w,wat}}} \quad (107)$$

$$D_{w,m} = 4.46\, E-6\, \frac{\varepsilon}{\tau} T^{2.334} \quad (108)$$

$$B_m = \frac{1}{R\, T} \frac{D_{w,k}\, D_{w,m}}{D_{w,m} + P_{air} D_{w,k}} \frac{M_{w,wat}}{\delta_m} \quad (109)$$

$$C_{m,hot} = C_{bulk,hot}\, e^{\frac{J_w}{k_{f,mass}\, \rho}} \quad (110)$$

Medium-hierarchy model

The medium-hierarchy model simulates a MD unit with a counter-current flow arrangement. It presents an iterative procedure that runs until the error between the calculated and the given values of inlet permeate flow rate and temperature is below a fixed tolerance. In fact, the flow arrangement makes necessary to guess a value for the outlet permeate flow rate and temperature and to use them to simulate the unit.

The MD unit is discretised along the feed flow direction into a certain number of elements and, for each discretisation element, the low-hierarchy model is run to estimate the vapour and the heat fluxes through the membrane. Once J_w and Q_m are estimated for the element, the mass and energy balances reported in Table 20 are applied to calculate the outlet feed flow rate ($m_{f,out}$ [kg/s]), concentration ($C_{f,out}$ [ppm]) and temperature ($T_{f,out}$ [K]) and the inlet permeate flow rate ($m_{p,out}$ [kg/s]) and temperature ($T_{p,out}$ [K]). The mass balances are applied to each discretisation element. At the end of each iteration, the flow rate and temperature of the permeate entering the unit are calculated and compared with the given values. Depending on their difference, the guess values of outlet permeate flow rate and temperature are updated and a new iteration starts.

Table 20. Equations of the medium-hierarchy MD model.

$$m_{f,out}[i] = m_{f,in}[i] - J_w[i]\, A_{elem} \quad (111)$$

$$m_{p,in}[i] = m_{p,out}[i] - J_w[i] A_{elem} \quad (112)$$

$$T_{f,out}[i] = \frac{m_{f,in}[i]\, C_{p,f,in}[i]\, T_{f,in}[i] - Q_m[i]\, A_{elem}}{m_{f,out}[i]\, C_{p,f,out}[i]} \quad (113)$$

$$T_{p,in}[i] = \frac{m_{p,out}[i]\, C_{p,p,out}[i]\, T_{p,out}[i] - Q_m[i]\, A_{elem}}{m_{f,in}[i] C_{p,f,in}[i]} \quad (114)$$

$$C_{f,out}[i] = \frac{m_{f,in}[i]\, C_{f,in}[i]}{m_{f,out}[i]} \quad (115)$$

High-hierarchy model

The MD plant is given by the combination of MD modules arranged in series and in parallel [150]. Firstly, the MD modules are composed of a certain number of MD membranes wounded together in a spiral-wound configuration. In other words, the MD module can be represented as some MD units in parallel, each having a feed and a permeate channel separated by a membrane. Secondly, the MD modules are arranged in parallel and the number of branches in parallel depends on the total feed flow rate. In fact, commercial MD modules have a design flow rate between 500 and 1500 l/h. Therefore, the ratio between the total flow rate and the design flow rate corresponds to the number of branches in parallel ($N_{parallel}$ [-] in equation 118). Thirdly, in each branch, a number of MD modules are put in series and the brine of one module is fed to the following module, to achieve the target recovery (defined as the ratio between $M_{dist,plant}$ and $M_{feed,plant}$).

In analogy with the RO plant, three plant arrangements are considered and the choice depends on the total recovery: a single-stage is used for recovery lower than 50%, a double-stage for recovery between 50% and 75% and a triple-stage for recovery higher than 75%.

Concerning the design procedure, the knowledge of the plant recovery or of the target brine concentration $C_{brine,plant}$ [ppm] allows for calculating the total required flow rates of brine and distillate produced by the plant ($M_{brine,plant}$ and $M_{dist,plant}$ [kg/s], equations 116 and 117).

Also, the model selects the arrangement (single-, double- or triple-stage) depending on the recovery and estimates $N_{parallel}$ starting from $M_{feed,plant}$. Note that $N_{parallel}$ is the number of branches in parallel in the first stage. If there are two or three stages, the number of branches in parallel is always defined as the half of the number of branches of the previous stage. In this way, significant variations of feed flow rate between two stages are avoided.

Thus, the modules within each branch are simulated and an iterative procedure is used to assess the number of modules in series. A guess value of $N_{module,series}$ is calculated from an average water flux, estimated at an average concentration between the inlet feed concentration and the one of the outlet brine (equation 119). Then, the modules are simulated and the brine produced by one module is supposed to be fed to the following module. Therefore, the inlet feed concentration changes along the series, whereas the inlet feed and permeate temperatures do not change, thanks to the employment of intermediate heaters and coolers that restore the initial temperatures. To reduce the external heat supply required to restore the inlet

temperatures, recovery heat exchangers are included to realise a thermal integration between the two streams.
The whole series is simulated and the outlet concentration of the brine is compared to the target one. The iterative procedure runs until the error between these values is below a given tolerance.

Table 21. Equations of the high-hierarchy MD model.

$$M_{brine,plant} = \frac{M_{feed,plant}\, C_{feed}}{C_{brine,plant}} \quad (116)$$

$$M_{dist,plant} = M_{feed,plant} - M_{brine,plant} \quad (117)$$

$$N_{parallel} = \mathrm{int}\left(\frac{M_{feed,plant}\, \rho_{feed,plant}}{M_{feed,in-design-lh} \times 1000}\right) \quad (118)$$

$$N^{guess}{}_{modules,series} = \mathrm{int}\left(\frac{M_{dist,plant}}{J_{w,aver} N_{parallel}\, A_{module}\, 3600}\right) \quad (119)$$

2.1.5.2 Economic model

The economic model estimates the capital and the operating costs of the MD plant, on the basis of literature data and correlations [95, 151]. The capital costs include direct and indirect costs. The direct ones are the costs of modules, membranes, pumps and heat exchangers, the costs for intake and pre-treatment and the costs for civil works [95]. The costs of modules, pumps and heat exchangers are calculated by using scale-up factors [151]. This is a common approach for the estimation of the equipment cost as a function of its size and, typically, a scale-up factor of 0.6 is used [128]. I use a factor of 0.6 for pumps and heat exchangers and a factor of 0.8 for the MD modules [151]. The cost of membranes depends on the specific cost of the MD membrane and the total area required in the plant. The costs of intake and pre-treatment and of the civil works are calculated according to equations 120 and 121 [95].

$$Cost_{intake\&pretreat} = 658 \left(Q_{feed}\left[\frac{m^3}{day}\right]\right)^{0.8} \quad (120)$$

$$Cost_{civil\ works} = 1945 \left(Q_{dist}\left[\frac{m^3}{day}\right]\right)^{0.8} \quad (121)$$

The indirect capital costs are estimated as 10% of the sum of the direct costs. The total investment cost is given by the sum of direct and indirect costs. This is annualised by using a depreciation time of 10 years and a discount rate of 6%.
The operating costs include the costs for electricity and heat demand, maintenance, labour, chemicals and membrane replacement. The electricity cost depends on the energy demand of the pumps used for feed and permeate streams entering in each module in series. The thermal cost is due to the heat required to increase the temperature of the feed from the intake to the inlet temperature and the heat required in the intermediate heaters. The maintenance cost is calculated as 2.5%/y of the investment cost, without the costs for membranes and modules because they are supposed to be replaced at the end of their lifetime [151]. The labour cost is

given by the product of the required number of workers and their average salary. The first term depends on the size of the plant, represented by the produced distillate flow rate [151]. Finally, the chemicals cost is given by the cost of the reactant to be used to pre-treat the feed solution and the membrane replacement cost is calculated by assuming a replacement rate of 15%/y [95].

2.2 Definition of inputs and outputs

Any industrial process has inlet and outlet material and energy streams, which are represented in the relevant models by input and output values. For the case of wastewater treatment processes, the inlet stream is the effluent or pre-treated effluent, with a certain temperature and composition depending on the industrial process responsible for its release. Different outlet streams can be generated by the treatment units: a target of purity and/or recovery defines the main product, whereas the other streams consist in by-products or waste to be further treated. Accordingly, the feed flow rate and composition are among the most important inputs of models of wastewater treatment units. If the model is used to design the plant, other important inputs regard the target that has to be achieved, for example the recovery of a RO plant or the outlet brine concentration in the MD plant. Conversely, if the model is used in the operation mode, the other important inputs concern the size of the plant, such as the total membrane area in the RO plant or the number of modules in series in the MD plant. The outputs typically include the characterisation of all outlet streams and the required size in the case of design models. In addition, the models require the knowledge of some parameters, which describe the operating conditions, such as the inlet temperatures or pressures, and the geometric features, for example the number of RO elements in series inside a pressure vessel or the size of the membrane sheet. These parameters can have a strong impact on the outputs, thus sensitivity analyses are often performed to find the most suitable values of the parameters for a specific case.

Concerning the economic models, the main outputs of all models described so far are the total annualised capital costs (CAPEX [$/y]) and the total operating costs (OPEX [$/y]). Generally speaking, the inputs of the economic models are produced by the technical models in the design mode. These mainly consist in the number of modules in the plant (for the modular membrane technologies like NF, RO and MD) or the size of the stages as for the MED plant and in the electricity and heat demand. Among the parameters used in the economic models, some are common to all technologies: the discount rate, the capacity factor of the plant, the efficiency of the pumps and the electricity and heat specific costs. Others are specific to the plant such as the chemicals cost and the depreciation time.

Table 22 reports the main inputs, outputs and parameters of the technical models, together with the inputs and parameters of the economic model. The outputs of the economic models are always CAPEX and OPEX of the relevant units.

Table 22. Main inputs, outputs and parameters of the models implemented in the doctoral thesis.

Model	Technical Inputs	Technical Parameters	Technical Outputs = *Economic Inputs*	Economic Parameters
Nanofiltration (NF)	- Feed flow-rate - Feed composition - Feed pressure - Plant recovery	- Membrane properties (r_{pore}, δ_m, ε_{pore}, X_d) - Membrane sheet area - Height of the channels - N° of elements per vessel	- Permeate and retentate flow-rate - Permeate and retentate conc. - *N° of vessels in parallel* - *Electricity demand*	- Investment/membrane costs - Depreciation time - Membrane replacement rate - Membrane specific cost - Electricity cost - Chemicals cost
Crystallization (cryst)	- Feed flow-rate - Feed composition (conc. of Mg^{2+} and Ca^{2+})	- Conc. of the NaOH solution - Length of the reactor - Fluid velocity in the reactor	- Effluent flow-rate and conc. - *Inlet flow-rate of NaOH solution* - *Outlet flow-rate of hydroxides* - *Electricity demand*	- Investment costs - Depreciation time - Cost of NaOH - Selling price of minerals - Electricity cost
Multi-Effect Distillation (MED)	- Feed flow-rate - Inlet salt conc. - Plant recovery / retentate outlet conc. - Intake temp.	- N° of effects - Steam temp. - Last effect temp. - Size of connecting lines and evaporator tubes	- Inlet steam flow-rate - *Area of heat exchangers (evaporators, preheaters and end-condenser)* - *Heat and electricity demand*	- Investment costs - Depreciation time - Electricity and heat costs - Selling price of pure water - Pre- and post-treatment costs
Reverse Osmosis (RO)	- Feed flow-rate - Inlet salt conc. - Plant recovery / retentate outlet conc.	- Membrane permeability (water and salt) - Salt rejection - Membrane sheet area - N° of elements per vessel	- Permeate and retentate flow-rate - Permeate and retentate conc. - *N° of vessels in parallel* - *Electricity demand*	- Investment/membrane costs - Depreciation time - Membrane replacement rate - Electricity cost - Selling price of pure water - Pre- and post-treatment costs
Membrane Distillation (MD)	- Feed flow-rate - Inlet salt conc. - Plant recovery / retentate outlet conc. - Intake temp.	- Inlet feed and permeate temp. - Membrane properties (ε, τ, r_{pore}) - Membrane sheet area - N° of membranes per module - Design flow rates of module -Minimum ΔT in heat exchanger	- Permeate and retentate flow-rate - Retentate composition - *Recovery heat exchangers area* - *N° of branches in parallel* - *N° of modules in series* - *Heat and electricity demand*	- Investment/membrane costs - Depreciation time - Membrane replacement rate - Electricity and heat costs - Selling price of pure water - Pre- and post-treatment costs

2.3 Development of treatment chains and implementation details

The techno-economic models described so far refer to single treatment processes, which constitute the building blocks of integrated treatment systems (treatment chains). To simulate the treatment chains, I used a simulation platform called Remote Component Environment (RCE), which is internally developed by DLR and freely available (http://rcenvironment.de/). RCE allows for implementing and interconnecting various blocks that can have the function of input provider, execution script, data processing script or output writer.
The input provider blocks can supply an input value, such as the feed flow rate, or an input file, for example a yaml file containing the parameters of the model called in the execution script. The execution scripts call and run external programs and collect their output values. The outputs of an execution script block can be passed directly as inputs of a following block or can be processed in a data processing script. The processing scripts are intermediate tools used for various scopes, such as to apply mass balances when two streams are mixed in the chain or to adjust units of measurements or to extract values from external files. The output writer blocks export the outputs in a text or an Excel file.
In the implementation proposed in this doctoral thesis, I used execution scripts to represent single processes: the script imports the model file corresponding to the process and calls the relevant solver procedure. In fact, all models have been suitably shaped in Python, by implementing wrapping functions.
To simulate a treatment chain given by a certain combination of processes, I introduced an execution script block for each process. The block calls the relevant model and it is connected to input provider blocks, which pass the inputs and the parameters required to run the model. The outputs of the model are defined as the outputs of the block and, in this way, they can be written into an external file through an output writer block or transferred as inputs to the following block or processed in a processing script block.
An example of implementation of a treatment chain in RCE is depicted in Figure 11. The treatment chain proposed for the brine produced by the regeneration of ion exchange resins is composed of four units: nanofiltration and crystallizer in the pre-treatment phase and reverse osmosis and membrane distillation in the concentration phase. Four corresponding execution script blocks (in blue) have been included in the chain. Each block receives inputs and parameters from a number of input providers (in green). For example, some inputs provided to the NF blocks are the feed flow rate (Q_{feed}), the feed pressure (P_{feed}), the composition of the feed (in the file "conc file") and the total recovery. Also, every execution script has an input provider block passing the configuration file ("config file") of the corresponding process: this file is a dictionary containing all the parameters required by the model.
Furthermore, three processing scripts are included and they contain mass balances (from the left, the first represents the mixing of the crystallizer effluent and the NF permeate and the second the mixing of the RO and the MD permeates) or equations to adjust the units of measurement (as in the last script from the left).
Finally, each execution script block is connected to an output writer producing an Excel file with the techno-economic results of the model. In addition, some processing scripts have been introduced to merge the Excel files and to calculate the global outputs of the treatment chain. These last units are not shown in Figure 11, to simplify the workflow.

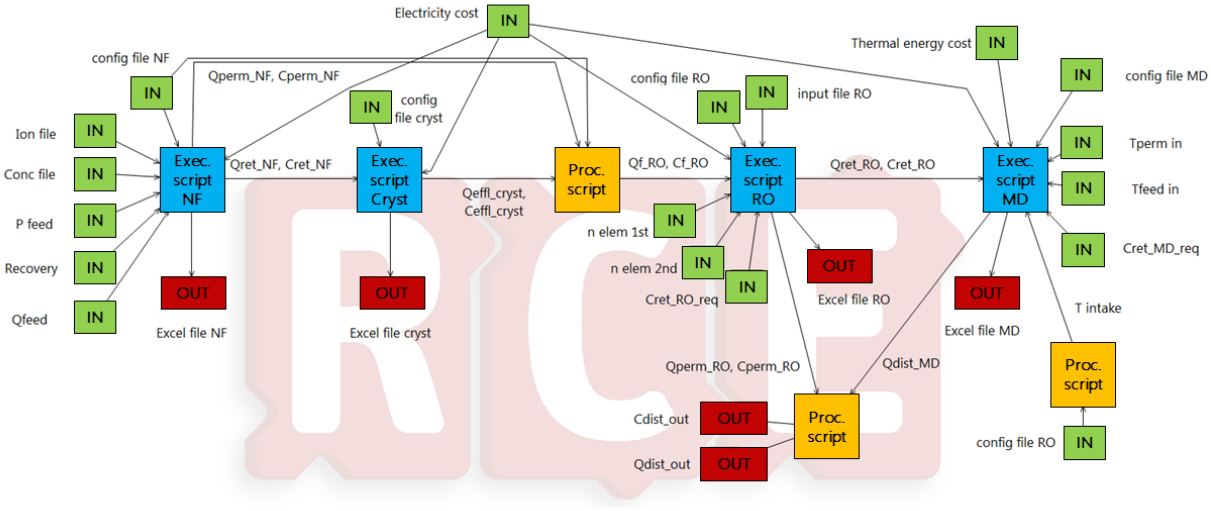

Figure 11. Example of a workflow implemented in RCE. The blue units represent the execution scripts calling the models, the yellow units represent the processing scripts, the green units are the input providers and the red units the outputs writers.

2.4 Definition of global assessment criteria

The implementation shown in section 2.3 allows for building easily various treatment chains for the same effluent. In fact, different integrated systems can be simulated by varying the technologies involved or by combining the pre-treatment or the concentration processes in different ways. To perform a proper comparison of the treatment chains devised for the same effluent, I selected some representative global assessment criteria able to inform about the technical, economic and environmental performances of the whole chain. Table 23 reports the global criteria used in this doctoral thesis.

Table 23. Criteria used to compare the treatment chains.

Technical	Electric power demand [kW] Thermal power demand [MW]
Economic	Total levelised cost of the main product LPC_{tot} [$/m$^3_{prod}$] - Total Levelised Brine Cost (LBC_{tot} [$/m$^3_{brine}$]) - Total Levelised Salt Cost (LSC_{tot} [$/m$^3_{salt}$])
Environmental	Operational CO_2 emissions per unit of main product [$kton_{CO2}/m^3_{prod}$]

The treatment systems are always investigated from the perspective of the water-energy nexus as “energy for water” systems [152]. Therefore, the technical comparison of the treatment chains refers to the global electric and thermal power demands, calculated as the sum of the demands of all integrated processes. In particular, the pre-treatment processes require only electricity, whereas the concentration processes require both heat and electricity and, typically, the heat demand is the highest term.
Moreover, the chains are devised with the aim to recover sellable raw materials and streams reusable in the industrial process. The combination of treatment technologies is designed to maximise the production of the main product of the chain, and to recover the other by-

products. Therefore, the economic comparison is performed by taking into account the main product and by estimating the selling price that the main product should have to allow the project to break-even. In this way, I calculate the levelised cost of the main product (LPC [$/m$^3_{prod}$]), in analogy with the levelised cost of water, typically used for the economic assessment of desalination plants, or the levelised cost of electricity, used for electricity supply systems.

The levelised cost of the main product (e.g. the concentrate brine in the treatment of the effluent of ion exchange regeneration and the salt in the treatment of the coal mine effluent) accounts for all the capital and operating expenditures of the processes integrated in the chain and for the revenues given by the by-products. The general definition of LPC_{tot} is reported in equation 122. It is given by the sum of two terms: the capital levelised cost (LPC_{cap} [$/m$^3_{prod}$]) and the operating levelised cost (LPC_{op} [$/m$^3_{prod}$]). The first is given by the ratio between the total annualised capital cost CAPEX [$/y] and the annual productivity Q_{prod} [m^3_{prod}/y]. The second is defined as the ratio between the total operating cost OPEX [$/y] minus the revenues of the by-products [$/y] and the annual productivity Q_{prod} [m^3_{prod}/y].

$$LPC_{tot} = LPC_{cap} + LPC_{op} = \frac{\sum_{units} CAPEX}{Q_{prod}} + \frac{\sum_{units} OPEX - \sum_{by-products} revenues}{Q_{prod}} \quad (122)$$

The calculation of LPC_{tot} has two scopes: (i) to assess the economic feasibility of a treatment chain, by comparing it with the market value of the main product and (ii) to compare different chains and to find the most economically profitable.

For what concerns the environmental analysis, all treatment systems allow for reducing the environmental impact of the industrial process by minimising the discharge of effluent into the natural environment. However, the treatment processes require material and energy supplies, which correspond to emissions of CO_2 into the environment. In this doctoral thesis, I referred only to the operational CO_2 emissions, since they turned out to be much higher than the ones due the material flows for desalination plants construction [153].

Therefore, the environmental comparison of different treatment chains focuses on the operational CO_2 emissions due to the thermal and electric energy demand of the treatment systems. Also in this case, I calculate the CO_2 emissions per unit of main product produced and this output is used both for comparison with the current industrial system used to produce the same product and for comparison with other treatment chains, to find the most environmentally-friendly solution.

3. Energy supply and energy demand

The estimation of the energy demands and the selection of the energy supply have a key role in our analyses, because the treatment chains often have significantly high heat and electricity demands and these may endanger the economic feasibility or the environmental friendliness of the whole chain. Therefore, a particular attention has been devoted to estimating the energy requirement of the involved processes and various options have been evaluated to supply electricity and heat to the treatment chains.

3.1 Energy supply

In this paragraph, the different energy supply systems considered for electricity and thermal energy are listed and the methods used to estimate the relevant specific costs of energy are described.

3.1.1 Electricity supply

Concerning the electricity supply, I considered two scenarios: grid supply and a combination of grid and photovoltaic (PV)-battery power system. I chose to investigate the PV technology rather than the wind technology, because it is more modular and easier to manage and because the power production has lower uncertainty. In fact, the lack of predictability of wind power production results in higher levelised cost of electricity (LCOE) due to the implementation of over-sized batteries.

3.1.1.1 Grid supply

For the case of grid supply, the specific cost of electricity and the CO_2 grid intensity are relevant to the country where the industrial plant is located and depend on the mix of electricity carriers of the grid in the specific country. The data about the current mix of electricity carriers in the different countries are taken from [154]. The current cost of electricity for non-household consumers is given by [155]. Once the shares of total electricity output covered by the different carriers are known, it is possible to estimate the global CO_2 emission factor by using the emission factors and the conversion efficiencies of the single carriers. The conversion efficiency is defined as the ratio between the output energy and the primary energy [156]. The CO_2 emission factors referred to the primary energy demand are reported in Table 24 [157].

Table 24. CO_2 emission factor for energy carriers [157].

Electricity carrier	CO_2 emission factor [kg/kWh_{prim}]
Lignite	0.399
Hard Coal	0.335
Mineral Oil	0.270
Natural Gas	0.202

3.1.1.2 PV-battery power system

The PV-battery system is simulated by using a tool implemented in INSEL [158]. The tool estimates how much power is produced by the system in a specific location, with given number of PV modules and size of the battery. In this way, for different configurations, it is possible to estimate the share of the total required power that can be covered by the PV-battery system. To characterise the specific location in the tool, the relevant meteorological data of a typical year with hourly resolution are required. In particular, the inputs to provide are: the global horizontal irradiance (GHI), the diffuse horizontal irradiance (DHI) and the ambient temperature. The other inputs refer to the size of the system and, in particular, these are the installed PV power [MW] and the capacity of the battery [h]. With these inputs, the model calculates the power produced by the PV-battery system that corresponds to a share of the total electricity demand of the treatment chain. This share is defined as self-sufficiency [%] (equation 123) because it is self-generated by an ad-hoc built plant, whereas the remaining fraction is always supplied by the grid.

$$Self-sufficiency\ [\%] = \frac{P_{PV-battery,prod}}{P_{demand}} 100 \quad (123)$$

Also, knowing the size of the system and the power produced, it is possible to calculate the capital and operating costs and the LCOE relevant to the PV-battery system. The capital costs are calculated as the sum of PV modules, battery and converter [159]. The operating costs are estimated as 1.5%/y and 2.5%/y of the investment cost for PV and battery, respectively [160]. The global LCOE is given by the combination of the cost of electricity from the grid and the LCOE calculated for the PV-battery system. The weights of the two terms in the combination correspond to the shares of the power demand covered by the two corresponding supply systems. Moreover, in the case of a combined grid-PV-battery supply, two sub-cases are included: one in which no taxation is imposed on the CO_2 emissions and one in which a given tax is applied to the CO_2 emissions generated by the fraction of power taken from the grid.
Finally, the CO_2 emission factor of the combined electricity supply system is calculated by dividing the CO_2 emissions due to the grid supply by the total power produced.
Overall, the INSEL tool can provide the global LCOE and CO_2 emission factor of an electricity supply system given by a certain combination of grid and PV-battery. A wide range of combinations can be realised by varying installed PV power and capacity of the battery and the different systems correspond to different costs and CO_2 emissions. As reported in the procedure in Figure 12, I performed parametric analyses by varying the ratio between the installed PV power and the power demand from 0.5 to 10 and by varying the full load hours of the battery from 0 to 17.5 h. These analyses gave rise to a scatter plot of LCOE values in function of the CO_2 emission factor that is directly correlated to the self-sufficiency of the plant, as shown in Figure 13. I selected the configurations of the supply system corresponding to the points in the lower envelope of the scatter plot to get a characteristic curve of LCOE vs. CO_2 emission factor (in black in Figure 13). The cost of electricity and the corresponding CO_2 emission factor are used as inputs in the simulation of the treatment chains to calculate the economic (LPC_{tot}) and the environmental (CO_2 emission per unit of product) global outputs.

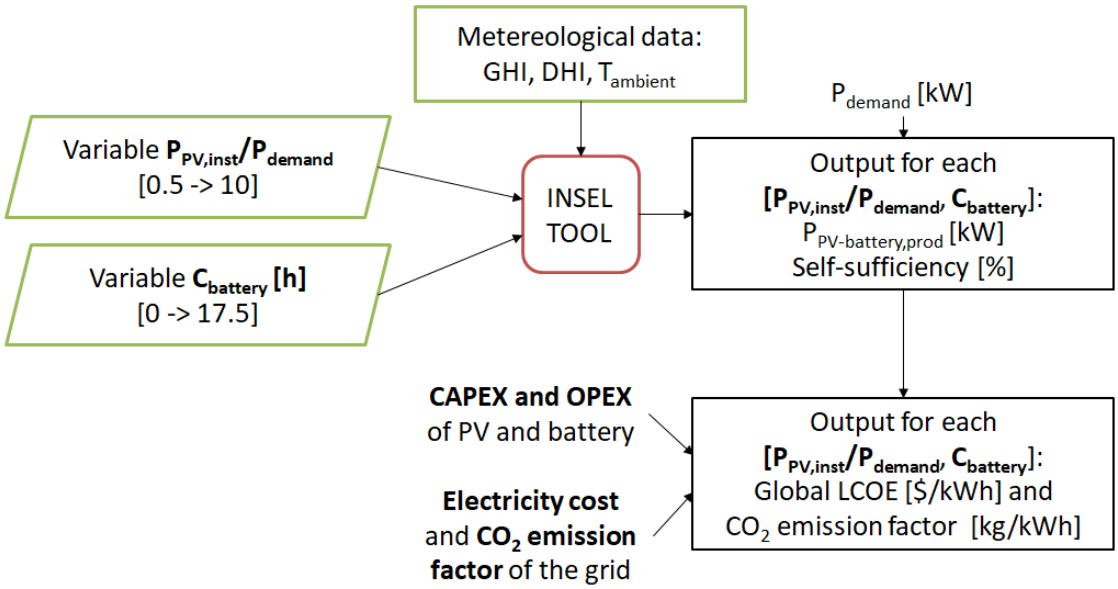

Figure 12. Procedure to estimate global LCOE and CO_2 emission factors of mixed PV-battery-grid supply systems with the INSEL tool.

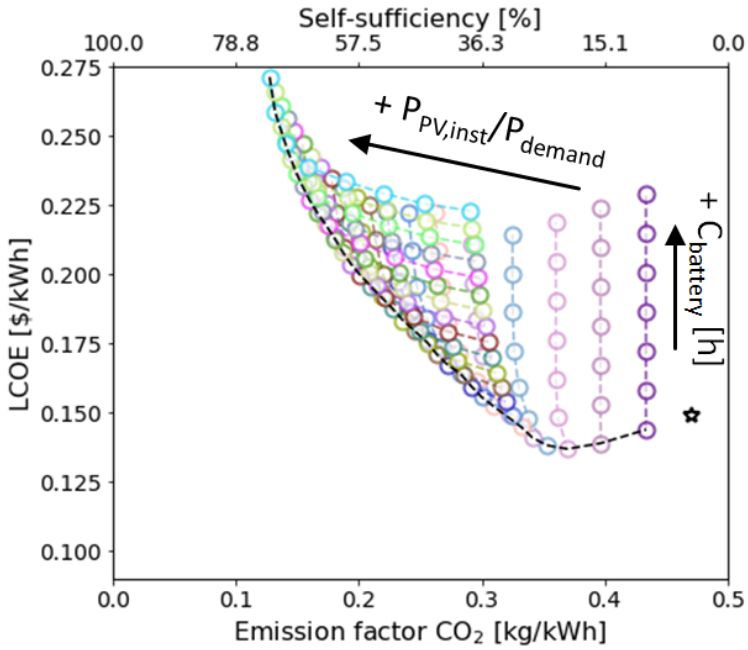

Figure 13. LCOE [$/kWh] of the PV-battery-grid supply as function of the CO_2 emission factor [kg/kWh] obtained by varying the $P_{PV,inst}/P_{demand}$ ratio from 0.5 to 10 (step of 0.5) and the full load hours of the battery from 0 to 17.5h (step of 2.5h). The CO_2 emissions have a cost of 80€/ton_{CO2}. The asterisk symbol (*) indicates the grid supply point.

3.1.2 Heat supply

I investigated two possible sources of thermal energy: waste heat available in the industrial site and a combined heat and power cycle.

3.1.2.1 Waste heat available in the industrial site

The reference case used for the analyses presented in this doctoral thesis provides the availability of low-temperature waste heat in the industrial site. In fact, previous studies showed that most industrial sectors produce high amounts of waste heat, especially in the temperature range between 100°C and 200°C [161]. This thermal energy is suitable to the concentration technologies involved in the treatment chains, because these typically require low temperature heat. The MED unit works with steam at a temperature comprised between 70°C and 120°C and the MD units operate with a maximum temperature of the hot stream ranging from 50°C to 80°C.
Therefore, in most cases, thermal energy is supposed to be supplied from low-pressure steam lines at pressure of 1 bar (temperature of 100°C). I fix a specific cost and CO_2 emission factor, mostly due to the electricity to be supplied for pumping and compressing the heat. The guidelines report that 0.09 GJ of electricity are required to recover 1 GJ of thermal energy [162]. Thus, I assumed a thermal energy cost of 0.01 $/kWh$_{th}$, in agreement with other works [163, 164] and with the equivalent cost of the electricity required, when the specific electric energy cost is 0.1 $/kWh$_{el}$ [155]. The CO_2 emissions are calculated on the basis of the electric consumption of the heat recovery operations.

3.1.2.2 Combined Heat and Power Cycle

An alternative thermal energy supply is a Combined Heat and Power (CHP) cycle with steam boiler and steam turbine. The system consists in a boiler fired by natural gas and a conventional steam turbine, which is used to provide thermal and electric energy simultaneously. To achieve this dual purpose, the steam is extracted at a given pressure. For desalination applications, the outlet steam pressure is typically between 0.9 and 2.5 bar.
The cost of the produced thermal energy depends on the outlet steam pressure and is estimated via the reference cycle method, proposed by [138]. This method calculates the price of steam extraction, by estimating the amount of electricity that could have been generated by further expanding the extracted steam in the low-pressure section of the turbine. The reference system is the turbine in which the steam is completely used for electricity generation. Therefore, the thermal energy cost is calculated on the basis of the opportunity cost (missed revenues) that would have been given by the electricity selling. Figure 14 depicts the trends of electricity losses in kWh$_{el}$ per ton of steam and the corresponding costs of the thermal energy in function of the pressure of the extracted steam.

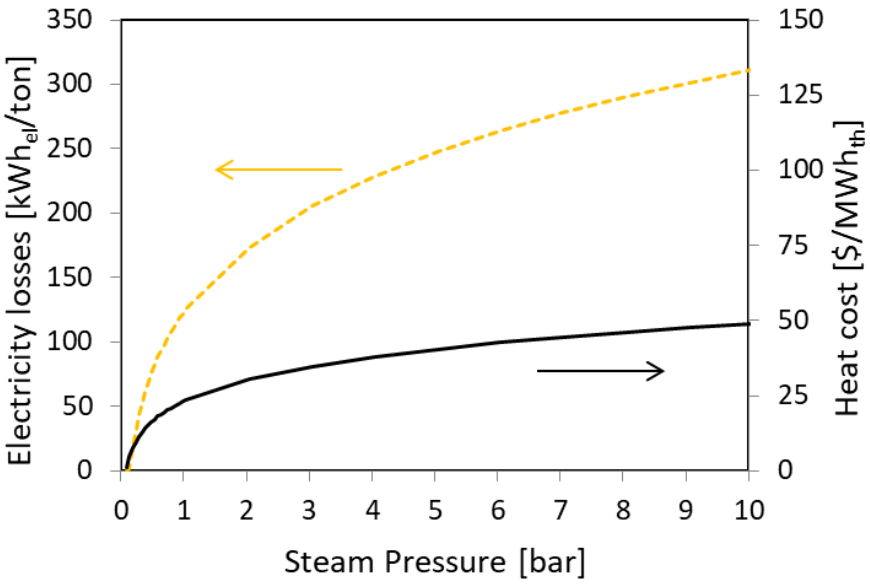

Figure 14. Specific electricity losses [kWh$_{el}$/ton] and heat costs [$/MWh$_{th}$] as functions of the steam pressure [bar].

3.*2 Energy demand*

All treatment processes have significant thermal and electric energy requirements, whose estimation is of crucial importance to assess the economic and environmental outputs of the treatment chains. Typical ranges of electricity and heat demands of the technologies modelled in this thesis are reported in Figure 15 [138, 163, 165]. In the following paragraphs, the thermal and electric energy requirements of each treatment process are described in detail.

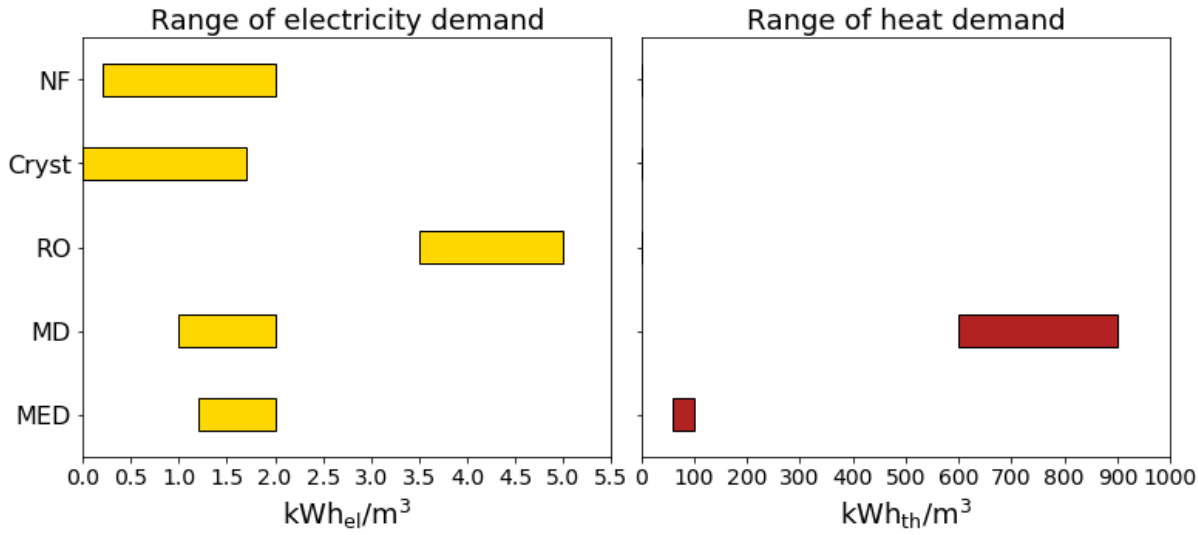

Figure 15. Typical ranges of electricity and heat demands of the five investigated technologies.

3.2.1 Electricity demand

The electricity demand is particularly significant for the pressure-driven membrane processes as NF and RO.

For the NF, the main energy consumption is due to the pumping of the feed solution up to a pressure comprised between 20 and 40 bar. The pumping energy is given by the product of the feed flow rate by the required final pressure, divided by the efficiency of the pumps (taken equal to 80%). An additional electricity demand term is accounted for NF unit and it consists in the average energy consumption of the membrane system equal to 40 Wh/m^3_{feed} [120].

Analogously, for the RO without energy recovery device, the electricity demand corresponds to the pumping energy required by the high-pressure pump to increase the pressure of the total feed flow rate up to a given value. The maximum feed pressure can be in the range from 70 to 85 bar [166]. Therefore, the energy demand can be very high and, to reduce it, energy recovery devices (ERD) are typically used to transfer a part of the pressure of the outlet brine to the inlet feed.
The ERD device has a given efficiency (taken equal to 98%), thus only a part of the total pressure change experienced by the brine (from the outlet brine pressure to ambient pressure) is transferred to the feed. The feed is pressurised in the ERD up to a certain pressure $P_{ERD,out}$ and the remaining pressure change from $P_{ERD,out}$ to P_{feed} is carried out in a booster pump.
Together with the energy consumption of the booster pump, the consumption of the high pressure pump has to be included but, with the ERD, the high pressure pump does not pressurise the total feed flow rate, but only the difference between the feed and the brine flow rates, i.e. the permeate flow rate [136]. In this way, the total energy consumption of the RO with ERD is lower than the one with RO only.

Concerning the crystallizer, electricity is required to pump the feed into the crystallizer and to overcome the pressure drops, mostly due to the nozzles. This term is relatively low, because the pressure drops have been estimated as approximately 0.5 bar per crystallizer. Concerning the filters, the electricity consumption is calculated with reference to an industrial-scale disc and drum filter with a nominal flow rate of 300 l/h, which works discontinuously for 3 hours per day and has a consumption of 4 kW. Switching to the continuous mode, I estimated a consumption of 1.7 kWh/m^3 of inlet solution.

The MED as well as the MD unit mostly make use of thermal energy for evaporation. However, they have also electricity demand to pump the solutions from one stage or module to the other. In the MED unit, I assume constant electricity consumption equal to 1.5 kWh_{el}/m^3 of distillate. Conversely, in the MD unit, I calculate the electricity required by each pump located between two adjacent modules. The pumps are used to compensate the pressure drops of the previous modules and to restore the inlet feed pressure for the following modules.

3.2.2 Heat demand

The two treatment processes requiring thermal energy are MED and MD. The specific thermal consumption of MD is typically higher than the one of MED. Typical values of

thermal consumption of MD range between 600 and 900 kWh/m^3 of distillate, while the thermal consumption of MED can be as low as 60 kWh/m^3 of distillate [163].

The thermal consumption of MED is calculated by multiplying the external steam flow rate by the latent heat at the steam temperature. The steam supplied to the first effect is the only external source of thermal energy. In fact, in the following effects, the heating steam is the one produced in the previous adjacent effect. Therefore, the higher the number of effects, the lower is the demand of external thermal energy. For many applications, the MED unit is coupled with a thermo-vapour compressor (TVC), which allows for recycling part of the vapour generated in one intermediate or in the last effect and for reusing it as a part of the heating steam in the first effect. By including the TVC, it is possible to reduce the amount of steam to supply from an external source and, generally speaking, also the thermal energy demand. However, it has to be mentioned that the steam required in the TVC has to be supplied at relatively higher pressures.

For what concerns the MD unit, the thermal consumption is given by the heat required to increase the temperature of the feed from the intake to the given inlet temperature (typically 80°C) plus the heat required in the intermediate heaters to restore the inlet temperature before each module in series. Since the recovery of single MD modules is thermodynamically low, many modules are typically arranged in series and the thermal requirement of the intermediate heaters covers a significant share of the total. In order to reduce the need for external thermal energy, recovery heat exchangers are used to perform heat integration between the outlet streams. The degree of integration depends on the given minimum temperature difference between the streams in the heat exchanger: lower temperature differences correspond to higher degrees of integration and lower external heat demands.

4. Papers

The research activities performed within this thesis aim at filling some gaps in the literature relevant to the treatment and recycling of industrial wastewater effluents. In particular, for many industrial sectors, previous studies investigated wastewater treatment strategies, but in most cases these aimed at purifying the water before discharge rather than recovering and recycling valuable materials. Also, the majority of the works proposed lab-scale treatment units that were very specific to the industrial application and did not present an economic analysis of a full-scale treatment plant. Thus, a more comprehensive approach to develop and analyse integrated treatment processes at the full-scale and to assess their economic feasibility was still missing.

To fill this gap, the main research questions of my thesis concern (i) the selection of suitable treatment processes and relevant operating conditions; (ii) the way in which the processes should be combined to develop economically feasible integrated chains and (iii) the estimation of the energy demands of such chains and the possibility to couple them with cleaner energy supply systems. These research questions can be applied to any industrial sector producing highly-concentrated brines. During the thesis, I focused on two industrial effluents: the spent regenerant solution produced during the regeneration of Ion Exchange Resins employed for water softening and the neutral highly-concentrated coal mine effluent produced in Poland.

The main findings of this doctoral thesis have been collected in five papers and Table 25 shows how these belong to the research questions and the objectives of the thesis.

In order to answer the research questions, I developed a novel method able to model, simulate and compare integrated treatment processes for industrial wastewater effluents. Therefore, this approach allows for implementing a circular economy approach and assessing various treatment strategies, given by the combination of different processes to remove the pollutants and recover raw materials.

As already shown in Figure 2, the methodological approach presents different inter-linked steps. The papers correspond to the main steps that I have gone through in the process of development and implementation of integrated treatment processes for industrial wastewater effluents.

Table 25. Summary of the papers corresponding to the research questions and the objectives of this thesis.

		Papers				
Research questions	**Objectives**	**1**	**2**	**3**	**4**	**5**
1. Which treatment processes can be used to purify industrial wastewater effluents and to recover raw materials?	1.1 Development of techno-economic models	■	■			
	1.2 Simulation with real inputs	■	■	■	■	■
	1.3 Sensitivity analyses	■		■	■	
2. How the treatment processes should be interconnected in integrated systems to be economically feasible?	2.1 Model integration in the simulation platform				■	■
	2.2 Construction of treatment chains			■	■	■
	2.3 Definition of assessment criteria	■		■	■	■
3. How high is the energy demand of the treatment chains and which energy supply systems can be used to make the chain more environmentally friendly and economically feasible?	3.1 Calculation of energy demands			■	■	■
	3.2 Inclusion of different energy supply systems	■			■	
	3.3 Estimation of costs and environmental impact	■		■	■	■

The development and validation of techno-economic models for the five investigated treatment processes are the starting point for the development of any treatment chain. This phase produced a library of reliable, flexible and widely usable tools. The implementation step is closely connected to the identification of the most suitable inputs and parameters of the technical models, which correspond to the optimal operating conditions of the process.

I have dedicated much effort to implementing novel fully-integrated, detailed techno-economic models; to calibrating and validating these models and to performing sensitivity analysis by varying a wide set of inputs and parameters. The main results of these activities are collected in the first three papers, which are more focused on single processes.

The first (Paper 1, section 4.1) concerns the techno-economic assessment of multi-effect distillation employed for the treatment of the effluent of ion exchange resins' regeneration process. The paper describes in detail the techno-economic model of MED used for the simulations, compares the performances of different plant configurations and shows the optimum number of effects in the various configurations and with different thermal energy costs.

The second paper (Paper 2, section 4.2) presents the characterisation of nanofiltration membranes in presence of the wastewater produced by the regeneration of ion exchange resins. The characterisation is performed via a joint experimental and simulation campaign, devised to find four membrane parameters useful to simulate the NF membrane through the Donnan Steric Pore Model with Dielectric Exclusion (DSPM-DE). Thus, this paper deals with the calibration of the NF model in presence of a multi-component solution. Also, it shows the main transport and exclusion mechanisms in the NF membranes.

The third paper (Paper 3, section 4.3) includes both the investigation of the techno-economic performances of a single unit (NF) and the economic analysis of an integrated treatment chain. Firstly, I investigated how the NF membrane rejection and the NF unit costs are influenced by the operating conditions. Secondly, I assessed the impact of NF recovery on the economic feasibility of an integrated system composed of NF, crystallizer and MED.

These first three papers constitute fundamental preliminary steps to the development and comparison of integrated treatment systems. These last research activities constitute the core of the doctoral thesis and the relevant results are presented for the two effluents mentioned above in the fourth and the fifth paper.
Paper 4 (section 4.4) shows different combinations of pre-treatment and concentration technologies, devised to treat the effluent of the regeneration of ion exchange resins. I compared the treatment chains from the technical, economic and environmental point of view via the definition of a set of global outputs. Moreover, I considered two scenarios characterised by different energy supply systems, to reduce the CO_2 emissions of the chains by including self-generated renewable energy.
Finally, the last paper (Paper 5, section 4.5) presents and compares five treatment chains devised to treat a highly-concentrated coal mine effluent. The chains are given by different combinations of pre-treatment and concentration units and they allow for recovering minerals and producing salt and water. The integrated systems are compared by estimating technical and economic global outputs.

Overall, each paper corresponds to a fundamental phase of the methodological approach devised and applied in this doctoral thesis. The results of the first papers constitute the basis of the final and more comprehensive papers, where the integrated systems include the already optimised units (i.e. with the inputs and the operating conditions that were found to improve the performances and/or minimise the costs). These papers make reference to specific case studies; however, the models are very flexible and applicable to very diverse effluents.
The following paragraphs introduce the five works. The whole papers are attached to the appendix.

4.1 Paper 1 - Techno-economic Assessment of Multi-Effect Distillation Process for the Treatment and Recycling of Ion Exchange Resin Spent Brines

This paper, published in Desalination in 2019, presents a detailed techno-economic analysis of the MED plant, when applied to treat and concentrate the effluent of the regeneration of ion exchange resins. In particular, the MED is used to increase the concentration of the pre-treated effluent, to enable its reuse as regenerant solution in the following regeneration cycles. This novel application of the MED makes necessary to define novel representative outputs, useful to find the most economically feasible configurations of the MED plant. Therefore, this paper introduces the Levelised Brine Cost (LBC) that is the selling price that the concentrate brine produced by the MED should have to break-even. This parameter is used to compare different systems and to assess their economic feasibility. In fact, the plant is considered economically feasible if its LBC is found to be lower than the current cost of the fresh regenerant solution. I analysed plain-MED and MED coupled with thermo-vapour compressor (MED-TVC) and I considered two thermal energy sources: a co-generation system and waste heat available in the industrial site. Also, I focused on the impact of the number of effects on the capital and operating costs and on the total LBC of the different configurations. In fact, higher numbers of effects correspond to higher thermal efficiencies but also to higher areas of the evaporators. Therefore, the increase of the number of effects leads to an increase of the capital costs and a decrease of the operating costs. The minimum in the total LBC trend corresponds to the optimal configuration at given operating conditions.
This work includes both a detailed theoretical description of the MED model and an application to a real case study. In the context of the real case study, the number of effects corresponding to the minimum LBC was reported at different thermal energy costs for the plain-MED and the MED-TVC. Also, I found the threshold value of thermal energy cost for the different configurations and different steam pressures, i.e. the value below which the optimised MED plant is economically feasible. I found a wide range of feasible thermal energy costs, for which the LBC relevant to the MED plant was lower than the current cost of the regenerant solution. Therefore, the MED plant turned out to be a very promising technology for the concentration of the spent regenerant solution.
Overall, this work gives important insights into the performances of the MED technology in a wide range of operating conditions and economic inputs and for an application different than desalination. The results show the most promising configurations to be used in the treatment chain and are included in the following papers to develop the treatment chains.

M. Micari, M. Moser, A. Cipollina, B. Fuchs, B. Ortega-Delgado, A. Tamburini, and G. Micale. 2019. Techno-economic assessment of multi-effect distillation process for the treatment and recycling of ion exchange resin spent brines. ***Desalination*** *456:38-52.*

Authors' contribution
I implemented the techno-economic model for the MED in Python, I devised and performed the simulations, I collected and analysed the data and wrote the paper. **M.Mo.**: Supervision, Funding acquisition. **A.C.**: Conceptualization, Supervision. **B.F.**: Software. **B.O.D.**: Validation. **A.T.**: Writing – Review and Editing. **G.M.**: Supervision, Funding acquisition.

4.2 Paper 2 - Experimental and Theoretical Characterization of Commercial Nanofiltration Membranes for the Treatment of Ion Exchange Spent Brine

This work presents a joint experimental and simulation campaign devised to characterise NF membranes in presence of the effluent produced by the regeneration of ion exchange resins employed for water softening. The characterisation consists in the estimation of four membrane parameters that are used to simulate the NF membranes through the Donnan Steric Pore Model with Dielectric Exclusion (DSPM-DE). The four parameters are pore radius, active layer membrane thickness, dielectric constant within the pores and membrane charge density. Experiments were conducted on two NF membranes and in presence of pure water, solutions of organic compounds and artificial multi-component solutions simulating the real effluent. Then, I performed a least square fitting of the model to the experimental results to find the four membrane parameters. The so-calibrated model was able to simulate reliably the behaviour of NF membranes in presence of the investigated effluent. Also, it allowed for identifying the main transport and exclusion mechanisms of NF membranes.
This work is very important in the framework of the multi-step method proposed in the thesis, because the characterisation allowed for defining the parameters of the NF model suitable to a specific industrial application. In fact, the membrane properties strictly depend on the fed solution and on the species that it contains. Therefore, the experimental and simulation campaign acquires a central role, since the obtained membrane properties can be used to simulate the NF membrane and to design the NF plant taking into account the specific effluent. In addition, the simulation of the NF unit with the estimated membrane properties gave insights into the transfer mechanisms within the membrane and into the exclusion mechanisms at the feed-membrane interface. This analysis allowed for correlating the membrane properties to the trans-membrane fluxes and exclusion mechanisms and for explaining the experimental rejections measured at different feed concentrations. In this context, the pore dielectric constant had the highest impact on the ionic rejections, whereas the membrane charge density did not affect the membrane performances significantly at the investigated concentrations. In fact, the most significant exclusion mechanism was the dielectric exclusion. Concerning the membrane fluxes, the highest term was always the diffusive flux. The knowledge of the exclusion and transfer mechanisms can have also practical applications, since it can indicate the directions to undertake for possible future membrane improvements.

M. Micari, D. Diamantidou, B. Heijman, M. Moser, A. Haidari, H. Spanjers, V. Bertsch. 2020. Experimental and Theoretical Characterization of Commercial Nanofiltration Membranes for the Treatment of Ion Exchange Spent Brine. ***Journal of Membrane Science****. 606. 118117*

Authors' contribution

I proposed and led this work: I planned and supervised the experimental campaign, I performed the simulations and the fitting, I analysed the results of the model and wrote the paper. **D.D.**: Validation, Investigation. **B.H.**: Supervision, Resources. **M.Mo.**: Funding acquisition. **A.H.**: Resources. **H.S.**: Funding acquisition, Writing – Review and Editing. **V.B.**: Supervision, Writing – Review and Editing.

4.3 Paper 3 - Combined Membrane and Thermal Desalination Processes for the Treatment of Ion Exchange Resins Spent Brine

This paper, published in Applied Energy in 2019, presents the first techno-economic analysis of an integrated treatment system composed by membrane and thermal processes and devised for the effluent of the regeneration of ion exchange resins. However, the main focus of this paper is the NF unit and the impact of the operating conditions of the NF plant on the integrated system. Firstly, the techno-economic model of the NF process used in this doctoral thesis was presented. Secondly, the results of sensitivity analyses performed on the NF model were reported to find the most suitable operating conditions of the NF plant within the integrated system. In this context, from the technical point of view, I investigated how much the ionic rejection was influenced by the total recovery of the NF plant, with given membrane properties. Also, the role of the feed pressure on the ionic rejections and on the annualised cost was assessed, with a given recovery of the NF plant. These first findings allowed for identifying the set of feed pressures to use at the different plant recovery values. Finally, I analysed the whole treatment chain composed by NF, crystallizer and MED from the energetic and the economic point of view. These analyses were performed at three values of NF plant recovery (25, 50 and 65%), in order to evaluate the impact of the NF recovery on the costs and energy consumption of each process in the chain.
This paper applied for the first time a comprehensive definition of levelised brine cost (LBC), including the terms of cost and revenue relevant to each process in the chain. The economic feasibility of the whole chain was then assessed by comparing the LBC with the current cost of the fresh regenerant solution. Moreover, the LBC values of the chains with different NF recovery were compared to find the most economically advantageous chain configuration. This analysis showed the weights of the different terms of cost of the integrated system: the operating costs due to the alkaline reactant used in the crystallizer were found to cover the highest share of the total costs. However, the revenues due to the production of magnesium and calcium hydroxide turned out to be high enough to offset the expenses of the reactant. Generally speaking, the three chains (with the three NF recovery values) had a total LBC lower than the current cost of the regenerant solution and the most economically feasible system was the one with the lowest NF recovery, i.e. 25%.
This work represents the first analysis of an integrated treatment chain composed of pre-treatment and concentration steps and shows the energetic and economic contributions of each process to the global outputs of the chain.

M. Micari, A. Cipollina, A. Tamburini, M. Moser, V. Bertsch, and G. Micale. 2019. Combined membrane and thermal desalination processes for the treatment of ion exchange resins spent brine. ***Applied Energy*** *254.*

Authors' contribution
I am the lead author of the paper. My role was to implement the techno-economic models, develop the mass balances to connect the units in the treatment chain, design and perform the simulations, analyse the data and write the paper. **A.C.**: Conceptualization, Supervision. **A.T.**: Supervision, Writing – Review and Editing. **M.Mo.**: Supervision, Funding acquisition. **V.B.**: Supervision, Writing – Review and Editing. **G.M.**: Supervision, Funding acquisition.

4.4 Paper 4 - Towards the Implementation of Circular Economy in the Water Softening Industry: A Technical, Economic and Environmental Analysis

This paper represents the comprehensive outcome of the methodological approach developed in the thesis, when applied to the case study about the treatment of the effluent produced by the regeneration of ion exchange resins.
I analysed treatment chains composed of NF, crystallizer and three different concentration technologies: MED, MD and the combination of RO and MD. Furthermore, I considered two electricity supply systems, i.e. grid supply and a mixed photovoltaic-battery-grid system. For the comparison, I used the global technical, economic and environmental outputs defined in section 2.4. The final objective of those analyses consisted in finding suitable strategies to implement circular economy in the water softening industry, by including an economically feasible and environmentally-friendly treatment chain able to recycle the effluent as regenerant solution. The global energy demands, total LBC and CO_2 emissions of the three chains were compared in a wide range of feed flow rates and with electricity supplied from the grid. I found that the chain with RO-MD was more economically convenient at lower feed flow rates, whereas the one with MED was more feasible at higher feed flow rates. The chain with MD reported always the highest LBC, because of the high thermal consumption. Thus, I considered only the chains with RO-MD and with MED in the analyses with the mixed renewable energy supply system. In this case, it was possible to increase significantly the electricity self-sufficiency (i.e. the share of electricity supplied by the PV-battery system) while the LBC was still lower than the current cost of the regenerant solution. The comparison between the CO_2 emissions per unit of regenerant solution recovered and the ones per unit of fresh solution currently produced showed that a 75% reduction of the emissions can be achieved, with economically competitive RO-MD and MED chains.
This work constitutes the final step of the proposed methodological approach applied to a specific case study. This modular approach resulted to be a powerful tool for the development and comparison of different treatment chains, also when these are coupled with different energy supply systems. The global results gave insights into the economic and environmental impact of the chains and can be used as the basis for decision tools to implement circular economy models in the industrial sector.

M. Micari, M. Moser, A. Cipollina, A. Tamburini, G. Micale, and V. Bertsch. 2020. Towards the Implementation of Circular Economy in the Water Softening Industry: A Technical, Economic and Environmental Analysis. ***Journal of Cleaner Production****. Article number 12029.*

Authors' contribution
I am the lead author of the paper. I developed the tools and integrated them into the simulation platform; I calculated the electricity cost with the different supply systems, performed the simulations, analysed the data and wrote the paper. **M.Mo.**: Software, Funding acquisition. **A.C.**: Methodology, Supervision. **A.T.**: Supervision, Writing – Review and Editing. **G.M.**: Supervision, Funding acquisition, **V.B.**: Supervision, Writing – Review and Editing.

4.5 Paper 5 - Techno-economic Analysis of Integrated Treatment Chains for the Valorisation of Coal Mine Effluents

This paper presents the results of the methodological approach devised in this thesis, if applied to the case study of the neutral effluent produced by coal mines in Poland. In this work, I developed and compared five treatment chains composed of pre-treatment and concentration processes. The chains present NF units, crystallizers to recover the minerals and concentration technologies coupled with an end crystallizer to produce pure water and sodium chloride crystals. In these analyses, the main product of the chain is sodium chloride. Therefore, I used a different global economic output, called levelised salt cost (LSC) that included the costs of the other processes and the revenues given by the by-products, i.e. water and minerals.

Firstly, each treatment chain was analysed by assessing the energy requirements of the single processes, the capital and operating costs and the revenues. Secondly, the integrated systems were compared in terms of total energy requirement, recovery of NaCl and total LSC. The recovery of NaCl is estimated as the ratio between the amount of NaCl produced in the form of crystals and the amount dissolved in the feed solution entering the treatment chain. I found that the chains with two crystallization steps were able to recover more than 95% of NaCl, since they were designed to enable the recycling of the crystallization effluents to the concentration step and to minimise the losses. Moreover, the chains presenting two NF units and MED were found to be economically competitive, since the LSC fell within the range of the market values of NaCl crystals.

This work showed that the methodological approach can be very flexible and usable with diverse effluents. Its modularity allowed for devising various chains composed by different combinations of pre-treatment and concentration technologies. Also in this case, the results gave indications about the most suitable strategies to implement circular economy in the industrial sector.

M. Micari, A. Cipollina, A. Tamburini, M. Moser, G. Micale, and V. Bertsch. 2020. Techno-economic Analysis of Integrated Treatment Chains for the Valorisation of Coal Mine Effluents. ***Journal of Cleaner Production****. 270. 122472*

Authors' contribution

I led the activities for this work: I integrated the models in the simulation platform and built the treatment chains, I performed the simulations, analysed the data and wrote the paper. **A.C.**: Methodology, Supervision. **A.T.**: Supervision, Writing – Review and Editing. **M.Mo.**: Funding acquisition. **G.M.**: Funding acquisition, **V.B.**: Supervision, Writing – Review and Editing.

5. Discussion of the results and conclusions

This doctoral thesis aims at making a contribution to the development of the industrial sector toward more sustainable solutions. The discharge of polluted industrial effluents into the environment has become a severe issue and the removal of pollutants before the release can be very energy consuming and costly. Therefore, various valorisation strategies of the waste streams have been proposed in the literature to purify the effluents and to recover raw materials. However, the literature review reported in sections 1.2 and 1.3 highlighted some literature gaps: the proposed treatment systems focus more on the purification of the effluent before discharge than on the recovery of raw materials; the processes are often tested at the lab-scale unit and the implementation at the full-scale as well as an economic feasibility assessment are not discussed yet; the treatment strategies are specific to the investigated wastewater and a general framework for various industrial effluents is missing.
With this thesis, I aim at filling these gaps by developing a novel flexible multi-step method able to build and analyse various technical strategies for the treatment of industrial effluents and to identify the most economically feasible and environmentally friendly one. This method can be applied to various industrial sectors producing highly-concentrated water solutions and its modularity allows for easily devising various combinations of treatment processes.
Each of the five paper included in the thesis constitutes an important step of the proposed methodological path and provides answers to the three main research questions of Table 1. The development of the models and the estimation of suitable sets of parameters is the main focus of the first two papers: the first deals with multi-effect distillation and the second with nanofiltration. The third paper concerns the identification of the optimal operating conditions of nanofiltration, within an integrated treatment chain. Finally, the development and comparison of various treatment chains composed by different pre-treatment or concentration units are the objectives of the fourth and the fifth paper, which deal with two different case studies.
In the following paragraphs, the methodological approach adopted are shortly described and discussed and the main results of the papers are discussed within the frameworks of the three research questions.

5.1 Methodological path

To reduce or minimise the environmental issue due to the discharge of polluted wastewaters into the environment, I developed and applied the method sketched in Figure 16. Each step of the method is strongly connected to the adjacent ones and has a strong impact on the final outcomes. Firstly, the effluent has to be identified and the concentration of each component has to be measured. Then, multiple sets of pre-treatment and concentration processes are investigated to purify the effluent and recover raw materials. During the thesis, I worked on the implementation of the techno-economic models of five treatment processes and these models are now part of a library of tools which can be easily integrated in a simulation platform. Depending on the effluent under consideration, different sets of input data are supplied to the models and different parameters can be used to simulate the optimal operating conditions. Thus, the models are interconnected in the simulation platform to reproduce the

integrated treatment chains and different combinations can be proposed and compared through the definition of global technical, economic and environmental outputs.
In this regard, global technical outputs are the total electric and thermal energy demand of the treatment chains. The global economic output is the levelised cost of the main product of the chain, i.e. the cost that the main product would have to allow the project to break-even. This value is meant to be compared with the market value of the main product, to assess the economic feasibility of the proposed system. The global environmental output is given by the CO_2 emissions due to the energy demand of the treatment processes per unit of main product produced by the chain.
The proposed approach is highly modular, since the models describing the single processes are separate tools but can be easily interconnected in the simulation platform used during the thesis. The modularity allows for devising a wide range of process combinations for the same application and for developing treatment schemes for different applications.
Moreover, the structure of the tools gives the possibility to easily perform sensitivity analysis by varying one or more parameters relevant to a single process and by assessing their impact on the global outputs of the treatment chain. In this context, it is possible to couple the treatment plant with different electric and thermal energy sources by varying the relevant parameters common to all units in the chain, and in particular the electricity and heat costs and the CO_2 emission factor. Thus, this approach allows for developing and comparing integrated treatment chains for various industrial wastewater effluents and with different energy supply systems.
Figure 16 shows also how the activities and the findings reported in the papers are located along this methodological path. Each paper constitutes an important part of a common development process and the results obtained while optimising single models are fundamental for the simulations and the comparisons of integrated systems.

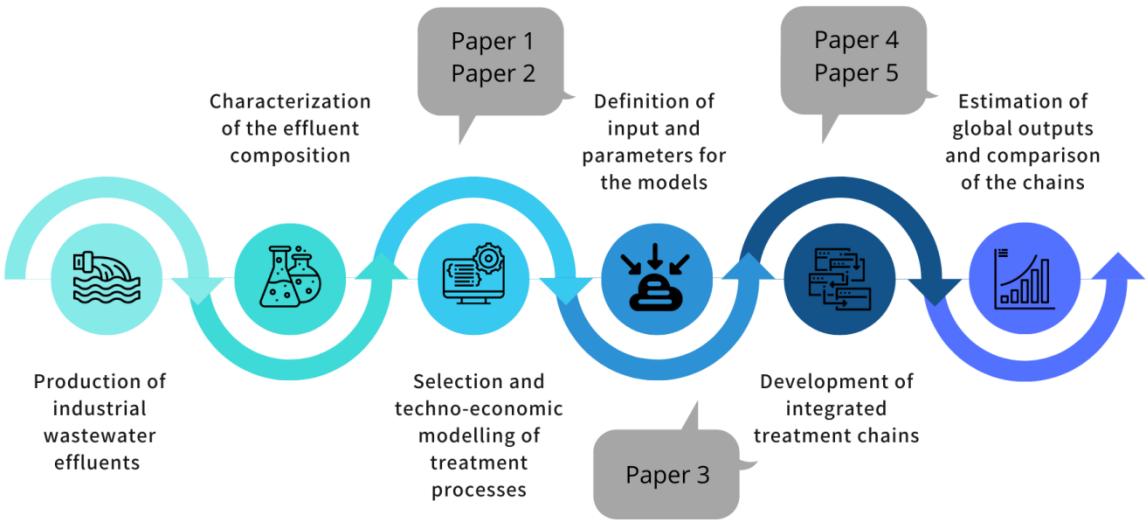

Figure 16. Schematic representation of the phases of the methodological approach when applied to a specific case study.

5.2 Research question 1

The first research question concerns the selection of the treatment processes and of their operating conditions to purify industrial wastewater effluents and to recover raw materials. In this regard, I performed the simulations and the sensitivity analyses reported in Paper 1, Paper 2 and Paper 3. Paper 1 and 3 focus on the techno-economic analysis of membrane and thermal processes when applied to novel applications, whereas Paper 2 presents an experimental and theoretical characterisation of NF membranes, aimed at calibrating the model for the application and at investigating the main transport mechanisms through the membrane.

In the first, I proposed a novel application of Multi-Effect Distillation technology in the context of the treatment of the industrial brine produced by the regeneration of ion exchange resins, employed for softening. The role of the MED plant was to concentrate the water solution up to the target concentration to reuse it in the industrial process. In this paper, I simulated the MED plant by giving as inlet feed concentration the concentration of the ion exchange spent brine after the pre-treatment in nanofiltration and crystallization units. I found that MED is a valuable option for this application, since, from the technical point of view, it allows for concentrating the NaCl-rich solution up to the target and, from the economic point of view, the levelised cost of brine was found to be in many cases competitive with the market value of the regenerant solution. When industrial waste heat at low temperature (100°C) was used as the heating steam, the MED plant was able to concentrate the solution with an optimum number of stages equal to 13 and the corresponding cost of the produced brine was 50% lower than the current cost of the regenerant solution. In addition, I assessed the sensitivity of the global cost to the thermal energy cost and for each thermal energy cost the optimum number of stages was estimated. This analysis constituted a powerful tool to assess the range of thermal energy costs for which the MED technology was economically feasible. In the range of thermal energy cost from 0 to 20 $\$/MWh_{th}$ the minimum levelised cost of brine (i.e. at the optimised number of effects) was lower than the current cost of the regenerant solution. Thus, the MED is very promising for this application and these analyses were a fundamental starting point to the research proposed in Paper 3.

Paper 3 simulates the whole treatment chain devised for this case study (spent regenerant produced by softeners), including nanofiltration, crystallization and multi-effect distillation. This paper focuses on the sensitivity analyses of the nanofiltration unit, to find the optimal operating conditions for the specific application. NF showed to be a very suitable pre-treatment unit for the present effluent, because of its ability to separate the divalent ions (in our case, Mg^{2+}, Ca^{2+} and SO_4^{2+} ions) from the monovalent ions (Na^+ and Cl^-). Also, whereas typically NF units work at very high recovery (i.e. ratio between permeate and feed flow rate) because the retentate is a waste to dispose, I found that a lower recovery was more suitable to this application. In fact, the retentate produced by the NF unit is not a waste but it is fed to the crystallizers and then, mixed with the NF permeate and sent to the concentration technology. Therefore, since a lower NF recovery allowed for working at lower pressures and with higher divalent ions rejection, this operating condition was selected for the treatment chain. Also, in this paper I introduced the definition of global levelised brine cost (LBC) that accounted for

all costs and revenues of the treatment processes in the chain. I found a global LBC of 4.9 $/m^3 for the treatment chain with a NF recovery of 25%, which demonstrated that the whole treatment chain was economically feasible since the current cost of the fresh regenerant solution is 8 $/m^3. In addition, the treatment chain was found to be feasible for all cases with feed flow rates higher than 50 m^3/h, thus the proposed system can be economically advantageous even for small-medium scale plants.

Finally, in Paper 2 I focused on the implementation and calibration of the NF model for the specific application. The NF model implemented during this thesis required some parameters (membrane pore radius, active layer membrane thickness, dielectric constant within the pore and charge density) to simulate accurately the membranes in presence of the specific water solution. Thus, experiments were performed to measure the ionic rejection of the membrane with the solution produced by the regeneration of ion exchange resins and I carried out simulations to find the parameters via least-square fitting. This study gave important insights into the transport and exclusion mechanisms of NF membranes with multi-ionic mixtures. I found that the charge density did not affect much the ionic rejection at high ionic strength, whereas the main exclusion mechanism was the dielectric exclusion, due to water confinement in the pores. These findings may be very helpful to understand the membrane behaviour with complex mixtures and to indicate directions for the development of future generations of highly-performing membranes.

Overall, these works show the results of the development, implementation and validation of techno-economic models to be included in integrated platforms simulating the treatment chains. Novel applications of the treatment processes made necessary to device novel performance parameters and to calibrate the models through ad-hoc experimental campaigns. The construction and the adaptation of the models is a fundamental step to make them suitable building blocks to simulate and compare more complex systems as the treatment chains.

5.3 Research question 2

The second research question deals with the comparison of treatment chains given by different combinations of treatment processes. The final aim is to identify the most suitable chain depending on the specific applications. Paper 4 and 5 reported various treatment chains, given by the combination of pre-treatment and concentration technologies, to treat the spent regenerant of the softeners and neutral coal mine effluents, respectively.

The findings obtained for the two case studies showed very promising results. Concerning the first case study, I compared treatment chains with the same pre-treatment step (composed by nanofiltration and crystallization) and different alternative concentration steps, i.e. multi-effect distillation, membrane distillation and the coupling of reverse osmosis and membrane distillation. The chains were devised in order to recover the hydroxides and to produce a concentrate brine reusable as regenerant solution in the regeneration process. Therefore, the main product of the chains was always the same, i.e. the recovered regenerant solution, but the energy requirements and the costs changed depending on the technologies involved.

For the economic comparison of the chains and for the assessment of the economic feasibility, I estimated the global levelised cost of the concentrate brine (LBC) for each chain and I compared these values with the current cost of the fresh solution. In this context, in a wide range of feed flow rates, electricity costs and heat costs, the chain composed by NF, crystallizers and MED as well as the one composed by NF, crystallizer, RO and MD showed a LBC lower than the current cost of the regenerant. Moreover, the most economically advantageous chain depends on the operating conditions and especially on the size of the plant. Interestingly, the chain with RO and MD had lower LBC values with smaller plant sizes (corresponding to lower feed flow rates), because the technologies are more modular and easier to handle. Conversely, the chain with MED showed lower LBC values for bigger plant sizes, because of the lower thermal energy demand of the MED technology, with respect to the MD technology.

Concerning the treatment chains proposed for the coal mine effluent in Paper 5, I developed different combinations with the aim to recover minerals, water and sodium chloride. In this case, the main product of the chains was sodium chloride, in the form of crystals to be produced in the end-crystallizer located after the main concentration technology. Therefore, the economic comparison was performed by defining a global levelised salt cost (LSC) that accounted for all terms of costs and revenues of the chain and for its salt productivity (i.e. the amount of NaCl produced). In the paper, I included five treatment chains having different pre-treatment and different concentration units. The pre-treatment steps were given by various combinations of nanofiltration and crystallization units and, consequently, produced different by-products contributing to the global economic feasibility. The concentration step was given by multi-effect distillation or the coupling of reverse osmosis and membrane distillation. In any case, an end-crystallizer was included to produce NaCl crystals from an almost saturated solution. As observed also in the first case study, the higher thermal demand of the MD unit, especially when high concentrations have to be achieved, made the corresponding chains less economically advantageous in most cases.
For a fixed feed flow rate, I found that the chains with multi-effect distillation as main concentration technology and with two nanofiltration units were economically feasible, because the LSC fell within the typical range of price of NaCl. In particular, the most feasible was the chain with two NF units, three crystallizers to produce magnesium hydroxide, calcium sulphate and calcium carbonate, multi-effect distillation and NaCl crystallizer: the corresponding LSC was around 90 $/ton$_{NaCl}$ that is comparable with the lower bound of the range of NaCl market value. However, the analogous chain with RO-MD in the concentration step instead of MED had a LSC slightly higher than the higher bound of the NaCl price range. Therefore, further improvements of the MD technology, which are expectable since its readiness level is much lower than the other technologies (RO and MED), may easily allow this chain to be economically feasible.

Overall, these studies showed examples of novel circular strategies designed to purify and recycle the effluents produced by various industrial sectors. Generally speaking, the application of circular economy models requires a comprehensive redesign of the industrial processes, to include the treatment steps and to recycle the purified effluent or the recovered

chemicals in the production process. In this regard, the proposed method allowed for developing various treatment options depending on the main product that had to be recycled or recovered to be sold. Moreover, the pre-treatment steps were designed with the aim to maximise the recovery of specific by-products, such as hydroxides or carbonates, which can be crucial for the economic feasibility.

5.4 Research question 3

The third research question focuses on the total electric and thermal energy demand of the treatment chains and on the different energy supply systems that may be coupled. The analysis of the energy demands of each treatment process in the chains and the assessment of the role of energy costs on total costs are central topics of all five papers. The global thermal and the electric energy demands of the treatment chains have been taken as global outputs to represent the technical performances of the chains. The selection of the energy supply systems was made by assessing the impact of the relevant energy cost and CO_2 emission factor on the global economic and environmental outputs of the chain.

In the first paper, I focused on the impact of thermal energy cost on the LBC calculated for the MED unit only, by considering two scenarios with two different energy supply systems: waste heat available in the industrial site at a certain cost and heat generated by a co-generation cycle. Within the last scenario, I considered a wide range of temperature of the heating steam (from 65 to 120°C) and I changed the specific cost of the thermal energy accordingly. MED was found to be feasible for any steam temperature lower than 80°C, whereas, for higher temperatures, the increasing operating expenditures, due to higher steam costs, affected the global expenditures more than the decreasing capital investment. However, in general, I observed that industrial waste heat, when available in the industrial site, allowed for devising more economically advantageous solutions.

In the paper about the comparison of treatment chains for the spent regenerant produced by the softening industry (Paper 4), I considered two scenarios with respect to the electricity supply. In the first, the electricity was completely taken from the grid, whereas, in the second, the electricity was partially produced by a photovoltaic power system with Li-Ion batteries in conjunction and partially taken from the grid. Within the second scenario, the installed capacity of the PV power system and the capacity of the battery were varied, to get a set of supply systems with different self-sufficiency (percent of the energy demand supplied by the PV-battery system), specific electricity cost and CO_2 emission factor (depending on the amount of electricity taken from the grid).
The economic and environmental outputs of the treatment chains in the two scenarios were calculated to find strategies that were simultaneously economically feasible and environmentally friendly. I found that the chains with MED and with RO-MD were economically feasible even when coupled with the most self-sufficient (and most expensive) supply systems, especially when the treatment plant was located in a region with higher solar potential. Moreover, I compared the CO_2 emissions due to the energy requirement of the treatment system with the ones currently given by the production of the fresh regenerant solution. The comparison of the emissions per unit of solution produced showed that the

emissions of the proposed systems were lower, even when the electricity was totally supplied by the grid. A much stronger reduction (up to 90%) was found when part of the electricity was self-generated via a photovoltaic system with battery storage.

Concerning the assessment of the energy demands, much attention was devoted to estimating the single terms of energy demand connected to the different processes in the chains. Paper 3 reported the components of the electricity demand and the MED thermal energy demand for the treatment chain composed by NF, crystallizer and MED. Furthermore, the role of electricity and heat cost of each process was highlighted in the breakdown of the operating costs of the chain. It was found that the cost relevant to the thermal energy required by the MED covered more than 30% of the total. This analysis is crucial to understand how the global system is sensitive to variations of the single units in the chain: the major impact of the thermal energy demand of MED and the relevant costs gives important directions for further improvement of the energy efficiency of the chain and reduction of the operating costs.

Furthermore, the paper about the treatment chains for coal mine effluents (Paper 5) presented a breakdown of the energy demand of each chain and, also in this case, it was found that the thermal energy demand of the main concentration technology (MD or MED) was significantly higher than any other term. However, sensitivity analyses performed by varying the specific cost of heat or electricity showed that the chains were similarly sensitive to the two costs variation and in one case, with three NF units operating at high pressure, the global LSC was slightly more sensitive to electricity cost variation than to heat cost variation.

Overall, the analysis of the thermal and electric energy demand of the treatment chains gave information about the prominent and most influencing term among the demands of the single processes. Then, the coupling of the treatment chains with different energy supply systems, realised by giving suitable inputs as energy cost and CO_2 emission factor, allowed for investigating more comprehensive systems. In this way, I proposed and analysed novel sustainable and feasible strategies, where electricity was self-produced by ad hoc built PV-battery systems or heat was recycled within the industrial park.

5.5 Limitations

The work performed within this doctoral thesis has some limitations that can be taken as starting points for future research. Firstly, I analysed the environmental impact of the proposed treatment processes by looking only at the operational CO_2 emissions connected to the energy demand of the technologies. However, it has to be said that the environmental impact includes many other aspects and the CO_2 emissions are also given by the manufacturing phase of the components of the processes. Therefore, to have an overview of the environmental impact of a process, it would be necessary to perform a Life Cycle Assessment analysis that requires the availability of significant amount of data, often very site-specific. This was beyond the scope of the doctoral thesis, but should be taken into account for further analyses.

Another limitation concerns the assumption of stationary operating conditions of the industrial plants. I considered constant feed flow rate of the treatment plant, thus a constant energy demand and plant productivity. The treatment plant operational flexibility would depend on the operation of the industrial plant producing the effluent and its consideration would also be helpful to select the most suitable processes, since they may handle process parameters changes in different ways.

5.6 Conclusions and future outlooks

Within the framework of this doctoral thesis, I developed a novel multi-step method to simulate and compare integrated treatment processes to purify wastewater effluents and to recover valuable raw materials. The works performed during the PhD showed the results of the application of the method to two industrial effluents: spent regenerant solution produced by the water softening industry and neutral coal mine effluents. The economic feasibility, energy consumption and environmental impact of the proposed chains were assessed and used to select the most suitable ones. In this way, it was possible to identify promising strategies to implement a circular economy approach in those industrial sectors.

Novel circular schemes were found to be beneficial from both the economic and the environmental perspective. Concerning the environmental impact, the introduction of treatment processes would allow for minimising the discharge of polluted effluent into the natural environment. In addition, the recovery of solutions or chemicals to be reused in the industrial process would reduce the need for fresh ones and, consequently, the demand for raw materials to produce them. Furthermore, in the first investigated case study, the treatment processes required to restore and recycle the water solution were found to have lower CO_2 emissions than the processes currently used to produce the fresh solution. Thus, a global net reduction of the environmental impact can be achieved, by minimising the pollution, the emissions and the consumption of raw materials. At the same time, such treatment schemes turned out to be economically feasible, since the levelised cost of the main product was lower or comparable with its current market value.

The method proposed in this thesis can be employed as a decision support tool by the industries to reduce the costs connected to the wastewater treatment and to reduce the requirements for fresh raw materials. For this reason, such a tool would be of crucial importance to limit the environmental pollution of the industrial sector, by minimising the discharge of the effluents into the environment and by reducing the emissions due to the production of fresh raw materials.

Concluding, the results reported in this thesis show the capability of the proposed method to develop and compare treatment schemes in different industrial sectors. The possibility to easily integrate and interconnect the tools corresponding to the techno-economic models of the treatment processes allows for applying the method to many case studies. Thus, the main outcome of this thesis concerns the development of a general framework including various techno-economic tools relevant to different treatment processes, able to simulate and analyse circular strategies to improve the sustainability of the industrial processes.

Future research activities should concern the investigation of case studies relevant to other industrial sectors producing highly-concentrated water solutions that are currently disposed

into the natural environment. Also, many industries produce wastewater solutions polluted by organic compounds and the library of available techno-economic tools may be extended in the future to include other pre-treatment processes for organics removal. Finally, a further development of the method may provide the building of a multi-objective optimisation algorithm able to select the most suitable treatment chain and operating conditions of each process for a given industrial effluent.

6. Acknowledgements

First of all, I would like to thank Professor Bertsch, whose support and suggestions have been very important for me in these years. Together with him, I have to deeply thank Professor Micale and Professor Cipollina, who have been always available and helpful whenever I needed. I would like to thank Massimo Moser for his supervision and daily support and Ben Fuchs that introduced me into the world of programming. I am also very thankful to Alessandro Tamburini, whose help and dedication in the phase of the revision and the submission of the papers are always precious. I cordially thank Professor Nieken for his availability and his support.

I want to thank all my colleagues at DLR for having supported in various forms my research activities and, in particular, I am thankful to Patrick Jochem, Thomas Pregger, Christoph Schillings and Tobias Naegler.

I would like to thank Dionysia Diamantidou for her commitment and her precious work in our nanofiltration project, Bartolome' Ortega-Delgado for his help in the development of the MED model and Francesco Giacalone for the great collaboration in the works about the RED closed loop. It has been very valuable to discuss and work with you during these years.

Now, a huge thank to all the colleagues and the PhD students that have been close friends since the beginning. I am very happy to have had the possibility to share my time at DLR with you!
Thank you, Hedda, Manuel, Tobias and Kai for your sincere friendship, for all the fun and the laughs together and for the support that you have given me in many ways. Thank you, Ben, Felix, Martin, Kien, Niklas, Mengzhu, Judith, Evelyn, Farzad, Andy and Shima. You made my years in Stuttgart very enjoyable, we had interesting and stimulating discussions and a lot of fun together.

I would like to thank also all the friends in Palermo that I am very grateful to find every time I go back to Italy. Among them, a great thank to my closest friends and my best-man and bridesmaid, Giovanni and Chiara. Also, I am very happy to thank my PhD colleagues and friends from Palermo and in particular Ninni, Rosa and Andrea.

Finally, my family! Grazie ai miei genitori, che mi hanno sempre supportato e consigliato in tutte le mie decisioni, in modi diversi ma sempre con attenzione e amore; alla mia cara sorella, per essermi sempre vicina pur stando lontane; a mia nonna Ghega, le cui amorevoli cure e lunghe telefonate rallegrano le mie giornate; ai miei zii e ai miei cugini, che mi fanno sempre sentire a casa, a maggior ragione adesso che le nostre case sono una di fronte all'altra. Grazie ai miei suoceri, che sono una parte importante della mia famiglia e a Sergio e Virginia, che sono fantastici cognati. Last but not least, grazie per tutto a mio marito Gioele, con cui adesso non vedo l'ora di cominciare un nuovo meraviglioso capitolo di vita insieme, sempre insieme!

7. Nomenclature

$f_{CO2,emission}$	CO_2 emission factor [kg_{CO2}/kWh]
C	Concentration
$C_{battery}$	Capacity of the battery [h]
$Cost_{El}$	Electricity cost [$/kWh]
$Cost_{Heat}$	Thermal energy cost [$/kWh]
Cryst	Crystallizer
P	Power [kW]
Q	Flow rate [m^3/h]

Acronyms

AMD	Acid Mine Drainage
CAPEX	Capital Expenditure [$/y]
CE	Circular Economy
COD	Chemical Oxygen Demand
TOC	Total Organic Carbon
DCMD	Direct Contact Membrane Distillation
DSPM-DE	Donnan Steric Pore Model with Dielectric Exclusion
DHI	diffuse horizontal irradiance
GHI	global horizontal irradiance
IEX	Ion Exchange resins
LBC	Levelised Brine Cost
LBC_{CAP}	Capital Levelised Brine Cost
LBC_{OP}	Operating Levelised Brine Cost
LCOE	Levelised Cost of Electricity
LSC	Levelised Salt Cost [$/$ton_{NaCl}$]
MD	Membrane distillation
MED	Multi-effect distillation
NF	Nanofiltration
NOM	Natural Organic Matter
NPV	Net Present Value
OPEX	Operating Expenditure [$/y]
PV	Photovoltaic
RCE	Remote Component Environment
RO	Reverse osmosis
SD	Sustainable Development
SWRO	Seawater Reverse Osmosis
VMD	Vacuum-enhanced Membrane Distillation
UV	Ultraviolet
ZLD	Zero Liquid Discharge

Nanofiltration

A	temperature correction factor for the activity coefficient [-]
$A_{membr,elem}$	membrane area of a single NF element [m^2]
C	concentration [mol/m^3]
C_{civil}	cost for the building [$]
C_{mech}	costs for pumps, filters and piping system [$]
$C_{electro}$	cost for energy supply systems [$]

$C_{membrane}$	cost for membranes [$]
$D_{i,pore}$	diffusion coefficient of the ion within the pore [m^2/s]
D_H	hydraulic diameter of the feed channel [m]
$D_{i,\infty}$	diffusion coefficient of the ion in the bulk [m^2/s]
e_0	electronic charge [1.602 x 10^{-19} C]
f	friction factor [-]
F	Faraday constant [9.64867 x 10^4 C/mol]
h_f	height of the NF feed channel [m]
I	ionic strength [mol/l]
j	trans-membrane flux [mol/(m^2s)]
J_v	permeate flux [m/s]
$k^{bulk}_{c,i}$	mass transfer coefficient in the bulk [m/s]
$k'^{bulk}_{c,i}$	corrected mass transfer coefficient in the bulk [m/s]
k_B	Boltzmann constant [1.38066 x 10^{-23} J/K]
$k_{i,c}$	hindered convective mass transfer coefficient [-]
$k_{i,d}$	hindered diffusive mass transfer coefficient [-]
l	length of the discretisation interval [m]
L_{mix}	mixing length of the spacer [m]
Lp	water permeability [LMH/bar]
M_b	inlet feed flow rate in the discretisation element [m^3/s]
M_{feed}	feed flow rate of the NF plant [m^3/h]
M_p	permeate flow rate [m^3/s]
M_{ret}	retentate flow rate [m^3/s]
N	number of discretisation elements within the membrane [-]
N_A	Avogadro number [6.023 x 10^{23} mol^{-1}]
$n_{discr,L}$	number of discretisation intervals along the NF element length [-]
n_{vessel}	number of vessels (30 m^2-area) for economic calculation [-]
$N_{vess,parall}$	number of vessels in parallel [-]
P	pressure [Pa]
Pe	Peclet number [-]
P_{feed}	feed pressure [bar]
R	ideal gas constant [8.314 J/(K mol)]
Re	Reynolds number [-]
r_i	ion radius [nm]
R_i	ionic rejection [-]
r_{pore}	pore radius [nm]
Sc	Schmidt number [-]
T	Temperature [K]
u_f	feed velocity [m/s]
x	direction of the feed flow [m]
X_D	charge density [mol/m^3]
y	direction across the membrane from the feed to the permeate side [m]
z_i	valence of the ion [-]

Greek symbol

γ	activity coefficient [-]
δ_m	active layer membrane thickness [µm]
ΔP	net pressure difference [Pa]
ΔP_{losses}	pressure losses along the element [bar]
$\Delta\Pi$	osmotic pressure difference [Pa]

$\Delta\psi_{D,feed}$	Donnan potential difference at the feed-membrane interface [V]
$\Delta\psi_{D,perm}$	Donnan potential difference at the permeate-membrane interface [V]
ΔW	Born solvation energy barrier [J]
ε	medium permittivity [F/m]
ε_0	vacuum permittivity [8.854 x 10^{-12} F/m]
ε_b	dielectric constant in the bulk [-]
ε_{pore}	pore dielectric constant [-]
η	solution viscosity [Pa s]
η_{mix}	mixing efficiency of the spacer [-]
λ_i	ratio between the ion Stokes radius and the pore radius [-]
ξ	electric potential gradient at the bulk-membrane interface [V/m]
Ξ	correction factor for the mass transfer coefficient [-]
ρ_f	feed density [kg/m^3]
Φ_i	steric coefficient [-]
Φ_B	Born solvation contribution for partitioning [-]
ψ	potential [V]

Subscripts

calc	calculated
exp	experimental
i	ion
j	index for the discretisation along the NF membrane thickness
lim	limit
w	interface

Superscripts

b	bulk
bm	bulk-membrane interface
f	feed
m	membrane
p	permeate
ret	retentate

Crystallizer

A_{filter}	filter area [m^2]
B	birth rate [m^{-4} s^{-1}]
C	concentration [ppm]
$C_{p,0}$	purchase cost of equipment [$]
D	death rate [m^{-4} s^{-1}]
G	growth rate [m/s]
J	nucleation rate [m^{-3} s^{-1}]
k	moment order
L	particle length [m]
L_i	abscissas [m]
M	mass flow rate [kg/s]
m_k	k^{th} moment of number density function [m^{k-3}]
M_T	mass of precipitated crystals [g]

n	number density function [m^{-4}]
n_{stoich}	stoichiometric coefficient
N_q	number of quadratures
Q^{mol}	molar flow rate [mol/s]
t	time [s]
V_{cryst}	crystallizer volume [m^3]
w_i	weights [m^{-3}]

Superscripts

effl	effluent
feed	inlet feed solution
alk	alkaline solution

Multi-Effect Distillation

A	heat exchanger area [m^2]
C_p	specific heat [kJ/(kg °C)]
C_p^0	purchased cost of equipment [US$]
F_{BM}	bare module factor [-]
h	specific enthalpy [kJ/kg]
i	effect index
M	mass flow rate [kg/s]
N	number of effects [-]
T	temperature [°C]
T_c	condensation temperature of the vapour in the following effect [°C]
T'_c	temperature of the vapour after crossing the connecting lines [°C]
T_{preh}	maximum feed temperature reached in the preheater [°C]
T_{vsat}	temperature of the saturated vapour [°C]
T'_{vsat}	temperature of the vapour after crossing the demister [°C]
X	salinity [ppm]
P	pressure [bar]
U	overall heat transfer coefficient [kW/(m^2 °C)]

Greek symbols

λ	latent heat [kJ/kg]
ΔT	temperature difference [°C]
α_{cond}	fraction of vapour condensed in the preheater

Subscripts

b	brine solution generated in the generic effect
brine	outlet brine
c	condensed pure water collected in the flash box
cond	end-condenser
cw	cooling water

d	vapour generated via evaporation
dist	outlet distillate
dist,real	fixed distillate flow rate to be produced
fb	vapour generated in the flash box
feed	feed entering into the first effect
f,brine	vapour generated via the brine flash
HX	heat exchanger
liq	pure water in the liquid state
n	last effect index
preh	preheater
s	total external steam
sw	salt water solution
vap	total vapour generated in the generic effect
vap	pure water in the vapour state

Acronyms

BPE	Boiling Point Elevation [°C]
CHP	Combined heat and power
DTML	Temperature logarithmic mean
GOR	Gain Output Ratio
FF	Forward Feed
TVC	Thermo-vapour compressor

Reverse Osmosis

A_{membr}	pure water permeability in the membrane [kg/(s m2 bar)]
B_{membr}	solute permeability in the membrane [kg/(s m2)]
F_w	water flux [kg/(s m2)]
F_s	salt flux [kg/(s m2)]
T	operating temperature [K]
ΔP	transmembrane pressure difference [bar]
k_p	membrane constant [-]
R_i	recovery of the i-th element [-]
X	concentration [ppm]
R_{salt}	salt rejection [%]
A	membrane active area [m]
C_{membr}	membrane constant for the temperature correction factor [K]
M	flow rate [kg/s]
n_{discr}	number of discretisation intervals [-]
R_{plant}	plant recovery [%]
P_{feed}	feed pressure [bar]
PRO	electric power consumption [W]
CPF	concentration polarisation factor

Subscripts

f,w	feed side at the membrane interface
f	feed side
p	permeate side
feed	feed solution
brine	brine solution
perm	permeate solution
$perm,out_{unit}$	permeate produced by the RO unit
perm,out	permeate produced by the plant
w	water
s	salt
elem	discretisation element

Greek symbols

$\Delta\Pi$	transmembrane osmotic pressure difference [bar]
$\Delta\Phi$	relative variation of the flux with time [-]
ρ	density of the solution [kg/m3]
η_{pump}	efficiency of the high pressure pump [-]

Acronyms

TCF	temperature correction factor
MAF	membrane ageing factor

Membrane Distillation

T	temperature [K]
m	volume flow rate [m3/s]
C	concentration [ppm]
Q	heat flux [W/m2]
h	heat transfer coefficient [W/(m2 K)]
J_w	water flux [kg/(m2 s)]
ΔH_{evap}	latent heat of vaporisation of water [J/kg]
k_m	membrane thermal conductivity [W/(m K)]
k_{air}	air thermal conductivity [W/(m K)]
$k_{membr,pol}$	polymeric structure thermal conductivity [W/(m K)]
k	thermal conductivity of the solution [W/(m K)]
Nu	Nusselt number [-]
Re	Reynolds number [-]
Pr	Prandtl number [-]
D_h	hydraulic diameter of the channel [m]
v	fluid velocity in the channel [m/s]
C_p	fluid specific heat [J/(kg K)]
B_m	mass transfer coefficient [kg / (m2 s Pa)]
R	ideal gas constant (8.314 J/(K mol))
k_B	Boltzmann constant (1.38066 x 10-23 J/K)

d_{wat}	collision diameter of water vapour [m]
P_{pore}	pressure within the pores [Pa]
r_{pore}	pore radius [m]
P_{air}	air pressure inside the pores [Pa]
$D_{w,k}$	Knudsen diffusion coefficient [m2/s)]
$D_{w,m}$	molecular diffusion coefficient [m2/s]
$D_{NaCl,wat}$	diffusivity of NaCl in water [m2/s]
$k_{f,mass}$	mass transfer coefficient in the feed channel [m/s]
$N_{parallel}$	number of branches in parallel [-]
$N_{tot,modules}$	total number of modules present in the plant [-]
A_{module}	membrane area of a single module [m2]

Subscripts

m	membrane
f	feed
p	permeate
m,hot	feed membrane interface
m,cold	permeate membrane interface
bulk,hot	feed bulk
bulk,cold	permeate bulk
conv,hot	convective flux, feed side
conv,cold	convective flux, permeate side
cond,m	conductive flux, membrane
evap,m	latent heat, membrane
in	inlet in the element
out	outlet of the element

Greek symbols

δ_m	membrane thickness [m]
ε	membrane porosity [-]
ρ	solution density [kg/m3]
μ	dynamic viscosity of the fluid [kg/(m s)]
λ	molecular mean free path [m]
τ	membrane tortuosity [-]

8. Bibliography

[1] D. Prabakar, K.S. Suvetha, V.T. Manimudi, T. Mathimani, G. Kumar, E.R. Rene, A. Pugazhendhi, Pretreatment technologies for industrial effluents: Critical review on bioenergy production and environmental concerns, J Environ Manage, 218 (2018) 165-180.
[2] D.B. Žarković, Ž.N. Todorović, L.V. Rajaković, Simple and cost-effective measures for the improvement of paper mill effluent treatment – A case study, Journal of Cleaner Production, 19 (2011) 764-774.
[3] V. Masindi, G. Madzivire, M. Tekere, Reclamation of water and the synthesis of gypsum and limestone from acid mine drainage treatment process using a combination of pre-treated magnesite nanosheets, lime, and CO2 bubbling, Water Resources and Industry, 20 (2018) 1-14.
[4] G.S. Simate, S. Ndlovu, Acid mine drainage: Challenges and opportunities, Journal of Environmental Chemical Engineering, 2 (2014) 1785-1803.
[5] P. Hobbs, S.H.H. Oelofse, J. Rascher, Management of Environmental Impacts from Coal Mining in the Upper Olifants River Catchment as a Function of Age and Scale, International Journal of Water Resources Development, 24 (2008) 417-431.
[6] C.R. Holkar, A.J. Jadhav, D.V. Pinjari, N.M. Mahamuni, A.B. Pandit, A critical review on textile wastewater treatments: Possible approaches, J Environ Manage, 182 (2016) 351-366.
[7] K. Sarayu, S. Sandhya, Current technologies for biological treatment of textile wastewater--a review, Appl Biochem Biotechnol, 167 (2012) 645-661.
[8] J.F. Perez, J. Llanos, C. Saez, C. Lopez, P. Canizares, M.A. Rodrigo, Treatment of real effluents from the pharmaceutical industry: A comparison between Fenton oxidation and conductive-diamond electro-oxidation, J Environ Manage, 195 (2017) 216-223.
[9] E. Salehi, S.S. Madaeni, A.A. Shamsabadi, S. Laki, Applicability of ceramic membrane filters in pretreatment of coke-contaminated petrochemical wastewater: Economic feasibility study, Ceramics International, 40 (2014) 4805-4810.
[10] M.N.I. Siddique, M.S.A. Munaim, Z.B.A. Wahid, The combined effect of ultrasonic and microwave pre-treatment on bio-methane generation from co-digestion of petrochemical wastewater, Journal of Cleaner Production, 145 (2017) 303-309.
[11] D. Ariono, M. Purwasasmita, I.G. Wenten, Brine Effluents: Characteristics, Environmental Impacts, and Their Handling, Journal of Engineering and Technological Sciences, 48 (2016) 367-387.
[12] T. Mezher, H. Fath, Z. Abbas, A. Khaled, Techno-economic assessment and environmental impacts of desalination technologies, Desalination, 266 (2011) 263-273.
[13] R. Einav, K. Harussi, D. Perry, The footprint of the desalination processes on the environment, Desalination, 152 (2002) 141-154.
[14] D.A. Roberts, E.L. Johnston, N.A. Knott, Impacts of desalination plant discharges on the marine environment: A critical review of published studies, Water Res, 44 (2010) 5117-5128.
[15] J. Morillo, J. Usero, D. Rosado, H. El Bakouri, A. Riaza, F.-J. Bernaola, Comparative study of brine management technologies for desalination plants, Desalination, 336 (2014) 32-49.
[16] A. Giwa, V. Dufour, F. Al Marzooqi, M. Al Kaabi, S.W. Hasan, Brine management methods: Recent innovations and current status, Desalination, 407 (2017) 1-23.
[17] S.G. Lehman, M. Badruzzaman, S. Adham, D.J. Roberts, D.A. Clifford, Perchlorate and nitrate treatment by ion exchange integrated with biological brine treatment, Water Res, 42 (2008) 969-976.
[18] S. Wadley, C.J. Brouckaert, L.A.D. Baddock, C.A. Buckley, Modelling of nanofiltration applied to the recovery of salt from waste brine at a sugar decolourisation plant, J. Membr. Sci., 102 (1995) 163-175.

[19] M. Kabsch-Korbutowicz, J. Wisniewski, S. Łakomska, A. Urbanowska, Application of UF, NF and ED in natural organic matter removal from ion-exchange spent regenerant brine, Desalination, 280 (2011) 428-431.
[20] N. Mirabella, V. Castellani, S. Sala, Current options for the valorization of food manufacturing waste: a review, Journal of Cleaner Production, 65 (2014) 28-41.
[21] M.R. Kosseva, Chapter 3 Processing of Food Wastes, in, 2009, pp. 57-136.
[22] N. Dabas, K.K. Yadav, A.K. Ganguli, M. Jha, New process for conversion of hazardous industrial effluent of ceramic industry into nanostructured sodium carbonate and their application in textile industry, J Environ Manage, 240 (2019) 352-358.
[23] M. Giagnorio, A. Amelio, H. Grüttner, A. Tiraferri, Environmental impacts of detergents and benefits of their recovery in the laundering industry, Journal of Cleaner Production, 154 (2017) 593-601.
[24] G. Jaria, C.P. Silva, C.I. Ferreira, M. Otero, V. Calisto, Sludge from paper mill effluent treatment as raw material to produce carbon adsorbents: An alternative waste management strategy, J Environ Manage, 188 (2017) 203-211.
[25] R. Gueccia, S. Randazzo, D. Chillura Martino, A. Cipollina, G. Micale, Experimental investigation and modeling of diffusion dialysis for HCl recovery from waste pickling solution, J Environ Manage, 235 (2019) 202-212.
[26] Ellen MacArthur Foundation, Towards the Circular Economy-Economic and business rationale for an accelerated transition (part 1), in, 2013.
[27] B. Suárez-Eiroa, E. Fernández, G. Méndez-Martínez, D. Soto-Oñate, Operational principles of circular economy for sustainable development: Linking theory and practice, Journal of Cleaner Production, 214 (2019) 952-961.
[28] P. Ghisellini, C. Cialani, S. Ulgiati, A review on circular economy: the expected transition to a balanced interplay of environmental and economic systems, Journal of Cleaner Production, 114 (2016) 11-32.
[29] Y. Geng, J. Fu, J. Sarkis, B. Xue, Towards a national circular economy indicator system in China: an evaluation and critical analysis, Journal of Cleaner Production, 23 (2012) 216-224.
[30] V. Castellani, S. Sala, N. Mirabella, Beyond the throwaway society: A life cycle-based assessment of the environmental benefit of reuse, Integrated Environmental Assessment and Management, 11 (2015) 373-382.
[31] A. Murray, K. Skene, K. Haynes, The Circular Economy: An Interdisciplinary Exploration of the Concept and Application in a Global Context, Journal of Business Ethics, 140 (2015) 369-380.
[32] Y. Geng, B. Doberstein, Developing the circular economy in China: Challenges and opportunities for achieving 'leapfrog development', International Journal of Sustainable Development & World Ecology, 15 (2008) 231-239.
[33] K. Ramani, D. Ramanujan, W.Z. Bernstein, F. Zhao, J. Sutherland, C. Handwerker, J.-K. Choi, H. Kim, D. Thurston, Integrated Sustainable Life Cycle Design: A Review, Journal of Mechanical Design, 132 (2010).
[34] Z. Yuan, J. Bi, Y. Moriguichi, The Circular Economy: A New Development Strategy in China, Journal of Industrial Ecology, 10 (2006) 4-8.
[35] R. Van Berkel, T. Fujita, S. Hashimoto, Y. Geng, Industrial and urban symbiosis in Japan: analysis of the Eco-Town Program 1997-2006, J Environ Manage, 90 (2009) 1544-1556.
[36] A. Perez-Gonzalez, A.M. Urtiaga, R. Ibanez, I. Ortiz, State of the art and review on the treatment technologies of water reverse osmosis concentrates, Water Res, 46 (2012) 267-283.
[37] F. Macedonio, E. Curcio, E. Drioli, Integrated membrane systems for seawater desalination: energetic and exergetic analysis, economic evaluation, experimental study, Desalination, 203 (2007) 260-276.

[38] E. Drioli, E. Curcio, G. Di Profio, F. Macedonio, A. Criscuoli, Integrating Membrane Contactors Technology and Pressure-Driven Membrane Operations for Seawater Desalination, Chemical Engineering Research and Design, 84 (2006) 209-220.
[39] M. Turek, Seawater desalination and salt production in a hybrid membrane-thermal process, Desalination, 153 (2002) 173-177.
[40] M. Reig, S. Casas, C. Aladjem, C. Valderrama, O. Gibert, F. Valero, C.M. Centeno, E. Larrotcha, J.L. Cortina, Concentration of NaCl from seawater reverse osmosis brines for the chlor-alkali industry by electrodialysis, Desalination, 342 (2014) 107-117.
[41] E. Drioli, E. Curcio, A. Criscuoli, G.D. Profio, Integrated system for recovery of CaCO3, NaCl and MgSO4·7H2O from nanofiltration retentate, Journal of Membrane Science, 239 (2004) 27-38.
[42] A. Shahmansouri, J. Min, L. Jin, C. Bellona, Feasibility of extracting valuable minerals from desalination concentrate: a comprehensive literature review, Journal of Cleaner Production, 100 (2015) 4-16.
[43] M. Reig, S. Casas, C. Valderrama, O. Gibert, J.L. Cortina, Integration of monopolar and bipolar electrodialysis for valorization of seawater reverse osmosis desalination brines: Production of strong acid and base, Desalination, 398 (2016) 87-97.
[44] G.P. Thiel, A. Kumar, A. Gómez-González, J.H. Lienhard, Utilization of Desalination Brine for Sodium Hydroxide Production: Technologies, Engineering Principles, Recovery Limits, and Future Directions, ACS Sustainable Chemistry & Engineering, 5 (2017) 11147-11162.
[45] P. Ortiz-Albo, S. Torres-Ortega, M. González Prieto, A. Urtiaga, R. Ibañez, Techno-Economic Feasibility Analysis for Minor Elements Valorization from Desalination Concentrates, Separation & Purification Reviews, 48 (2018) 220-241.
[46] M. Turek, K. Mitko, E. Laskowska, M. Chorążewska, K. Piotrowski, A. Jakóbik-Kolon, P. Dydo, Energy Consumption and Gypsum Scaling Assessment in a Hybrid Nanofiltration-Reverse Osmosis-Electrodialysis system, Chemical Engineering & Technology, 41 (2018) 392-400.
[47] J.K. Choe, A.M. Bergquist, S. Jeong, J.S. Guest, C.J. Werth, T.J. Strathmann, Performance and life cycle environmental benefits of recycling spent ion exchange brines by catalytic treatment of nitrate, Water Res, 80 (2015) 267-280.
[48] H.R. Flodman, B.I. Dvorak, Brine reuse in ion-exchange softening: salt discharge, hardness leakage, and capacity tradeoffs, Water Environ Res, 84 (2012) 535-543.
[49] L. Birnhack, O. Keller, S.C.N. Tang, N. Fridman-Bishop, O. Lahav, A membrane-based recycling process for minimizing environmental effects inflicted by ion-exchange softening applications, Separation and Purification Technology, 223 (2019) 24-30.
[50] Y. Chen, J.R. Davis, C.H. Nguyen, J.C. Baygents, J. Farrell, Electrochemical Ion-Exchange Regeneration and Fluidized Bed Crystallization for Zero-Liquid-Discharge Water Softening, Environ Sci Technol, 50 (2016) 5900-5907.
[51] O. Ashrafi, L. Yerushalmi, F. Haghighat, Wastewater treatment in the pulp-and-paper industry: A review of treatment processes and the associated greenhouse gas emission, J Environ Manage, 158 (2015) 146-157.
[52] L.H. Buruberri, M.P. Seabra, J.A. Labrincha, Preparation of clinker from paper pulp industry wastes, J Hazard Mater, 286 (2015) 252-260.
[53] M. Pervaiz, M. Sain, Recycling of Paper Mill Biosolids: A Review on Current Practices and Emerging Biorefinery Initiatives, CLEAN - Soil, Air, Water, 43 (2015) 919-926.
[54] N.R. Khalili, J.D. Vzas, W. Weangkaew, S.J. Westfall, S.J. Parulekar, R. Sherwood, Synthesis and characterization of activated carbon and bioactive adsorbent produced from paper mill sludge, Separation and Purification Technology, 26 (2002) 295-304.

[55] K. Pirzadeh, A.A. Ghoreyshi, Phenol removal from aqueous phase by adsorption on activated carbon prepared from paper mill sludge, Desalination and Water Treatment, 52 (2013) 6505-6518.
[56] A. Battaglia, N. Calace, E. Nardi, B.M. Petronio, M. Pietroletti, Paper mill sludge–soil mixture: kinetic and thermodynamic tests of cadmium and lead sorption capability, Microchemical Journal, 75 (2003) 97-102.
[57] M. Turek, P. Dydo, R. Klimek, Salt production from coal-mine brine in NF — evaporation — crystallization system, Desalination, 221 (2008) 238-243.
[58] M. Turek, P. Dydo, R. Klimek, Salt production from coal-mine brine in ED–evaporation–crystallization system, Desalination, 184 (2005) 439-446.
[59] M. Turek, P. Dydo, A. Surma, Zero discharge utilization of saline waters from "Wesola" coal-mine, Desalination, 185 (2005) 275-280.
[60] M. Sivakumar, M. Ramezanianpour, G. O'Halloran, Mine Water Treatment Using a Vacuum Membrane Distillation System, APCBEE Procedia, 5 (2013) 157-162.
[61] G. Naidu, S. Ryu, R. Thiruvenkatachari, Y. Choi, S. Jeong, S. Vigneswaran, A critical review on remediation, reuse, and resource recovery from acid mine drainage, Environ Pollut, 247 (2019) 1110-1124.
[62] F. Fu, Q. Wang, Removal of heavy metal ions from wastewaters: a review, J Environ Manage, 92 (2011) 407-418.
[63] A. Dabrowski, Z. Hubicki, P. Podkoscielny, E. Robens, Selective removal of the heavy metal ions from waters and industrial wastewaters by ion-exchange method, Chemosphere, 56 (2004) 91-106.
[64] M. Mullett, R. Fornarelli, D. Ralph, Nanofiltration of Mine Water: Impact of Feed pH and Membrane Charge on Resource Recovery and Water Discharge, Membranes, 4 (2014) 163-180.
[65] J. Hu, G. Chen, I.M.C. Lo, Selective Removal of Heavy Metals from Industrial Wastewater Using Maghemite Nanoparticle: Performance and Mechanisms, Journal of Environmental Engineering, 132 (2006) 709-715.
[66] Y.H. Li, Y.M. Zhao, W.B. Hu, I. Ahmad, Y.Q. Zhu, X.J. Peng, Z.K. Luan, Carbon nanotubes - the promising adsorbent in wastewater treatment, Journal of Physics: Conference Series, 61 (2007) 698-702.
[67] Y. Nleya, G.S. Simate, S. Ndlovu, Sustainability assessment of the recovery and utilisation of acid from acid mine drainage, Journal of Cleaner Production, 113 (2016) 17-27.
[68] M.C. Martí-Calatayud, D.C. Buzzi, M. García-Gabaldón, E. Ortega, A.M. Bernardes, J.A.S. Tenório, V. Pérez-Herranz, Sulfuric acid recovery from acid mine drainage by means of electrodialysis, Desalination, 343 (2014) 120-127.
[69] J. López, M. Reig, O. Gibert, J.L. Cortina, Recovery of sulphuric acid and added value metals (Zn, Cu and rare earths) from acidic mine waters using nanofiltration membranes, Separation and Purification Technology, 212 (2019) 180-190.
[70] U. Kesieme, A. Chrysanthou, M. Catulli, C.Y. Cheng, A review of acid recovery from acidic mining waste solutions using solvent extraction, Journal of Chemical Technology & Biotechnology, 93 (2018) 3374-3385.
[71] J. López, M. Reig, O. Gibert, J.L. Cortina, Integration of nanofiltration membranes in recovery options of rare earth elements from acidic mine waters, Journal of Cleaner Production, 210 (2019) 1249-1260.
[72] D. Sapsford, M. Santonastaso, P. Thorn, S. Kershaw, Conversion of coal mine drainage ochre to water treatment reagent: Production, characterisation and application for P and Zn removal, J Environ Manage, 160 (2015) 7-15.
[73] S. Vajnhandl, J.V. Valh, The status of water reuse in European textile sector, J Environ Manage, 141 (2014) 29-35.

[74] E. Ozturk, N.C. Cinperi, Water efficiency and wastewater reduction in an integrated woolen textile mill, Journal of Cleaner Production, 201 (2018) 686-696.
[75] L. Bilińska, M. Gmurek, S. Ledakowicz, Textile wastewater treatment by AOPs for brine reuse, Process Safety and Environmental Protection, 109 (2017) 420-428.
[76] I. Koyuncu, Reactive dye removal in dye/salt mixtures by nanofiltration membranes containing vinylsulphone dyes: Effects of feed concentration and cross flow velocity, Desalination, 143 (2002) 243-253.
[77] J.M. Gozálvez-Zafrilla, D. Sanz-Escribano, J. Lora-García, M.C. León Hidalgo, Nanofiltration of secondary effluent for wastewater reuse in the textile industry, Desalination, 222 (2008) 272-279.
[78] B. Van der Bruggen, B. Daems, D. Wilms, C. Vandecasteele, Mechanisms of retention and flux decline for the nanofiltration of dye baths from the textile industry, Sep. Purif. Technol., 22-23 (2001) 519-528.
[79] S. Cheng, D.L. Oatley, P.M. Williams, C.J. Wright, Characterisation and application of a novel positively charged nanofiltration membrane for the treatment of textile industry wastewaters, Water Res, 46 (2012) 33-42.
[80] K. Nadeem, G.T. Guyer, B. Keskinler, N. Dizge, Investigation of segregated wastewater streams reusability with membrane process for textile industry, Journal of Cleaner Production, 228 (2019) 1437-1445.
[81] E. Sahinkaya, S. Tuncman, I. Koc, A.R. Guner, S. Ciftci, A. Aygun, S. Sengul, Performance of a pilot-scale reverse osmosis process for water recovery from biologically-treated textile wastewater, J Environ Manage, 249 (2019) 109382.
[82] F. Li, J. Huang, Q. Xia, M. Lou, B. Yang, Q. Tian, Y. Liu, Direct contact membrane distillation for the treatment of industrial dyeing wastewater and characteristic pollutants, Separation and Purification Technology, 195 (2018) 83-91.
[83] N.M. Mokhtar, W.J. Lau, A.F. Ismail, S. Kartohardjono, S.O. Lai, H.C. Teoh, The potential of direct contact membrane distillation for industrial textile wastewater treatment using PVDF-Cloisite 15A nanocomposite membrane, Chemical Engineering Research and Design, 111 (2016) 284-293.
[84] M. Laqbaqbi, M.C. García-Payo, M. Khayet, J. El Kharraz, M. Chaouch, Application of direct contact membrane distillation for textile wastewater treatment and fouling study, Separation and Purification Technology, 209 (2019) 815-825.
[85] W.J. Lau, A.F. Ismail, Polymeric nanofiltration membranes for textile dye wastewater treatment: Preparation, performance evaluation, transport modelling, and fouling control — a review, Desalination, 245 (2009) 321-348.
[86] N.C. Cinperi, E. Ozturk, N.O. Yigit, M. Kitis, Treatment of woolen textile wastewater using membrane bioreactor, nanofiltration and reverse osmosis for reuse in production processes, Journal of Cleaner Production, 223 (2019) 837-848.
[87] S.H. Lin, M.L. Chen, Treatment of textile wastewater by chemical methods for reuse, Water Research, 31 (1997) 868-876.
[88] V. Buscio, V. López-Grimau, M.D. Álvarez, C. Gutiérrez-Bouzán, Reducing the environmental impact of textile industry by reusing residual salts and water: ECUVal system, Chemical Engineering Journal, 373 (2019) 161-170.
[89] C. Gadipelly, A. Pérez-González, G.D. Yadav, I. Ortiz, R. Ibáñez, V.K. Rathod, K.V. Marathe, Pharmaceutical Industry Wastewater: Review of the Technologies for Water Treatment and Reuse, Industrial & Engineering Chemistry Research, 53 (2014) 11571-11592.
[90] W. Zhang, G. He, P. Gao, G. Chen, Development and characterization of composite nanofiltration membranes and their application in concentration of antibiotics, Separation and Purification Technology, 30 (2003) 27-35.

[91] R. Gupta, B. Sati, A. Gupta, Treatment and Recycling of Wastewater from Pharmaceutical Industry, in: Advances in Biological Treatment of Industrial Waste Water and their Recycling for a Sustainable Future, 2019, pp. 267-302.
[92] B.G. Mahendra, S. Mahavarkar, Treatment of wastewater and electricity generation using microbial fuel cell technology, International Journal of Research in Engineering and Technology, 1 (2013) 277-282.
[93] X. Wei, S. Zhang, Y. Sun, S.A. Brenner, Petrochemical Wastewater and Produced Water, Water Environ Res, 90 (2018) 1634-1647.
[94] S. Sarmin, B. Ethiraj, M.A. Islam, A. Ideris, C.S. Yee, M.M.R. Khan, Bio-electrochemical power generation in petrochemical wastewater fed microbial fuel cell, Sci Total Environ, 695 (2019) 133820.
[95] S. Al-Obaidani, E. Curcio, F. Macedonio, G. Diprofio, H. Alhinai, E. Drioli, Potential of membrane distillation in seawater desalination: Thermal efficiency, sensitivity study and cost estimation, Journal of Membrane Science, 323 (2008) 85-98.
[96] C. Li, W. Deng, C. Gao, X. Xiang, X. Feng, B. Batchelor, Y. Li, Membrane distillation coupled with a novel two-stage pretreatment process for petrochemical wastewater treatment and reuse, Separation and Purification Technology, 224 (2019) 23-32.
[97] S.A. Mirbagheri, S.N. Hosseini, Pilot plant investigation on petrochemical wastewater treatmentfor the removal of copper and chromium with the objective of reuse, Desalination, 171 (2005) 85-93.
[98] M. Viuda-Martos, J. Fernandez-Lopez, E. Saya-Barbera, E. Sendra, J.A. Perez-Alvarez, Physicochemical caracterization of the orange juice wastewater of a cytrus by-product, Journal of Food Processing and Presenvation, 35 (2011) 264-271.
[99] A. Gopinath, A. Bahurudeen, S. Appari, P. Nanthagopalan, A circular framework for the valorisation of sugar industry wastes: Review on the industrial symbiosis between sugar, construction and energy industries, Journal of Cleaner Production, 203 (2018) 89-108.
[100] S. Cartier, M.A. Theoleyre, M. Decloux, Treatment of sugar decolorizing resin regeneration waste using nanofiltration, Desalination, 113 (1997) 7-17.
[101] A. Cardinali, S. Pati, F. Minervini, I. D'Antuono, V. Linsalata, V. Lattanzio, Verbascoside, isoverbascoside, and their derivatives recovered from olive mill wastewater as possible food antioxidants, J Agric Food Chem, 60 (2012) 1822-1829.
[102] F. Federici, F. Fava, N. Kalogerakis, D. Mantzavinos, Valorisation of agro-industrial by-products, effluents and waste: concept, opportunities and the case of olive mill wastewaters, J Chem Technol Biotechnol 84 (2009) 895-900.
[103] J. Luo, L. Ding, B. Qi, M.Y. Jaffrin, Y. Wan, A two-stage ultrafiltration and nanofiltration process for recycling dairy wastewater, Bioresour Technol, 102 (2011) 7437-7442.
[104] Z. Chen, J. Luo, X. Hang, Y. Wan, Physicochemical characterization of tight nanofiltration membranes for dairy wastewater treatment, J. Membr. Sci., 547 (2018) 51-63.
[105] I.G. Wenten, D. Ariono, M. Purwasasmita, Khoirudin, Integrated processes for desalination and salt production: A mini-review, AIP Conference Proceedings, 1818 (2017).
[106] J. Dasgupta, J. Sikder, S. Chakraborty, S. Curcio, E. Drioli, Remediation of textile effluents by membrane based treatment techniques: A state of the art review, Journal of Environmental Management, 147 (2015) 55-72.
[107] I. Vergili, Y. Kaya, U. Sen, Z.B. Gönder, C. Aydiner, Techno-economic analysis of textile dye bath wastewater treatment by integrated membrane processes under the zero liquid discharge approach, Resour Conserv Recycl, 58 (2012) 25-35.
[108] K. Praneeth, D. Manjunath, S.K. Bhargava, J. Tardio, S. Sridhar, Economical treatment of reverse osmosis reject of textile industry effluent by electrodialysis–evaporation integrated process, Desalination, 333 (2014) 82-91.

[109] C. Nicolaidis, I. Vyrides, Closing the water cycle for industrial laundries: An operational performance and techno-economic evaluation of a full-scale membrane bioreactor system, Resources, Conservation and Recycling, 92 (2014) 128-135.
[110] Z. Zhou, D. Ruan, L.M. Jiang, Y. Yang, H. Ge, L. Wang, Comparison on treatment strategy for chemical cleaning wastewater: Pollutants removal, process design and techno-economic analysis, J Environ Manage, 235 (2019) 161-168.
[111] S. Sujak, S.R. Wan Alwi, J.S. Lim, Z.A. Manan, A Mathematical Model for Techno-Economic Evaluation of Industrial Wastewater Sludge to Resources Sehnaz Chemical Engineering Transactions, 56 (2017) 115-120.
[112] S. Sujak, Z.B. Handani, S.R. Wan Alwi, Z.A. Manan, H. Hashim, S. Lim Jeng, A holistic approach for design of Cost-Optimal Water Networks, Journal of Cleaner Production, 146 (2017) 194-207.
[113] X.-Y. Fan, A.-H. Li, J.J. Klemeš, Z.-Y. Liu, Advances in designing and targeting of water systems involving regeneration/treatment units, Journal of Cleaner Production, 197 (2018) 1394-1407.
[114] W.R. Bowen, A.W. Mohammad, N. Hilal, Characterisation of nanofiltration membranes for predictive purposes use of salts, uncharged solutes and atomic force microscopy, J. Membr. Sci., 126 (1997) 91-105.
[115] J. Schaep, C. Vandecasteele, A.W. Mohammad, W.R. Bowen, Analysis of the Salt Retention of Nanofiltration Membranes Using the Donnan–Steric Partitioning Pore Model, Separation Science and Technology, 34 (1999) 3009-3030.
[116] O. Labban, C. Liu, T.H. Chong, J.H. Lienhard V, Fundamentals of low-pressure nanofiltration: Membrane characterization, modeling, and understanding the multi-ionic interactions in water softening, J. Membr. Sci., 521 (2017) 18-32.
[117] V. Geraldes, A.M. Brites Alves, Computer program for simulation of mass transport in nanofiltration membranes, J. Membr. Sci., 321 (2008) 172-182.
[118] S. Senthilmurugan, A. Ahluwalia, S.K. Gupta, Modeling of a spiral-wound module and estimation of model parameters using numerical techniques, Desalination, 173 (2005) 269-286.
[119] Y. Roy, M.H. Sharqawy, J.H. Lienhard, Modeling of flat-sheet and spiral-wound nanofiltration configurations and its application in seawater nanofiltration, J. Membr. Sci., 493 (2015) 360-372.
[120] B. Van der Bruggen, K. Everaert, D. Wilms, C. Vandecasteele, Application of nanofiltration for removal of pesticides, nitrate and hardness from ground water: rejection properties and economic evaluation, Journal of Membrane Science, 193 (2001) 239-248.
[121] A.W. Mohammad, N. Hilal, H. Al-Zoubib, N.A. Darwish, N. Ali, Modelling the effects of nanofiltration membrane properties on system cost assessment for desalination applications, Desalination, 206 (2007) 215-225.
[122] H.M. Omar, S. Rohani, Crystal Population Balance Formulation and Solution Methods: A Review, Crystal Growth & Design, 17 (2017) 4028-4041.
[123] D.L. Marchisio, R.D. Vigil, R.O. Fox, Quadrature method of moments for aggregation–breakage processes, Journal of Colloid and Interface Science, 258 (2003) 322-334.
[124] D.L. Marchisio, J.T. Pikturna, R.O. Fox, R.D. Vigil, A.A. Barresi, Quadrature Method of Moments for Population-Balance Equations, AIChE Journal, 49 (2003) 1266-1276.
[125] V. John, F. Thein, On the efficiency and robustness of the core routine of the quadrature method of moments (QMOM), Chemical Engineering Science, 75 (2012) 327-333.
[126] A. Alamdari, M.R. Rahimpour, N. Esfandiari, E. Nourafkan, Kinetics of magnesium hydroxide precipitation from sea bittern, Chemical Engineering and Processing: Process Intensification, 47 (2008) 215-221.

[127] A. Cipollina, M. Bevacqua, P. Dolcimascolo, A. Tamburini, A. Brucato, H. Glade, L. Buether, G. Micale, Reactive crystallisation process for magnesium recovery from concentrated brines, Desalination and Water Treatment, 55 (2014) 2377-2388.
[128] R. Turton, R.C. Bailie, W.B. Whiting, J.A. Shaeiwity, D. Bhattacharzza, Analysis, Synthesis and Design of Chemical Processes, Prentice Hall, 2012.
[129] Personal Communication with the company WESTECH, in, 2019.
[130] H. El-Dessouky, H. Ettouney, Multiple-effect evaporation desalination systems: thermal analysis, Desalination, 125 (1999) 259-276.
[131] B. Ortega-Delgado, L. García-Rodríguez, D.-C. Alarcón-Padilla, Opportunities of improvement of the MED seawater desalination process by pretreatments allowing high-temperature operation, Desalination and Water Treatment, 97 (2017) 94-108.
[132] K.S. Pitzer, G. Mayorga, Thermodynamics of Electrolytes. I I. Activity and Osmotic Coefficients for Strong Electrolytes with One or Both Ions Univalent, Journal of Physical Chemistry, 77 (1973) 2300-2308.
[133] ESDU, Condensation inside tubes: pressure drop in straight horizontal tubes, in: ESDU Series on Heat Transfer, 1993.
[134] S. Shen, Thermodynamic Losses in Multi-effect Distillation Process, IOP Conference Series: Materials Science and Engineering, 88 (2015).
[135] H. El-Dessouky, I. Alatiqi, S. Bingulac, H. Ettouney, Steady-State Analysis of the Multiple Effect Evaporation Desalination Process, Chem. Eng.. Technol., 21 (1998) 437-451.
[136] J. Gebel, S. Yuce, An Engineer's Guide to Desalination, VBG PowerTech, 2008.
[137] T. Laukemann, R. Baten, T. Fichter, MENA Regional Water Outlook, Phase II, Desalination using Renewable Energy, (2012).
[138] C. Sommariva, Desalination and Advanced Water Treatment-Economics and Financing, Balaban Desalination Publications, 2010.
[139] M. Wilf, The Guidebook to Membrane Desalination Technology, Balaban Desalination Publications, 2007.
[140] M. Moser, Combined Electricity and Water Production Based on Solar Energy, in: Institute for Energy Storage, University of Stuttgart, 2015.
[141] V. Geraldes, N.E. Pereira, M.N. De Pinho, Simulation and Optimization of Medium-Sized Seawater Reverse Osmosis Processes with Spiral-Wound Modules, Ind. Eng. Chem. Res., 44 (2005) 1897-1905.
[142] A. Malek, M.N.A. Hawlader, J.C. Ho, Design and economics of RO seawater desalination, Desalination 105 (1996) 245-261.
[143] M. Wilf, C. Bartels, Optimization of seawater RO systems design, Desalination, 173 (2005) 1-12.
[144] F. Vince, F. Marechal, E. Aoustin, P. Bréant, Multi-objective optimization of RO desalination plants, Desalination, 222 (2008) 96-118.
[145] M. Qtaishat, T. Matsuura, B. Kruczek, M. Khayet, Heat and mass transfer analysis in direct contact membrane distillation, Desalination, 219 (2008) 272-292.
[146] A. Alkhudhiri, N. Darwish, N. Hilal, Membrane distillation: A comprehensive review, Desalination, 287 (2012) 2-18.
[147] M. Khayet, A. Velázquez, J.I. Mengual, Modelling mass transport through a porous partition: Effect of pore size distribution, Journal of Non-Equilibrium Thermodynamics, 29 (2004).
[148] Ó. Andrjesdóttir, C.L. Ong, M. Nabavi, S. Paredes, A.S.G. Khalil, B. Michel, D. Poulikakos, An experimentally optimized model for heat and mass transfer in direct contact membrane distillation, International Journal of Heat and Mass Transfer, 66 (2013) 855-867.
[149] I. Hitsov, L. Eykens, W.D. Schepper, K.D. Sitter, C. Dotremont, I. Nopens, Full-scale direct contact membrane distillation (DCMD) model including membrane compaction effects, Journal of Membrane Science, 524 (2017) 245-256.

[150] A. Ali, J.-H. Tsai, K.-L. Tung, E. Drioli, F. Macedonio, Designing and optimization of continuous direct contact membrane distillation process, Desalination, 426 (2018) 97-107.
[151] I. Hitsov, K.D. Sitter, C. Dotremont, I. Nopens, Economic modelling and model-based process optimization of membrane distillation, Desalination, 436 (2018) 125-143.
[152] J. Dai, S. Wu, G. Han, J. Weinberg, X. Xie, X. Wu, X. Song, B. Jia, W. Xue, Q. Yang, Water-energy nexus: A review of methods and tools for macro-assessment, Applied Energy, 210 (2018) 393-408.
[153] J. Liu, S. Chen, H. Wang, X. Chen, Calculation of Carbon Footprints for Water Diversion and Desalination Projects, Energy Procedia, 75 (2015) 2483-2494.
[154] International Energy Agency, World Energy Outlook 2018, in, 2018.
[155] Eurostat, Electricity prices for non-household consumers - bi-annual data (from 2007 onwards), in, 2019.
[156] IPCC, 2006 IPCC Guidelines for National Greenhouse Gas Inventories, in: E. H.S., B. L., M. K., N. T., T. K. (Eds.), National Greenhouse Gas Inventories Programme, IGES, Japan, 2006.
[157] Greenpeace International, Global Wind Energy Council, SolarPowerEurope, Energy Revolution - A sustainable world - 5th edition, in, 2015.
[158] M. Moser, F. Trieb, T. Fichter, J. Kern, D. Hess, A flexible techno-economic model for the assessment of desalination plants driven by renewable energies, Desalination and Water Treatment, (2014) 1-15.
[159] Fraunhofer ISE, Current and Future Cost of Photovoltaics. Long-term Scenarios for Market Development, System Prices and LCOE of Utility-Scale PV Systems, in, Agora Energiewende, 2015.
[160] C. Breyer, S. Afanasyeva, D. Brakemeier, M. Engelhard, S. Giuliano, M. Puppe, H. Schenk, T. Hirsch, M. Moser, Assessment of mid-term growth assumptions and learning rates for comparative studies of CSP and hybrid PV-battery power plants, in, 2017.
[161] M. Papapetrou, G. Kosmadakis, A. Cipollina, U. La Commare, G. Micale, Industrial waste heat: Estimation of the technically available resource in the EU per industrial sector, temperature level and country, Applied Thermal Engineering, 138 (2018) 207-216.
[162] M. Harmelink, L. Bosselaar, Allocating CO2 emissions to heat and electricity, in, Harmelink consulting, 2013.
[163] U.K. Kesieme, N. Milne, H. Aral, C.Y. Cheng, M. Duke, Economic analysis of desalination technologies in the context of carbon pricing, and opportunities for membrane distillation, Desalination, 323 (2013) 66-74.
[164] M.Z. Stijepovic, P. Linke, Optimal waste heat recovery and reuse in industrial zones, Energy, (2011).
[165] A. Cipollina, G. Micale, L. Rizzuti, Seawater Desalination - Conventional and Renewable Energy Processes, Springer, 2009.
[166] Dow Water and Process Solutions, Filmtec Reverse Osmosis Membrane. Technical Manual, (2018).

Appendix – Papers

Paper 1

M. Micari, M. Moser, A. Cipollina, B. Fuchs, B. Ortega-Delgado, A. Tamburini, G. Micale, "*Techno-economic assessment of multi-effect distillation process for the treatment and recycling of ion exchange resin spent brines*", Desalination, 2019, vol. 456, p- 38-52, https://doi.org/10.1016/j.desal.2019.01.011

Paper 2

M. Micari, D. Diamantidou, B. Heijman, M. Moser, A. Haidari, H. Spanjers, V. Bertsch, *"Experimental and Theoretical Characterization of Commercial Nanofiltration Membranes for the Treatment of Ion Exchange Resins Spent Brine"*, Journal of Membrane Science, 2020, Article number 118117, https://doi.org/10.1016/j.memsci.2020.118117

Paper 3

M. Micari, A. Cipollina, A. Tamburini, M. Moser, V. Bertsch, G. Micale, "*Combined Membrane and Thermal Desalination Processes for the Treatment of Ion Exchange Resins Spent Brine*", Applied Energy, 2019, Article number 113699, https://doi.org/10.1016/j.apenergy.2019.113699

Paper 4

M. Micari, M. Moser, A. Cipollina, A. Tamburini, V. Bertsch, G. Micale, "*Towards the Implementation of Circular Economy in the Water Softening Industry: A Technical, Economic and Environmental Analysis*", Journal of Cleaner Production, 2020, Article number 120291, https://doi.org/10.1016/j.jclepro.2020.120291.

Paper 5

M. Micari, A. Cipollina, A. Tamburini, M. Moser, G. Micale, V. Bertsch, *"Techno-economic Analysis of Integrated Treatment Chains for the Valorisation of Neutral Coal Mine Effluents",* Journal of Cleaner Production, 2020, Article number 122472, https://doi.org/10.1016/j.jclepro.2020.122472

Desalination 456 (2019) 38–52

Contents lists available at ScienceDirect

Desalination

journal homepage: www.elsevier.com/locate/desal

Techno-economic assessment of multi-effect distillation process for the treatment and recycling of ion exchange resin spent brines

M. Micari[a], M. Moser[a,*], A. Cipollina[b], B. Fuchs[a], B. Ortega-Delgado[b], A. Tamburini[b,*], G. Micale[b]

[a] German Aerospace Center (DLR), Institute of Engineering Thermodynamics, Pfaffenwaldring 38-40, 70569 Stuttgart, Germany
[b] Dipartimento dell'Innovazione Industriale e Digitale (DIID), Università degli Studi di Palermo (UNIPA), viale delle Scienze Ed. 6, 90128 Palermo, Italy

ARTICLE INFO

Keywords:
Industrial brines
Multi-effect distillation
Circular economy
Techno-economic analysis
Brine recycling

ABSTRACT

A treatment chain including nanofiltration, crystallization and multi-effect distillation (MED) is for the first time proposed for the treatment of an effluent produced during the regeneration of Ion Exchange resins employed for water softening. The goal is to recover the minerals and to restore the regenerant solution to be reused in the next regeneration cycle. MED is the most crucial unit of the treatment chain from an economic point of view. A techno-economic analysis on the MED unit was performed and a novel performance indicator, named Levelized Brine Cost, was introduced as a measure of the economic feasibility of the process. Different scenarios were analysed, assuming different thermal energy sources and configurations (plane-MED or MED-TVC). It was found that the plane-MED fed by waste-heat at 1 bar is very competitive, leading to a reduction of 50% of the fresh regenerant current cost. Moreover, the thermal energy cost of 20US$/MWh$_{th}$ was identified as the threshold value below which producing regenerant solution in the MED is economically more advantageous than buying a fresh one. Overall, MED allows reducing the environmental impact of the industrial process and it results competitive with the state of the art for a wide range of operating conditions.

1. Introduction and literature review

The disposal of polluted brines coming from industrial processes constitutes a very critical environmental issue of our time. Industrial brines are water solutions, containing sodium chloride, magnesium and calcium salts and, eventually, organic pollutants, released as a waste by several industrial processes. Even the brine generated as by-product by desalination processes has adverse environmental effects if discharged into the sea, because of the higher specific weight of the concentrated brine and the potential presence of additional chemicals [1]. Conventional approach consists in disposing brines directly to water bodies or in injecting them to inland wells [2]. Several studies were conducted to improve the disposal methods and to reduce the environmental impact. In particular, the position of the brine outlet [3] and the possibility to mix the concentrate brine with wastewater or exhaust cooling water [4] were investigated. Currently, some strategies are proposed to treat the brines with a combination of an evaporator with a crystallizer (Zero Liquid Discharge schemes) [5–7]. These strategies allow producing water at a very high purity, but the remaining solid by-product, given by the mixture of different components, is generally a waste, which has to be disposed. In order to tackle this problem and to reduce the disposal requirements, it is possible to develop treatment chains, given by the combination of different processes suitable to treat industrial brines by recovering each of their components. A properly selected treatment chain may lead to the recovery of the valuable products from the brine and to the minimization of the energy requirement of the process, making the brines a source of raw materials, such as water, NaCl and minerals. The definition of the most suitable processes and the process combination in a treatment chain depends on several factors, namely the reject brine volume, the chemical composition, the geographical position of the plant, the feasibility of the process based on the capital and operating costs, the availability of storage and transportation of the brine [6]. In particular, the brine composition strictly depends on the industrial process, which produces the brine. Several industrial processes can be accounted, e.g. desalination and demineralization plants, textile industry and coal mining industry. Many studies were conducted to identify the composition of the brines in the different cases and the possible processes to treat them [7–11]. For example, the brine coming from the textile industry is rich of organic components, while the brine coming from desalination plants is rich of bivalent ions, such as Mg^{++} and Ca^{++} [11]. With regard to the brine coming from Reverse Osmosis (RO) desalination processes, the profitability of different possible scenarios were compared taking into account the cost of the fresh-water production and the produced salt sale. Drioli et al. investigated the

* Corresponding authors.
E-mail addresses: massimo.moser@dlr.de (M. Moser), alessandro.tamburini@unipa.it (A. Tamburini).

https://doi.org/10.1016/j.desal.2019.01.011
Received 21 July 2018; Received in revised form 3 January 2019; Accepted 10 January 2019

performances of a Microfiltration, Nanofiltration and Reverse Osmosis (MF-NF-RO) membrane system, integrated with a membrane crystallizer, which is employed to bring the RO-concentrate above its saturation limit and to generate NaCl crystal nucleation and growth [12].

Another possible strategy of wastewater treatment consists in producing a water solution, at a defined composition, which can be used as a reactant in the industrial process itself. This approach is commonly used in the textile industry, where the contaminated waste stream is treated via oxidation processes and then re-used for next dyeing operations [13]. Ion Exchange resins operations is another industrial sector where this approach is employed. Ion-exchange resins (IEXs) are often employed for purification (e.g. for the removal of nitrates or perchlorates) or for water softening purposes [14]. Spent IEX resins are usually regenerated via the employment of a regenerant solution which is capable of reversing the ion-exchange equilibrium, displacing the ions removed from the treated solution [15]. For the case of demineralization, strong acids like HCl or H_2SO_4 are employed for the regeneration, conversely, in the case of water softening, the regenerant is typically a NaCl-water solution at a concentration ranging between $8\%^{w/w}$ and $12\%^{w/w}$, usually around $10\%^{w/w}$ [16]. During the regeneration, a wastewater solution enriched in the components displaced from the resin is produced. A proper combination of treatment processes allows restoring the regenerant solution required for the regeneration process, starting from the effluent itself. Some studies aimed at closing the loop and reusing the effluent coming from the IEX regeneration to reduce the amount of fresh regenerant solution. Wadley et al. modelled a NF unit used to separate the colorants from the regeneration effluent produced by an IEX in a sugar decolourisation plant [17]. In this case, the employed regenerant solution was a NaCl-water solution ($10\%^{w/w}$) and according to the presented process scheme, the NF permeate was mixed with a make-up NaCl-water solution and then sent back to the IEX as the regenerant. Moreover, IEX technology is widely used to remove pollutants from groundwater, especially nitrate which is the most common contaminants of groundwater and of drinking water sources [18]. The regeneration of the exhaust resins is carried out through a regenerant rich of sodium chloride or sodium bicarbonate, which, at the end of the regeneration process, is enriched of nitrate. Van der Hoek et al. suggested employing a biological denitrification reactor to carry out a regeneration in a closed circuit [19]. Lehman et al. tested a biological enhanced treatment system to remove both perchlorate and nitrate from the spent IEX brine [20]. Choe et al. investigated the applicability and the environmental sustainability of a catalytic reduction technology for treating nitrate in spent IEX brine [21]. Other studies focused on the recovery of the regenerant solution, for the case of IEX used for water purification from Natural Organic Matters (NOM). The study from Kabsch-Korbutowicz et al. was devoted to assessing the performances of pressure or electrically driven membrane processes in the removal of NOM from the spent IEX regenerant, in order to reuse it for the regeneration process [22]. Finally, Gryta et al. evaluated the employment of a Membrane Distillation (MD) unit for the concentration of IEX effluents with or without a preliminary treatment to avoid the scaling of the membranes [23]. In this case, the solution was concentrated up to the saturation point, to separate the salt crystals.

Ion Exchange resins are also widely used in water softening plants. In this case, the spent regenerant brine is rich of Mg^{++} and Ca^{++}, at a concentration of around 3000 and 12,500 ppm respectively, while the concentration of nitrate and other species is negligible [24]. This brine has a very low concentration of NaCl (between 10,000 and 15,000 ppm), since a very strong dilution is required to flash out all the high-density spent brine from the softener. A possible treatment chain suitable for this case is reported in Fig. 1. This has been developed within the framework of the EU-funded project Zero Brine [25], whose goal is the development of pilot plants able to treat different kinds of industrial brines. In particular, the one schematically represented in Fig. 1 is devoted to treating the brine produced in the softening section of the EVIDES company plant, in the Rotterdam port (The Netherlands). In this case, a NF stage is employed to separate most of the bivalent ions. Then, the retentate of the NF stage, rich of Mg^{++} and Ca^{++}, is processed in a crystallization section, where magnesium hydroxide and calcium hydroxide are precipitated and recovered. Conversely, the permeate of the NF stage, rich of NaCl, together with the liquid stream from the crystallization section, is sent to a Multi-Effect Distillation (MED) unit. In this stage, the NaCl-water solution is concentrated up to the required regenerant concentration.

MED can play a key role in the treatment of the IEX brines. MED process found a very large application in the desalination field, but there is still room for further investigation of this process in a higher range of feed salinity and brine salinity. Moreover, the presence of a NF stage before the MED can ensure the separation of the bivalent ions. Consequently, the risk of scaling in the heat exchangers, occurring usually with seawater at temperatures higher than 70 °C, is negligible and higher Top Brine Temperatures and higher steam temperatures are allowed. In literature, several efforts were made to investigate the coupling of a NF unit with thermal or membrane desalination processes, in order to reduce the risk of scaling due to the presence of hardness in seawater. With this regard, the idea to couple a NF pretreatment step with the traditional thermal or membrane desalination process was firstly proposed by the Saline Water Conversion Corporation (SWCC) [26]. Then, many studies proposed NF-RO, NF-MSF or NF-MED couplings, where the employment of the NF stage allowed a net reduction of the energy and the chemicals consumption of the desalination process [27–31]. Finally, Al-Rawajfeh investigated the possibility to employ a NF unit as CO_2 deaerator to pretreat the feed of a MSF distiller, in order to reduce the alkaline scale formation [32,33].

In literature, several case studies and several models for the MED plant have been proposed so far. The very first Forward Feed MED (FF-MED) model was proposed by El-Sayed and Silver: it was a design model, relying on some simplified thermodynamic assumptions [34]. Then, El-Dessouki et al. proposed a more sophisticated model for the FF-MED, indicating this arrangement as the most suitable to high temperature application [47]. They also proposed some approximate correlations to calculate the specific heat transfer area, the specific cooling flow rate and the thermal performance ratio as function of the top brine temperature and the number of effects. Kamali et al. presented a model for the MED coupled with a Thermo-Vapor Compressor (MED-TVC) [35,36] and Bin Amer et al. developed an optimization tool to maximize the Gain Output Ratio (GOR), varying top brine temperature, entrainment ratio and temperature difference per effect [37]. Recently, Mistry et al. proposed a modular MED model for different flow arrangements, which was compared with the previous models present in literature, showing good agreement and requiring less simplifying assumptions [38]. Finally, Ortega-Delgado et al. developed a detailed model for the FF-MED process and showed a net increase of the performance with higher heating steam temperatures [62]. Almost all these models were referred to a desalination process, considering a limited range of concentration and, in some cases, neglecting the influence of some parameters, whose estimation might become very relevant at higher concentration, such as the Boiling Point Elevation (BPE) variation with the composition or the temperature.

Moreover, various economic models were reported in literature for the MED process. Most of these were based on exergy analysis, to identify source and relevance of thermodynamic inefficiencies. Sayyadi et al. proposed an economic model, based on exergy analysis, for a parallel-cross (PC) MED-TVC system, with equal temperature differences for each effect and neglecting the pressure drops in the pipelines [39]. Then, the same authors presented three optimization scenarios: (i) the maximization of the exergy efficiency of the MED-TVC, (ii) the minimization of the cost of the fresh water production, (iii) a combination of the previous two [40]. Esfahani et al. proposed a multi-objective optimization to minimize the total annual costs and maximize the GOR [41]. Recently, Piacentino presented a detailed thermo-

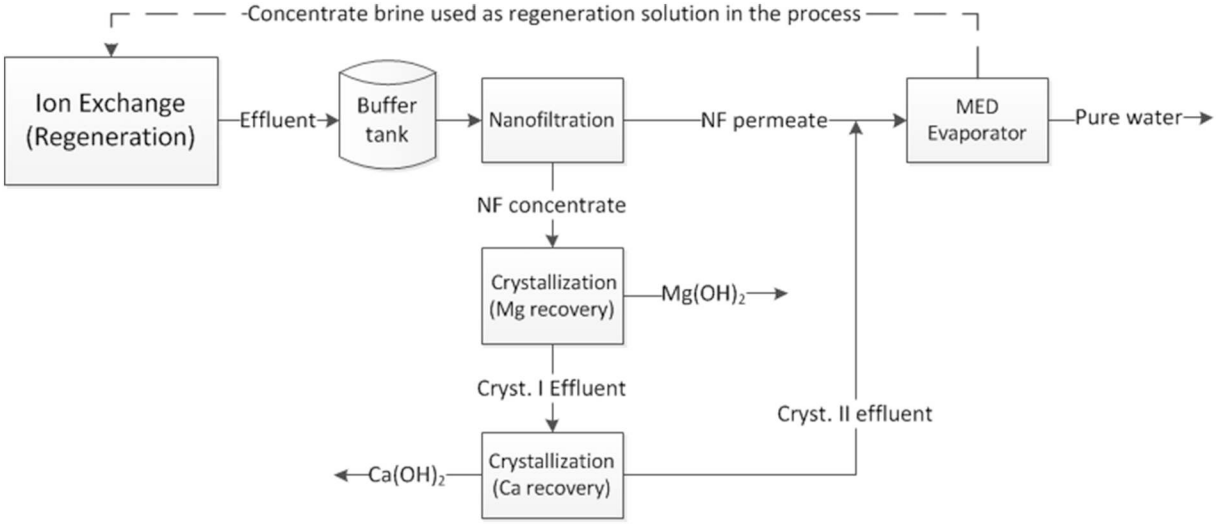

Fig. 1. Block Flow Diagram of the proposed treatment chain for industrial brines rich of bivalent ions, coming from Ion Exchange resins regeneration.

economic analysis for the case of a FF-MED plant. The research allowed identifying a cost for each material stream and describing all the single contributions to the final distillate cost [42]. Finally, Papapetrou et al. reviewed the methodologies used in literature for the estimation of the costs in the desalination plants, their range of validity and their limits [60].

In the present work, a fully-integrated techno-economic model for the MED process is presented: in the same simulation, the economic section of the model receives the main inputs directly from the technical model calculations (i.e. size of the equipment and energy requirement) to evaluate the capital and the operating costs, thus providing the final feasibility assessment of the MED technology. The model is applicable to a wide range of input parameters (e.g. feed salinity, steam temperature, number of effects) and able to easily switch between design methods (i.e. equal heat exchanger areas or equal temperature changes in the effects) and between feed flow arrangements (i.e. parallel cross and forward feed). For the first time, the application of the MED process to the treatment of the brines coming from the regeneration of spent IEXs is investigated. This new application of the MED made necessary to introduce a new parameter to define its performance. This has to be different from the most common performance parameter used for desalination plants, i.e. the Levelized Cost of Water (LCOW). With this aim, the Levelized cost of Brine (LBC) is introduced here for the first time, since the concentrate solution (brine) produced by the MED is the main valuable product of the treatment process. Therefore, the feasibility of this novel application of MED technology is assessed via the comparison of the calculated LBC with the current cost of the regenerant solution, i.e. the cost of a fresh NaCl-water solution for every regeneration cycle. Two scenarios are investigated, with reference to different thermal energy supplies. In the first one, the thermal energy is assumed to be completely provided by a gas turbine co-generation system, with a cost depending on the steam pressure. Conversely, the second scenario provides the utilization of waste heat available in the industrial site, at given quality and cost. In both scenarios, the performances of a plane MED and a MED-TVC are compared and a sensitivity analysis including the number of effects, the steam temperature and the motive steam pressure (for the case of MED-TVC) is carried out. Moreover, once the system configuration has been optimized on the basis of the thermal energy cost, the effects of the electric energy cost and of the revenue coming from the pure water production on the LBC are assessed. Finally, the influence of the feed flow rate on the LBC is assessed, in order to investigate the effect of the economy of scale on the proposed system.

Overall, the present work aims at proposing a new technological solution to treat an industrial wastewater effluent, whose treatment has not been investigated yet in literature and at evaluating the most suitable conditions to operate the MED unit in the treatment chain.

2. Model

2.1. Integrated techno-economic model

The techno-economic model is composed of a technical and an economic part that are fully integrated and implemented in Python. The technical/design model is mainly based on mass and energy balances at steady-state conditions and on the evaluation of thermo-physical properties of water, in the liquid or in the vapor state, and of the NaCl-water solution [62,63]. These properties are estimated via correlations reported in literature. The economic model evaluates the capital costs, via the estimation of the costs of the single equipment, and the operating costs, making reference to the calculated energy requirements. The main input variables for the technical model are: feed salinity, temperature and flow rate, steam temperature, motive steam pressure (in presence of the TVC), required brine salinity, temperature of the last effect and number of effects. All the geometrical features, such as the size of the tubes in the tube bundles or of the connecting lines, are given as parameters. Conversely, the key output variables of the design model are the heat exchanger areas, the preheater areas and the end-condenser area, the steam flow rate and the motive steam flow rate in the case of the MED-TVC. These variables (along with other financial parameters) constitute the inputs of the economic model, whose results are the annualized capital and operating costs, the revenue from the pure water production and the capital, operating and total Levelized Brine Cost. The most relevant inputs and outputs of the techno-economic model are summarized in Table 1.

The integrated model takes advantage from a purposely developed resolution algorithm which includes minimization steps (via iterative procedures) allowing design requirements to be fulfilled. The model is able to run for different feed arrangements (FF-MED and PC-MED) and different design methods, which refer to different design requirements, i.e. one provides equal heat exchangers area (A_{HX}) and equal preheaters area (A_{preh}) while the other provides equal temperature differences (ΔT_{eff}) for each effect. For the case under investigation, i.e. the concentration of the effluent coming from the IEX resins, the FF arrangement was selected as the most suitable, given the high concentrations which have to be reached and the possibility to employ high Top Brine Temperatures to enhance the performances in absence of TVC [47]. Moreover, for easiness of comparison with other technical models, the

Table 1
Main inputs and outputs of the technical and the economic model for the MED process.

Model	Inputs	Outputs
Technical model	Number of effects (N [−]) Feed flow rate (M_{feed} [kg/s]) Feed salinity (X_{feed} [ppm]) Intake feed temperature (T_{feed} [°C]) Brine salinity (X_{brine} [ppm]) Steam temperature (T_s [°C]) Motive steam pressure (P_m [bar]) Temperature in the last effect (T_N [°C])	Distillate flow rate (M_{dist} [kg/s]) Brine flow rate (M_{brine} [kg/s]) Heat exchanger areas (A_{HX} [m^2]) Preheater areas (A_{preh} [m^2]) End-condenser area (A_{cond} [m^2]) Cooling-water flow rate (M_{cw} [kg/s]) Steam flow rate (M_s [kg/s]) and motive steam flow rate for MED-TVC (M_m [kg/s]) Specific area (sA [m^2/(kg/s)]) and specific thermal consumption (sQ [kJ/kg])
Economic model	Heat exchanger areas (A_{HX} [m^2]) Preheater areas (A_{preh} [m^2]) End-condenser area (A_{cond} [m^2]) Cooling-water flow rate (M_{cw} [kg/s]) Steam flow rate (M_s [kg/s]) for MED or motive steam flow rate for MED-TVC (M_m [kg/s]) Electric energy requirement (P_{el} [kWh_{el}/m^3])	Annualized capital cost (CAPEX [US$/y]) Annualized operating cost (OPEX [US$/y]) Water revenue ($R_{wat}$ [US$/y]) Capital Levelized Brine Cost (LBC_{CAP} [US$/$m^3$]) Operating Levelized Brine Cost (LBC_{OP} [US$/$m^3$]) Total Levelized Brine Cost (LBC_{tot} [US$/$m^3$])

design method with equal areas of the heat exchangers and the preheaters was selected.

The structure of the resolution algorithm is reported in Fig. 2. As shown in the figure, the technical model presents three minimization loops, since it is required that (i) the areas of the heat exchangers (A_{HX}) and (ii) the areas of the preheaters (A_{preh}) have to be equal and (iii) a given distillate flow rate (M_{dist}) corresponding to a given brine salinity has to be produced. Once all the three requirements are satisfied, the technical results are available and are given as inputs to the economic model. Additional details on both the technical and the economic part of the model are reported in the following sections.

2.2. Technical model

The main output variables are the specific area (sA), the specific thermal consumption (sQ) and the GOR, which are defined as follows.

$$sA = \frac{\sum_N A_{HX} + \sum_{N-1} A_{preh} + A_{cond}}{M_{dist}} \quad (1)$$

$$sQ = \frac{M_s\, \lambda(T_s)}{M_{dist}} \quad (2)$$

$$GOR = \frac{M_s}{M_{dist}} \quad (3)$$

where $\lambda(T_s)$ is the latent heat of water at a temperature equal to T_s.

A short description and a table containing the main equations of the FF-MED steady-state model used for the simulations are reported in the following.

2.2.1. Forward feed model

The schematic representation of the MED plant described in the present FF-MED model is reported in Fig. 3. It shows the first effect, a generic intermediate effect and the last effect with the end condenser. In fact, three slightly different systems of mass and energy balance equations are used to model these three classes of effects.

All the equations relevant to the model of the FF-MED are reported in Table 2 where λ is the latent heat of water, h_{vap} is the enthalpy of the steam, h_{liq} is the enthalpy of the liquid water, h_{sw} is the enthalpy of the NaCl salt-water solution and $c_{p,sw}$ is the NaCl salt-water solution specific heat. The water properties are function of temperature, while the NaCl-water solution properties are functions of temperature and composition.

Basically, each run starts from the calculation of global mass and salinity balances, to estimate the brine flow rate (M_{brine}), the distillate flow rate (M_{dist}) and the brine salinity (X_{brine}), under the assumption that the distillate is pure water. Then, all the variables, such as mass flow rate, temperature and pressure, related to each single effect are estimated. Regarding the temperature profiles, six main quantities have to be calculated: temperature of the brine generated in the effect (T), temperature reached by the feed in the preheater of the effect (T_{preh}), temperature of the saturated vapor generated in the effect (T_{vsat}), temperature of the vapor after crossing the demister (T'_{vsat}), temperature of the vapor after crossing the connecting lines (T'_c) and condensation temperature of the vapor in the following effect (T_c). These are interdependent according to the Eqs. (6)–(9), through the boiling point elevation (BPE) and the pressure drops, which lead to temperature drops ($\Delta T_{demister}$, ΔT_{lines}, ΔT_{grav}, ΔT_{acc}), in the case of saturated vapor. The boiling point elevation is estimated through the Pitzer model, which is valid in a wider range of salinity compared to the other correlations in literature [43,44]. The pressure drops are estimated according to some correlations present in literature [45,46]. Concerning the modelling of the effects, the first effect is the only one which receives heat from an external source (M_s at temperature equal to T_s) and in which the feed (M_{feed} at a concentration equal to X_{feed}) enters after having crossed all the preheaters. The feed is sprayed on a tube bundle, while M_s flows inside the tubes. In this effect, the vapor generated (M_{vap}) is given only by the partial evaporation of the feed (M_d). This crosses the demister and the first preheater, where it partially condenses. The remaining part is sent to the following effect, as the heating steam. The brine generated in the first effect (M_b at a concentration equal to X_b) is sent to the following effect as the feed, sprayed on the external surface of the tube bundle. The intermediate effects' modelling includes the two energy balances on the preheater and on the heat exchanger to know the condensed fraction on the preheater tube surface (α_{cond}) and M_d, respectively (Eqs. (17)–(18)). Moreover, other two vapor contributions have to be considered: the vapor generated by the inlet brine flash (M_{fbrine} from Eq. (16)) and the vapor coming from the flashing box M_{fb}, which is generated by the flash of the condensed distillate collected in the flashing box (M_{fb} and M_c, the condensate exiting from the flash box, are derived from Eqs. (14), (15)). Finally, the last effect differs from the others because it does not have any preheater and the entire vapor generated in the last effect is sent to the end condenser, where it condenses completely. This leads to a slightly different expression of the energy balances on the effect (Eq. (19)) and on the last flashing box, since the total M_{vap} generated in the last effect condenses in the end condenser and then is collected in the flash box. The brine generated in the last effect (M_b [N]) constitutes the final brine produced by the plant, while the condensate exiting from the last flash box (M_c [N]) constitutes the final distillate. These have to satisfy the global balance in Eqs. (4)–(5). Regarding the end condenser, usually, the feed itself is used to condensate the vapor. The necessary

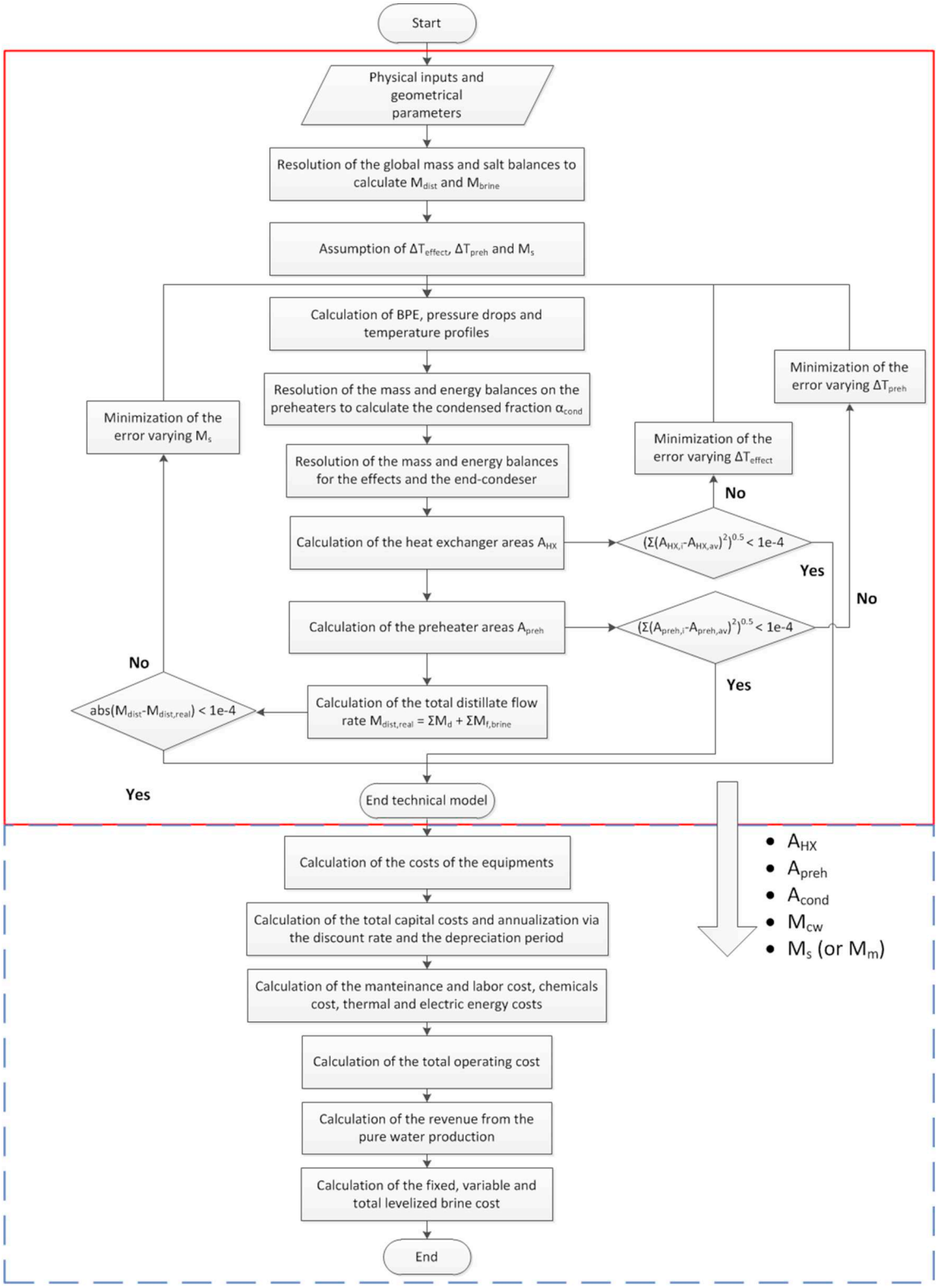

Fig. 2. Resolution algorithm for the MED model. The solid red rectangle encompasses the technical model procedure, while the broken blue rectangle contains the economic model one.

total cooling water flow rate (M_{cw}) is calculated through the heat balance reported in Eq. (20) and the surplus ($M_{cw} - M_{feed}$) is cooled down and can be reused.

Finally, the areas of the heat exchangers, of the preheaters and of the end condenser are calculated according to Eqs. (21)–(24) reported in Table 3. In these equations, $DTML_{preh}$ and $DTML_{cond}$ are the temperature logarithmic mean in the preheater and in the condenser and U_{cond} and U_{evap} are the heat transfer coefficients for the condenser and the evaporator respectively, derived from correlations by El-Dessouky et al. [47].

The described technical model was validated through the comparison with another FF-MED model, which is reported in literature [62].

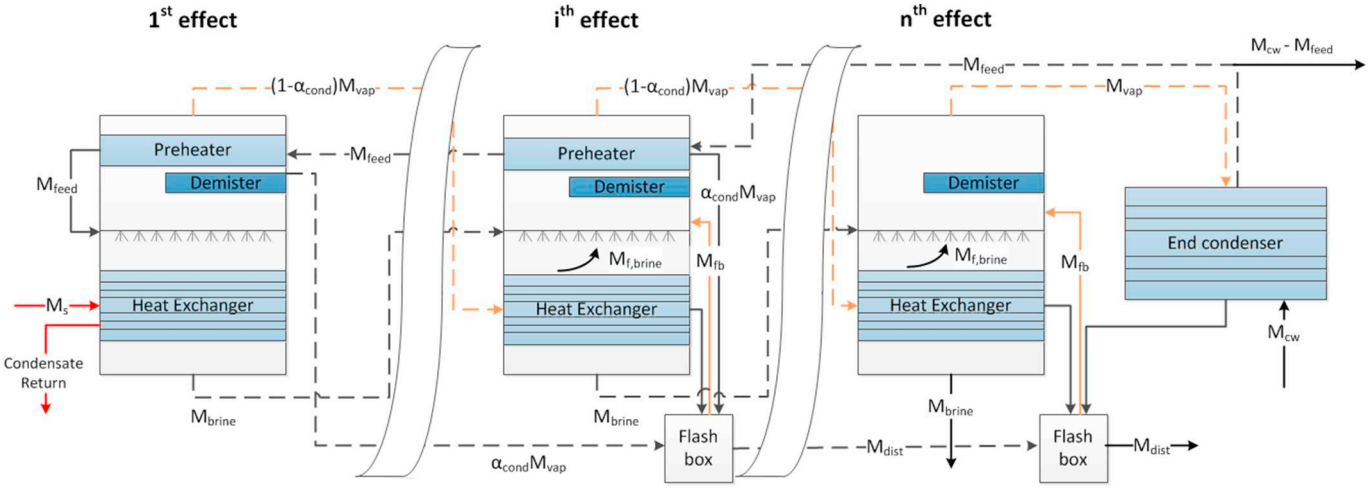

Fig. 3. Schematic representation of the MED plant.

The results of one of the sensitivity analyses carried out for validation purposes are reported in the Appendix A - Supplementary data.

2.2.2. Thermo-vapor compressor

In the case of a MED-TVC system, a certain amount of vapor generated in one effect is recycled to the first effect as part of the heating steam. More in detail, this is possible using a compression device, such as a thermo-compressor, in which a fraction of the vapor coming from the last effect or from an intermediate (i.e. entrained vapor) is mixed with the vapor coming from an external source (i.e. motive steam). In this work, the entrained vapor is always taken from the last effect. The discharged vapor is rejected as super-heated vapor at a pressure equal

Table 3
Equations to calculate the heat exchangers, preheaters and end condenser areas of the MED plant.

N	Equation
(21)	$A_{hx}[0] = \frac{M_{feed} c_{P\,sw}\left(T_{mean}, X_f\right)(T[1] - T_{preh}[1]) + M_d[1]\,\lambda(T_{vsat}[1])}{U_{evap}(T[1])(T_{steam} - T[1])}$
(22)	$A_{hx}[i] = \frac{(1-\alpha_{cond}[i-1])M_{vap}[i-1]\,\lambda(T_c[i-1])}{U_{evap}(T[i])(T_c[i-1] - T[i])}$
(23)	$A_{preh}[i] = \frac{\alpha_{cond}[i]\,M_{vap}[i]\,\lambda(T'_{vsat}[i])}{U_{cond}(T'_{vsat}[i])\,DTML_{preh}}$
(24)	$A_{cond} = \frac{M_{cw}\,c_{P\,sw}\left(\overline{T_{cw}}, X_{feed}\right)(T_{cw,out} - T_{cw,in})}{U_{cond}(T'_c[N])\,DTML_{cond}}$

Table 2
Main mass and energy balance equations of the forward-feed MED model.

N	Equation	Short description
(4)	$M_{feed} = M_{dist} + M_{brine}$	Global mass balance
(5)	$M_{feed}\,X_{feed} = M_{brine}\,X_{brine}$	Global salt balance
(6)	$T_{vsat}' = T - BPE(T, X_{brine})$	Temperature drop for the BPE
(7)	$T_{vsat}' = T_{vsat} - \Delta T_{demister}$	Temperature drop in the demister
(8)	$T_c' = T_{vsat}' - \Delta T_{lines}$	Temperature drop in the connecting lines
(9)	$T_c = T_c' - \Delta T_{grav} - \Delta T_{acc}$	Temperature drop in the evaporator
(10)	$M_s\lambda(T_s) + M_{feed}\,h_{sw}(T_{preh}[1], X_{feed})$ $= M_b[1]\,h_{sw}(T[1], X_b[1])$ $+(1-\alpha_{cond}[1])\,M_{vap}[1]\,h_{vap}(T_{vsat}'[1])$ $+\alpha_{cond}[1] M_{vap}[1]\,h_{liq}(T'_{vsat}[1])$	Energy balance on the first effect
(11)	$M_b[i-1] = M_d[i] + M_{fbrine}[i] + M_b[i]$	Mass balance on a generic effect
(12)	$M_{feed}\,X_{feed} = M_b[i]\,X_b[i]$	Salt balance on a generic effect
(13)	$M_{vap}[i] = M_d[i] + M_{fbrine}[i] + M_{fb}[i]$	Mass balance on the vapor phase
(14)	$M_c[i-1] + \alpha_{cond}[i]\,M_{vap}[i]$ $+(1-\alpha_{cond}[i-1])M_{vap}[i-1] = M_{fb}[i] + M_c[i]$	Mass balance on the generic flash-box
(15)	$M_c[i-1]\,h_{liq}(T_{v,\,sat}'[i-1])$ $+\alpha_{cond}[i]\,M_{vap}[i]\,h_{liq}(T_{vsat}'[i]) +$ $(1-\alpha_{cond}[i-1])M_{vap}[i-1]\,h_{liq}(T_c[i-1])$ $= M_{fb}[i]h_{vap}(T'_{vsat}[i]) + M_c[i]h_{liq}(T'_{vsat}[i])$	Energy balance on the generic flash-box
(16)	$M_{fbrine}[i]\,\lambda(T_{brine,\,f}[i])$ $= M_{brine}[i-1]\,c_{Psw}(T_{mean}, X_b[i-1])$ $(T[i-1] - T_{brine,\,f}[i])$	Energy balance on the brine entering as the feed ($T_{brine,f}$ calculated via the Non Equilibrium Allowance [47])
(17)	$M_{feed}\,c_{Psw}(T_{mean}, X_f)\,(T_{preh}[i] - T_{preh}[i+1]) = \alpha_{cond}[i]\,M_{vap}[i]\,\lambda(T'_{vsat}[i])$	Energy balance on a generic preheater
(18)	$(1-\alpha_{cond}[i-1])M_{vap}[i-1]\,\lambda(T_c[i-1])$ $+M_{fbrine}[i](h_{sw}(T[i-1], X_b[i-1]) - h_{vap}(T_{vsat}'[i]))$ $+M_b[i](h_{sw}(T[i-1], X_b[i-1]) - h_{sw}(T[i], X_b[i]))$ $= M_d[i](h_{vap}(T_{vsat}'[i]) - h_{sw}(T[i-1], X_b[i-1]))$	Energy balance on a generic heat exchanger
(19)	$(1-\alpha_{cond}[N-1])M_{vap}[N-1]\,\lambda(T_c[N-1])$ $+M_{fb}[N]\,h_{vap}(T_{vsat}'[N])$ $+M_b[N-1]\,h_{sw}(T[N-1], X_b[N-1])$ $= M_b[N]\,h_{sw}(T[N], X_b[N])$ $+M_{vap}[N]\,h_{vap}(T'_{vsat}[N])$	Energy balance on the last effect
(20)	$M_{cw}\,c_{P\,sw}(\overline{T_{cw}}, X_{feed})\,(T_{cw,out} - T_{cw,in}) = M_{vap}[N]\,\lambda(T'_c[N])$	Energy balance on the end condenser

to the saturation pressure at $T = T_s$. In order to model the TVC, some correlations reported in literature are employed [48,56]. Given the pressure of the motive steam P_m, the saturation pressure at T_s (P_s) and the pressure of the entrained vapor (P_{ev}, i.e. the saturation pressure at T_n), it is possible to calculate the compression ratio ($C_R = P_s / P_{ev}$) and the expansion ratio ($ER = P_m / P_{ev}$). Thus, the correlations allow calculating the entrainment ratio ($Ra = M_m / M_{ev}$) and, consequently, the amount of steam which has to be supplied externally (M_m).

2.3. Economic model

The economic model receives as input parameters the main outputs of the technical model, i.e. the areas of the heat exchangers, the preheaters and the end condenser, the required steam flow rate (M_s for the plane MED system and M_m for the MED-TVC) and the cooling water flow rate. The outputs of the economic model are the capital and the operating costs and the Levelized Brine Cost (LBC).

2.3.1. Capital costs

The capital costs are evaluated through the module costing technique, described extensively in [52] and widely used in literature as a standard tool for economic assessments of chemical plants [49–51]. This technique estimates the capital cost of every unit included in the process as a function of its purchased cost. The basis purchased cost of each element (C_p^0) is evaluated for some base conditions, i.e. equipment operating at ambient pressure and fabricated from most common material, usually carbon steel. The basis C_p^0 values are reported in database where these refer to a specific unit scale and are relevant to a specific year. The actual C_P^0 values are calculated for all equipment as function of their actual size, i.e. the area in the case of the heat exchangers and the condenser and the volume in the case of the pressure vessels. The C_P^0 values are then actualized through the Chemical Engineering Plant Cost Index (CEPCI). In the case of construction materials different from the ones employed for the base case (usually carbon steel) and pressures different from ambient pressure, suitable correction factors relevant to both purchased and installation costs are estimated for any kind of equipment. Finally, the bare module cost of the equipment C_{BM} is calculated multiplying the C_p^0 by a bare module factor F_{BM}, which takes into account all the above factors, together with the terms of cost related to freight, overhead and engineering:

$$C_{BM} = C_P^0 F_{BM} \tag{25}$$

In this way, it is possible to evaluate the cost of the single effect, considering each effect as the combination of two heat exchangers (i.e. the evaporator and the preheater) and one vessel (i.e. the flash box). Regarding the heat exchangers, these are supposed to have the shell in carbon steel and the tubes in a nickel-based alloy, which has an excellent resistance to saltwater and high temperatures [52,61]. The total cost of the equipment is calculated as the sum of the costs of the single effect, plus the cost of the end condenser and of the thermo-vapor compressor (for the case of MED-TVC). The estimation of the thermo-vapor compressor cost makes reference to a TVC whose cost and plant size, in terms of produced distillate flow rate, are known [57]. Finally, the total module cost (C_{TM}) is evaluated adding the contingency and fee cost to the cost of equipment, which are commonly assumed as 15% and 3% of the cost of equipment, respectively [52]. The auxiliary facility cost is neglected, since the plant is supposed to be built in an already developed industrial area. The total module cost is annualized (CAPEX in US$/y), through the discount rate (i) and assuming a certain plant lifetime (n_{years}), according to the following definition:

$$CAPEX = C_{TM} \frac{(1+i)^{n_{years}} i}{(1+i)^{n_{years}} - 1} \tag{26}$$

CAPEX definition intrinsically requires the adoption of a straight-line depreciation method. This choice commonly adopted in literature should be regarded as conservative as other deprecation methods would provide higher depreciation rates during the first years thus resulting into a better profitability of the economic analysis.

2.3.2. Operating costs

The operating costs take into account maintenance and labor costs, personnel costs, chemicals costs, thermal and electric energy costs. The maintenance cost is estimated as the 3% of the CAPEX (on an annual basis), while the labor cost for maintenance is defined as the 20% of the personnel cost [57]. This last term is given by the average cost of the personnel multiplied by the number of required workers, estimated according to [57]. The chemicals cost is given by the sum of the costs relevant to the required pretreatment to apply to the feed (e.g. anti-scalant or antifoaming) and to the cooling water (e.g. chlorination) and the post-treatment to the distillate (e.g. chlorination) [57]. The electric energy cost is calculated multiplying the specific electric consumption (assumed equal to 1.5 kWh_{el}/m^3 [64]) by the specific electric energy cost [US$/$kWh_{el}$]. Finally, the thermal energy cost is given by the product of the required thermal energy (i.e. the required steam times its latent heat) and the specific heat cost, which depends on the source of the heat which is available. In the case of no waste heat available, the heat is supposed to come from a gas turbine co-generation system and its price is function of the required steam pressure and is calculated via the Reference Cycle Method [64] reported in the Appendix A - Supplementary data section. If waste heat is supposed to be available in the industrial site, a certain cost for the thermal energy is given, depending on its quality. This cost is different from zero to account for the cost of the infrastructures necessary to supply the steam and, for the case of a higher-pressure steam, since this does not constitute a waste stream, a purchase price has been estimated on the bases of industrial practical data. In the case under investigation, part of the feed itself is employed as the cooler in the end condenser, so this cost has not to be accounted among the operating costs. The total annual operating cost (OPEX in US $/y) is given by the sum of all the described operating cost terms.

2.3.3. Levelized Brine Cost

The capital and the operating costs can be estimated also per unit of valuable solution produced, being expressed in this case in US$/$m^3$. As reported by Papapetrou et al. [60], in order to compare the feasibility of different desalination technologies, the Levelized Cost of Water (LCOW) is commonly used, i.e. the selling price that the water would have to reach the break-even point after a certain plant lifetime. In formula:

$$LCOW = \frac{C_{TM} + \sum_{t=1}^{n_{years}} \frac{OPEX(t)}{(1+i)^t}}{\sum_{t=1}^{n_{years}} \frac{M_{dist}(t)}{(1+i)^t}} \tag{27}$$

In most of the cases, the LCOW is calculated under the assumption that the produced water flow rate (M_{dist}) and the operating costs are the same for every year in the plant lifetime, thus the definition of the LCOW is as follows.

$$LCOW = \frac{CAPEX + OPEX}{M_{dist}} \tag{28}$$

Literature reports many examples of techno-economic analysis of processes producing water where the Levelized Water Cost is the only profitability index commonly adopted. The MED process investigated in the present work is meant as a unit able to produce a concentrated brine as main product to be sold. Thus, an evaluation standard akin to the LCOW was proposed, namely the Levelized Brine Cost (LBC), as reported in Eq. (29):

$$LBC = \frac{CAPEX + OPEX - REVENUE}{M_{brine}} \tag{29}$$

where M_{brine} is the brine flow rate produced by MED in one year [m^3/y]. Notably, the investigated MED unit produces also distillate being a by-product which can be sold. Relevant revenues must be subtracted to the expenses as reported in Eq. (29). Throughout the work, the

definition in Eq. (29) corresponds to the total Levelized Brine Cost LBC_{tot}, given by the sum of the Levelized Brine Cost relevant to the CAPEX (LBC_{CAP}) and the Levelized Brine Cost relevant to the OPEX (LBC_{OP}).

3. Description of the case study: treatment of the IEX effluent

The present work focuses on the investigation of the MED performances within the treatment of the effluent produced by the regeneration process of the Ion Exchange Resins employed in a water softening plant. The results are collected under two assumptions: (i) the effluent does not present organics or other pollutants (such as nitrate or boron) in an appreciable quantity, (ii) the stage of nanofiltration and crystallization ensures the total separation of the bivalent cations. The solution which is fed to the MED presents NaCl and water only and this allows considering a wide range of steam temperatures in the first effect. Two scenarios are investigated: (i) in the first one, all the steam is supposed to be supplied by an external source and, in particular, a gas turbine co-generation system, which is also the source of the electric energy; (ii) in the second one, waste heat is available in the industrial site at certain conditions and at a certain cost, namely either at 1 bar and a cost of 10 US$/$MWh_{th}$ or at 5 bar and a very conservative cost of 30 US$/$MWh_{th}$ [53,54]. Details are reported in Table 4.

In both scenarios, the concentration of the feed is given by the average salinity of the effluent produced during the regeneration of the resins (an overall salinity of around 36,000 ppm, including around 11,000 ppm of NaCl). Usually, this salinity is quite low because of a strong dilution, carried out in the last stages of the regeneration cycle via softened water, in order to flash out completely the spent regenerant from the resins. The concentration of the brine, which has to be produced by the MED plant, is set equal to the required regenerant concentration (90,000 ppm), thus a concentration factor of almost 9 has to be guaranteed by the MED evaporator. All simulations are performed varying the number of effects, both for the plane MED and the MED-TVC system, always with a forward-feed arrangement. In the first scenario, the temperature of the steam supplied to the plane MED varies from 65 °C up to 120 °C [55,62]. Conversely, concerning the MED-TVC, the temperature of the steam is fixed equal to 70 °C, in order to ensure a stable behavior of the thermo-vapor compressor ($C_R < 6$) [56], while the pressure of the motive steam is let free to vary from 3 bar up to 21 bar. In the second scenario, the temperature of the steam in the plane MED is selected as the highest temperature possible ($\leq$120 °C), depending on the quality of the waste heat. Regarding the MED-TVC, its performances are investigated only for the higher-pressure waste heat and the pressure of the motive steam is equal to the pressure of the available waste heat, while the Top Brine Temperature is fixed equal to 70 °C. Finally, in both scenarios, the temperature of the last effect is equal to 38 °C, in order to ensure a minimum terminal temperature difference of 3 °C in the case of the maximum temperature change in the end condenser (10 °C). The main technical assumptions are reported in Table 5.

Regarding the economic parameters, the thermal energy cost depends on the pressure of the steam in the first scenario and on the quality of the waste heat in the second scenario. All other parameters are fixed. The electric energy cost is calculated for the electricity produced by a gas turbine co-generation system, the water price is equal to an average distillate price produced in a desalination plant [57]. Since the water price is kept constant in the two scenarios and the produced distillate flow rate is always the same (because the feed flow rate as well as the salinity of the feed and of the brine have been defined), the water revenue is the same in all cases and it is equal to 8.15 $/$m^3_{brine}$. The depreciation period, the average personal cost and the number of workers are also typical of commercial-scale desalination plants [57,60,64]. These parameters are reported in Table 6. It is worth noting that many cost items reported in Table 6 may change significantly when different countries are investigated. Among the cost items, unitary personnel cost of 50,000 US$/y should be regarded again as a conservative choice. Nevertheless, preliminary analysis showed that even doubling this cost, the corresponding LBC remains competitive compared to the fresh regenerant solution cost.

Regarding the first scenario, the steam is assumed to be completely supplied by a combined cycle CHP system, fired by natural gas, and its cost is reported as a function of the steam pressure P_m in Fig. 4. The costs are calculated via the application of the Reference Cycle Method [64,65], described in the Appendix A - Supplementary data. It is evident that the heat cost increases more deeply in the range of pressure between 0 and 1 bar; conversely, for pressures higher than 1 bar the increasing trend is smoother. The trend of the cost vs. the pressure of the steam is fitted via a logarithmic equation, as reported in Eq. (30), which is valid for the natural gas cost shown in Table 6.

$$Heat\ cost\left[\frac{US\$}{MWh_{th}}\right] = 10.7 \ln P_{steam} + 24.2 \quad (30)$$

This has important consequences in the estimation of the operating costs of both MED and MED-TVC in the first scenario. In fact, the temperature of the total steam to supply to the plane MED ranges from 65 °C to 120 °C and, consequently, its pressure ranges from 0.25 bar to 1.98 bar. Conversely, the pressure of the motive steam, which can be supplied to the TVC, in the case of the MED-TVC system, can vary from 3 bar up to 21 bar, as it is defined as the maximum pressure of the steam produced by the co-generation system.

Finally, as already mentioned, the feasibility of the MED technology is evaluated comparing the calculated LBC_{tot} with the current cost of the regenerant solution, equal to 8 US$/$m^3$. This cost is estimated for a

Table 5
Technical inputs for the case study analysis.

Main technical parameters			
X_{feed} [ppm]		11,000	
X_{brine} [ppm]		90,000	
N [−]		Variable	
T_s [°C]	Variable (MED)		70 (MED-TVC)
P_m [bar]	$P_{sat}(T_s)$ (MED)		Variable (MED-TVC)
T_n [°C]		38	
T_{feed} [°C]		25	
M_{feed} [kg/s]		200	

Table 4
Summary of the investigated scenarios.

			T_s	P_m	Heat cost
Scenario 1 (Section 4.1)	Case 1	Plane MED	Variable (65–120 °C)	$P_{sat,steam}$ (T_s)	Variable with P_m, see Eq. (30)
	Case 2	MED-TVC	70 °C	Variable (3–21 bar)	Variable with P_m, see Eq. (30)
Scenario 2 (Section 4.2)	Case 1	Plane MED	100 °C	$P_{sat,steam}$ (T_s) 1 bar	10 US$/$MWh_{th}$ (Section 4.2.1.1) Variable (Section 4.2.2)
	Case 2	Plane MED	120 °C	$P_{sat,steam}$ (T_s)	30 US$/$MWh_{th}$ (Section 4.2.1.2) Variable (Section 4.2.2)
		MED-TVC	70 °C	5 bar	30 US$/$MWh_{th}$ (Section 4.2.1.2) Variable (Section 4.2.2)

Table 6
Main economic inputs for the case study analysis.

Main economic parameters	
Thermal energy cost	Variable
Electric energy cost	0.215 US$/kWh$_{el}$
Discount rate (i)	6%
Depreciation period (n_{years})	25 years
Average unitary personnel cost	50,000 US$/y
Number of workers	10
Pure water price	1 US$/m^3
Fuel cost (gas)	65.9 US$/MWh[a]

[a] See Appendix A - Supplementary data section.

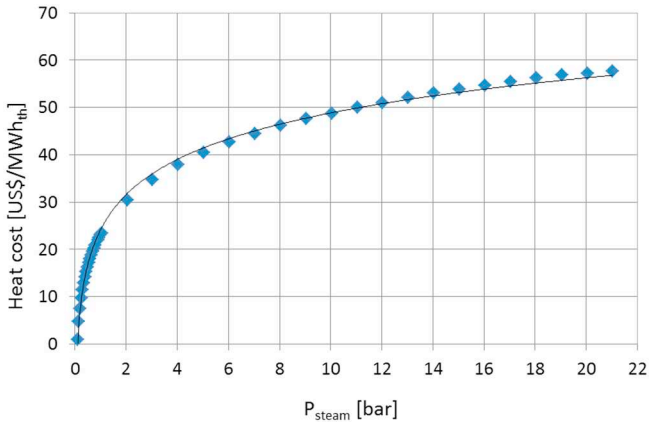

Fig. 4. Thermal energy cost vs. the steam pressure for the case of a gas turbine co-generation system (as a reference, the pressures of 1, 5, 10, 15 and 20 bar correspond to temperatures of 99.7, 151.9, 179.9, 198.2, 212.2 °C).

9%$^{w/w}$ NaCl-water solution, considering a cost of the pure NaCl salt equal to 65 euro/ton (80.2 US$/ton) and a cost of water equal to 1 US $/m^3. Notably, a preliminary analysis on the treatment chain of Fig. 1 showed that the revenues deriving from the selling of $Ca(OH)_2$ and $Mg(OH)_2$ more than counterbalance all the costs relevant to the crystallization and filtration steps [58]. Thus, the value of 8 US$/m^3 of the current regenerant solution is used as a benchmark for the MED technology only.

4. Results and discussion

4.1. First scenario: steam supplied by a gas turbine co-generation system

In the first scenario, the influence of T_s in the plane MED and of P_m in the MED-TVC is evaluated at 6, 9, 12 and 15 effects. Fig. 5 reports the trend of the total Levelized Brine Cost (LBC_{tot} in US$/m^3), considering the contributions of the capital (LBC_{CAP}) and the operating costs (LBC_{OP}) for a plane MED with different number of effects varying the steam temperature. The (threshold) purchase cost of fresh regenerant solution is also reported for comparison purposes. Basically, the capital costs slightly decrease with T_s because of the higher overall temperature differences, which correspond to higher available driving forces in each effect. Therefore, whenever the available temperature driving force increases, the area required for the heat transfer decreases. Conversely, the operating costs increase very sharply, because of the higher thermal energy cost. The analysis at different number of effects highlights the different weights of the capital and the operating costs in the different configurations, i.e. the higher the number of effects, the higher the impact of the fixed costs on the total LBC compared to the operating costs. Therefore, at 6 and 9 effects, the operating costs are higher than the capital costs in most of the range of T_s. Conversely, at 12 and especially at 15 effects, the two cost terms are comparable and, although the LBC_{tot} increases also in these two cases in the entire range of T_s, it is possible to notice a low-slope trend at low temperatures, because the capital and operating cost trends are opposite. Finally, it is also worth mentioning that, especially for high number of effects, for any temperature lower than 80 °C, the total LBC is lower than the current cost of the regenerant solution (i.e. 8 US$/m^3).

Conversely, Fig. 6 shows the trend of the LBC_{tot}, together with the LBC_{CAP}, LBC_{OP} and the regenerant solution cost for a MED-TVC system with different number of effects, varying the motive steam pressure. In this case, as already mentioned, T_s is fixed and equal to 70 °C and this leads to constant capital costs. Conversely, P_m is free to vary and its variation leads to a variation of the operating costs. The slope is higher at low P_m and decreases at higher pressures in accordance with Fig. 4. Overall, comparing the results at different number of effects, as expected, the capital costs increase as the number of effects increases, while the operating costs strongly decrease. Note that, in this case, at 6 and 9 effects the operating costs are always higher than the capital costs, at 12 effects there is a cross at low pressures, while at 15 effects the capital costs are always higher that the operating costs. Finally, for the MED-TVC system, the cost of the thermal energy is too high to make this system competitive with the current regenerant solution supply. In fact, for any configuration and for any pressure in the investigated range, the LBC_{tot} is higher than the estimated cost of the required regenerant solution of 8 US$/m^3.

4.2. Second scenario: waste heat available in the industrial site

4.2.1. Fixed revenue and operating costs

In the second scenario, the thermal energy is assumed to be supplied via waste heat, available in the industrial site. In particular, two sets of thermo-physical conditions of the available steam (i.e. temperature and pressure) are selected and coupled with a value of the thermal energy cost: saturated steam at 1 bar at a cost of 10 US$/MWh$_{th}$ and saturated steam at 5 bar and a cost of 30 US$/MWh$_{th}$ (see Table 4). In the first case, only the plane MED is investigated, since the pressure is too low for a MED-TVC (typically $P_m > 3$ bar [59]). For the second accounted waste heat quality, the plane MED and the MED-TVC systems are both investigated and a sensitivity analysis varying the number of effects is performed. For the MED-TVC system, the pressure of the motive steam is equal to the pressure of the available steam (5 bar). Conversely, for the plane MED, the temperature of the steam in the first effect is set equal to the maximum reachable temperature of the steam, taking into account the steam pressure and the maximum allowed temperature in the first effect (i.e. 120 °C). This is because the higher the temperature of the steam, the lower the fixed costs, which are the most relevant costs for the definition of the LBC_{tot}, when the thermal energy cost is fixed.

4.2.1.1. First case: waste heat available at 1 bar. In Fig. 7 the trends of the LBC_{CAP}, LBC_{OP} and LBC_{tot} are reported as functions of the number of effects. As expected, the capital costs increase with the number of effects, while the operating costs decrease. The combination of these two opposite trends gives rise to a minimum in LBC_{tot}, which occurs at 13 effects. Interestingly, for any number of effects higher than 5, LBC_{tot} results lower than 8 US$/m^3, showing that, in these conditions, the technology is competitive with the current regenerant solution supply. In particular, the minimum LBC_{tot} is around 4 US$/m^3.

4.2.1.2. Second case: waste heat available at 5 bar. The results relevant to this case are reported in Fig. 8. Both in the case of the plane MED and of the MED-TVC, the operating costs play the most prominent role in the definition of LBC_{tot} and, for this reason, a wider range of number of effects has to be investigated to detect the minimum. The minimum corresponds to the optimum configuration of the system, and it is found at different number of effects because of the different weights of the capital and the operating costs in the plane MED and in the MED-TVC. The capital costs are higher in the MED-TVC in the entire range of number of effects, because of the presence of the TVC but, mainly,

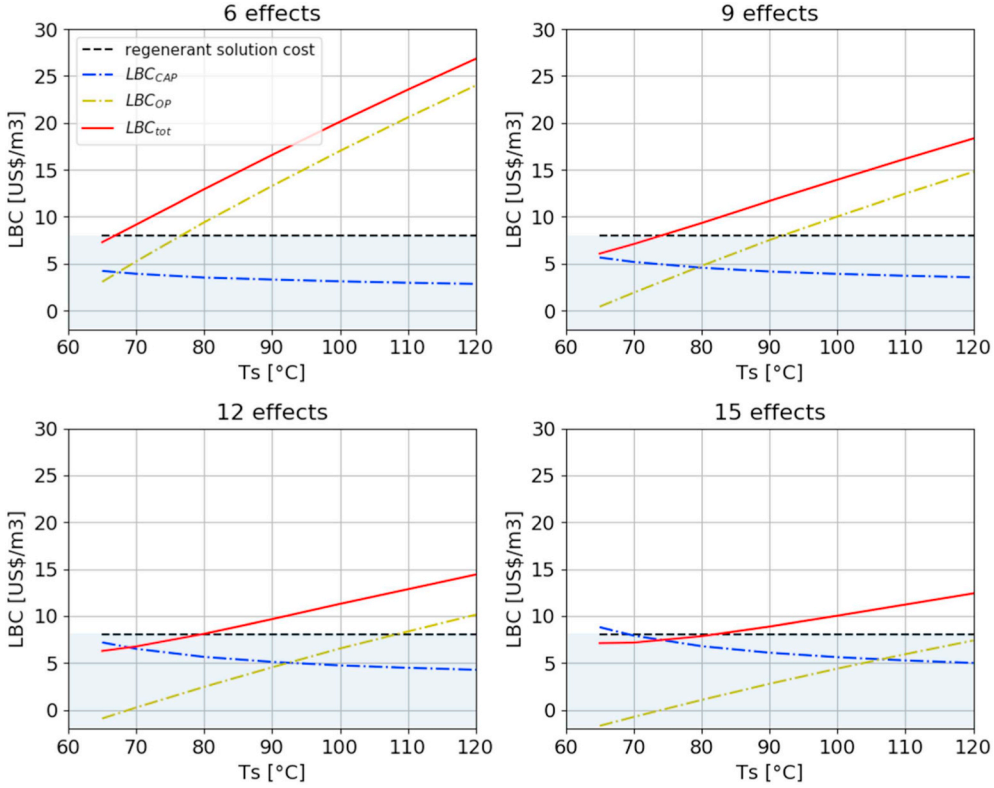

Fig. 5. Levelized Brine Cost for a plane MED system with variable number of effects (6, 9, 12, 15 effects) as a function of the steam temperature.

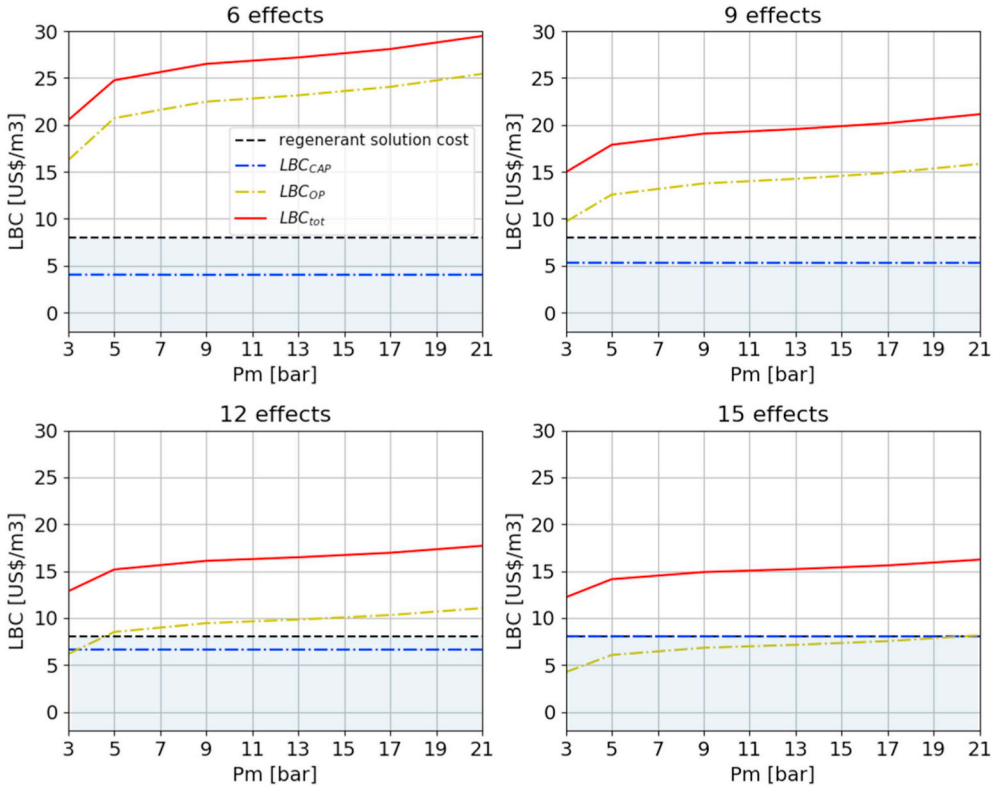

Fig. 6. Levelized Brine Cost for a MED-TVC system with variable number of effects (6, 9, 12, 15 effects) as a function of the motive steam pressure.

because of the lower available driving force, due to the fixed $T_s = 70\,^{\circ}C$. At the same time, the operating costs are much higher in the plane MED, especially at low number of effects, because the total steam, which has to be supplied, is higher than the motive steam supplied at the same cost in the MED-TVC. In both cases (MED and MED-TVC) it is possible to recognize a minimum in LBC_{tot}, which occurs at 25 effects for the plane MED and at 15 effects for the MED-TVC. These two LBC_{tot} minimum values are around 10 US$/m^3, which is higher than the

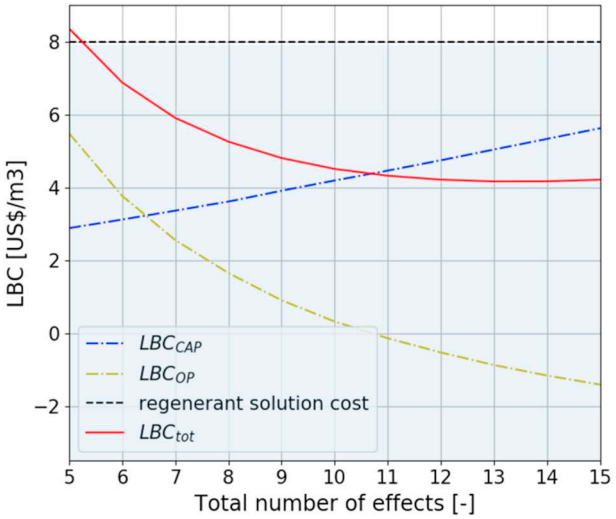

Fig. 7. Levelized Brine Cost for a plane MED system with T_s = 100 °C varying the number of effects (5–15 effects) and fixing the thermal energy cost equal to 10 US$/MWh$_{th}$.

current cost of the fresh regenerant solution. This means that the employment of this waste heat stream does not make this technology competitive with the current state.

4.2.2. Sensitivity analysis

A sensitivity analysis is carried out varying the thermal energy cost from 0 [60] up to the cost of the steam (see Fig. 4) produced by the co-generation system at the corresponding pressure (1 bar for the first case in Figs. 7 and 5 bar for the second case in Fig. 8). This analysis aims at investigating quantitatively the role of the thermal energy cost on the LBC_{tot} and at defining the optimum system configuration (i.e. the number of effects, for plane MED and MED-TVC), for the two different steam qualities of Case 1 and Case 2. Fig. 9 reports the minimum LBC_{tot} varying the thermal energy cost from 0 up to the selling price at 1 bar (i.e. 26 US$/MWh$_{th}$ from Fig. 4), for the plane MED described in the Case 1 of the second scenario. The chart shows an increasing trend of the minimum LBC_{tot} with the thermal energy cost, as expected. Moreover, the number of effects corresponding to the optimum configuration increases with the thermal energy cost. Therefore, since the heat cost increases, the operating costs constitute a larger fraction of the total costs and the optimum system configuration corresponds to a higher number of effects and a lower thermal consumption. Finally, it is remarkable that at very low heat cost, the minimum LBC_{tot} is negative and this means that the revenue coming from the water production overcomes the annualized capital and operating costs.

Fig. 10 reports the trends of the minimum LBC_{tot} for the plane MED and the MED-TVC described in Case 2 of the second scenario. Here, the optimum number of effects ranges up to 30 effects for the plane MED and up to 17 effects for the MED-TVC, because of the higher maximum thermal energy cost (i.e. 42 US$/MWh$_{th}$ at P_m = 5 bar, see Fig. 4). It is worth noting that, in the entire range of heat cost, the plane MED system ensures the lowest minimum LBC_{tot}, but employing always a higher number of effects, for a given heat cost. Moreover, it is possible to notice that the higher the heat cost, the larger the difference between the optimum configurations in the two systems. The plane MED has higher thermal consumptions on the one hand. On the other hand, it allows a larger reduction of operating costs, increasing the number of effects, with respect to the MED-TVC. Therefore, the capital costs increase much more deeply with the number of effects in the MED-TVC, because of the stronger depletion of the driving force, due to the lower steam temperature (70 °C). This leads to a higher value of the minimum LBC_{tot} with respect to the plane MED. It is also possible to notice that the trends relevant to the two configurations starts at 0 with a certain difference, they get closer at low heat costs and start diverging at higher heat costs. For a heat cost equal to 0, the CAPEX is the prominent term and it is lower for the plane MED, because of the higher T_s. As the heat cost increases, the OPEX acquires a more significant role and the minimum LBC_{tot} values get similar. At very high heat cost, both systems tend to a configuration, which minimizes the operating costs increasing the number of effects and at this point the capital costs are the prominent term in the calculation of LBC_{tot}. This explains why the plane MED is the most competitive arrangement, especially at high thermal energy costs. Finally, when comparing the minimum LBC_{tot} for the plane MED at the two different T_s (i.e. 100 °C in Fig. 9 and 120 °C in Fig. 10), similar results can be observed. This is not surprising since the values correspond to the minimum costs and the optimum configuration (i.e. the optimum number of effects) takes into account the different operating conditions. Therefore, the optimum number of effects for the plane MED is always lower (or equal for very low heat cost) for the case of T_s = 100 °C, which allows having a higher temperature difference in each effect. Finally, it is worth noting that, in both cases, at a heat cost of around 20 US$/MWh$_{th}$, the minimum LBC_{tot} reaches a value of 8 US$/m^3, which is the current cost of the fresh regenerant solution. This means that the competitiveness of the process presented in the present work with respect to the traditional one is achieved when heat cost is lower than the threshold value of 20 US$/MWh$_{th}$.

Finally, for both Case 1 and Case 2 a parametric analysis is

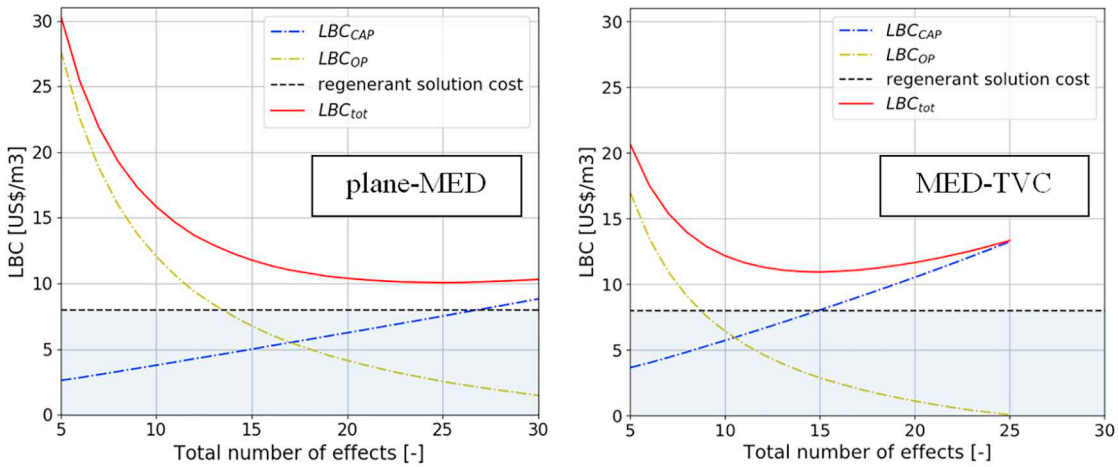

Fig. 8. Levelized Brine Cost for a plane MED system (left) with T_s = 120 °C and for a MED-TVC system (right) with P_m = 5 bar varying the number of effects and fixing the thermal energy cost equal to 30 US$/MWh$_{th}$.

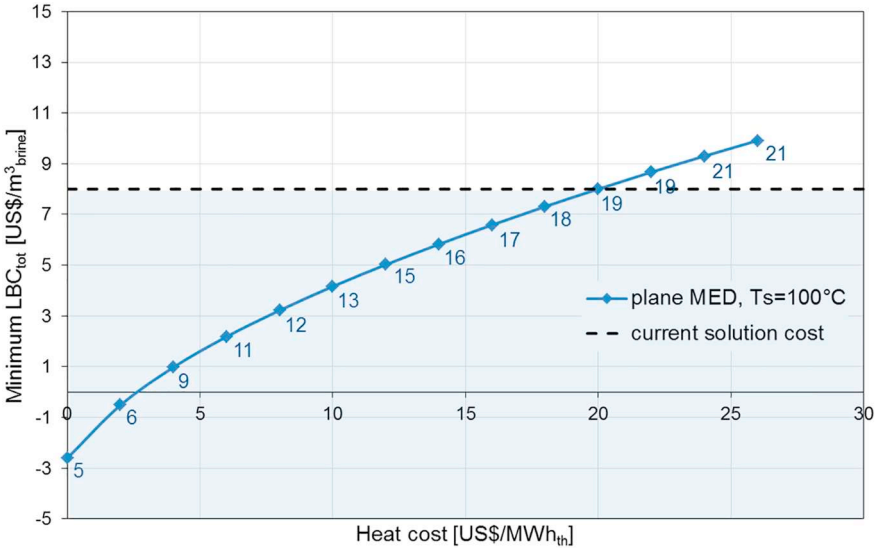

Fig. 9. Minimum LBC_{tot} as a function of the heat cost [US$/$MWh_{th}$] for a plane MED (steam at P = 1 bar, T_s = 100 °C). The labels correspond to the number of effects, which minimizes LBC_{tot}.

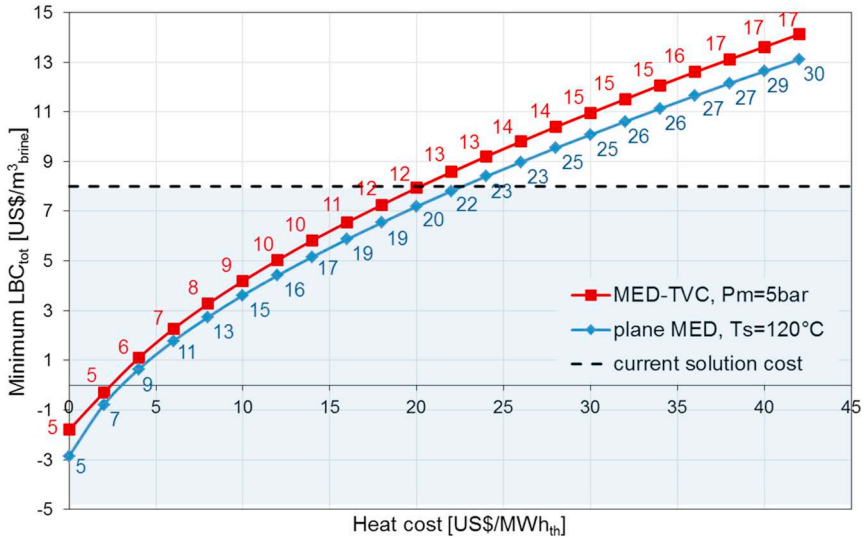

Fig. 10. Minimum LBC_{tot} as a function of the heat cost [US$/$MWh_{th}$] for a plane MED ($T_s$ = 120 °C) and for a MED-TVC (P_m = 5 bar). The labels correspond to the number of effects which minimize LBC_{tot}.

performed taking as a reference the configuration which minimizes LBC_{tot} and varying independently the main operating costs, i.e. electric energy cost, thermal energy cost and the water selling price, in a range within −100% and +100% of the corresponding costs in the reference case. The energy cost and the water price variations are not related to a variation in the quality of the supplied energy (e.g. the steam temperature) or of the produced water (since the distillate produced by the MED plant is supposed to be pure water in all cases). The analyses aim at investigating how much the single costs influence the overall LBC and which are the ranges of costs and prices that ensure the economic feasibility of the plant. These analyses are reported in Fig. 11 and in Fig. 12. Fig. 11 is relevant to Case 1, i.e. a plane MED with T_s = 100 °C and N = 13. In the reference case, the thermal energy cost is fixed equal to 10 US$/kWh$_{th}$. It is evident that the water selling price has the highest impact on LBC_{tot}, since its 100% variation leads to an opposite variation of LBC_{tot} of about 200%. The second term for relevance is the thermal energy cost, followed by the electric energy cost, as expected since the thermal energy is the main energy form required. Note that the percentage variation of LBC_{tot}, which corresponds to the current price of the salt solution (i.e. 8 US$/m^3) is also observable in Fig. 11 and in Fig. 12. One can observe that for the whole range of variation of the electric energy cost, the LBC_{tot} keeps lower than the threshold value, while a maximum increase of 80% of the thermal energy cost or a maximum decrease of around 50% of the water selling price could still ensure the competitiveness of the technology.

Conversely, the two charts in Fig. 12 are relevant to Case 2, i.e. for the plane MED T_s = 120 °C and N = 25, while for the MED-TVC P_m = 5 bar and N = 15. As it can be seen, the dependence of LBC_{tot} on the operating costs variation is much weaker than in the previous case, because these configurations are characterized by the prominence of the capital costs, as already mentioned. As a difference from Case 1, here the water selling price and the thermal energy cost have a comparable, yet opposite, role. Conversely, also in this case, the variation of the electric energy cost has a slight impact compared to the other two. Note that the variation of the minimum LBC_{tot} leading to LBC_{tot} equal to the current regeneration solution cost is negative, since in both cases the minimum LBC_{tot} is higher than 8 US$/m^3, even for the optimum configuration. In particular, a water selling price increase or a thermal

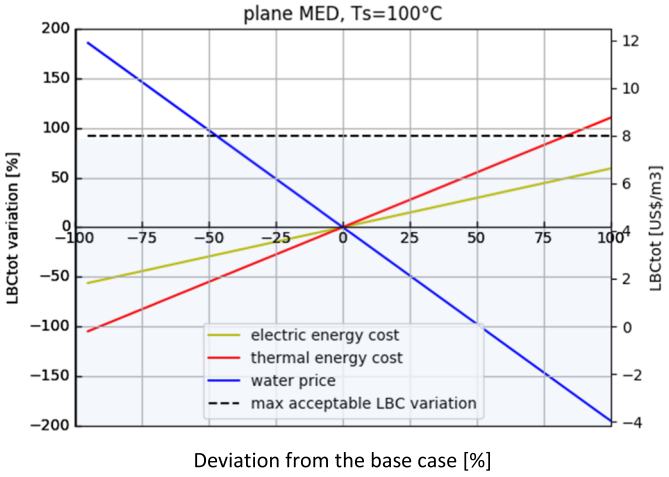

Fig. 11. Parametric analysis of the LBC_{tot} of a plane MED varying the main operating costs (thermal energy cost, electric energy cost and water selling price) with respect to the reference case: thermal energy cost = 10 US$/$MWh_{th}$, electric energy cost = 0.215 $/$kWh_{el}$, water price = 1 US$/m^3, N = 13.

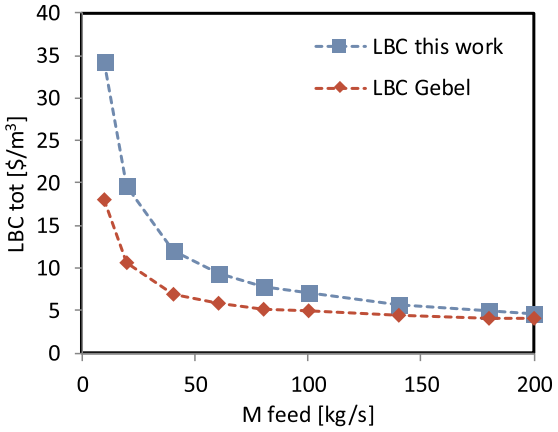

Fig. 13. Sensitivity analysis of the LBCtot as function of the feed flow rate (Mfeed [kg/s]) for the reference case 1: thermal energy cost = 10 US$/$MWh_{th}$, electric energy cost = 0.215 $/$kWh_{el}$, water price = 1 US$/m^3, N = 13.

energy cost decrease of the same amount, which is 25% for MED and around 30% for MED-TVC could make the technology competitive with the current purchase of fresh regenerant solution. Finally, in this last case, the charts for the plane MED and for the MED-TVC are almost identical, because in both systems the steam requirement was minimized by increasing the number of effects, in order to limit the role of the heat cost as much as possible.

The analyses reported in Results and discussion section are relevant to a certain size of the plant. In order to evaluate how much the size affects the overall costs, a sensitivity analysis is performed varying the feed flow rate, which determines the plant design and the relevant economic assessment. With this regard, the results given by the module costing technique adopted are compared with the results of another method (here referred as Gebel method) proposed in literature for thermal desalination plants [61,64]. As shown in Fig. 13, LBC_{tot} shows a decreasing trend as M_{feed} increases, as expected due to economy of scale. It is also remarkable that the two correlations show a very good agreement in the range of flow rates higher than 100 kg/s, while the values diverge at lower flow rates. This occurs because the present method intrinsically account for equipment size, thus being suitable also for very low scales (e.g. the correlation for the heat exchangers is valid down to a heat exchanger area equal to 10 m^2). Conversely, the Gebel method was developed for desalination plants of higher scale and, for this reason, the costs are allegedly underestimated at smaller scales.

5. Conclusions

In the present work, the feasibility to apply the Multi-Effect Distillation technology to the treatment of the IEX spent regenerant solution was investigated via a techno-economic analysis. The treatment aims at the recycling of the solution through a purification and a re-concentration stage. The re-concentration occurs in the MED plant, which has to concentrate the solution from 11,000 ppm up to 90,000 ppm. Because of this wide concentration range, the forward-feed arrangement was selected and the performances of a plane MED were compared with those of a MED-TVC system. An integrated techno-economic model was developed in order to assess the present process feasibility. To this aim, a novel performance indicator, named the total Levelized Brine Cost (LBC_{tot}), was proposed and provided as output by the model. This value, given by the combination of the capital and the operating costs and the revenue coming from the selling of the produced pure water, was compared with the current cost of the fresh regenerant solution (i.e. 8 US$/$m^3$). Two scenarios were investigated: in the first one, the steam was assumed to be supplied by a gas turbine co-generation system and its cost was a function of the pressure. In this scenario, the temperature of the steam in the plane MED and the

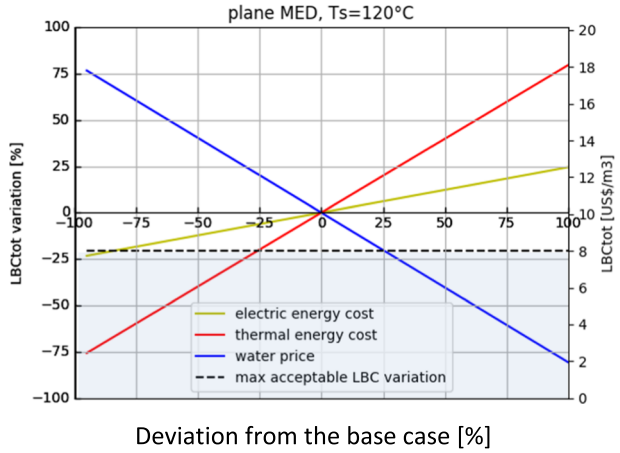

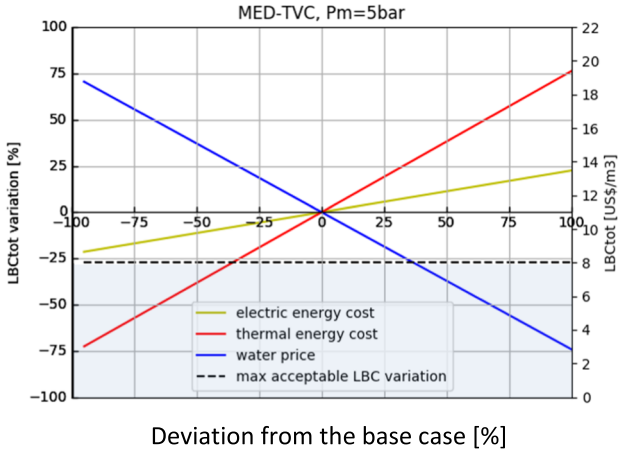

Fig. 12. Parametric analysis of the LBC_{tot} for plane MED (left) and for MED-TVC (right) varying the main operating costs (thermal energy cost, electric energy cost and water selling price) with respect to the reference case: thermal energy cost = 30 US$/$MWh_{th}$, electric energy cost = 0.215 $/$kWh_{el}$, water price = 1 US$/m^3, N_{MED} = 25, $N_{MED\text{-}TVC}$ = 15.

pressure of the motive steam in the MED-TVC were varied, at different number of effects. The results showed that producing the regenerant solution with the plane MED with high number of effects (> 12) and low T_s (< 80–90 °C) costs less than buying a fresh regenerant solution. This is not the case for all the analysis performed with the MED-TVC. The second scenario concerned the availability of waste heat, to be employed as the heating steam. Two different waste heat qualities and costs were tested: saturated steam at 1 bar and 10 US$/MWh$_{th}$ and saturated steam at 5 bar and 30 US$/MWh$_{th}$. Firstly, a sensitivity analysis varying the number of effects was performed for a plane MED and a MED-TVC (only in the case of higher-pressure waste steam). In the first case, the plane MED showed the lowest LBC_{tot} of around 4 US$/m^3 at 13 effects. Conversely, in the second case, the prominence of the thermal energy cost determined a net increase of the LBC_{tot} both for the MED and the MED-TVC and the lowest LBC_{tot} was relevant to a MED system with 25 effects and equal to around 10 US$/m^3. This means that only the employment of the waste heat at 1 bar and 10 US$/MWh$_{th}$ may allow the MED technology to be more convenient than the employment of fresh regenerant.

Moreover, a sensitivity analysis varying the thermal energy cost was performed, in order to evaluate the optimum number of effects (i.e. those that minimize the LBC_{tot}) at the different costs. It resulted that the plane MED reported always a lower LBC_{tot} with higher optimum number of effects in comparison to the MED-TVC. More important, the thermal energy cost of 20 US$/MWh$_{th}$ was identified as the threshold cost value below which the MED technology is economically more advantageous.

Finally, taking into account the optimum configuration (i.e. the optimum number of effects) in the two different cases, for the plane MED and the MED-TVC, a sensitivity analysis varying the thermal energy cost, the electric energy cost and the water selling price was carried out. In the case of the waste steam at lower pressure (first case), the pure water selling price had the highest impact in the definition of LBC_{tot}. Conversely, in the case of the higher waste steam pressure (second case), the water selling price and the thermal energy cost had a comparable role, but it should be pointed out that the overall impact of the operating cost was lower, because the optimum configuration was meant to minimize the operating costs, increasing the number of effects.

Overall, the present study results suggest that applying the MED technology instead of supplying fresh NaCl solution in every regeneration cycle may result not only into a net reduction of raw material consumption and of environmental pollution, but also into a cost saving in a wide range of conditions (both technical and economical). The next steps will address the economic optimization of the whole treatment chain reported in Fig. 1, taking into account the use of different reactants, operating conditions and different unit configurations (e.g. different crystallizers). The outcome of this analysis should boost future and more in-depth analysis of other treatment processes involving the production of saline solutions, also in other industrial sectors, such as the textile or the mining industry, aiming at increasing the level of sustainability of the industrial processes.

Nomenclature

N	number of effects [−]
M	mass flow rate [kg/s]
T	temperature [°C]
X	salinity [ppm]
P	pressure [bar]
A	heat exchanger area [m^2]
sA	specific area [m^2/(kg/s)]
sQ	specific thermal consumption [kJ/kg]
h	specific enthalpy [kJ/kg]
C_p	specific heat [kJ/(kg °C)]
U	overall heat transfer coefficient [kW/(m^2 °C)]
C_R	compression ratio [−]
ER	expansion ratio [−]
Ra	entrainment ratio [−]
C_{BM}	bare module cost [US$]
C_p^0	purchased cost of equipment [US$]
F_{BM}	bare module factor [−]
F_M	correction factor due to construction materials [−]
F_P	correction factor due to the working pressure [−]
C_{TM}	total module cost [US$]
i	discount rate [−]
n_{years}	depreciation period
CAPEX	annualized capital costs [US$/y]
OPEX	annualized operating costs [US$/y]

Greek letters

λ	latent heat [kJ/kg]
ΔT	temperature difference [°C]
α_{cond}	fraction of vapor condensed in the preheater

Subscripts

feed	feed entering into the first effect
dist	outlet distillate
brine	outlet brine
HX	heat exchanger
preh	preheater
cond	end-condenser
s	total steam
m	motive steam
vap	total vapor generated in the generic effect
d	vapor generated via evaporation
f,brine	vapor generated via the brine flash
fb	vapor generated in the flash box
b	brine solution generated in the generic effect
c	condensed pure water collected in the flash box
cw	cooling water
sw	salt water solution
liq	pure water in the liquid state
vap	pure water in the vapor state
n	last effect index
ev	entrained vapor
_real	fixed distillate flow rate to be produced
grav	gravitational component
acc	accelarational component
vsat	saturated vapor

Acronyms

IEX	Ion Exchange Resins
MED	Multi-Effect Distillation
TVC	thermo-vapor compressor
GOR	Gain Output Ratio
FF	Forward Feed
NF	nanofiltration
RO	Reverse Osmosis
LBC	Levelized Brine Cost [US$/m^3]
BPE	Boiling Point Elevation [°C]
DTML	temperature logarithmic mean
LCOW	Levelized Cost of Water [US$/m^3]
SCOW	Simplified Cost of Water [US$/m^3]
CHP	combined heat and power

Acknowledgements

This work was performed within the ZERO BRINE project (ZERO BRINE – Industrial Desalination – Resource Recovery – Circular

Economy), funded by the European Union's Horizon 2020 research and innovation programme under grant agreement No 730390. www.zerobrine.eu.

Appendix A. Supplementary data

Supplementary data to this article can be found online at https://doi.org/10.1016/j.desal.2019.01.011.

References

[1] R. Einav, K. Harussi, D. Perry, The footprint of the desalination processes on the environment, Desalination 152 (2002) 141–154.
[2] T. Mezher, H. Fath, Z. Abbas, A. Khaled, Techno-economic assessment and environmental impacts of desalination technologies, Desalination 266 (2011) 263–273.
[3] T. Bleninger, G.H. Jirka, Modelling and environmentally sound management of brine discharges from desalination plants, Desalination 221 (2008) 585–598.
[4] A. Giwa, S. Daer, I. Ahmed, P.R. Marpu, S.W. Hasan, Experimental investigation and artificial neural networks ANNs modeling of electrically-enhanced membrane bioreactor for wastewater treatment, J. Water Process Eng. 11 (2016) 88–97.
[5] J. Morillo, J. Usero, D. Rosado, H.E. Bakouri, A. Riaza, F.J. Bernaola, Comparative study of brine management technologies for desalination plants, Desalination 336 (2014) 32–49.
[6] A. Giwa, V. Dufour, F.A. Marzooqi, M.A. Kaabi, S.W. Hasan, Brine management methods: recent innovations and current status, Desalination 407 (2017) 1–23.
[7] A. Pérez-González, A.M. Urtiaga, R. Ibáñez, I. Ortiz, State of the art and review on the treatment technologies of water reverse osmosis concentrates, Water Res. 46 (2) (2012) 267–283.
[8] C.M. Tun, A.M. Groth, Sustainable integrated membrane contactor process for water reclamation, sodium sulfate salt and energy recovery from industrial effluent, Desalination 283 (2011) 187–192.
[9] M. Turek, P. Dydo, A. Surma, Zero discharge utilization of saline waters from 'Wesola' coal-mine, Desalination 185 (2005) 275–280.
[10] S.H. Zyoud, A.E. Al-Rawaifeh, H.Q. Shaheen, D. Fuchs-Hanusch, Benchmarking the scientific output of industrial wastewater research in Arab world by utilizing bibliometric techniques, Environ. Sci. Pollut. Res. 23 (2016) 10288–10300.
[11] D. Ariono, M. Purwasasmita, I.G. Wenten, Brine effluents: characteristics, environmental impacts and their handling, J. Eng. Technol. Sci. 48 (4) (2016) 367–387.
[12] E. Drioli, E. Curcio, G.D. Profio, F. Macedonio, A. Criscuoli, Integrating membrane contactor technology and pressure-driven membrane operations for seawater desalination energy, exergy and costs analysis, Chem. Eng. Res. Des. 84 (2006) 209–220.
[13] L. Bilińska, M. Gmurek, S. Ledakowicz, Textile wastewater treatment by AOPs for brine reuse, Process. Saf. Environ. Prot. 109 (2017) 420–428.
[14] S.D. Alexandratos, Ion-exchange resins: a retrospective from industrial and engineering chemistry research, Ind. Eng. Chem. Res. 48 (2009) 388–398.
[15] W.S. Miller, C.J. Castagna, A.W. Pieper, Understanding Ion-Exchange Resins for Water Treatment Systems, Water Technologies and Solutions, 1981.
[16] Lenntech, Ion Exchange Introduction, www.lenntech.com, (2008).
[17] S. Wadley, C.J. Brouckaert, L.A.D. Baddock, C.A. Buckley, Modelling of nanofiltration applied to the recovery of salt from waste brine at a sugar decolourisation plant, J. Membr. Sci. 102 (1995) 163–175.
[18] A. Kapoor, T. Viraraghavan, Nitrate removal from drinking water-review, J. Environ. Eng. 123 (1997).
[19] J.P. Van der Hoek, A. Klapwijk, Reduction of regeneration salt requirement and waste disposal in an ion exchange process for nitrate removal from ground water, Waste Manag. 9 (2008) 203–210.
[20] S.G. Lehman, M. Badruzzaman, S. Adham, D.J. Roberts, D.A. Clifford, Perchlorate and nitrate treatment by ion exchange integrated with biological brine treatment, Water Res. 42 (4) (2008) 969–976.
[21] J.K. Choe, A.M. Bergquist, S. Jeong, J.S. Guest, C.J. Werth, T.J. Strathmann, Performance and life cycle environmental benefits of recycling spent ion exchange brines by catalytic treatment of nitrate, Water Res. 80 (2015) 267–280.
[22] M. Kabsch-Korbutowicz, J. Wisniewski, S. Łakomska, A. Urbanowska, Application of UF, NF and ED in natural organic matter removal from ion-exchange spent regenerant brine, Desalination 280 (2011) 428–431.
[23] M. Gryta, K. Karakulski, M. Tomaszewska, A. Morawski, Treatment of effluents from the regeneration of ion exchangers using the MD process, Desalination 180 (2005) 173–180.
[24] EVIDES INDUSTRIEWATER, "Pers. Commun.."
[25] www.zerobrine.eu, "Zero Brine." n.d.
[26] A.M. Hassan, M.A.K. Al-Sofi, A.M. Al-Amoudi, A.T.M. Jamaluddin, A.M. Farooque, A. Rowaili, A.G.I. Dalvi, N.M. Kither, G.M. Mustafa, I.A.R. Al-Tisan, A new approach to membrane and thermal seawater desalination processes using nanofiltration membranes (part 1), Desalination 118 (1998) 35–51.
[27] A.A. Al-Hajouri, A.S. Al-Amoudi, A.M. Farooque, Long term experience in the operation of nanofiltration pretreatment unit for seawater desalination at SWCC SWRO plant, Desalin. Water Treat. 51 (7–9) (2013) 1861–1873.
[28] W.L. Ang, A.W. Mohammad, N. Hilal, C.P. Leo, A review on the applicability of integrated/hybrid membrane processes in water treatment and desalination plants, Desalination 363 (2015) 2–18.
[29] E. Drioli, F. Lagana, A. Criscuoli, G. Barbieri, Integrated membrane operations in desalination processes, Desalination 122 (1999) 141–145.
[30] A.E. Al-Rawajfeh, Influence of nanofiltration pretreatment on scale deposition in multi-stage flash thermal desalination plants, Therm. Sci. 15 (1) (2011) 55–65.
[31] A.E. Al-Rawaifeh, H.E.S. Fath, A.A. Mabrouk, Integrated salts precipitation and nano-filtration as pretreatment of multistage flash desalination system, Heat Tran. Eng. 33 (2011) 272–279.
[32] A.E. Al-Rawajfeh, Nanofiltration pretreatment as CO_2 deaerator of desalination feed: CO_2 release reduction in MSF distillers, Desalination 380 (2016) 12–17.
[33] A.E. Al-Rawajfeh, H. Glade, J. Ulrich, Scaling in multiple-effect distillers: the role of CO_2 release, Desalination 182 (2005) 209–219.
[34] Y.M. El-Sayed, R.S. Silver, K.S. Spiegler, A.D.K. Laird (Eds.), Principles of Desalination, 1980.
[35] R.K. Kamali, A. Abbassi, S.A.S. Vanini, A simulation model and parametric study of MED–TVC process, Desalination 235 (2009) 340–351.
[36] R.K. Kamali, A. Abbassi, S.A. Sadough Vanini, M.S. Avval, Thermodynamic design and parametric study of MED-TVC, Desalination 222 (2008) 596–604.
[37] A.O. Bin Amer, Development and optimization of ME-TVC desalination system, Desalination 249 (2009) 1315–1331.
[38] K.H. Mistry, M.A. Antar, V.J.H. Lienhard, An improved model for multiple effect distillation, Desalin. Water Treat. 51 (2013) 807–821.
[39] H. Sayyadi, A. Saffari, Thermoeconomic optimization of multi effect distillation desalination systems, Appl. Energy 87 (2010) 1122–1133.
[40] H. Sayyadi, A. Saffari, A. Mahmoodian, Various approaches in optimization of multi effects distillation desalination systems using a hybrid meta-heuristic optimization tool, Desalination 254 (2010) 138–148.
[41] I.J. Esfahani, A. Ataei, K.V. Shetty, T.S. Oh, J.H. Park, C.K. Yoo, Modeling and genetic algorithm-based multi-objective optimization of the MED-TVC desalination system, Desalination 292 (2012) 87–104.
[42] A. Piacentino, Application of advanced thermodynamics, thermoeconomics and exergy costing to a Multiple Effect Distillation plant: in-depth analysis of cost formation process, Desalination 371 (2015) 88–103.
[43] K.S. Pitzer, G. Mayorga, Thermodynamics of electrolytes. II. Activity and osmotic coefficients for strong electrolytes with one or both ions univalent, J. Phys. Chem. 77 (19) (1973) 2300–2308.
[44] M. Bialik, P. Sedin, H. Theliander, Boiling point rise calculations in sodium salt solutions, Ind. Eng. Chem. Res. 47 (2008) 1283–1287.
[45] ESDU, Condensation inside tubes: pressure drop in straight horizontal tubes, ESDU Series on Heat Transfer, 1993.
[46] S. Shen, Thermodynamic losses in multi-effect distillation process, Mater. Sci. Eng. 88 (2015) 1–12.
[47] H. El-Dessouky, I. Alatiqi, S. Bingulac, H. Ettouney, Steady-state analysis of the multiple effect evaporation desalination process, Chem. Eng. Technol. 21 (5) (1998) 437–451.
[48] A.S. Hassan, M.A. Darwish, Performance of thermal vapor compression, Desalination 335 (2014) 41–46.
[49] S. Lemmens, Cost engineering techniques and their applicability for cost estimation of organic Rankine cycle systems, Energies 9 (2016) 485.
[50] S. Georgiu, N. Shah, C.N. Markides, A thermo-economic analysis and comparison of pumped-thermal and liquidair electricity storage systems, Appl. Energy 226 (2018) 1119–1133.
[51] Z. Han, P. Li, X. Han, Z. Mei, Z. Wang, Thermo-economic performance analysis of a regenerative superheating organic Rankine cycle for waste heat recovery, Energies 10 (2017) 1593.
[52] R. Turton, R.C. Bailie, W.B. Whiting, J.A. Shaeiwitz, D. Bhattacharyya, Analysis, Synthesis and Design of Chemical Processes, Prentice Hall, 2012.
[53] M.Z. Stijepovic, P. Linke, Optimal waste heat recovery and reuse in industrial zones, Energy 36 (2011) 4019–4031.
[54] A.K. Kralj, P. Glavic, M. Krajnc, Waste heat integration between processes, Appl. Therm. Eng. 22 (2002) 1259–1269.
[55] O.A. Hamed, Overview of hybrid desalination systems — current status and future prospects, Desalination 186 (2005) 207–214.
[56] H.T. El-Dessouki, H.M. Ettouney, Fundamentals of Salt Water Desalination, Elsevier, 2002.
[57] T. Laukemann, R. Baten, T. Fichter, MENA Regional Water Outlook, Phase II, Desalination Using Renewable Energy, Fichtner and DLR, 2012.
[58] M. Micari, M. Moser, A. Cipollina, M. Bevacqua, A. Tamburini, B. Fuchs, G. Micale, Combined membrane and thermal desalination processes for the treatment of ion exchange resins spent brine, 13th Conference on Sustainable Development of Energy, Water and Environmental Systems, 2018.
[59] S. Shen, S. Zhou, Y. Yang, L. Yang, X. Liu, Study of steam parameters on the performance of a TVC-MED desalination plant, Desalin. Water Treat. 33 (2011) 300–308.
[60] M. Papapetrou, G. Micale, G. Zaragoza, G. Kosmadakis, Assessment of methodologies and data used to calculate desalination costs, Desalination 419 (2017) 8–19.
[61] J. Gebel, S. Yüce, An Engineer's Guide to Desalination, VBG PowerTech (2008).
[62] B. Ortega-Delgado, L. Garcia-Rodriguez, D.C. Alarcon-Padilla, Opportunities of improvement of the MED seawater desalination process by pretreatments allowing high-temperature operation, Desalin. Water Treat. 97 (2017) 94–108.
[63] M.H. Sharqawy, H. John, V. Lienhard, S.M. Zubair, The thermophysical properties of seawater: a review of existing correlations and data, Desalin. Water Treat. 16 (2010) 354–380.
[64] C. Sommariva, Desalination and Advanced Water Treatment-Economics and Financing, Balaban Desalination Publications, 2010.
[65] M. Moser, F. Trieb, J. Kern, Development of a flexible tool for the integrated techno-economic assessment of renewable desalination plants, Desalin. Water Treat. 76 (2017) 53–70.

Journal of Membrane Science 606 (2020) 118117

Contents lists available at ScienceDirect

Journal of Membrane Science

journal homepage: http://www.elsevier.com/locate/memsci

Experimental and theoretical characterization of commercial nanofiltration membranes for the treatment of ion exchange spent regenerant

M. Micari [a,*], D. Diamantidou [b], B. Heijman [c], M. Moser [a], A. Haidari [c], H. Spanjers [c], V. Bertsch [a,d]

[a] German Aerospace Center (DLR), Institute of Engineering Thermodynamics, Department of Energy System Analysis, Pfaffenwaldring 38-40, 70569, Stuttgart, Germany
[b] Lenntech, Water Treatment Solutions, Distributieweg 3, 2645 EG, Delfgauw, The Netherlands
[c] Delft University of Technology, Department of Water Management, Stevinweg 1, 2628 CN, Delft, The Netherlands
[d] Ruhr-Universität Bochum, Chair of Energy Systems and Energy Economics, Universitätsstr. 150, 44801, Bochum, Germany

ARTICLE INFO

Keywords:
Nanofiltration
Wastewater treatment
Membrane characterization
Ionic rejection
Water softening

ABSTRACT

This work presents a joint experimental and simulation campaign aimed at characterizing two nanofiltration membranes (TS80 and NF270) in the presence of a multi-ionic water solution simulating the spent regenerant of cationic ion exchange resins employed for water softening. We identified the membrane parameters, which allowed for predicting the performances through the Donnan Steric Pore Model with Dielectric Exclusion. A good agreement between model and experimental trends of rejection as a function of the applied pressure was observed (error < 15%). The analysis of trans-membrane fluxes and exclusion coefficients showed that dielectric exclusion was the crucial mechanism for the ionic partition. In fact, the lower pore dielectric constant found for TS80 justified the higher rejections to divalent cations with respect to NF270. Moreover, negative charge densities were found for both membranes, because of the high concentration of chloride ions in the feed, which likely adsorbed onto the membrane. However, it was observed that the experimental rejections did not change significantly with the feed pH. This result, in line with the minor role of the Donnan exclusion resulting from the model, suggested that the membrane performances were not much affected by the charge density at high feed ionic strengths (~1 M).

1. Introduction

Nanofiltration (NF) is a membrane technology widely used as a treatment process or as a pre-treatment step in various industrial sectors, for its ability to selectively separate multivalent ions from water solutions. The performances of NF membranes are intermediate between those of Reverse Osmosis (RO) and Ultrafiltration, their pore size is in the order of 1 nm [1] and their molecular weight cut-off (MWCO) typically ranges between 100 and 1000 Da [2,3]. NF membranes constitute selective barriers to remove various compounds, such as organics, inorganic metal ions and microorganisms, thanks to the combination of three exclusion mechanisms: steric, Donnan and dielectric exclusion [4]. Therefore, various industrial applications of NF are reported in the literature, which concern the concentration and separation of specific components or the fractionation of a liquid solution into two at different concentrations [5].

NF is widely used in environmental applications and in particular, for the production of high-quality water from groundwater, surface water and wastewater [6]. In this context, extensive research has been carried out on the removal of arsenic (As) and pesticides from groundwater [7,8] and on the removal of natural organic matter, dissolved organic carbon and heavy metals from surface water [9].

Furthermore, NF is used to treat various industrial wastewater effluents and in particular, to remove ions and compounds from waste streams. In the textile industry, for instance, NF is employed to treat the spent dyeing solution produced by the industrial process, to separate dye and salts (NaCl and Na_2SO_4) [10,11] and to remove the colour and enable the reuse of the permeate as fresh reactant solution [12–14]. Other applications of NF include the removal of heavy metals such as barium, strontium [15], cadmium, nickel [16] and lead [17] from wastewater, the removal of lithium from salt lake brines [18], the recovery of boric acid present in radioactive wastewater produced by nuclear power plants [19] and the treatment of acidic coal mine drainage [20].

* Corresponding author.
E-mail address: Marina.Micari@dlr.de (M. Micari).

https://doi.org/10.1016/j.memsci.2020.118117
Received 17 December 2019; Received in revised form 13 March 2020; Accepted 31 March 2020
Available online 5 April 2020

Within the food industry, NF is widely applied in the beverage industry for juice concentration [21] and in the dairy industry for lactose recovery and whey demineralization [22,23]. Another industrial food sector that uses membrane processes is the sugar industry, where NF is used to treat the sugar beet press water [24] or to purify and recover the brine produced by the regeneration of the ion exchange resins used for sugar decolourisation [25].

In the water industry, NF has found several applications in water softening and typically as a pre-treatment of desalination processes. The use of NF reduces the risks of scaling and fouling in downstream equipment by removing divalent ions and organic compounds, and it leads to a decrease in the osmotic pressure of the solution [26]. Different integrated systems have been evaluated, which present (i) the coupling of NF with other membrane desalination processes, such as RO or Electrodialysis and (ii) the coupling of NF with thermal processes, as multi-effect distillation or multi-stage flash (MSF) [27]. Concerning the integration of NF with membrane processes, the decrease of the osmotic pressure due to the NF pre-treatment corresponds to an enhancement of the available driving force at the same applied pressure and, consequently, to an increase of the water recovery in the desalination unit [28]. With this regard, the Saline Water Conversion Corporation proposed the employment of NF as a pre-treatment step for seawater RO and relevant works in the literature showed that the water recovery increases by 60% and the cost decreases by about 30% [29,30]. Regarding the integration of NF with thermal processes, the removal of divalent ions, and in particular of calcium and sulphate ions, allows for operating at higher temperatures in the desalination unit. Some authors presented NF-MSF systems with MSF operating at a Top Brine Temperature (TBT) of 120 °C without any scaling [31].

Another application of NF within the water industry concerns the treatment of the spent brine produced by the regeneration of ion exchange resins. Ion exchange resins are employed in various sectors and the composition of the spent solution produced by the regeneration of the resins depends on the application. For example, NF has been used to remove the Natural Organic Matter from the spent regenerant of the resins used in municipal wastewater purification [32] or to purify the effluent produced by the resins used for sugar decolourisation [5,25]. In this work, we deal with the effluent produced by the regeneration of resins employed for water softening. In particular, this work aims at characterizing NF membranes in the presence of an artificial brine simulating the industrial effluent, containing magnesium and calcium ions and sodium chloride. The characterization is fundamental to be able to simulate the NF unit within an integrated treatment system (chain). The treatment chain is devised in order to recover raw materials and recycle the purified effluent to the industrial process. In particular, NF is used as the first treatment step to separate magnesium and calcium from the NaCl-rich solution that can be concentrated and recycled to the regeneration process. Conversely, the concentrate solution produced by the NF, which includes magnesium and calcium ions, is further treated to produce crystals of $Ca(OH)_2$ and $Mg(OH)_2$. The latter is identified by the European Commission as a critical raw material [33]. Therefore, NF plays a crucial role in the brine treatment process, since a highly-performing separation step leads to an almost total recovery of the divalent ions in the form of hydroxides, which is crucial for the economic profitability of the process [34].

Given the importance of the NF unit in the treatment chain described above, it is fundamental to predict accurately the NF membrane behaviour by introducing suitable calibration parameters obtained via a full characterization of the membranes.

The characterization of NF membranes has been a very active field of research in the last twenty years. Membranes are typically described as charged porous structures, characterized by parameters including pore radius (r_p), active layer membrane thickness (δ_m), dielectric constant within the pores (ε_{pore}) and charge density (X_D). Various methods have been proposed in the literature for characterization purposes. Among these, direct methods include atomic force microscopy to estimate the pore size on the membrane surface [35] and membrane surface zeta potential, used as a measure of the Donnan potential [36]. Conversely, indirect methods consist in the combination of experimental measurements of neutral and ionic solutes rejection and model simulations [37].

As far as the modelling is concerned, the first model, proposed by Spiegler and Kedem, was based on irreversible thermodynamics and considered the membrane as a black box, where the membrane porosity was neglected [38]. Later, Tsuru et al. proposed a model based on the extended Nernst-Planck equation [39], which was followed by two other models: the space charge model and the Teorell-Meyer-Sievers model [40]. Finally, Bowen et al. proposed the Donnan Steric Pore Model (DSPM) that was able to predict the NF performances with neutral solutes and monovalent salts solutions [37]. Further development of the DSPM, i.e. the DSPM-DE, proposed by Vezzani and Bandini, consisted in the incorporation of the dielectric exclusion mechanism [41]. They showed that the prediction of rejections of divalent ions, such as Mg^{2+} and Ca^{2+}, significantly improves including this mechanism in the ionic partition.

Many works in the literature presented a characterization of NF membranes with different salt solutions, by performing ad hoc designed experiments coupled with DSPM-DE simulations. Most of the works focused on the characterization of commercial NF membranes in the presence of single salt solutions. Mohammad et al. investigated the impact of the solution concentration on the membrane charge density with NF90 membranes and six single salt solutions (NaCl, KCl, $MgCl_2$, Na_2SO_4, Na_2CO_3, $MgSO_4$) [42]. They found that the DSPM-DE can predict the water flux and the salt rejection also at high concentrations. Moreover, since dielectric exclusion and charge density are interconnected, in order to split the two effects, many authors focused on the identification of the isoelectric point, i.e. the pH at which the membrane charge is equal to zero. The identification of the isoelectric point allows first for estimating the dielectric constant and secondly for calculating the charge density, by fitting model simulations to rejection data. Following this procedure, Mazzoni et al. characterized Desal DK membranes with NaCl and $CaCl_2$ solutions [43] and Hussain et al. characterized two commercial membranes with NaCl solution and investigated how the membrane charge density is affected by different concentrations in the presence of NaCl and $MgCl_2$ solutions [44]. Kotrappanavar et al. reported membrane parameters for NF250 and NF300 with NaCl and $MgCl_2$ solutions at different concentrations, by using the Stokes-Einstein, Born effective and Pauli radii for the model simulations [45]. Oatley et al. focused on the identification of the isoelectric point with NaCl and KCl solutions and reported the dielectric constant within the pores found via model fitting for four different salt solutions with two membranes (NF270 and NF99HF) [3].

Only a few papers report a comprehensive characterization of membranes in the presence of multi-ionic solutions with experimental results and model fitting [4,46,47]. Roy et al. performed a fit of the DSPM-DE to experimental data to estimate the NF membrane parameters for seawater [48]. A study by Labban et al. reports the characterization of low-pressure hollow fibre membranes [49]. They identified the isoelectric point by varying the pH of a NaCl solution and they found the membrane charge density for three different mixtures via model fitting to rejection data: NaCl–$MgCl_2$; NaCl–Na_2SO_4 and artificial seawater.

Overall, the characterization of NF membrane is essential to predict the performances of the NF process in the presence of different solutions. Only a few studies have characterized NF membranes with multi-ionic mixtures, although these are much more common than the single salt solutions in industrial applications and nature. In addition, despite the large number of works on the assessment of NF performances for different industrial applications, very few focus on the investigation of the membrane parameters with industrial streams.

To fill this gap, we performed the characterization of commercial NF membranes in the presence of an artificial solution simulating the effluent produced by the regeneration of ion exchange resins employed

for water softening. The joint experimental and simulation campaign carried out with two commercial membranes, NF270 and TS80, allowed for estimating the membrane parameters (pore radius, membrane thickness, pore dielectric constant and charge density) with a water-salt mixture (hereby referred to as "brine") simulating the real wastewater effluent. Since the NF membrane properties strongly depend on the feed composition and concentration, performing a comprehensive characterization for the specific industrial application is very important. In fact, the results of the present work allow for predicting accurately the membrane behaviour in the industrial application and for designing bigger-scale NF plants, accounting for real membrane properties. Moreover, the same experimental campaign was performed with a ten-time diluted solution (hereby referred to as "diluted brine"), to assess the role of the concentration of the multi-ionic solutions on the membrane properties.

Overall, the analysis of the collected data with the two membranes and at two different concentrations gives insights into the exclusion and the trans-membrane transfer mechanisms that are responsible for the ionic rejections.

2. Theoretical background: the Donnan Steric Pore Model with Dielectric Exclusion

This section describes the theory about the transfer and exclusion mechanisms in NF membrane and reports the main equations of the Donnan Steric Pore Model with Dielectric Exclusion (DSPM-DE), which has been widely used in the literature to simulate NF membranes.

The DSPM-DE is based on the extended Nernst-Planck equation that defines the flux of ions through the membrane as the combination of three transport mechanisms, i.e. convection, diffusion, and electromigration [37]. Other fundamental equations are related to the equilibrium partition at the interfaces and the electro-neutrality condition. The partition of the ions at the solution-membrane interface depends on the ionic size (steric partition), the charge of the ions and of the membrane (Donnan partition) and the dielectric constant within the pores, that determines the solvation energy (dielectric partition) [50]. These exclusion mechanisms have been widely investigated in literature and many efforts have been dedicated to identifying the impact of the membrane parameters (pore radius, membrane thickness, pore dielectric constant and charge density) on the performance. In particular, many studies focused on the estimation of the pore dielectric constant and the charge density, which are responsible for the dielectric exclusion and the Donnan exclusion, respectively [47,51]. The dielectric exclusion is mostly caused by the different solvent structure in the narrow pores, which is responsible for the increase of the ion solvation energy within the pores. The charge density depends on various mechanisms that take place once the membrane comes in contact with an aqueous solution, such as the dissociation of the functional groups and the adsorption of ions from the solution onto the membrane [52]. Experimental evidence showed that the two parameters are dependent and that both are a function of the solution composition [43]. The dielectric constant of a membrane may significantly change when varying the feed composition: Oatley et al. found similar values of dielectric constant in the presence of solutions of NaCl, KCl and Na_2SO_4 (between 31 and 35 for Desal DK membrane and between 38 and 42 for NF270) and higher values with $MgSO_4$ solutions (46.6 for Desal DK membrane and 65.1 for NF270) [3,50]. Moreover, the ions present in the solution have a crucial role in the charge density: the ions can adsorb onto the membrane surface and can affect the charge significantly, depending on their concentration. For example, it was found that high concentrations of divalent cations may cause an increase of membrane charge, which can turn into positive, even in presence of negatively charged functional groups [52–54].

2.1. Mathematical formulation of the DSPM-DE

The extended Nernst-Planck equation, reported below (equation (1)), defines the flux of each ion through the membrane.

$$j_i = J_v C_i^p = -D_{i,pore}\frac{dC_i^m}{dy} - z_i C_i^m D_{i,pore}\frac{F}{RT}\frac{d\psi}{dy} + k_{i,c} C_i^m J_v \quad (1)$$

The flux j_i of each ion *i* through the membrane, which is equal to the product of the water flux J_v and the concentration of the ion *i* in the permeate solution C^p_i, is given by the sum of three terms. The first (diffusive flux) depends on the diffusion coefficient of the ion inside the pore ($D_{i,pore}$) and the concentration C^m_i change within the membrane itself (y-axis). The second (migrative flux) depends on the potential profile (ψ) along the membrane thickness, the diffusion coefficient of the ion inside the pore ($D_{i,pore}$), the ionic concentration C^m_i, the ion valence (z_i), the Faraday (F) and the ideal gas constants (R) and the temperature (T). Finally, the third (convective flux) is a function of the convective coefficient of the ions inside the pores ($k_{i,c}$), the water flux and the ionic concentration inside the membrane. Fig. 1 depicts the water and the ionic fluxes through the membrane and typical profiles of concentration and electric potential.

The water flux through the membrane can be expressed as a function of the net pressure difference ΔP, the pore radius r_p, the membrane thickness δ_m and the solution dynamic viscosity η, according to the Hagen-Poiseuille equation (equation (2)). The net pressure difference ΔP is given by the difference of the applied pressures in the feed-concentrate and in the permeate channel minus the osmotic pressure difference $\Delta\Pi$, as shown in equation (3).

$$J_v = \frac{\Delta P\, r_p^{\,2}}{8\,\eta\,\delta_m} \quad (2)$$

$$\Delta P = \left(P^f - P^p\right) - \Delta\Pi = \left(P^f - P^p\right) - RT\sum_i \left(C^{bm}{}_i - C^p{}_i\right) \quad (3)$$

The diffusion and the convective coefficients require a specific definition, given the size of the pores where these transports occur. Therefore, "hindered" or "restricted" transport can be described through the introduction of the hindrance factors for diffusion and for convection, $k_{i,d}$ and $k_{i,c}$ [55].

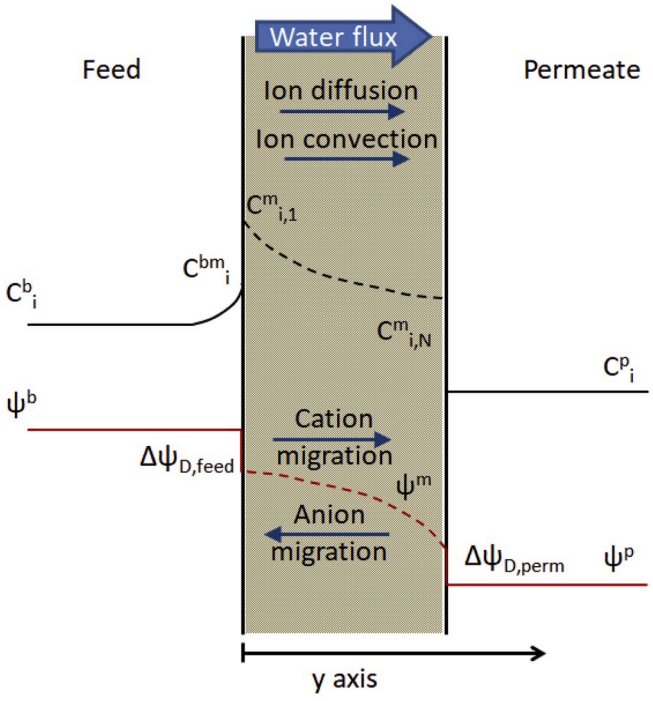

Fig. 1. Schematic of the NF membrane, including the indication of the ionic and water fluxes and exemplary ionic concentration and potential profiles.

$$D_{i,pore} = k_{i,d} D_{i,\infty} \tag{4}$$

$$k_{i,d} = \frac{1}{\varphi_i}\left(1 + \tfrac{9}{8}\,\lambda_i\, ln(\lambda_i) - 1.56034\,\lambda_i + 0.528155\,\lambda_i^2 + 1.91521\,\lambda_i^3 - 2.81903\,\lambda_i^4 + 0.270788\,\lambda_i^5 + 1.10115\,\lambda_i^6 - 0.435933\,\lambda_i^7\right) \tag{5}$$

$$k_{i,c} = \frac{1 + 3.867\,\lambda_i - 1.907\,\lambda_i{}^2 - 0.834\,\lambda_i{}^3}{1 + 1.867\,\lambda_i - 0.741\,\lambda_i{}^2} \tag{6}$$

The coefficients $k_{i,d}$ and $k_{i,c}$ are functions of the parameter λ_i, which is given by the ratio between the ion Stokes radius and the pore radius.

Concerning the solution-membrane interface, the equilibrium partition can be described by equation (7) for the feed-membrane interface and by equation (8) for the permeate-membrane interface.

$$\frac{\gamma^m{}_{i,1} C^m{}_{i,1}}{\gamma^{bm}{}_i C^{bm}{}_i} = \varphi_i \varphi_{Bi} \exp\left(-\frac{z_i F}{RT}\Delta\psi_{D,feed}\right) \tag{7}$$

$$\frac{\gamma^m{}_{i,N} C^m{}_{i,N}}{\gamma^p{}_i C^p{}_1} = \varphi_i \varphi_{Bi} \exp\left(-\frac{z_i F}{RT}\Delta\psi_{D,perm}\right) \tag{8}$$

In equation (7), the ratio between the activity of the ion just inside the membrane on the feed-concentrate side (index 1) and just outside the membrane in the feed solution (index bm) is proportional to the steric coefficient φ_i, the Born solvation coefficient φ_{Bi} and the Donnan term. The latter depends on the Donnan potential at the solution membrane interface $\Delta\psi_{D,feed}$ [56]. The same can be said for equation (8), where the ratio is between the activity of the ions just inside the membrane on the permeate side (index N) and the activity in the permeate solution. In the permeate solution, the concentration polarization is negligible, thus there is no need to define a concentration of the permeate solution just outside the membrane (as $C^{bm}{}_i$).

The activity coefficients are calculated via the Davies equations, given in equations (9) and (10) [57].

$$\log \gamma_i = -A\, z_i{}^2\left(\frac{\sqrt{I}}{1+\sqrt{I}} - 0.3\, I\right) \tag{9}$$

$$A = \frac{e_0{}^3\, N_A{}^{1/2}}{\ln(10)\, 4\pi\, \sqrt{2}\, (\varepsilon\, k_B T)^{3/2}} \tag{10}$$

The exclusion coefficients are calculated as below. The steric coefficient depends on the parameter λ_i, whereas the Born solvation coefficient depends on the solvation energy barrier, calculated using the Born model as a function of the dielectric constants in the pore (ε_{pore}) and in the solution bulk (ε_b) [58].

$$\varphi_i = (1 - \lambda_i)^2 \tag{11}$$

$$\varphi_{Bi} = \exp\left(-\frac{\Delta W_i}{k_B T}\right) \tag{12}$$

$$\Delta W_i = \frac{z_i{}^2 e_0{}^2}{8\pi\varepsilon_0 r_i}\left(\frac{1}{\varepsilon_{pore}} - \frac{1}{\varepsilon_b}\right) \tag{13}$$

The concentration at the feed membrane interface depends on the concentration polarization that consists in a concentration gradient between bulk and membrane interface. This gradient is due to the fact that the ions would have different rates in crossing the membrane and in moving from the bulk to the membrane. The concentration polarization leads typically to higher concentrations of the ions at the membrane interface that contribute to decreasing the permeate flux and the ionic rejections. This phenomenon can be quantified by equating the ion flux through the membrane to the one from the bulk to the membrane interface, as in equation (14) [59].

$$j_i = -k'^b_{c,i}\left(C^{bm}{}_i - C^b{}_i\right) + J_v C^{bm}{}_i - z_i C^{bm}{}_i D_{i,\infty}\frac{F}{RT}\xi \tag{14}$$

The mass transfer coefficient (equation (15)) is estimated using the equation given for spiral wound membranes by Senthilmurugan et al. and is corrected using the coefficient Ξ, which accounts for the "suction effect" due to the membrane permeation [60].

$$k'^b_{c,i} = k^b_{c,i}\,\Xi = k^b_{c,i}\left[\frac{J_v}{k^b_{c,i}} + \left(1 + 0.26\left(\frac{J_v}{k^b_{c,i}}\right)^{1.4}\right)^{-1.7}\right] \tag{15}$$

$$k^b_{c,i} = 0.753\left(\frac{\eta_{mix}}{2-\eta_{mix}}\right)^{1/2}\left(\frac{D_{i,\infty}}{h_f}\right) Sc^{-1/6}\left(\frac{Pe_i h_f}{L_{mix}}\right)^{1/2} \tag{16}$$

In equation (16), η_{mix} is the mixing efficiency of the net of the spacer, h_f is the height of the feed channel, L_{mix} is the mixing length of the spacer, Pe and Sc are the Peclet and the Schmidt adimensional numbers, respectively.

Furthermore, other conditions to be fulfilled are the electroneutrality at the feed-membrane interface, in the permeate solution and inside the membrane. These conditions are given in equations (17)–(19).

$$\sum_i z_i C^{bm}{}_i = 0 \tag{17}$$

$$\sum_i z_i C^p{}_i = 0 \tag{18}$$

$$\sum_i z_i C^m{}_{i,j} + X_d = 0 \tag{19}$$

The system of equations was solved following the implementation proposed by Geraldes et al. [61]. The equations were discretized within the membrane and linearized, by defining linear coefficients containing guess values of electric potential and ionic concentrations. The linear system of equations was solved simultaneously in Python via the *LAPACK routine_gesv*, then the coefficients of the linear system were recalculated and the updated system was solved again. The iterative procedure was repeated until all conditions were fulfilled and the residuals were below 10^{-4} [61].

3. Materials and methods: experiments for membrane characterization

This section focuses on the description of the experimental activities performed for characterization purposes. The experiments are schematically reported in Table 1.

Membrane filtration experiments were carried out in a laboratory-scale flat sheet cross-flow SEPA-CFII cell by Osmonics, depicted in Fig. 2. The membrane, with an active area of 0.014 m^2, was placed into the membrane housing that was kept pressurized during the experiments. The module contained a piston feed pump, pressure indicators on the feed and the concentrate side, and a regulation needle valve for the concentrate stream, which was manually controlled to adjust the transmembrane pressure. The permeate and the concentrate flows were measured by mass flowmeters (Mini Cori-Flow and Gems Sensors, respectively). Two different NF membranes were tested in this study: (i) NF270 (DOW Filmtec, USA) and (ii) TS80 (Trisep Microdyn Nadir, Germany). NF270 has been widely used in the literature and in industrial applications for the removal of divalent ions. Therefore, it has been chosen as a reference membrane, because the availability of published data relevant to NF270 membrane allowed for assessing the validity of our experimental methods [62]. Conversely, TS80 is much less common and, from a preliminary comparison of various membranes, it resulted particularly suitable to divalent cations separation. Both membranes are made of a thin polyamide active layer and a polysulfone support layer but they belong to different categories in terms of membrane chemistry. NF270 is a semi-aromatic membrane (PIP-TMC), whereas TS80 (MPD-TMC) is a fully aromatic membrane. The membranes were wetted

Table 1
Experimental activities performed in the present work.

Experiment	Operating solution	Variable input	Measured output	Membrane parameter to estimate
Permeability test (Sections 3.1, 4.1)	Pure water	Trans-membrane pressure	Permeate flux	Pore radius and active layer membrane thickness
Organics rejection (Sections 3.1, 4.1)	Solutions of organics	Trans-membrane pressure	Permeate concentration	
Ionic rejection varying pH (Sections 3.2, 4.2)	Feed solution (brine and diluted brine)	Solution pH	Permeate concentration	Pore dielectric constant and charge density
Ionic rejection varying permeate flux (Sections 3.3, 4.3)	Feed solution (brine and diluted brine)	Permeate flux	Permeate concentration	

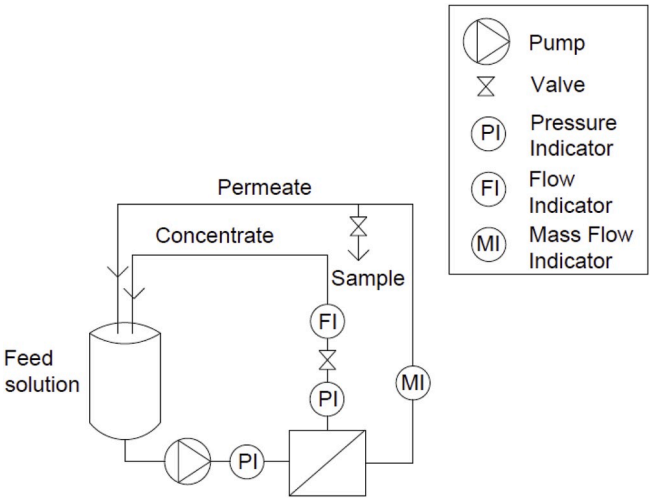

Fig. 2. Scheme of the laboratory-scale flat sheet cross-flow cell SEPA-CFII by Osmonics, used for the experiments.

and kept immersed in demineralized water for 24 h prior to each experiment. The feed water temperature was monitored by a thermometer and remained constant at 21 °C during the experiments through a cooling spiral that was immersed in the feed tank. Before each experiment, the membrane was pressurized for 2 h at a constant flux and the permeate and the concentrate streams were mixed with the feed solution. After this stabilization period, the solutions were circulated and samples were collected after 30 min and 1 h. The cross-flow velocity was 1 m/s, in order to diminish the effect of concentration polarization and to ensure the equality between observed and real ion rejections. The ion rejection was calculated using equation (20) and the experiments were repeated twice to validate the data.

$$R_i = 1 - \frac{C^p{}_i}{C^f{}_i} \tag{20}$$

3.1. Permeability test and organics rejection

Permeability test and organics rejection measurement are fundamental to evaluate membrane pore radius and active layer membrane thickness, which are closely related.

3.1.1. Procedure to estimate the pore radius

The calculation of the pore radius of the two membranes was performed by testing three neutral solutes (glycerol, glucose and sucrose) as it was proposed by Bowen et al. and then applied by many authors [37, 63]. Low concentrations of the neutral solutes (200 mg/l) and relatively high cross-flow velocity (1 m/s) were used to minimize the effect of concentration polarization and the difference between the observed and the real rejections. Four different permeate fluxes were tested and used for model calibration: 35, 70, 105 and 170 L/(m^{2}h). The experimental rejection of the single organic solutions was calculated from Total Organic Carbon (TOC) analysis of the permeate and the feed samples by using the TOC-V_{CPH} analyser and the ASI-V autosampler (Shimadzu, Japan).

The trans-membrane flux of the neutral solutes is based only on diffusion and convection and their theoretical rejection is due to steric interactions with the pore wall. The values of organics rejection were calculated as functions of the pore radius, according to equation (21) [50]. Thus, the pore radius of the membrane was calculated by minimizing the sum of squared errors (SSE) between the calculated and the experimental ionic rejections, as reported in equation (23). Then, an average pore radius based on the fitting values found for the three employed neutral solutes (i.e. glycerol, glucose and sucrose) was estimated. The physical properties of the three organics are summarized in Table 2.

$$R_i = 1 - \frac{C^p{}_i}{C^f{}_{i,w}} = 1 - \frac{k_{i,c}\varphi_i}{1 - [1 - k_{i,c}\varphi_i]\exp(-Pe_i)} \tag{21}$$

$$Pe_i = \frac{k_{i,c}J_v\delta_m}{D_{i,p}} = \frac{k_{i,c}r_p{}^2}{8\eta D_{i,p}}\Delta P \tag{22}$$

$$SSE = \sum_i \left(R_{i,exp} - R_{i,calc}\right)^2 \tag{23}$$

The neutral solute rejection increases when the applied pressure increases because convection becomes the primary transport mechanism and the permeate stream is less concentrated. A plateau is reached when any further increase in the applied pressure does not contribute to an increase in the uncharged solute rejection. In fact, the rejection remains constant because the effect of higher convective fluxes is counterbalanced by an increase of concentration polarization and, consequently, of the solute transport to the permeate side [49]. This rejection, namely the limiting rejection (R_{lim}), is defined in equation (24) and it is obtained when the Peclet number (Pe) reaches very high values.

$$R_{i,lim} = 1 - k_{i,c}\varphi_i \tag{24}$$

In this study, high permeate fluxes were tested in order to reach the

Table 2
Properties of the neutral solutes and the ions used for the experiments [49].

Solute	MW (g/mol)	r_i (nm)	$D_{i,oo}$ (x 10^{-9} m^2 s^{-1})
Glycerol	92	0.260	0.95
Glucose	180	0.365	0.69
Sucrose	342	0.471	0.52
Na^+	23	0.184	1.33
Cl^-	35	0.121	2.03
Mg^{2+}	24	0.347	0.706
Ca^{2+}	40	0.309	0.792

limiting rejection of the solutes.

3.1.2. Procedure to estimate the active layer membrane thickness

The active layer membrane thickness (δ_m) is defined as the ratio between the effective thickness and the porosity [37] and it is calculated via membrane permeability experiments once the pore radius is known. In this study, the membrane permeability was measured by filtering demineralized water at different transmembrane pressures and by monitoring the permeate flux. A linear trend between the applied pressure and the permeate flux was observed in membrane filtration experiments [44]. The effective membrane thickness was calculated by the Hagen-Poiseuille equation (see equation (2) in section 2) and by assuming that the pore radius of the membrane is cylindrical and uniform [49].

3.2. Ionic rejection varying pH

To assess the behaviour of the membranes in the presence of salt mixtures, we measured the ionic rejections at different values of feed solution pH.

For these experiments, a brine given by the mixture of three salts (NaCl, $CaCl_2{\cdot}2H_2O$, and $MgCl_2{\cdot}6H_2O$), simulating the real wastewater produced by the ion exchange columns, was used as feed solution. Additional experiments were conducted to investigate the influence of the ionic strength on the exclusion effects, by diluting the artificial brine ten times. The properties of the ions (Stokes radius and bulk diffusivity) are reported in Table 2 and the concentrations of the brine and the diluted brine are reported in Table 3. The pH of the feed solution was varied between 3 and 9 with the addition of NaOH and HCl and it was measured using a multi-parameter portable meter (Multi 3510 IDS) with a WTW pH electrode. Permeate fluxes of 15, 30 and 45 L/(m^2h) were tested for each membrane (TS80 and NF270), solution (brine and diluted brine) and pH. Samples were taken after the stabilization period, and the electrical conductivity was measured with a WTW EC probe to check the stability of the permeate water quality and the representativeness of the sample. The samples were analysed by Inductively Coupled Plasma Mass Spectrometry (ICP-MS) and by Inductively Coupled Plasma - Optical Emission Spectrometry (ICP-OES).

3.3. Ionic rejection varying permeate flux: estimation of pore dielectric constant and membrane charge density

For the estimation of the pore dielectric constant and the charge density of each membrane, a curve fitting was performed by minimizing the sum of squared errors (SSE) between the measured and the calculated rejection of the feed solution (defined in equation (25)).

$$f_{obj}(\varepsilon_{pore},\ X_d) = SSE = \sum_{fluxes}\sum_{i}\left(R_{i,exp} - R_{i,calc}\right)^2 \tag{25}$$

For this analysis, membrane experiments were conducted at four fluxes (15, 30, 45 and 70 L/(m^2h)) and by using the salt mixtures of Table 3. The sampling and ion analysis procedures were the same as described in section 3.2.

The range of fluxes was selected in order to cover a wide range of operating conditions and in particular pressures since these fluxes correspond to feed pressures from 1 to 32 bar. Although typical fluxes for long-run operations with wastewater do not exceed 25 L/(m^2h) [64], we performed experiments also at higher fluxes to obtain a broader set of data for model calibration.

In literature, the estimation of the pore dielectric constant has been often performed via the least-square fitting of the ionic rejections at the isoelectric point, i.e. the pH at which the rejection reaches a minimum because the charge density equals zero and the steric and the dielectric effects are the only exclusion mechanisms. In the presence of multi-component systems, the isoelectric point often corresponds to the pH range where a net variation of the ionic rejection trends occurs, because this is likely due to a switch in the membrane charge [62].

In the present work, we also implemented this second method, to confirm the findings of the first method. The pore dielectric constant was assessed by minimizing the error between the ionic rejections calculated by fixing the charge density to zero and the values measured at the pH range corresponding to a net variation of the trend. Once the pore dielectric constant was known, the membrane charge density was estimated by minimizing the error between the calculated and the measured ionic rejections in the presence of the feed solution.

Table 3
Concentrations of the artificial brine and the diluted brine.

Solute	Ion concentration (ppm)		Ion concentration (mol/m^3)	
	Brine	Diluted brine	Brine	Diluted brine
Sodium	4030	403	175	17.5
Calcium	7640	764	191	19.1
Magnesium	1260	126	52.5	5.25
Chloride	23,200	2320	662	66.2

4. Results and discussion

In this section, the results of the experimental and simulation campaigns are reported, with the aim to present a full characterization of two commercial NF membranes with a salt mixture (brine) analogous to the wastewater produced by ion exchange resins. Firstly, we show the results of the permeability tests together with the values of rejections found for organic solutes, which allow for estimating the pore radius and the active layer membrane thickness. Secondly, we present the experimental values of rejection of the different ions when the solution pH is varied, to assess how the ionic rejections are affected by the pH and, consequently, by the membrane charge density. Thirdly, we report the ionic rejections at different permeate fluxes, which we used to calculate the pore dielectric constant and membrane charge density, through a least-square fitting of the model to the experimental results.

4.1. Permeability test and organics rejection: estimation of pore radius and active layer membrane thickness

The results of the permeability test for NF270 and TS80 are depicted in Fig. 3. A linear relationship between water flux and applied pressure was found, as expected, and the slope, corresponding to the membrane

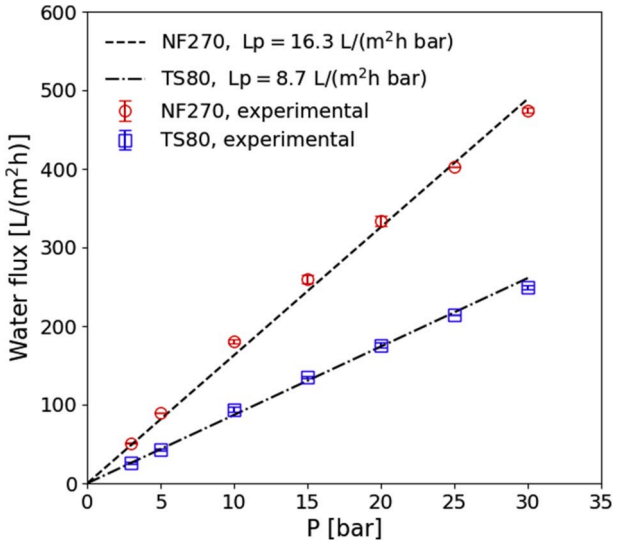

Fig. 3. Experimental water flux through the membrane [L/(m^2h)] vs. the applied pressure [bar] for NF270 and TS80.

permeability, resulted equal to 16.3 L/(m^2h)/bar for NF270 and 8.7 L/(m^2h)/bar for TS80. The two membranes showed very different values of permeability, which suggested that the steric exclusion mechanism was more effective in TS80 and this might lead to higher solute rejections.

The rejection values found for glycerol, glucose, and sucrose with NF270 and TS80 are depicted in Fig. 4. Solutes with lower Stokes radius showed lower rejection with both membranes. Moreover, the rejection of glucose and sucrose became constant already at low pressure, meaning that these solutes reached the limiting rejection. Conversely, almost constant rejection of glycerol was observed only with TS80 at the highest investigated pressures. Regarding the fitting of the theoretical curves to the experimental data, different pore radii were found for the different solutes and the lower the solute radius, the lower the fitting pore radius. This finding was already reported by previous authors, who found that the solutes experience different pore sizes and different membrane thicknesses depending on their size because the network of pores is more complex and tortuous than how it is usually represented [65]. In particular, smaller solutes such as glycerol have longer paths within the membrane and are able to detect smaller pore radii [66]. Therefore, to obtain a uniform pore size, the pore radius was estimated for each membrane as the average of the radii found with the different solutes [67]. In this way, we found a pore radius of 0.507 nm for NF270 and 0.488 nm for TS80. The pore radius of NF270 is in agreement with other studies in literature, which report values in the range of 0.43–0.54 nm [3,67,68]. As already predicted by the permeability test, the NF270 membrane showed a larger pore radius than the TS80 and this was already highlighted by Wadekar et al., who found that semi-aromatic membranes as NF270 show larger effective pore sizes in comparison with fully aromatic membranes as TS80 [54]. The pore radii were slightly higher than the sucrose radius, whose rejection was equal to or higher than 90% in both membranes. Similarly, Labban et al. found rejection values of sucrose of 93% and a pore radius of 0.5 nm [49].

To assess the validity of assuming an average pore radius for each membrane, Fig. 5 shows the comparison between the experimental limiting rejection values and the theoretical curve, defined in equation (24). Since glycerol did not reach the limiting rejection within the investigated pressure range, the value of limiting rejection used in Fig. 5 corresponds to the plateau reported in Fig. 4. A good agreement was found for both membranes between theoretical and experimental values, with errors lower than 11%. Therefore, we can conclude that the membranes could be reliably modelled, assuming the aforementioned average pore radii.

Once the pore radius and the permeability (Fig. 3) were assessed for each membrane, the active layer membrane thickness was estimated, using the Hagen-Poiseuille equation (equation (2)). The membrane thickness obtained was equal to 0.8 μm for NF270 and 1.38 μm for TS80.

4.2. Ionic rejections varying the solution pH

To assess the membrane behaviour with the brine and the diluted brine and to estimate the other two membrane parameters (pore dielectric constant and membrane charge density), we measured the ionic rejections at different solution pH values and permeate fluxes. The data collected at different pH values are depicted in Fig. 6.

Firstly, the ions showed different values of rejections and, in particular, the order of rejection, in any case, was $R_{Mg} > R_{Ca} > R_{Cl} > R_{Na}$. This is because NF membranes are able to selectively separate ions on the basis of their Stokes radius, diffusivity, and valence. In all cases, the rejection rate of divalent ions was higher, as predicted by the values of Stokes radius and diffusivity reported in Table 2. Moreover, the rejections found with TS80 are higher than the ones with NF270 and this is in agreement with the lower pore radius and higher active layer membrane thickness found in section 4.1. A negative rejection of Na^+ was observed in the case of NF270 membrane, whereas positive values were found with TS80. In the first case, the higher transmembrane flux of Cl^- led to higher fluxes of the most mobile cation, i.e. Na^+, which had to compensate for the negative charge on the permeate side, since the divalent ions were more screened by the membrane [49].

Secondly, relatively flat trends of ionic rejections vs. the pH were found with both brine and diluted brine and for both membranes. Therefore, even if the membrane charge density changed with pH, the system did not seem to be significantly affected by these variations. In general, this finding suggests that, at the investigated concentrations, the Donnan exclusion mechanism does not give a significant contribution to the ionic rejection. This is in line with other studies that reported a flat membrane potential for solutions with ionic strengths higher than 0.1 M [4,54]. However, the semi-aromatic membrane (NF270) showed a more enhanced variation with pH in comparison with the fully aromatic membrane (TS80). In particular, while the rejections of Ca^{2+} and Mg^{2+} were almost constant with the TS80 membrane, they were more sensitive to pH variation with NF270. This can be explained because semi-aromatic membranes present more fixed charges on their surface in comparison with multi-aromatic membranes, thus they may be more affected by the Donnan potential [54]. Note that NF270 showed a significant change in the ionic rejection when the pH was between 4 and 5, while the profiles of ionic rejection with TS80, especially the Na^+ rejection, changed their slope for pH values between 5 and 6. In particular, with NF270, Ca^{2+} reported a more evident decrease in rejection when the pH increased, whereas Mg^{2+} was more stable. In fact, Mg^{2+} has a higher Stokes radius and can be more screened by the steric effect. Conversely, Ca^{2+} can be more influenced by the Donnan exclusion, especially at lower pH values, since the membrane is more positively charged [52]. For pH higher than 5 for NF270 and higher than 6 for TS80, the ionic rejections were almost constant. Furthermore, the lower ionic rejections found with NF270 at the highest investigated pH

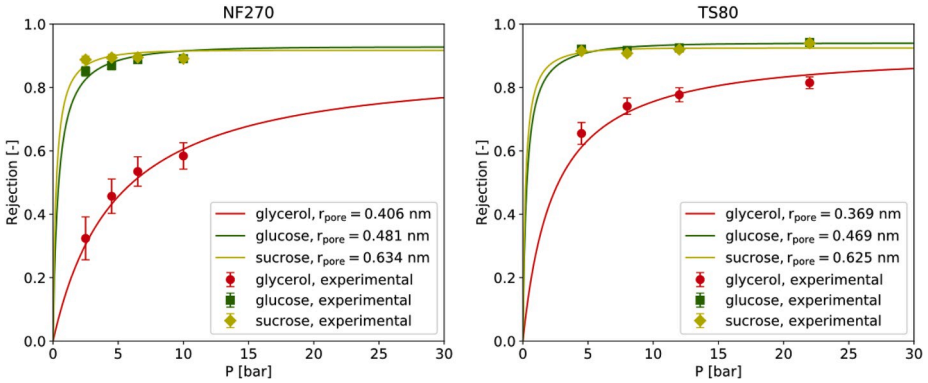

Fig. 4. Experimental rejections of neutral solutes at different applied pressures and model fitting curves at different pore radius for NF270 membrane (left) and TS80 membrane (right).

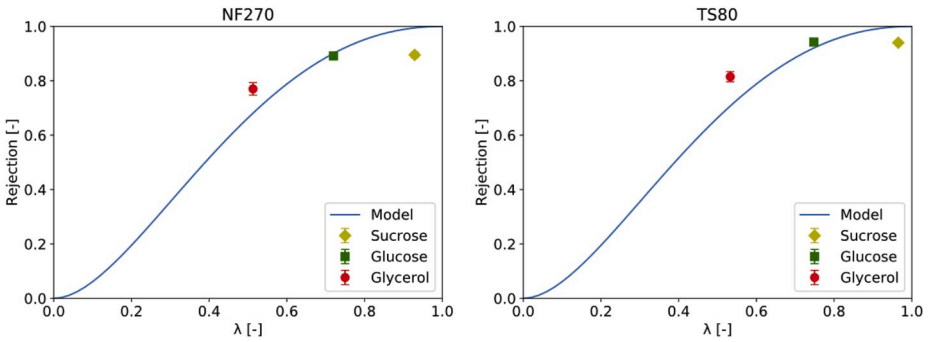

Fig. 5. Experimental values of limiting rejection of the three neutral solutes vs. the lambda ratio (solute Stokes radius divided by the pore radius) and the theoretical curve of limiting rejection vs. the lambda ratio for NF270 (left) and for TS80 (right).

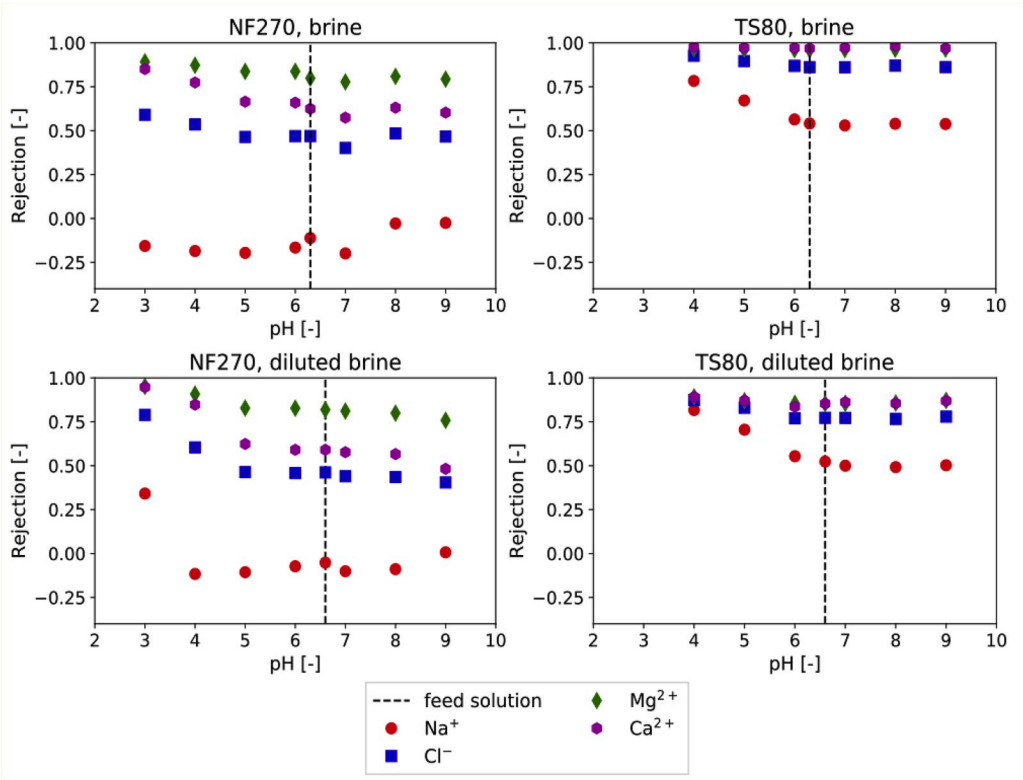

Fig. 6. Experimental rejection of each ion vs. the pH with NF270 and TS80 membranes and with the brine and the diluted brine, reported in Table 3. Flux = 45 L/(m^{2}h).

(i.e. 9) can be explained by considering the change of membrane morphology, because the pore radius tends to increase with alkaline solutions [68]. Overall, the trends of the ionic rejection vs. the solution pH gave essential insights into the transport mechanisms through the membrane at different operating conditions but did not allow for identifying a pH corresponding to a minimum rejection for every ion.

4.3. Ionic rejection varying permeate flux: estimation of pore dielectric constant and membrane charge density

To identify the pore dielectric constant and the charge density of the two membranes, firstly, we carried out experiments to measure the ionic rejections in presence of the synthetic wastewater (brine) and the diluted brine at four permeate fluxes (15, 30, 45 and 70 L/(m^{2}h)), corresponding to four different applied pressures (in the range between 1 and 32 bar). Secondly, we found the set of pore dielectric constant and membrane charge density by minimizing the SSE calculated as in equation (25) in Section 3.4.

The impact of the simultaneous variation of pore dielectric constant and membrane charge density on the SSE is reported in the maps in Fig. 7. The maps show that the charge density influences only slightly the systems at higher concentrations (brine) since the variation of the SSE is almost completely due to the change in the pore dielectric constant. Conversely, the maps relevant to the diluted brine present significant variations in both directions. This difference is explicable considering that the higher the ionic strength of the solution, the flatter the membrane potential and the lower the system dependence on the Donnan exclusion mechanism. However, it is worth noting that both maps for TS80 show a good fitting (low SSE) along an entire line of charge density vs. dielectric constant. This evidence, in line with the trends depicted in Fig. 6, demonstrates that the performances of the TS80 membrane are always governed by the dielectric constant, rather than the charge density.

From the minimization of the SSE, we identified the couples (ε_{pore},

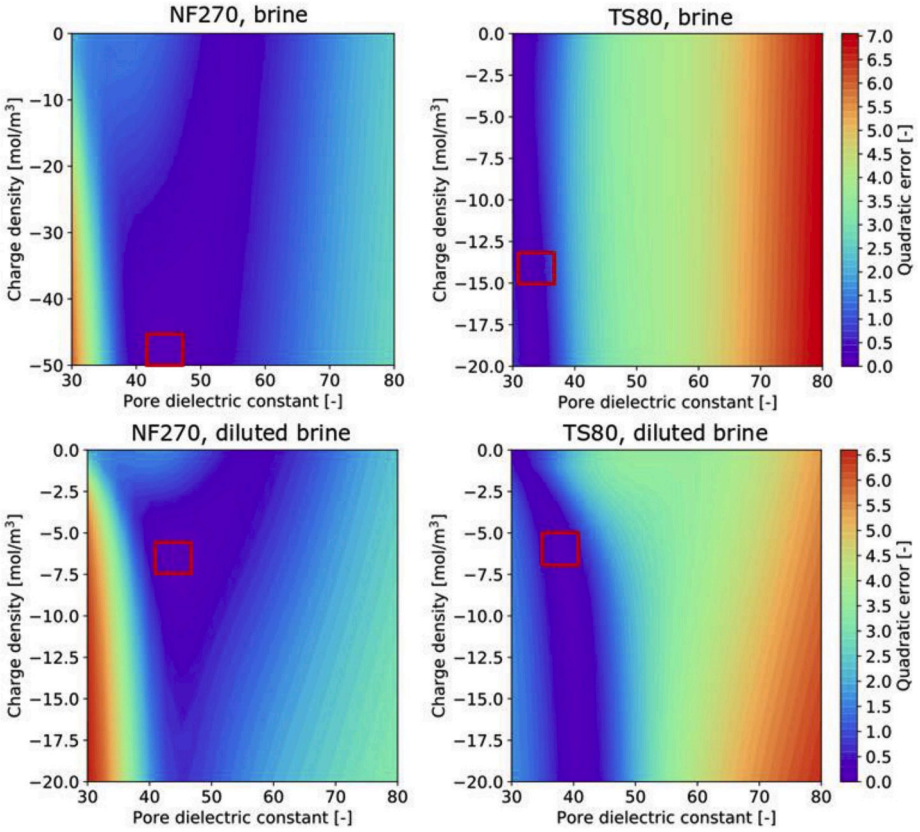

Fig. 7. Maps reporting the quadratic error (SSE) between the experimental and the calculated feed rejection values varying the pore dielectric constant and the charge density with brine and diluted brine and with NF270 and TS80 membranes. The red squares represent the minimum errors. (For interpretation of the references to colour in this figure legend, the reader is referred to the Web version of this article.)

X_d) able to describe the membrane behaviour with the minimum error. The estimated values of the membrane parameters, highlighted with the red squares in Fig. 7, are reported in Table 4. The results show that NF270 presented a higher ε_{pore} and a lower (more negative) X_d. Both findings justify the lower ionic rejections found with NF270, as reported in Fig. 6. Moreover, both membranes presented a higher ε_{pore} and a higher (less negative) X_d in the presence of the diluted brine. The lower dielectric constant at higher concentrations is due to the higher confinement of water within the pores when more ions are present. In fact, the dielectric exclusion is typically more effective in the presence of more concentrated solutions. Concerning the charge density, since Cl^- had a much higher concentration in comparison with the divalent ions, its adsorption had likely the greatest influence on the membrane charge density. In fact, the brine presented higher amounts of Cl^-, whose adsorption led to more negative charges. This is in line with the charge density found by Deon et al. who varied the concentration of NaCl and $CaCl_2$ [69].

Furthermore, we applied an additional method to identify one of the two parameters of the couple (ε_{pore}, X_d) of each membrane, to validate the results of the minimization algorithm, since the minimum was not always easily distinguishable, as shown in the maps of Fig. 7.

Table 4
Values of pore dielectric constant (ε_{pore}) and membrane charge density (X_d) estimated in the presence of the artificial brine and the diluted one with NF270 and TS80 membranes.

Membrane	Brine		Diluted brine	
	ε_{pore} [−]	X_d [mol/m^3]	ε_{pore} [−]	X_d [mol/m^3]
NF270	42.5	−50	45	−7
TS80	32.5	−14	37.5	−6

Such method consisted in estimating the pore dielectric constant by fitting the model trends to the ionic rejections found at the pH range corresponding to the isoelectric point. This was identified, in agreement with previous studies, by assuming that a change in the trends of the ionic rejection is attributed to a switch of the membrane charge sign [62]. Therefore, to assess the validity of the results reported in Table 4, the ionic rejections found between a pH of 4 and 5 for NF270 and between 5 and 6 for TS80 were used to recalculate the pore dielectric constant, assuming a charge density of zero. The least-square fitting gave values of pore dielectric constant between 45 and 50 for NF270 and between 30 and 35 for TS80. These values are in line with those found via the minimization algorithm (reported in Table 4) and fall within the range of previous results reported in the literature for seawater or solutions containing divalent ions [3,4,49,70]. Therefore, the application of an additional method for the estimation of pore dielectric constant and the comparison with results from the literature allow for validating the minimization method. Thus, the parameters obtained via such a method can be considered robust and reliable for model calibration.

Once the set of membrane parameters was found for each of the four membrane-solution combinations, simulations of the DSPM-DE were performed to compare the trends of the ionic rejections predicted by the model with all the collected experimental data. The results are depicted in Fig. 8. Note that the lowest permeate flux considered for the NF270 membrane with the diluted brine was 22 L/(m^{2}h) because lower pressure differences could not be imposed to reach lower fluxes. The error bars reported for the experimental points correspond to a 10% error in the permeate concentration, due to the precision of the instrument used for the concentration measurement. A good agreement between the trends given by the model and the experimental data was found: the errors were lower than 15% and the predicted values were within the error bars of the experimental values in almost all cases. Therefore, we

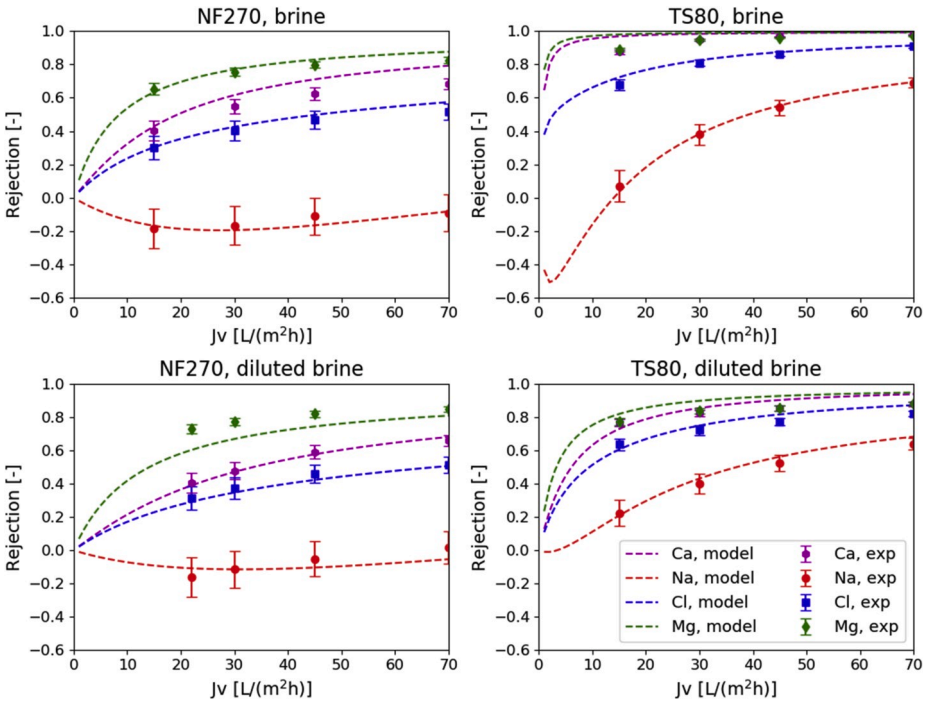

Fig. 8. Simulated trends of ionic rejection vs. the water flux Jv [L/(m^{2}h)] (dotted line) and experimental values of rejection at four fluxes (15, 30, 45 and 70 L/(m^{2}h)) obtained with brine and with diluted brine and for NF270 and TS80 membranes.

can conclude that the DSPM-DE was able to predict the performances of the NF membranes reliably in the presence of wastewater solutions, using the novel sets of four membrane parameters presented in this work.

5. Model results and discussion

Finally, an analysis of the ionic transmembrane fluxes estimated by the model was performed to get insights into the main transport and exclusion mechanisms occurring in the investigated systems. In particular, experimental rejections of the divalent ions at different feed concentrations and with the two membranes were compared and put in relation with the trans-membrane fluxes and the exclusion coefficients estimated by the model. The ionic rejections vs. the permeate flux are shown in Fig. 9. Firstly, in all cases, the rejections of the divalent ions increased with the flux since more water was forced to pass through the membrane and this led to a higher dilution of the permeate stream and a lower permeate concentration. Secondly, we found always higher rejections in the presence of the brine if compared with the diluted brine, except for Mg^{2+} that showed similar values of rejection at the two concentrations in the presence of NF270 membranes. Thus, the main experimental evidence concerns the decrease of rejections in the presence of diluted feed solutions and the stronger variation of rejection with TS80 membranes than with NF270.

The decrease in rejection at lower concentrations has been observed in literature for the case of solutions containing divalent cations. As a matter of fact, while with NaCl solutions the rejection increases when the concentration decreases, an opposite behaviour is observed with solutions of $MgCl_2$ or mixtures containing Mg^{2+} ions [44,46,71]. In these works, it was stated that the decrease of rejection with the concentration is due to the partial screening of the negative membrane charge caused by the adsorption of divalent cations, which occurs more at higher concentrations.

Our results are in line with those findings and in particular, the reduction of rejection is due to the fact that the concentration of the permeate solution decreased less than proportionally with the concentration of the feed. In fact, while the ratio between the feed concentrations in the brine and in the diluted brine was 10:1, the one between the experimental permeate concentrations was 12:1 for NF270 and 50:1 for TS80 (for a permeate flux of 45 L/(m^{2}h)).

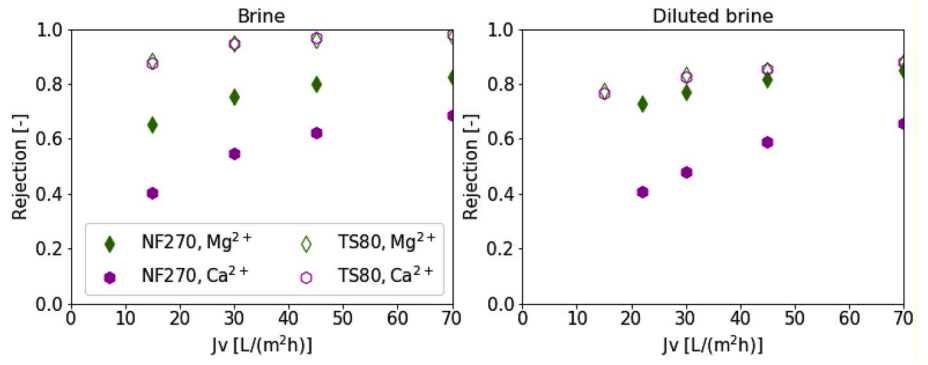

Fig. 9. Experimental ionic rejections for Mg^{2+} and Ca^{2+} vs. the permeate flux with the two membranes (NF270 and TS80) and the two feed solutions (synthetic brine and diluted brine).

This can be explained by analysing the transmembrane fluxes that are calculated by the model. The fluxes of Mg^{2+} and Ca^{2+} estimated for NF270 and TS80 membranes, with the two feed concentrations and a permeate flux of 45 L/(m^2h) are depicted in Fig. 10. The charts show the three contributions to the total ion fluxes. The total fluxes were related to the feed concentration but they did not decrease proportionally with the concentration: this led to a lower rejection with diluted feed solutions. Furthermore, the reduction of the total ionic fluxes was more enhanced with NF270 than with TS80 and this is in line with the stronger decrease of the ionic rejections with concentration found for TS80.

Concerning the analysis of the different fluxes, the diffusive flux was the highest term, and it decreased with the feed concentration because of the lower driving force, i.e. the concentration difference. Moreover, the migrative flux was lower for diluted brine because the potential profile within the membrane became flatter than the one with the brine. This variation was due to the decrease in the magnitude of membrane charge density, and consequently of the membrane potential difference, with the feed concentration, as already found in the literature [72]. Conversely, the convective flux with the diluted brine turned out to be slightly higher than the one with brine, in the presence of TS80 membranes. The concentration of ions in the membrane, as calculated by the model, was higher when a diluted feed solution was used. This effect can be explained by analysing the exclusion mechanisms at different feed concentrations.

The coefficients used to define the steric (φ_i), dielectric (φ_{Bi}) and Donnan (depending on $\Delta\psi_{D,bm}$) exclusion mechanisms for Mg^{2+} and Ca^{2+} are reported in Fig. 11, for the two membranes and the two feed solutions investigated. Firstly, the higher the exclusion coefficient, the lower was the impact of the corresponding exclusion mechanism. In all cases, the exclusion coefficients found for NF270 were higher than those found for TS80, which is in line with the higher rejections measured with TS80. Only the Donnan exclusion coefficients of the two membranes at high feed concentration were comparable since the charge density did not play a significant role in any case. At both concentrations and with both membranes, the steric coefficient was the largest term, meaning that the steric effect was always the least important one.

Conversely, the dielectric exclusion was the primary factor, in line with other studies showing how crucial the addition of the dielectric exclusion effect is to improve the model reliability in the presence of divalent ions [41]. The dielectric exclusion coefficient decreased at higher concentrations because the water was more confined within the pores, and the Donnan exclusion coefficient increased because the charge density effect was more screened. These findings are in agreement with previous works, reporting that the Donnan effect is more relevant at low feed concentrations and the dielectric effect at high feed concentrations [73,74].

Concerning the TS80 membrane, the dielectric exclusion mechanism had the highest impact and the increase of the relevant coefficient at lower feed concentrations led to an increase of the ionic concentration within the membrane (C^m). This caused higher convective fluxes of Mg^{2+} and Ca^{2+} through the membrane in comparison to the ones with brine. The increase in the convective flux was also responsible for the minor decrease of permeate concentration for TS80 (stronger reduction of rejection) when switching from the brine to the diluted brine if compared to the one found for NF270.

The analysis of the transmembrane ionic fluxes was also performed at a lower permeate flux (25 L/(m^2h)), to simulate operating conditions more similar to real NF units treating industrial wastewater. We found that the three fluxes and the three exclusion coefficients followed the same order for both bivalent ions and membranes: the diffusive was always the highest flux and the dielectric was always the primary exclusion mechanism. However, as expected, the convective flux was significantly lower because of the lower permeate flux driving it.

Overall, the analysis of the transmembrane fluxes and the exclusion mechanisms estimated by the model allowed highlighting the significant factors influencing the ionic rejections at different feed concentrations and with different membranes.

As mentioned in the introduction, to simulate the NF membranes reliably, it is crucial to characterize them by calibrating the membrane properties with the specific solution. In fact, among the available literature studies about the characterization of NF membranes, most works presented experiments performed with seawater or with peculiar solutions containing mixtures of magnesium and sodium chloride, whereas

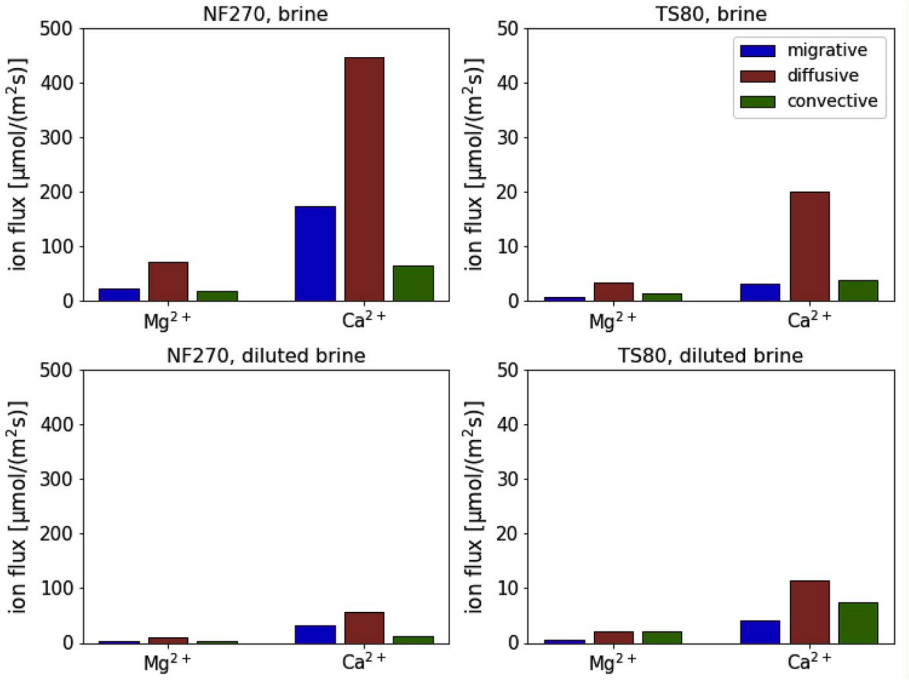

Fig. 10. Trans-membrane fluxes of Mg^{2+} and Ca^{2+} with NF270 and TS80 membranes, in the presence of synthetic brine and diluted brine. The permeate flux was 45 L/(m^2h).

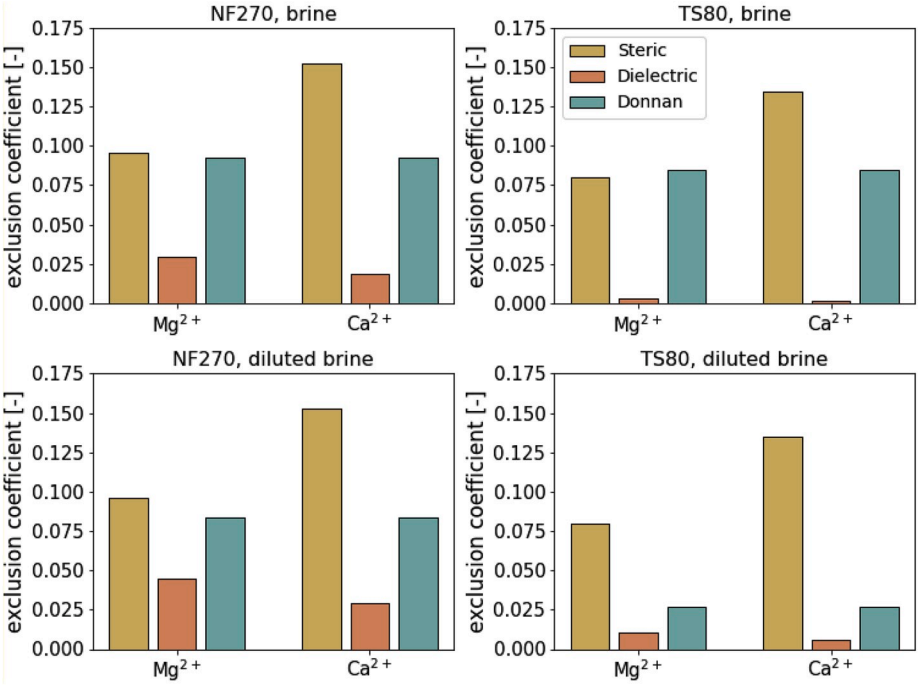

Fig. 11. Exclusion coefficients of Mg^{2+} and Ca^{2+} with NF270 and TS80 membranes, in presence of brine and diluted brine. The permeate flux was 45 L/(m^2h).

there are no studies about the characterization of NF membranes with the brines produced by ion exchange columns used in water softening.

With this respect, we run the DSPM-DE adopting our set of parameters of NF270 and other two found in the literature. In particular, we considered the membrane parameters found by Roy et al. for NF270 membrane and seawater [48] and the ones found by Labban et al. for hollow fibre membranes and seawater [49]. In all simulations, the feed solution of the NF unit corresponded to the spent regenerant of ion exchange resins used for water softening. The calculated rejection values for the different cases are shown in Fig. 12. We found that the two sets of parameters obtained for seawater were not suitable to simulate the NF membrane with our feed solution, characterized by higher ionic strength and relatively high concentrations of divalent ions. This analysis showed how much feed-dependant are the NF membrane parameters adopted in the model. Therefore, the joint experimental and simulation campaign is particularly important, since the knowledge of the suitable set of parameters allows for modelling the NF membranes reliably and for designing bigger-scale NF plant to purify the wastewater and implement

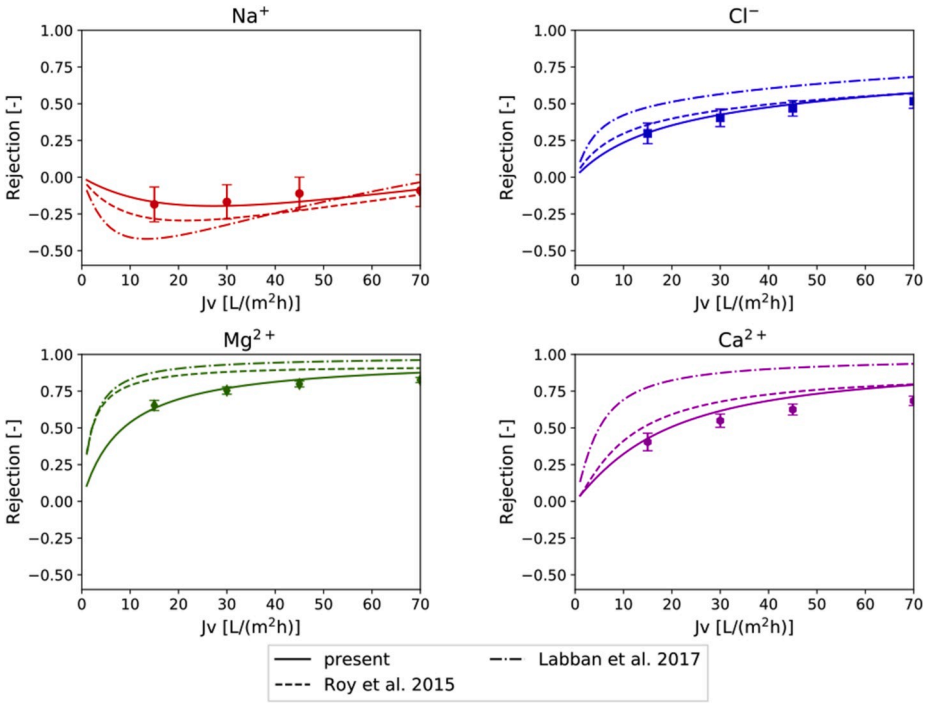

Fig. 12. Comparison of the ionic rejections calculated by the model for the brine solution with the parameters found in the present work and with the ones found for seawater in the works by Roy et al. and Labban et al.

a circular scheme in the water softening industry.

6. Conclusions

This study presents the characterization of NF membranes in the presence of a multi-ionic solution simulating the effluent produced by the regeneration of ion exchange resins employed for water softening. We performed experiments with two NF membranes and two solutions, the synthetic brine and a 10 times diluted brine, in a wide range of pH and permeate fluxes. Then, we found the four parameters to characterize the membranes by fitting the DSPM-DE to the experimental results. A good agreement between the experimental values and the simulated trends of ionic rejections vs. permeate flux was observed with errors lower than 15%. Finally, we analysed the trans-membrane fluxes and the exclusion coefficients given by the model.

Concerning the membrane parameters, we found negative values of membrane charge density and this could be explained by the high concentration of Cl^- in the feed, because Cl^- likely adsorbed onto the membrane surface and generated negatively charged sites. With diluted brine, higher ε_{pore} and higher (less negative) X_d were encountered because the water was less confined in the pores and because less Cl^- adsorption could take place. However, the trends of rejection obtained by varying the pH of the feed solutions were relatively flat and this suggested that, at the investigated concentrations, the membrane charge density did not affect the membrane performances significantly.

Generally speaking, the experimental rejections found with TS80 were always higher than the ones with NF270. This finding was supported by the lower ε_{pore} calculated for TS80, which corresponded to a stronger dielectric exclusion mechanism.

The analysis of the transmembrane fluxes of the divalent cations highlighted that the diffusive flux was the highest term in all cases. Moreover, the migrative flux decreased at lower concentrations and the Donnan exclusion term increased, because of the less negative membrane charge density. The convective flux with TS80 membranes was the only term that was slightly higher with the diluted brine because of a higher concentration of divalent ions in the membrane. This was because the dielectric exclusion mechanism played the most crucial role in the partition of the ions and it became weaker at lower concentrations.

Overall, the novel membrane parameters reported in this work allowed for simulating reliably two NF membranes in the presence of a multi-ionic solution reproducing the spent regenerant of ion exchange resins employed for water softening. Thus, the next step will consist in including them in full-scale models to design the NF plant to be employed for the treatment and recycling of the regeneration brine.

Credit author statement

Marina Micari: Conceptualization, Methodology, Software, Writing – Original Draft, Writing – Review and Editing; **Dionysia Diamantidou**: Investigation, Validation, Writing – Original Draft; **Bas Heijman**: Resources, Supervision; **Massimo Moser**: Methodology, Funding acquisition; **Amir Haidari**: Supervision, Writing – Review and Editing; **Henri Spanjers**: Writing – Review and Editing, Funding acquisition; **Valentin Bertsch**: Supervision, Writing – Review and Editing.

Declaration of competing interest

The authors declare that they have no known competing financial interests or personal relationships that could have appeared to influence the work reported in this paper.

Acknowledgments

This work was funded by the ZERO BRINE project (ZERO BRINE – Industrial Desalination – Resource Recovery – Circular Economy) - Horizon 2020 program, Project Number: 730390: www.zerobrine.eu.

Nomenclature

A	temperature correction factor for the activity coefficient [−]
C	concentration [mol/m^3]
$D_{i,pore}$	diffusion coefficient of the ion within the pore [m^2/s]
$D_{i,\infty}$	diffusion coefficient of the ion in the bulk [m^2/s]
e_0	electronic charge [1.602×10^{-19} C]
F	Faraday constant [9.64867×10^4 C/mol]
h_f	height of the NF feed channel [m]
I	ionic strength [mol/l]
j	trans-membrane flux [mol/(m^{2}s)]
J_v	permeate flux [m/s] or [L/(m^{2}h)]
$k^{bulk}_{c,i}$	mass transfer coefficient in the bulk [m/s]
$k^{,bulk}_{c,i}$	corrected mass transfer coefficient in the bulk [m/s]
k_B	Boltzmann constant [1.38066×10^{-23} J/K]
$k_{i,c}$	hindered convective mass transfer coefficient [−]
$k_{i,d}$	hindered diffusive mass transfer coefficient [−]
L_{mix}	mixing length of the spacer [m]
Lp	water permeability [L/(m^{2}h)/bar]
N	number of discretization elements within the membrane [−]
N_A	Avogadro number [6.023×10^{23} mol^{-1}]
P	pressure [Pa]
Pe	Peclet number [−]
R	ideal gas constant [8.314 J/(K mol)]
r_i	ion radius [nm]
R_i	ionic rejection [−]
r_p	pore radius [nm]
Sc	Schmidt number [−]
T	Temperature [K]
X_D	charge density [mol/m^3]
y	direction across the membrane from the feed to the permeate side [m]
z_i	valence of the ion [−]

Greek symbol

γ	activity coefficient [−]
δ_m	active layer membrane thickness [μm]
ΔP	net pressure difference [Pa]
$\Delta\Pi$	osmotic pressure difference [Pa]
$\Delta\psi_{D,feed}$	Donnan potential difference at the feed-membrane interface [V]
$\Delta\psi_{D,perm}$	Donnan potential difference at the permeate-membrane interface [V]
ΔW	Born solvation energy barrier [J]
ε	medium permittivity [F/m]
ε_0	vacuum permittivity [8.854×10^{-12} F/m]
ε_b	dielectric constant in the bulk [−]
ε_{pore}	pore dielectric constant [−]
η	solution viscosity [Pa s]
η_{mix}	mixing efficiency of the spacer [−]
λ_i	ratio between the ion Stokes radius and the pore radius [−]
ξ	electric potential gradient at the bulk-membrane interface [V/m]
Ξ	correction factor for the mass transfer coefficient [−]
Φ_i	steric coefficient [−]
Φ_B	Born solvation contribution for partitioning [−]
ψ	potential [V]

Subscripts

calc	calculated
exp	experimental
i	ion
j	index for the discretization along the NF membrane thickness
lim	limit

w	interface

Superscripts

b	bulk
bm	bulk-membrane interface
f	feed
m	membrane
p	permeate

Acronyms

DSPM	Donnan Steric Pore Model
DSPM-DE	Donnan Steric Pore Model with Dielectric Exclusion
MPD	m-phenylenediamine
MW	Molecular Weight [g/mol]
MWCO	Molecular Weight Cut-Off
NF	Nanofiltration
PIP	Piperazine
RO	Reverse Osmosis
SSE	sum of the squared errors [−]
TMC	trimesoyl chloride
TOC	Total Organic Carbon

References

[1] P. Eriksson, Nanofiltration extends the range of membrane filtration, Environ. Prog. 7 (1988) 58–62.
[2] N. Hilal, H. Al-Zoubi, N.A. Darwish, A.W. Mohamma, M. Abu Arabi, A comprehensive review of nanofiltration membranes:Treatment, pretreatment, modelling, and atomic force microscopy, Desalination 170 (2004) 281–308.
[3] D.L. Oatley, L. Llenas, R. Perez, P.M. Williams, X. Martinez-Llado, M. Rovira, Review of the dielectric properties of nanofiltration membranes and verification of the single oriented layer approximation, Adv. Colloid Interface Sci. 173 (2012) 1–11.
[4] A. Escoda, S. Déon, P. Fievet, Assessment of dielectric contribution in the modeling of multi-ionic transport through nanofiltration membranes, J. Membr. Sci. 378 (2011) 214–223.
[5] F. Salehi, S.M.A. Razavi, M. Elahi, Purifying anion exchange resin regeneration effluent using polyamide nanofiltration membrane, Desalination 278 (2011) 31–35.
[6] A.W. Mohammad, Y.H. Teow, W.L. Ang, Y.T. Chung, D.L. Oatley-Radcliffe, N. Hilal, Nanofiltration membranes review: recent advances and future prospects, Desalination 356 (2015) 226–254.
[7] F.F. Chang, W.J. Liu, X.M. Wang, Comparison of polyamide nanofiltration and low-pressure reverse osmosis membranes on As(III) rejection under various operational conditions, Desalination 334 (2014) 10–16.
[8] A. De Munari, A.J.C. Semiao, B. Antizar-Ladislao, Retention of pesticide endosulfan by nanofiltration: influence of organic matter-pesticide complexation and solute-membrane interactions, Water Res. 47 (2013) 3484–3496.
[9] M.A. Abdel-Fatah, Nanofiltration systems and applications in wastewater treatment: review article, Ain Shams Engineering Journal 9 (2018) 3077–3092.
[10] Q. Li, Z. Liao, X. Fang, D. Wang, J. Xie, X. Sun, L. Wang, J. Li, Tannic acid-polyethyleneimine crosslinked loose nanofiltration membrane for dye/salt mixture separation, J. Membr. Sci. 584 (2019) 324–332.
[11] M. Jiang, K. Ye, J. Lin, Y. Zhang, W. Ye, S. Zhao, B. Van der Bruggen, Effective dye purification using tight ceramic ultrafiltration membrane, J. Membr. Sci. 566 (2018) 151–160.
[12] I. Koyuncu, Reactive dye removal in dye/salt mixtures by nanofiltration membranes containing vinylsulphone dyes: effects of feed concentration and cross flow velocity, Desalination 143 (2002) 243–253.
[13] J.M. Gozálvez-Zafrilla, D. Sanz-Escribano, J. Lora-García, M.C. León Hidalgo, Nanofiltration of secondary effluent for wastewater reuse in the textile industry, Desalination 222 (2008) 272–279.
[14] B. Van der Bruggen, B. Daems, D. Wilms, C. Vandecasteele, Mechanisms of retention and flux decline for the nanofiltration of dye baths from the textile industry, Separ. Purif. Technol. 22–23 (2001) 519–528.
[15] S.S. Wadekar, R.D. Vidic, Insights into the rejection of barium and strontium by nanofiltration membrane from experimental and modeling analysis, J. Membr. Sci. 564 (2018) 742–752.
[16] Z.V.P. Murthy, L.B. Chaudhari, Separation of binary heavy metals from aqueous solutions by nanofiltration and characterization of the membrane using Spiegler–Kedem model, Chem. Eng. J. 150 (2009) 181–187.
[17] C.-V. Gherasim, P. Mikulášek, Influence of operating variables on the removal of heavy metal ions from aqueous solutions by nanofiltration, Desalination 343 (2014) 67–74.
[18] Y. Li, Y. Zhao, H. Wang, M. Wang, The application of nanofiltration membrane for recovering lithium from salt lake brine, Desalination (2019) 468.
[19] X. Chen, T. Chen, J. Li, M. Qiu, K. Fu, Z. Cui, Y. Fan, E. Drioli, Ceramic nanofiltration and membrane distillation hybrid membrane processes for the purification and recycling of boric acid from simulative radioactive waste water, J. Membr. Sci. 579 (2019) 294–301.
[20] S.S. Wadekar, R.D. Vidic, Comparison of ceramic and polymeric nanofiltration membranes for treatment of abandoned coal mine drainage, Desalination 440 (2018) 135–145.
[21] J. Warczok, M. Ferrando, F. López, C. Güell, Concentration of apple and pear juices by nanofiltration at low pressures, J. Food Eng. 63 (2004) 63–70.
[22] Z. Chen, J. Luo, X. Hang, Y. Wan, Physicochemical characterization of tight nanofiltration membranes for dairy wastewater treatment, J. Membr. Sci. 547 (2018) 51–63.
[23] F. Salehi, Current and future applications for nanofiltration technology in the food processing, Food Bioprod. Process. 92 (2014) 161–177.
[24] M.S. Noghabi, S.M.A. Razavi, S.M. Mousavi, M. Elahi, R. Niazmand, Effect of operating parameters on performance of nanofiltration of sugar beet press water, Procedia Food Science 1 (2011) 160–164.
[25] S. Wadley, C.J. Brouckaert, L.A.D. Baddock, C.A. Buckley, Modelling of nanofiltration applied to the recovery of salt from waste brine at a sugar decolourisation plant, J. Membr. Sci. 102 (1995) 163–175.
[26] W.L. Ang, A.W. Mohammad, N. Hilal, C.P. Leo, A review on the applicability of integrated/hybrid membrane processes in water treatment and desalination plants, Desalination 363 (2015) 2–18.
[27] D. Zhou, L. Zhu, Y. Fu, M. Zhu, L. Xue, Development of lower cost seawater desalination processes using nanofiltration technologies — a review, Desalination 376 (2015) 109–116.
[28] L. Llenas, X. Martínez-Lladó, A. Yaroshchuk, M. Rovira, J. de Pablo, Nanofiltration as pretreatment for scale prevention in seawater reverse osmosis desalination, Desalination and Water Treatment 36 (2012) 310–318.
[29] A.A. Al-Hajouri, A.S. Al-Amoudi, A.M. Farooque, Long term experience in the operation of nanofiltration pretreatment unit for seawater desalination at SWCC SWRO plant, Desalination and Water Treatment 51 (2013) 1861–1873.
[30] M.A.K. Al-Sofi, Seawater desalination - SWCC experience and vision, Desalination 135 (2001) 121–139.
[31] M.A.K. Al-Sofi, A.M. Hassan, G.M. Mustafa, A.G.I. Dalvi, N.M. Kither, Nanofiltration as a means of achieving higher TBT of $\geq 120^{\circ}$C in MSF, Desalination 118 (1998) 123–129.
[32] M. Kabsch-Korbutowicz, J. Wisniewski, S. Łakomska, A. Urbanowska, Application of UF, NF and ED in natural organic matter removal from ion-exchange spent regenerant brine, Desalination 280 (2011) 428–431.
[33] European Commission, Communication from the Commission to the European Parliament, the Council, the European Economic and Social Committe and the Committe of the Regions on the 2017 List of Critical Raw Materials for the EU, 2017.
[34] M. Micari, A. Cipollina, A. Tamburini, M. Moser, V. Bertsch, G. Micale, Combined membrane and thermal desalination processes for the treatment of ion exchange resins spent brine, Appl. Energy (2019) 254.
[35] S. Singh, K.C. Khulbe, T. Matsuura, P. Ramamurthy, Membrane characterization by solute transport and atomic force microscopy, J. Membr. Sci. 142 (1998) 111–127.
[36] M. Ernst, A. Bismarck, J. Springer, M. Jekel, Zeta-potential and rejection rates of a polyethersulfone nanofiltration membrane in single salt solutions, J. Membr. Sci. 165 (2000) 251–259.
[37] W.R. Bowen, A.W. Mohammad, N. Hilal, Characterisation of nanofiltration membranes for predictive purposes use of salts, uncharged solutes and atomic force microscopy, J. Membr. Sci. 126 (1997) 91–105.
[38] K.S. Spiegler, O. Kedem, Thermodynamics of hyperfiltration (reverse osmosis): criteria for efficient membranes, Desalination 1 (1966) 311–326.
[39] T. Tsuru, S.I. Nakao, S. Kimura, Calculation of ion rejection by extended Nernst-Planck equation with charged reverse osmosis membranes for single and mixed electrolyte solutions, J. Chem. Eng. Jpn. 24 (1991) 511–517.
[40] X.L. Wang, T. Tsuru, S.I. Nakao, S. Kimura, Electrolyte transport through nanofiltration membranes by the space-charge model and the comparison with Teorell- Meyer-Sievers model, J. Membr. Sci. 103 (1995) 117–133.
[41] D. Vezzani, S. Bandini, Donnan equilibrium and dielectric exclusion for of nanofiltration membranes, Desalination 149 (2002) 477–483.
[42] A.W. Mohammad, N. Hilal, H. Al-Zoubi, N.A. Darwish, Prediction of permeate fluxes and rejections of highly concentrated salts in nanofiltration membranes, J. Membr. Sci. 289 (2007) 40–50.
[43] C. Mazzoni, L. Bruni, S. Bandini, Nanofiltration: role of the electrolyte and pH on desal DK performances, Ind. Eng. Chem. Res. 46 (2007) 2254–2262.
[44] A.A. Hussain, S.K. Nataraj, M.E.E. Abashar, I.S. Al-Mutaz, T.M. Aminabhavi, Prediction of physical properties of nanofiltration membranes using experiment and theoretical models, J. Membr. Sci. 310 (2008) 321–336.
[45] N.S. Kotrappanavar, A.A. Hussain, M.E.E. Abashar, I.S. Al-Mutaz, T. M. Aminabhavi, M.N. Nadagouda, Prediction of physical properties of nanofiltration membranes for neutral and charged solutes, Desalination 280 (2011) 174–182.
[46] V. Silva, V. Geraldes, A.M. Brites Alves, L. Palacio, P. Prádanos, A. Hernández, Multi-ionic nanofiltration of highly concentrated salt mixtures in the seawater range, Desalination 277 (2011) 29–39.
[47] S. Déon, P. Dutournié, L. Limousy, P. Bourseau, Transport of salt mixtures through nanofiltration membranes: numerical identification of electric and dielectric contributions, Separ. Purif. Technol. 69 (2009) 225–233.
[48] Y. Roy, M.H. Sharqawy, J.H. Lienhard, Modeling of flat-sheet and spiral-wound nanofiltration configurations and its application in seawater nanofiltration, J. Membr. Sci. 493 (2015) 360–372.

[49] O. Labban, C. Liu, T.H. Chong, J.H. Lienhard V, Fundamentals of low-pressure nanofiltration: membrane characterization, modeling, and understanding the multi-ionic interactions in water softening, J. Membr. Sci. 521 (2017) 18–32.
[50] D.L. Oatley, L. Llenas, N.H.M. Aljohani, P.M. Williams, X. Martínez-Lladó, M. Rovira, J. de Pablo, Investigation of the dielectric properties of nanofiltration membranes, Desalination 315 (2013) 100–106.
[51] J.V. Nicolini, C.P. Borges, H.C. Ferraz, Selective rejection of ions and correlation with surface properties of nanofiltration membranes, Separ. Purif. Technol. 171 (2016) 238–247.
[52] M. Teixeira, M. Rosa, M. Nystrom, The role of membrane charge on nanofiltration performance, J. Membr. Sci. 265 (2005) 160–166.
[53] R. Epsztein, E. Shaulsky, N. Dizge, D.M. Warsinger, M. Elimelech, Role of ionic charge density in donnan exclusion of monovalent anions by nanofiltration, Environ. Sci. Technol. 52 (2018) 4108–4116.
[54] S.S. Wadekar, R.D. Vidic, Influence of active layer on separation potentials of nanofiltration membranes for inorganic ions, Environ. Sci. Technol. 51 (2017) 5658–5665.
[55] P. Dechadilok, W.M. Deen, Hindrance factors for diffusion and convection in pores, Ind. Eng. Chem. Res. 45 (2006) 6953–6959.
[56] F.G. Donnan, Theory of membrane equilibria and membrane potentials in the presence of non-dialysing electrolytes. A contribution to physical-chemical physiology, J. Membr. Sci. 100 (1995) 45–55.
[57] D.L. Parkhurst, C. Appelo, User's Guide to PHREEQC (Version 2): A Computer Program for Speciation, Batch-Reaction, One-Dimensional Transport and Inverse Geochemical Calculations, 2008.
[58] M. Born, Volumen und Hydratationswärme der Ionen, Z. Phys. Chem. 1 (1920).
[59] V. Geraldes, M.D. Afonso, Generalized mass-transfer correction factor for nanofiltration and reverse osmosis, AIChE J. 52 (2006) 3353–3362.
[60] S. Senthilmurugan, A. Ahluwalia, S.K. Gupta, Modeling of a spiral-wound module and estimation of model parameters using numerical techniques, Desalination 173 (2005) 269–286.
[61] V. Geraldes, A.M. Brites Alves, Computer program for simulation of mass transport in nanofiltration membranes, J. Membr. Sci. 321 (2008) 172–182.
[62] M. Mullett, R. Fornarelli, D. Ralph, Nanofiltration of mine water: impact of feed pH and membrane charge on Resource recovery and water discharge, Membranes 4 (2014) 163–180.
[63] J. Schaep, C. Vandecasteele, A.W. Mohammad, W.R. Bowen, Analysis of the salt retention of nanofiltration membranes using the donnan–steric partitioning pore model, Separ. Sci. Technol. 34 (1999) 3009–3030.
[64] Dow Water and Process Solutions, Filmtec Reverse Osmosis Membrane, Technical Manual, 2018.
[65] S.I. Nakao, S. Kimura, Analysis of solutes rejection in ultrafiltration, J. Chem. Eng. Jpn. 14 (1981) 32–37.
[66] J. Schaep, B. Van der Bruggen, C. Vandecasteele, D. Wilms, Influence of ion size and charge in nanofiltration, Separ. Purif. Technol. 14 (1998) 155–162.
[67] Y.L. Lin, P.C. Chiang, E.E. Chang, Removal of small trihalomethane precursors from aqueous solution by nanofiltration, J. Hazard Mater. 146 (2007) 20–29.
[68] M. Dalwani, N.E. Benes, G. Bargeman, D. Stamatialis, M. Wessling, Effect of pH on the performance of polyamide/polyacrylonitrile based thin film composite membranes, J. Membr. Sci. 372 (2011) 228–238.
[69] S. Déon, A. Escoda, P. Fievet, P. Dutournié, P. Bourseau, How to use a multi-ionic transport model to fully predict rejection of mineral salts by nanofiltration membranes, Chem. Eng. J. 189–190 (2012) 24–31.
[70] Y. Roy, D.M. Warsinger, J.H. Lienhard, Effect of temperature on ion transport in nanofiltration membranes: diffusion, convection and electromigration, Desalination 420 (2017) 241–257.
[71] G. Hagmeyer, R. Gimbel, Modelling the salt rejection of nanofiltration membranes for ternary ion mixtures and for single salts at different pH values, Desalination 117 (1998) 247–256.
[72] B.W. Su, X.J. Duan, M.W. Dou, X.L. Gao, C.J. Gao, Charge characteristics of nanofiltration membrane by streaming potential method, Adv. Mater. Res. 396–398 (2011) 547–551.
[73] D.-X. Wang, M. Su, Z.-Y. Yu, X.-L. Wang, M. Ando, T. Shintani, Separation performance of a nanofiltration membrane influenced by species and concentration of ions, Desalination 175 (2005) 219–225.
[74] K. Zhao, G. Ni, Dielectric analysis of nanofiltration membrane in electrolyte solutions: influences of permittivity of wet membrane and volume charge density on ion permeability, J. Electroanal. Chem. 661 (2011) 226–238.

Applied Energy 254 (2019) 113699

Contents lists available at ScienceDirect

Applied Energy

journal homepage: www.elsevier.com/locate/apenergy

Combined membrane and thermal desalination processes for the treatment of ion exchange resins spent brine

M. Micari[a,*], A. Cipollina[b], A. Tamburini[b,*], M. Moser[a], V. Bertsch[a,c], G. Micale[b]

[a] German Aerospace Center (DLR), Institute of Engineering Thermodynamics, Pfaffenwaldring 38-40, 70569 Stuttgart, Germany
[b] Dipartimento di Ingegneria (DI), Università degli Studi di Palermo (UNIPA), viale delle Scienze Ed. 6, 90128 Palermo, Italy
[c] University of Stuttgart, Institute for Building Energetics, Thermotechnology and Energy Storage, Pfaffenwaldring 6, 70569 Stuttgart, Germany

HIGHLIGHTS

- A treatment chain for the effluent of ion exchange resins regeneration is analysed.
- The chain results feasible for any nanofiltration recovery between 25 and 65%.
- The lowest levelized brine cost is 4.9 $/m^3 at a nanofiltration recovery of 25%.
- The multi-effect distillation is the most energy-intensive unit in the chain.
- Crystallization cost and relevant revenues are key players for feasibility.

GRAPHICAL ABSTRACT

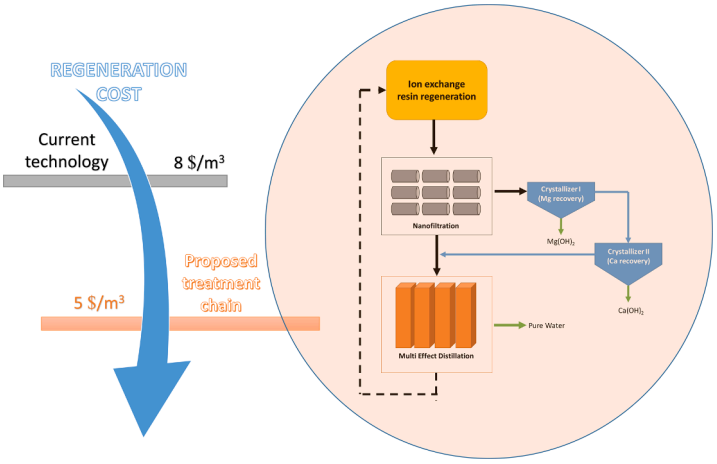

ARTICLE INFO

Keywords:
Industrial wastewater
Nanofiltration
Wastewater treatment
Techno-economic analysis
Circular economy
Waste heat recovery

ABSTRACT

The disposal of industrial wastewater effluents represents a critical environmental issue. This work focuses on the treatment of the spent brine produced by the regeneration of ion exchange resins employed for water softening. For the first time, a comprehensive techno-economic assessment and an analysis of the energy requirements of the treatment chain are carried out, via the simulation of *ad hoc* implemented models. The chain is composed of nanofiltration, double-stage crystallization and multi-effect distillation. The valuable product is the brine produced by the multi-effect distillation, which can be re-used for the regeneration. Therefore, the treatment chain's economic feasibility is evaluated via the Levelized Brine Cost, which includes the terms of cost and revenue of every unit in the chain. Varying the nanofiltration recovery, the treatment system always turns out to be economically competitive, since the Levelized Brine Cost is lower than the current cost of the fresh regenerant solution (8 $/m^3). In particular, the lowest value of 4.9 $/m^3 is found for a nanofiltration recovery of 25%. Moreover, the cost of the reactant used in the crystallization and the revenues of $Mg(OH)_2$ and $Ca(OH)_2$ play a prominent role in all scenarios. Regarding the energy demand, the thermal energy required by the evaporator is the main contribution and covers more than 30% of the operating costs (excluding the cost of the crystallization reactant, which is balanced by the hydroxides revenues). Therefore, the costs can be significantly

* Corresponding authors.
E-mail addresses: marina.micari@dlr.de (M. Micari), alessandro.tamburini@unipa.it (A. Tamburini).

https://doi.org/10.1016/j.apenergy.2019.113699
Received 31 May 2019; Received in revised form 2 August 2019; Accepted 3 August 2019
Available online 22 August 2019

reduced when waste heat is available in the industrial site. Overall, the treatment chain is economically feasible and allows reducing the industrial environmental impact by recycling waste streams and waste heat.

1. Introduction

The increasing environmental pollution along with the growing demand for energy and raw materials is leading to the need of a more sustainable development. With this respect, one of the most important requirements to fulfil, consists in saving water and energy simultaneously [1]. The consumption of water and energy has significantly increased in the past years and their applications are often interconnected and mutually reinforcing [2]. Water is used in power plants and energy is fundamental for fresh water production and water treatment processes [3]. The concept of the 'water-energy nexus' describes all the interdependencies and the dynamic linkages between water and energy [4]. This topic has drawn more and more attention in recent years and it may constitute the basis of future energy and water planning. The water-energy nexus has been investigated from several different angles and on different scales. Comprehensive studies were carried out from the 'water for energy' as well as the 'energy for water' perspective. Regarding the first one, water is widely needed in the energy sector, such as in the fuel production and in the hydropower generation [5–8]. For what concerns the 'energy for water' perspective, water systems are among the major consumers of energy resources [9]. The energy requirement depends on the water quality and on the process involved [10]. Wastewater treatment is a very electricity-intensive process and the energy consumption cost was found to cover up to 40% of the overall municipal wastewater treatment plants' operating costs [11]. Therefore, increasing the plants' energy efficiency may lead to a net reduction of the expenses [12]. The optimization of the energy efficiency and the identification of the energy inefficiencies in the wastewater treatment plants are very popular topics in literature [13,14]. Many strategies to optimize the energy efficiency are focused on the energy recovery within the wastewater treatment plants, which may be realized in self-sufficient plants [15] or via networks containing industrial processes using water, wastewater treatment units and recovery heat exchangers [16]. In general, the exploitation of the thermal energy stored in the water streams circulating in the network, through the development of a suitable flowsheet and the design of heat exchangers, allows a net reduction of the total energy requirement [17]. Overall, the investigation of the energy efficiency of wastewater treatment plants has mostly focused on municipal wastewater, although some studies evaluated also the energy performances of drinking water treatment plants, applying the energy benchmarks defined for the wastewater treatment plants [18].

However, nowadays, a rising attention is devoted to the treatment of industrial wastewater effluents. Therefore, a smart treatment of industrial effluents may represent a double advantage: (i) it would reduce the amount of wastes injected into the environment and (ii) it would make the effluents a new source of raw materials. In this context, several industrial effluents can be considered [19]: among others, brines produced in desalination plants or effluents deriving from the textile industry. Different ways to manage the desalination brines were investigated and implemented, such as brine minimization via thermal- or membrane-based technologies, direct re-use or extraction of minerals and salts for other applications [20–21]. In many cases, especially when organic compounds have to be removed, energy consumption may be a major issue. The same can be said for the treatment of textile wastewaters, which represent a very critical issue for the environment, because of the high volumes produced and because of their high content of organic pollutants (due to the dyes used in the industrial textile processes). For this reason, the contaminated textile wastewaters are typically treated via membrane processes [22] or via advanced oxidation processes [23], with the purpose of recycling the treated brine to the following dyeing operation.

Another industrial brine which has been taken into consideration is the one produced during the regeneration of Ion Exchange resins (IEXs), which are employed for a wide range of applications. Usually, the regeneration of the resins is carried out by using a regenerant solution at a certain concentration and the spent regenerant composition depends on the resins application. For example, IEXs are commonly used for water purification purposes, to remove perchlorates or nitrates from groundwater. The removal of these pollutants, for instance via catalytic reduction technology [24] or via biological treatment makes the re-use of the treated brine in the IEX regeneration viable and allows the reduction of the amount of fresh salt-water (regenerant) solution to be employed.

The IEX resins are also commonly used for water softening. In this case, the spent IEX resins are rich of the hardness (the ions Mg^{2+} and Ca^{2+}) removed from the softened water and the solution employed for the regeneration is a NaCl-water solution. Thus, the waste effluent arising from the regeneration of the spent resins is a water solution rich of sodium, chloride, magnesium and calcium ions. The discharge of the spent regenerant solution may cause serious environmental issues, especially because of the large volumes produced. A few studies in literature investigated alternative methods for the regeneration of the resins and strategies for the brine recycling. Flodman and Dvorak proposed brine reclaim operations or strategies to reduce salt consumption during regeneration [25]. They found that brine recycling systems, consisting of a single or a double tank where the spent brine effluent was partially recycled, allowed reducing the salt consumption and discharge without an increase of hardness leakage, but with a reduction of the removal efficiency. Hu et al. proposed a novel method to purify desalinated seawater instead of the conventional two-bed ion exchange. This process, called Chemical-Free Ion Exchange (CFIE), consisted of a mixed bed with strong acid and weak basic resins and an anion bed [26]. Other methods include the employment of thermally regenerable resins, whose capacity of removing salts from solutions by sorption depends on the temperature [27] and the introduction of other cation exchange forms, for example resins charged with Al^{3+} or with K^{+} [28,29]. Regarding the recycling strategies, Chen et al. proposed a closed-loop consisting of a bipolar membrane electrodialysis stack and a crystallizer, to restore the acid and the basic solutions used for the regeneration of weak resins and to recover the hardness minerals [30]. For most of these novel regeneration processes, the economic feasibility is not assessed, while it may constitute a crucial point.

This work proposes a recycling strategy for the spent regenerant solution of strong resins employed for water softening and presents, for the first time, a detailed and comprehensive techno-economic and energetic analysis of the whole treatment chain. The chain was developed within the framework of the EU-funded project Zero Brine [31], whose aim is to introduce new solutions to treat different types of industrial brines, promoting a circular economy approach at industrial scale. In particular, this work deals with the treatment of the industrial brine produced by the water softening plant, owned by the water industry Evides, in Rotterdam, The Netherlands. Currently, a fresh regenerant solution is continuously supplied to the resins and the effluent is disposed into the sea, without a treatment process. On the contrary, the system analysed in this work presents a treatment chain, which is depicted in Fig. 1. It consists of a Nanofiltration (NF) stage to concentrate the bivalent cations in the retentate, which is then fed to a double crystallization stage to produce $Mg(OH)_2$ and $Ca(OH)_2$ crystals. Conversely, the permeate of the NF stage, together with the effluent of the

Nomenclature

A	temperature correction factor for the activity coefficient [–]
$A_{membr,elem}$	membrane area of a single NF element [m^2]
$A_{membr,tot}$	total membrane area for each vessel [m^2]
C	concentration [mol/m^3]
D_H	hydraulic diameter relevant to the feed channel [m]
$D_{i,p}$	diffusivity of the species i within the pore [m^2/s]
$D_{i,\infty}$	diffusivity of the species i in the bulk [m^2/s]
e_0	electronic charge [1.602×10^{-19} C]
F	Faraday constant [9.64867×10^4 C/eq]
f	friction factor [–]
h_f	height of the NF feed channel [m]
I	ionic strength [mol/l]
j_i	flux of the ion i [m/s]
J_v	water flux through the NF membrane [m/s]
k_B	Boltzmann constant [1.38066×10^{-23} J/K]
$k_{i,c}$	hindered convective mass transfer coefficients of the ions within the pore [–]
$k_{i,d}$	hindered diffusive mass transfer coefficients of the ions within the pore [–]
$k_{c,i}^{bulk}$	mass transfer coefficient in the bulk [m/s]
$k'^{bulk}_{c,i}$	corrected mass transfer coefficient in the bulk [m/s]
l	length of the discretization interval [m]
L_{mix}	mixing length of the spacer [m]
M	flow rate [m^3/s] (if the unit is not specified)
N_A	Avogadro number [6.023×10^{23} mol^{-1}]
$n_{discr,L}$	number of discretization intervals along the NF element length [–]
n_{elem}	number of elements in each vessel [–]
n_{vessel}	number of vessels in parallel [–]
P	pressure [bar]
Pe	Peclet number [–]
R	ideal gas constant [8.314 J/(K mol)]
Re	Reynolds number [–]
r_i	ion radius [nm]
r_{pore}	NF membrane pore radius [nm]
Sc	Schmidt number [–]
T	Temperature [K]
u_w	feed velocity [m/s]
x	direction of the feed flow in the NF element [m]
X_d	NF membrane charge density [mol/m^3]
y	direction across the membrane from the feed to the permeate side [m]
z	ion valence [–]

Greek symbols

γ	activity coefficient [–]
δ_m	NF membrane active layer thickness [μm]
$\Delta\Pi$	osmotic pressure [bar]
ΔP_{losses}	pressure losses along the element [bar]
ΔP	net driving pressure [bar]
$\Delta\psi_{D,bm}$	Donnan potential difference at the bulk-membrane interface [V]
$\Delta\psi_{D,pm}$	Donnan potential difference at the permeate-membrane interface [V]
ΔW	Born solvation energy barrier [J]
ε	medium permittivity [F/m]
ε_{bulk}	dielectric constant in the bulk [–]
ε_{pore}	dielectric constant within the pore [–]
ε_0	vacuum permittivity [8.854×10^{-12} F/m]
η	solution viscosity [Pa s]
η_{mix}	mixing efficiency of the spacer [–]
λ	ratio between the solute radius and the pore radius [–]
ξ	electric potential gradient at the bulk-membrane interface [V]
Ξ	correction factor for the mass transfer coefficient [–]
ρ_w	solvent density [kg/m^3]
Φ_i	steric coefficient [–]
Φ_B	Born solvation contribution for partitioning [–]
ψ	electric potential across the membrane [V]

Subscripts and superscripts

b	solution entering into the interval along the NF element
bm	bulk-membrane interface (NF element)
feed	solution entering into the element
i	ion index
j	index for the discretization along the NF membrane thickness
m	inside the NF membrane
out	outlet of the NF unit
p	NF permeate along the NF element
ret	NF retentate along the element
x	index for the discretization along the NF membrane length

Acronyms

CAPEX	Capital Expenditure [US$/y]
COD	Chemical Oxygen Demand
DSPM-DE	Donnan Steric Pore Model with Dielectric Exclusion
FF	Forward Feed
IEX	Ion Exchange Resins
LBC	Levelized Brine Cost [US/m^3$]
MED	Multi-Effect Distillation
NF	Nanofiltration
OPEX	Operating Expenditure [US$/y]
TVC	Thermo-vapor compressor

crystallization, is sent to a Multi-Effect Distillation (MED) stage, where the NaCl concentration reaches the one required for the IEX regeneration process. For each stage, we developed a detailed techno-economic model and then, we connected the models via mass balances to simulate the treatment chain. The proposed approach allows (i) a net decrease of the salt and water consumption, (ii) the reduction of the environmental impact of the industrial process and the amount of produced waste and (iii) the re-utilization of waste materials and waste heat. The case study was already presented in a previous work by the same authors [32]. There, only the MED unit was investigated in detail in order to identify the most suitable operating conditions in presence of different steam qualities and costs.

This work presents the whole treatment chain as an 'energy for water' system and reports the energy demand of the single units, since this may constitute a crucial point for industrial wastewater treatment and its estimation is very much dependent on the effluent under investigation. We therefore make reference to a real case study and the properties of the effluent to be treated, such as composition and flow rate, are defined on the basis of the real wastewater effluent generated by the Evides water softening plant. The technical design of the plant is always performed with reference to a full-scale, where the whole amount of effluent produced by IEX regeneration is processed in the treatment chain. Concerning the economic analysis, the contributions of the single units are highlighted in terms of costs and revenues given by the by-products. The economic feasibility of the chain is defined via the introduction of the global Levelized Brine Cost (LBC), which

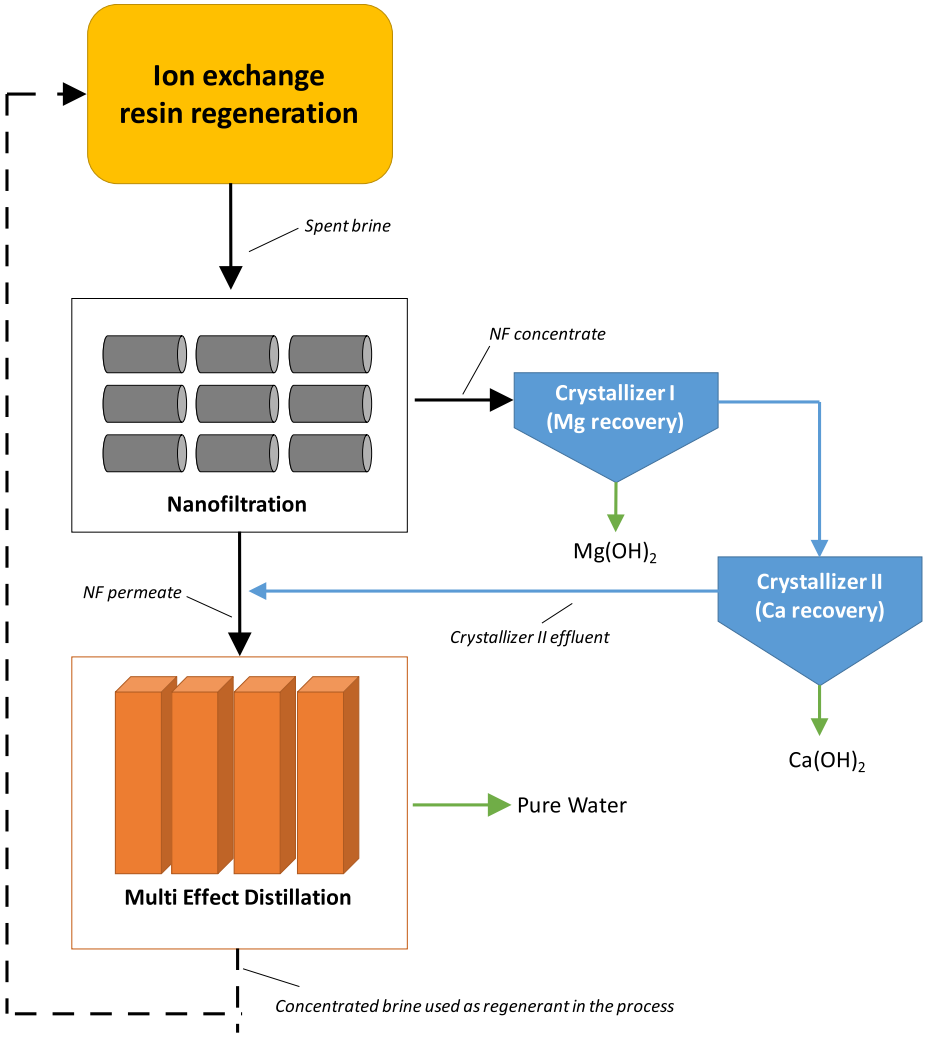

Fig. 1. Schematic representation of the treatment chain for the wastewater effluent produced by the regeneration of IEX resins employed in a water softening plant.

represents the cost that the concentrate brine would have at the break-even point (see Eq. (6) in Section 3). This performance parameter includes for the first time all the terms of cost of the treatment chain and it is meant to be compared with the cost of the fresh regenerant NaCl-water solution, currently employed for the resins regeneration, to evaluate the competitiveness of the proposed technology. The results reported in this work concern the impact of some operating conditions, in particular the nanofiltration recovery and the inlet feed flow rate, on the global economic feasibility, to identify the most suitable operating conditions and the most energy-intensive and cost-intensive units in the treatment chain. Overall, this work focuses on the global treatment plant design and on the estimation of the energy requirements for the real case study, with the aim of enhancing the sustainability of the industrial process producing the effluent.

2. Models

The treatment chain shown in Fig. 1 presents a NF stage, coupled with a double-stage crystallizer and a MED unit. For each unit, a technical model was implemented and coupled with an economic tool for the estimation of the capital and the operating costs. Then, the models were interconnected via suitable mass-balances to simulate the treatment chain. Table 1 shows the main inputs and outputs of the three models: different colours and marks are used in the table to show how

Table 1
Main inputs and outputs of the single models and interconnections in the treatment chain.

	Nanofiltration	Crystallizer	Multi-Effect Distillation
INPUTS	Feed flow rate	**(ii) -> Inlet flow rate**	***(i) -> Inlet flow rate***
	Ions concentration	**(ii) -> Concentration of Mg^{2+}**	***(i) -> Inlet NaCl concentration***
	Feed pressure	**(ii) -> Concentration of Ca^{2+}**	Required brine composition
	Plant Recovery	Concentration of the alkaline solution (NaOH)	Steam temperature
OUTPUTS	Ions rejection	Alkaline solution flow rate	Heat exchanger area
	Water flux	Flow rate of $Mg(OH)_2$	Preheater area
	Plant size	Flow rate of $Ca(OH)_2$	End condenser area
	Permeate flow rate and composition -> (i)	***Effluent flow rate -> (i)***	Cooling water flow rate
	Retentate flow rate and composition -> (ii)	***Effluent composition -> (i)***	Steam flow rate
	Electric energy requirement	Electric energy requirement	Electric and thermal energy requirements

the models are interconnected for the simulation of the treatment chain. In the real chain, the output retentate produced by the NF unit constitutes the feed solution of the crystallizer (the relevant input of the crystallizer model and output of the NF model are bolded, index (ii)), while the solution resulting from the mixing of the nanofiltration permeate and the crystallizer effluent (see Fig. 1) is the feed solution of the MED unit (the relevant input of the MED model and outputs of the NF and the crystallizer models are bolded and in italics, index (i)).

The main modelling activity reported in this work concerns the NF process, whose implementation at different scales is described in Section 2.1 and in the Appendix A. Crystallizers are simulated through the implementation of mass balances to evaluate the flow rates of the required alkaline solution and the produced hydroxides. The model adopted for the MED unit is extensively described elsewhere [32] and it is not reported here for brevity. The MED operating conditions which resulted to be the best performing [32] are employed for the simulation of the treatment chain. In the following, a short description of the developed models is reported.

2.1. Nanofiltration

2.1.1. Technical model

The NF model is developed on different scales, i.e. the lowest scale describes the mechanisms within the membranes; the middle-scale is relevant to a single NF element; the high scale regards the whole NF plant, given by a certain amount of vessels arranged in parallel, each one containing some NF elements in series. The schematic representation of the NF plant, as it is described in the multiscale model, is reported in Fig. 2.

The detailed description of the multi-scale model, including the equations employed for the low-scale and the middle-scale model and the description of the iterative procedures is reported in the Appendix A. For what concerns the low-scale model, the mechanisms within the membranes are described via the Donnan Steric Pore Model with Dielectric Exclusion (DSPM-DE). In literature, there are numerous studies regarding the modelling approaches of NF membranes and the DSPM-DE model is the most widely used [33–36]. The model allows a full characterization of the NF membrane, knowing four parameters, i.e. the membrane pore radius (r_{pore}), the active layer membrane thickness (δ_m), the dielectric constant within the pores (ε_{pore}) and the fixed charge density (X_d). These parameters are needed to estimate the membrane rejection of a species *i*, defined below.

$$R_i = 1 - \frac{C^p{}_i}{C^{feed}{}_i} \quad (1)$$

where C_i^p is the concentration of the species *i* in the permeate solution and C_i^{feed} is the concentration of the species *i* in the feed.

The DSPME-DE model derives from the resolution of the extended Nernst-Plank equation along the thickness of the membrane, which takes into account the three different mechanisms of ion transport, i.e. convection, diffusion and electro-migration, as shown in Fig. 3. Along the y axis, which corresponds to the thickness of the membrane, the membrane is discretized in a certain number of elements, taken equal to 50 in the present work on the basis of a preliminary sensitivity analysis (see Appendix A.4). The index employed for the elements along the y axis is 'j', while the index 'i' represents the different ionic species, as typically used in literature.

At the middle scale, the membrane model is integrated for the resolution of a whole NF membrane element. A schematic representation of the NF element, as described in the model, is reported in Fig. 4. The membrane length, along the main feed flow direction, is discretized and mass balances are applied to each discretization interval. Note that a one-dimensional model can be applied to a spiral wound element without significant errors, as shown by Roy et al. [37], since the variation of the permeate concentration and flow rates along the width of the membrane is negligible.

Typically, in spiral-wound elements, a certain number of membrane leaves are wounded together in a parallel arrangement [38]. The spiral-wound elements are placed in series within a pressure vessel, where the concentrate flow rate produced by one element is fed to the following one, while the produced permeates are mixed together. In analogy with high-scale plants described in literature, each pressure vessel includes 6 elements, each one composed of 5 membrane leaves wounded together. The total membrane area exposed by each pressure vessel is equal to 30 m^2 [39]. Also, according to the recovery rate to be achieved ($M_{p,out}/M_{feed}$, which corresponds to a required permeate flow rate), several vessels are typically arranged in parallel in order to increase the available membrane area [39].

The high-scale model deals with the design of the whole NF plant and the estimation of the required number of pressure vessels arranged in parallel (see Fig. 2). A schematic representation of the arrangement of the NF plant is reported in Fig. 5.

2.1.2. Economic model

Regarding the economic model, the Verberne cost model is employed [39–41]. All the equations of the model are based on practical data provided by NF units suppliers and its first applications were related to treatment systems for the removal of pesticides, hardness and nitrate from soil water [39]. The number of vessels, the feed flow rate and the operating feed pressure are the required inputs. The equations used for the calculation of the capital costs are reported in Table 2, where C_{civil} [$] represents the cost for the buildings housing the plant, C_{mech} [$] the cost for pumps, filters and piping system, $C_{electro}$ [$] the costs for the energy supply systems and $C_{membrane}$ [$] the investment for the membrane modules.

In all equations, M_{feed} is the total feed flow rate in [m^3/h] and P_{feed} is the inlet feed pressure in [bar]. These correlations make reference to vessels with a membrane area of 30 m^2. The capital costs are then linearly depreciated, the depreciation period is assumed equal to 30 years for the civil investment, 15 years for the mechanical and electro-technical equipment and 5 years for the membranes [39]. These costs are updated using the Chemical Engineering Plant Cost Index (CEPCI). A discount rate equal to 6% is considered for the calculation of the annuity, in line with typical values reported in the literature for water purification and desalination plants [42–43]. Among the operating costs, the energy cost is calculated taking into account the pump energy consumption and an average energy consumption of the membrane system equal to 40 Wh/m^3_{feed} [39]. The cost of chemicals is estimated as 0.020–0.025 $/$m^3$ of permeate [41]. Other costs including maintenance, quality control and daily operation are estimated to sum up to 2% of the capital costs [39].

2.2. Crystallizer

The treatment chain for the IEX spent brine includes two

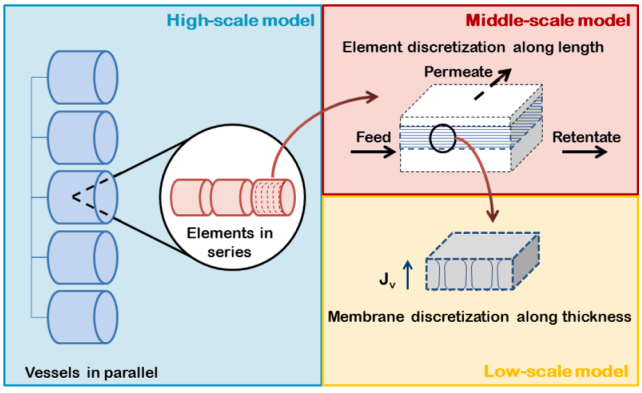

Fig. 2. Different scales of modelling of the nanofiltration unit.

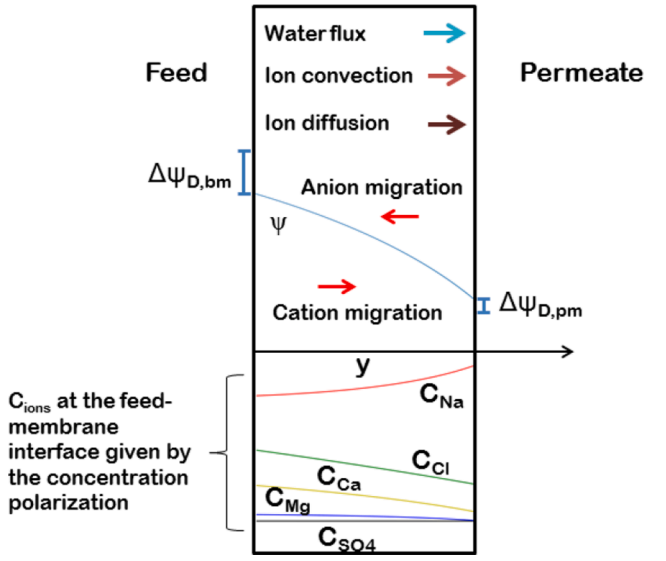

Fig. 3. Profiles of electric potential and ionic concentration through the membrane and relevant fluxes.

crystallization steps: one for the recovery of $Mg(OH)_2$, the other for $Ca(OH)_2$. A detailed simulation of the crystallizers is beyond the scope of this work: a simplified model based on mass balances was implemented to calculate the inlet flow rate and the outlet products flow rate. These figures are then used for the estimation of the economic parameters. The underlying assumption is that the hydroxide crystals produced via this process have the purity, the specific area and the size distribution suitable to be sold. In the present crystallization process, a first crystallization step is meant to separate the Mg^{2+} from the solution in the form of $Mg(OH)_2$; the produced suspension from the first crystallizer is filtered to get the solid crystals and the filtration effluent is fed to a second crystallizer where $Ca(OH)_2$ is produced and subsequently filtered. The investigated crystallizer is a plug-flow reactor, where the brine is fed at the entrance of the tube while the alkaline reactant (a NaOH solution) is injected into the tube in different equidistant points, in order to avoid too high supersaturation and to reduce the role of the primary nucleation. Because of the very low solubility of the two hydroxides, especially of $Mg(OH)_2$, a conversion of 100% typically occurs in the reactors. Consequently, the total inlet molar flow rate of Mg^{2+} and Ca^{2+} is converted into an outlet molar flow rate of $Mg(OH)_2$ and $Ca(OH)_2$. Furthermore, the estimation of the alkaline solution flow rate needed for the two separation stages is particularly important: it is calculated multiplying the entering molar flow rates of Mg^{2+} and Ca^{2+}, coming from the nanofiltration, by the stoichiometric coefficient (i.e. 2) and considering an excess of 10% with respect to the stoichiometric concentration. The volume flow rate is estimated assuming a concentration of the NaOH solution equal to 1 mol/l. For what concerns the economic estimations, the capital cost of the equipment is calculated via the Module Costing Technique starting from the purchasing cost of two crystallizers [44], one for each mineral, calculated as a function of the volume [m^3] and of two filters, calculated as a function of the area [m^2]. A disc and drum filter is selected as filter unit since its maximum capacity (i.e. 300 m^2 of filtration area) is higher than the one of a plate and frame filter (i.e. 80 m^2). For the calculation of the annualized capital costs (CAPEX of the crystallization) a discount rate of 6% and a depreciation period of 20 years are assumed. The operating costs include the cost of the energy required by the pumps of the feed solution and the reactant solution and the energy required by the filter, considering two filtration stages, one for the $Mg(OH)_2$ solution and one for the $Ca(OH)_2$ solution.

2.3. Multi-effect distillation

The last model employed for this work describes the Multi-Effect Distillation process. The process has been investigated in detail in the literature [45–46] and the model employed in the present work is extensively reported elsewhere [32]. The adopted MED plant has a forward feed arrangement (FF), because of the high operating concentrations and the high temperatures [47] and it is supposed to work in steady-state conditions. The model allows a full characterization of the flow rates, concentration and temperature profiles along the effects. The model inputs are the number of effects, the feed flow rate and salinity, the feed intake temperature, the steam temperature in the first effect and the temperature of the last effect. The main outputs are the heat exchanger areas of the evaporators, the preheater and the end-condenser, together with the steam flow rate required in the first effect. The steam flow rate allows estimating the thermal energy demand of the plant, which is given by the product of the steam flow rate and its latent heat at the corresponding pressure (in the present case at 1 bar). The model is able to simulate the behaviour of a plain MED or a MED coupled with a Thermo-Vapour Compressor (MED-TVC) and in this last case, the pressure of the motive steam is one of the inputs, while the output is the required motive steam flow rate. The technical model is fully coupled with an economic model, in which the estimation of the capital costs is performed via the application of the Module Costing Technique [44]. For the calculation of the CAPEX of the MED [$/y], again, we assumed a discount rate of 6% and a depreciation period of 25 years [43]. Finally, the estimation of the operating costs is based on the thermal and electric energy cost and on data relevant to real plants [48].

3. Case study under investigation and relevant model inputs

This section describes in detail the case study under investigation: it includes the description of the operating conditions used for the simulations, the parameters of the nanofiltration membranes (Section 3.1), the geometric properties and the main economic inputs (Section 3.2).

In the presented case, the economic feasibility of the proposed treatment chain is evaluated comparing a global parameter, called Levelized Brine Cost (LBC), with the cost of the currently used regenerant solution, equal to 8 US$/$m^3$. This cost corresponds to a 9%$^{w/w}$ NaCl-water solution, estimated considering a cost of the pure NaCl salt

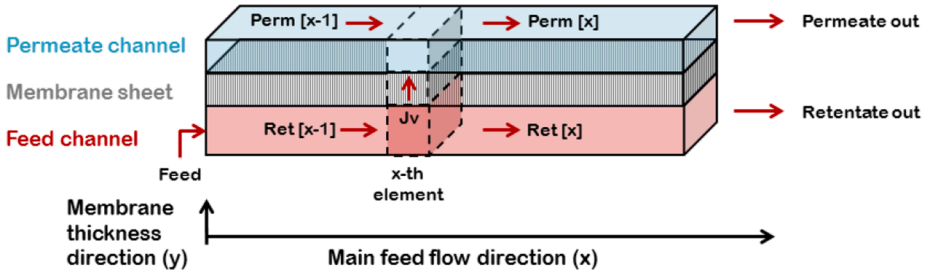

Fig. 4. Schematic representation of an unwound spiral-wound NF membrane element.

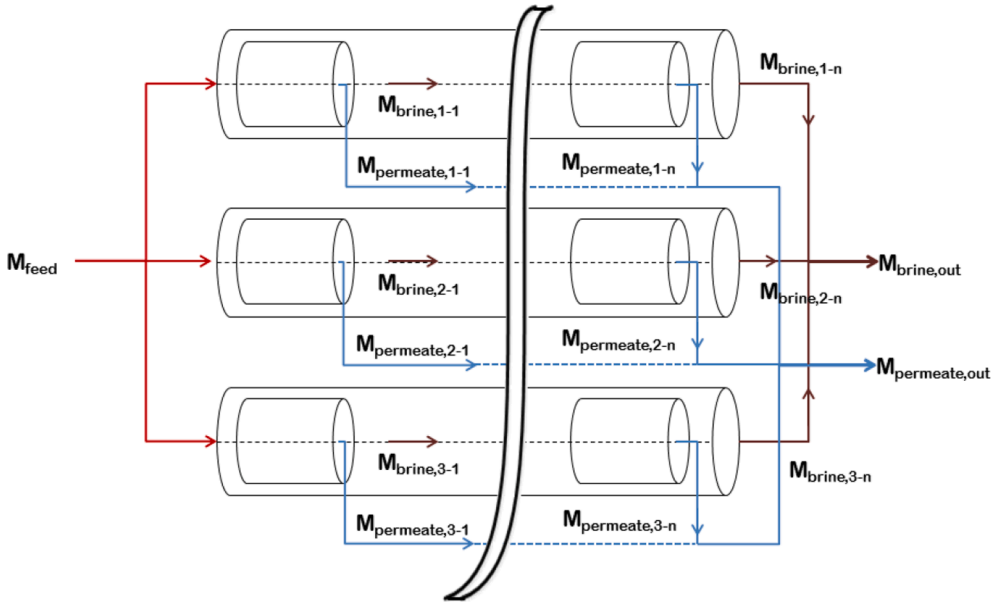

Fig. 5. Schematic representation of the arrangement of the pressure vessels in parallel in the NF plant.

Table 2
Capital cost estimation for the NF plant [39].

Equation	Equation number
$C_{civil} = 1034.4M_{feed} + 1487n_{vessel}$	(2)
$C_{mech} = 4329.6{M_{feed}}^{0.85} + 1089.6n_{vessel}$	(3)
$C_{electro} = 1.68*10^6 + 64.8P_{feed}M_{feed}$	(4)
$C_{membrane} = 1200n_{vessel}$	(5)

equal to 65 €/ton (80.2 US$/ton) and a cost of water equal to 1 US $/m^3.

The LBC is given by the sum of the annualized capital and operating costs minus the revenues of the chain by-products, divided by the amount of concentrate brine produced by the MED unit (see Eq. (6)).

$$LBC\left[\frac{\$}{m^3}\right] = \frac{CAPEX + OPEX - Revenue_{Mg(OH)_2} - Revenue_{Ca(OH)_2} - Revenue_{H_2O}}{M_{brine,MED}} \quad (6)$$

The definition of the LBC as the measure of the economic feasibility of the treatment chain is built in analogy with the definition of the Levelized Water Cost (LWC) for desalination plants. Therefore, several works in literature report techno-economic analyses of desalination processes, whose profitability is defined through the LWC, which includes the total costs of the technology and the distillate productivity of the plant [43].

The composition and the flow rate of the effluent, reported in Table 3, are based on the investigated case study (regeneration of the IEX resins in EVIDES water softening plant). Regarding the target product, the concentrate solution produced by the MED and re-usable for the IEX regeneration must have a fixed concentration of NaCl equal to 90,000 ppm (~1550 mol/m^3). This concentration is used as a design parameter, together with the steam temperature, the number of effects and the feed flow rate and concentration, to calculate the required steam flow rate and the area of heat exchangers and preheaters.

3.1. NF membrane properties

For what concerns the NF membranes, several works in the literature are devoted to estimating the parameters (pore radius r_{pore}, active layer membrane thickness δ_m, pore dielectric constant ε_{pore} and charge density X_d) in different operating conditions. These values are strongly dependent on the solutes and determine the membrane performances, in particular the solute rejections and the recovery. For the present study, the set of membrane parameters is based on previous literature works concerning NF units fed by solutions with a composition similar to the one under investigation. Each property is considered independent of the others, as already stated in [49]. In particular, the membrane pore radius is often found to be between 0.4 and 0.5 nm [35,50–51], while some studies showed that the active membrane thickness depends on the solute size, because of the complex and interconnected internal structure of the pores [52]. However, the most common range of membrane thickness is from 1 to 7 μm.

Regarding the dielectric pore constant (ε_{pore}), if the dielectric constant variation between bulk and pore is neglected, the value of ε_{pore} is taken equal to 80. In presence of NaCl, this is often found around 40 (values of 33.7 and 42.2 were found in literature for commercial membranes), while in presence of Mg^{2+} it has typically higher values (values of 46.6 and 65.1 were found) [51,53]. Next, the estimation of the charge density is a much discussed topic in literature, since its value depends not only on the solutes but also on their concentration. Most of the membranes are negatively charged at a neutral pH and the charge is given by the dissociation of sulfonic and/or carboxylic acid groups [54]. However, the membrane charge is significantly affected by the pH of the fed solution and its ionic strength. Therefore, the active sites can be more protonated or deprotonated varying the solution pH and other charged sites can be given by the adsorption of the ions present in the solution [55]. For example, Mazzoni et al. showed the trend of the membrane charge density with the concentration for NaCl and for $CaCl_2$ in presence of commercial membranes [56]. This study, in agreement with others reported in [57], demonstrated that in a very wide range of concentration of $CaCl_2$, the membrane presents a positive charge because of the preferential adsorption of Ca^{2+} on the membrane surface. Schaep et al. showed how the presence of Mg^{2+} ions leads to a positively charged membrane in a wide range of concentration [35]. This study also stated that, in presence of more ions, each component adds its own independent contribution to the overall membrane charge. In

Table 3
Feed flow rate and concentration values.

M_{feed} [m^3/h]	C_{Na} [mol/m^3]	C_{Cl} [mol/m^3]	C_{Mg} [mol/m^3]	C_{Ca} [mol/m^3]	C_{SO4} [mol/m^3]
130.0	173.9	662.2	55.6	191.7	3.125

the case under investigation, the presence of Mg^{2+} and Ca^{2+} in concentration much higher than in seawater may likely generate a positive charge on the membrane surface, which corresponds to higher values of Mg^{2+} and Ca^{2+} rejections. Having said that, in order to characterize a highly-performing membrane in presence of the investigated solution, the values of r_{pore}, δ_m and ε_{pore} are taken equal to the ones considered in previous works for seawater [37] and equal to 0.45 nm, 3 μm and 56.5 respectively. In fact, the components of the investigated brine are the same of seawater and these values proved to be much performing also for the case under investigation (see Section 4.1). Conversely, the value of charge density is assumed equal to 40 mol/m^3, since the concentrations are very different from seawater (much higher concentration of Mg^{2+} and Ca^{2+}) and the value used by Roy et al. in [37] (−80 mol/m^3) may not be suitable for this system. In this way, it is possible to achieve values of rejection of Mg^{2+}, Ca^{2+} and SO_4^{2-} within the typical intervals reported for the NF units integrated in desalination processes, i.e. from 85% to 97% for Mg^{2+}, from 70 to 97% for Ca^{2+} and higher than 95% for SO_4^{2-} [58]. The values of the membrane parameters employed in the present work are reported in Table 4.

3.2. Geometric properties of the units and main economic parameters

For what concerns the second part of the results, which is focused on the economic analysis of the whole treatment chain, the basic geometry of the plants has to be defined. With this respect, the area of the NF membrane leaf is equal to 1x1 m^2 and the feed spacer thickness is taken equal to 0.5 mm. The specifications of the crystallizer cannot be reported due to a confidentiality agreement with the company working on the joint development of the system. Regarding the MED, a plain MED, fed by waste heat with a pressure of 1 bar, is considered and the number of effects is fixed and equal to 13, as this is the optimal MED plant size under these operating conditions [32]. Regarding the economic analysis, the operating costs and the revenues depend on the cost of the alkaline reactant used in the crystallizer, on the selling price of the hydroxides and of the water and on the thermal and electric energy costs. These values are reported in Table 5.

4. Results and discussion

The results collected within this work are subdivided into two parts: in the first part (Section 4.1), the results relevant to the NF plant at different feed pressures and recovery values are reported, with a particular focus on the impact of the electric energy consumption on the total cost. Conversely, in the second part (Section 4.2) the overall treatment chain is analysed from the energetic and economic point of view, through the estimation of the costs relevant to each unit in the system (NF, crystallizer and MED) and the calculation of the Levelized Brine Cost (LBC).

4.1. Influence of the operating conditions of the nanofiltration unit

In the following, the NF unit performances are investigated to identify the most suitable operating conditions to be adopted for the treatment of the brine produced by IEX resins. The typical recovery of a NF unit used in desalination plants or in the removal of pollutants from water is very high (~80%), since in those cases the useful product is the permeate [58–60]. In this case, both permeate and retentate (after the crystallization steps) are fed to the MED unit, thus it may be interesting to investigate also NF units at a lower recovery. The role of feed pressure and recovery is investigated with respect to the performance of the whole NF plant. For a system with a fixed recovery (25%), the impact of the feed pressure on the ion rejection and on the overall cost of the plant is detected and the results are reported in Fig. 6. In this case, three pressures are considered, i.e. 20, 30 and 40 bar. Notably, it is not possible to consider lower pressures, since the high concentrations of the brine lead to a very high osmotic pressure. At the same time, higher pressures are not investigated since the maximum operating pressure in a NF system is generally around 40 bar. Fig. 6a depicts the trends of the rejection of the ions vs. the feed pressure, with a fixed recovery of 25% and with the feed flow rate and concentration values reported in Table 3. Notably, the higher the feed pressure, the higher the rejection of every ion. This is expected, because a higher feed pressure leads to a higher water flux through the membrane, when the pore radius and the membrane thickness are fixed. However, the most significant increase of the rejection is reported for Na^+ and Cl^-, while the Ca^{2+} rejection growth is less than 10% and the change in Mg^{2+} and SO_4^{2-} rejection is almost negligible. Fig. 6b reports the terms of cost of the NF plant at different P_{feed}, estimated according to the equations reported in Section 2.1.2. Firstly, the capital costs (annualized via linear depreciation) slightly decrease as the feed pressure increases, because the water flux through the membrane grows and the number of vessels in parallel required for the fixed recovery is lower. At the same time, the cost relevant to the energy supply system ($C_{electro}$) increases with the feed pressure and this effect becomes predominant at higher pressures, leading to a slight increase of the total capital costs. Conversely, all operating costs, especially the energy consumption, rise. Since the latter effect is prominent, the total annualized cost of the NF unit increases with the feed pressure.

Moreover, the effect of different recovery ratios is studied ranging from 25% up to 65% (i.e. 25%, 50% and 65%). The range is limited up to a maximum recovery of 65% because, with a single stage, higher recoveries would require operating pressures higher than 40 bar. Fig. 7 shows the trends of the rejection of the ions vs. the recovery at a feed pressure equal to 40 bar and with the values of feed flow rate and concentrations reported in Table 3. The rejection decreases as the recovery rises, for all ions apart from Na^+, whose rejection is almost constant. The rejection trends are explicable considering that, at higher recovery, the required number of vessels in parallel is higher and each vessel is crossed by a lower feed flow rate. This leads to a growing concentration polarization, which causes a higher driving force for the ion fluxes through the membrane and a lower rejection.

4.2. Treatment chain

4.2.1. Economic analysis and assessment of the energy demand varying the NF recovery

The following section reports the results of the economic analysis of the whole chain and the assessment of the energy requirements, collected at three different NF recovery values. As shown in Fig. 6b, for the present case, the most convenient condition for the NF plant is at the lowest feed pressure. For this reason, the comparison is carried out at different NF feed pressures, i.e. 20 bar for a recovery of 25%, 30 bar for 50% and 40 bar for 65%.

The variation of the recovery has several consequences on the chain performances, which are analysed from the economic and energetic point of view in Fig. 8 and Fig. 10. Regarding the NF plant, its size (i.e. the number of required vessels) increases with the recovery and the ion rejection decreases (as shown in Fig. 7). The first effect leads to a growth of the total capital costs relevant to the NF unit, while the operating costs increase because the systems work at higher feed pressure, as shown in Fig. 8. Moreover, for the definition itself of recovery, its rise corresponds to a reduction of the NF retentate flow rate, which is fed to the crystallizer. This causes the reduction of the crystallizer volume and, consequently, the drop of both capital and operating costs.

Table 4
Employed NF membrane parameters.

r_{pore} [nm]	δ_m [μm]	ε_{pore} [–]	X_d [mol/m^3]
0.45	3	56.5	40

Table 5
Costs of the reactants, utilities and products used for the economic analysis.

$Cost_{NaOH}$ [$/ton]	$Price_{Mg(OH)2}$ [$/ton]	$Price_{Ca(OH)2}$ [$/ton]	$Price_{water}$ [$/m^3]	$Cost_{therm.energy}$ [$/kWh$_{th}$]	$Cost_{el.energy}$ [$/kWh$_{el}$]
350	1200	300	1	0.01	0.06

However, these variations are relatively small (compared to other costs) and are not very evident in the cost overview reported in Fig. 8. At the same time, the diminution of the bivalent ion rejection with the recovery has various effects. Since the concentration of bivalent ions in the NF retentate decreases, the required NaOH solution flow rate decreases, but the produced flow rates of $Mg(OH)_2$ and $Ca(OH)_2$ are lower. From the economic point of view, in the crystallizer, we found a simultaneous decrease of the expenses due to the reactant used in the crystallizer and of the revenues due to the minerals' production, with the rise of the recovery. It has to be said that the cost of the NaOH solution constitutes an operating cost in the crystallization stage; however, it is separated in Fig. 8 on purpose in order to highlight its weight in the treatment chain. Furthermore, the MED feed is significantly affected by the NF recovery, since it is given by the NF permeate mixed with the effluent from the crystallizer. The flow rate fed to the MED slightly decreases with the recovery, because of the different NaOH-water solution flow rate. The NaCl concentration of the MED feed depends on the NaOH solution concentration and, assuming a fixed NaOH concentration equal to 1 M, the MED feed concentration decreases at higher recovery values, because of the higher permeate flow rates. At the same time, the higher permeate flow rate causes the growth of the concentration of bivalent ions in the MED feed, and consequently in the MED brine. This is because the concentration of bivalent ions in the NF permeate is higher than in the crystallizer effluent and the rejection worsens when recovery increases. However, these concentrations are very low in all cases and for the chain with a recovery of 25%, the concentrations of Mg^{2+} and Ca^{2+} in the recirculated brine are around 1.5 mol/m^3 and 18 mol/m^3, which are less than 10% of their concentration in the initial resins effluent.

In terms of costs, the decrease of the feed flow rate and NaCl concentration with the recovery growth causes a slight reduction of both capital and operating costs relevant to the MED plant.

Concerning the global costs, Fig. 8 clearly shows that both the expenses and the revenues decrease with the increase of the recovery. It has also to be underlined that the costs relevant (i) to the reactant employed in the crystallizer and (ii) to the MED unit (mostly thermal energy cost) play the most prominent role among the expenses. Regarding the capital costs, the MED covers the highest percentage, while the capital costs of the NF unit and the crystallizers, which include also the filter cost, represent a very small fraction of the total (the cost of the crystallizer is almost negligible). Turning to the revenues, these are found to play a crucial role for the feasibility of the system, especially the ones due to the minerals production. Notably, although the price of the $Mg(OH)_2$ is much higher than that of $Ca(OH)_2$, the net difference in their concentration in the effluent makes their revenues comparable and their sum is similar to or even higher (at low recovery) than the total cost of the NaOH solution. Also the revenue coming from the water production in the MED is significant, although it is much lower than the other two terms, as expected. Overall, the total cost is given by the difference between the annualized expenses (column on the left for each recovery value) and the annualized revenues (column on the right for each recovery value). The total annualized cost is almost constant

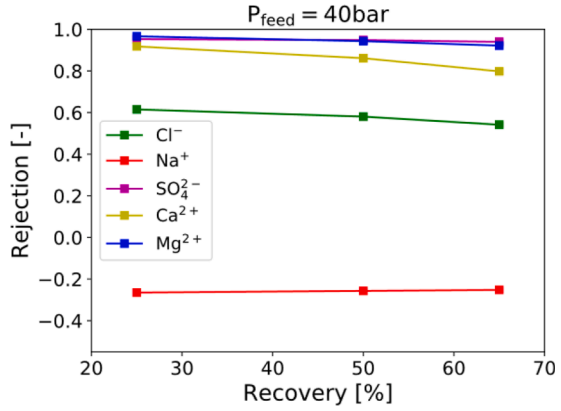

Fig. 7. Rejection of the ions at different recovery ratios. (P_{feed} = 40 bar; M_{feed} and C_{bulk} values reported in Table 3 and membrane properties reported in Table 4).

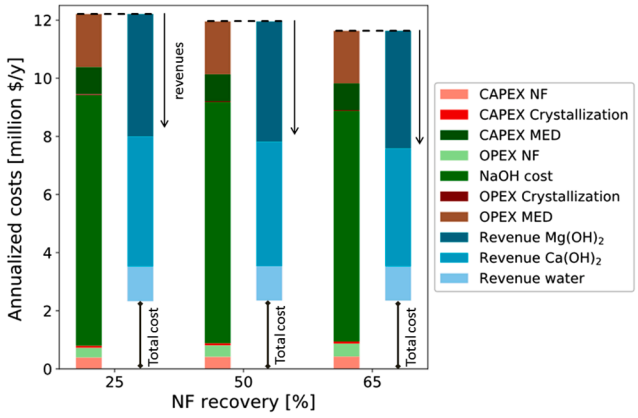

Fig. 8. Annualized costs [$/y] relevant to each unit in the treatment chain for three NF recovery values.

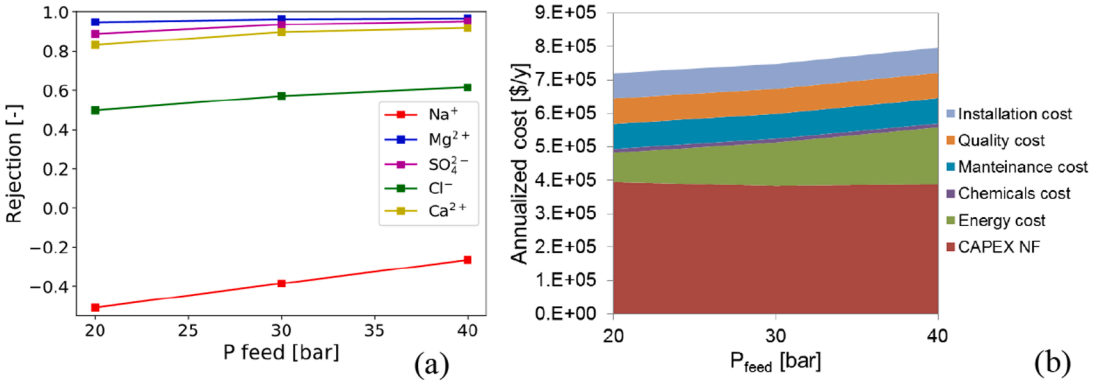

Fig. 6. Rejection of the ions (a) and analysis of the cost terms of the nanofiltration plant (b) at different P_{feed} [bar]. (Recovery = 25%; M_{feed} and C_{bulk} values reported in Table 3 and membrane properties reported in Table 4).

across the three cases. This is mostly due to the fact that, in all scenarios, the dominant terms are the cost of the NaOH solution and the revenues given by the minerals' production. These terms are almost balanced and this leads to a relatively stable total cost.

On the one hand, this analysis highlights the role of nanofiltration membranes, whose rejection to the different ions has a crucial role for the revenue estimation. Therefore, from the practical point of view, the membrane selection plays a fundamental role for the definition of the performances of the whole treatment system. On the other hand, it is worth noting the critical weight of the cost of the alkaline solution. Even if, in the presented cases, the revenues counterbalance the expenditure for the reactant, less expensive alternatives may be considered to further reduce the total costs. However, it has to be said that the NaOH solution is particularly advantageous because it ensures the production of pure hydroxide crystals and, importantly, it does not add other chemicals to the solution than Na^+, whose excess can be neutralized with HCl producing NaCl.

Moreover, in order to assess the feasibility of the treatment chain, another aspect to be considered is the productivity of the system, i.e. the concentrate solution ($M_{brine,MED}$) produced by the MED, which is the main product of the chain (Fig. 9a). Also in this case, the recovery plays a role because the concentration of NaCl in the solution fed to the MED changes. In particular, the MED inlet concentration decreases with the recovery, while the outlet concentration of the MED brine is fixed and equal to 90,000 ppm in all cases. Therefore, according to the global mass balance in the MED unit, the produced concentrate flow rate results lower at a higher recovery. The combination of these terms leads to the definition of the Levelized Brine Cost (LBC), reported in Fig. 9b. Notably, the decrease of the produced $M_{brine,MED}$ determines an increasing trend of the LBC with the recovery. However, the increase is relatively moderate and the maximum value, at the maximum recovery, is around 5.4 $/m^3, while the minimum LBC (at a recovery of 25%) is equal to 4.9 $/m^3. This makes the technology very competitive with the state of the art, since currently, a fresh solution of NaCl is provided for each regeneration cycle at a cost of 8 $/m^3 [32]. Thus, the proposed treatment chain reduces the consumption of raw materials (i.e. NaCl and pure water) and the disposal of brines into the environment, and is also more convenient than the current system from the economic point of view.

In relation to the energy demand, Fig. 10a reports the electricity requirement of each unit, while Fig. 10b shows the total electric and thermal demands. Notably, thermal consumption is driven by the MED unit only. The electric energy required by nanofiltration is given by the pumping energy and a general consumption for the membrane system. This last term depends on the feed flow rate, so it is constant in the three cases, while the pumping energy depends on the feed pressure, thus it rises with the recovery. The electric energy required to pump the feed in the crystallizer decreases when the recovery increases, however this term is very low, because of the low pressure required at the crystallizer inlet (mostly depending on the pressure drops in the nozzles). The electric energy demand of the filtration system is also calculated, starting from the energy consumption data given by the supplier for a certain filter size and scaling this value with the flow rate. In particular, the energy requirement of the filtration system slightly decreases with the NF recovery. Finally, both thermic and electric energy demand of the MED unit show a decreasing trend, since the produced distillate flow rate decreases at higher value of the NF recovery. Overall, the total electric energy requirement increases with the recovery, because of the increase of the pumping energy in the NF unit (Fig. 10b). Conversely, the thermal energy consumption decreases with the NF recovery, since the only contribution is given by the MED unit.

Overall, our analysis shows that the chain including the NF plant with the lowest recovery (25%) is the best performing from an economic point of view, since it corresponds to the lowest LBC and it allows for reducing the amount of bivalent ions in the recirculated regenerant solution. Regarding the energy requirements, this system presents the lowest electricity demand but the highest thermal demand. However, since the real case study provides the presence of low-grade waste heat at a low cost, a higher heat demand can be met within the feasibility range of LBC.

In Fig. 11 the operating costs are compared for one case (recovery equal to 25%), in order to evaluate the role of the energy costs. Since Fig. 8 showed that the expense due to the reactant in the crystallizer and the revenues coming from $Mg(OH)_2$ and $Ca(OH)_2$ production are almost balanced, these terms were excluded. It is worth noting that the main term of cost corresponds to the thermal energy required by the MED unit, which covers more than 30% of the total. This is due to the fact that the thermal energy requirement is much higher (around 60 kWh/$m^3_{dist,chain}$) than the electric energy requirement of NF (around 1 kWh/$m^3_{dist,chain}$, which corresponds to around 3 kWh/$m^3_{permeate,NF}$) and MED (1.5 kWh/$m^3_{dist,chain}$).

This analysis shows that the specific cost of the thermal energy may have a crucial impact on the total cost and the utilization of waste heat allows for reducing significantly the LBC.

4.2.2. Sensitivity analyses

4.2.2.1. Sensitivity analysis on the estimation of CAPEX and operating costs. The estimation of the capital costs is performed via literature correlation or using data provided by technology suppliers. However, the degree of uncertainty in these estimations may be relatively significant. For this reason, a sensitivity analysis on the capital costs is performed, introducing a variation of 50% in the total capex and evaluating the corresponding LBC variation. The results are reported in Fig. 12, where the error bars correspond to the maximum and the

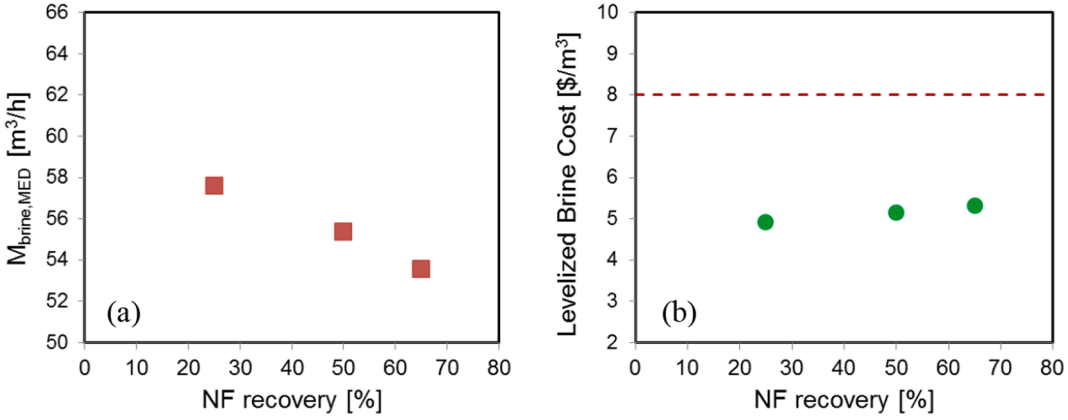

Fig. 9. Produced brine flow rate (in the MED) [m^3/h] vs. the NF recovery (a) and Levelized Brine Cost [$/$m^3$] vs. the NF recovery (b). In chart (b), the red dashed line corresponds to the current cost of the fresh regenerant solution.

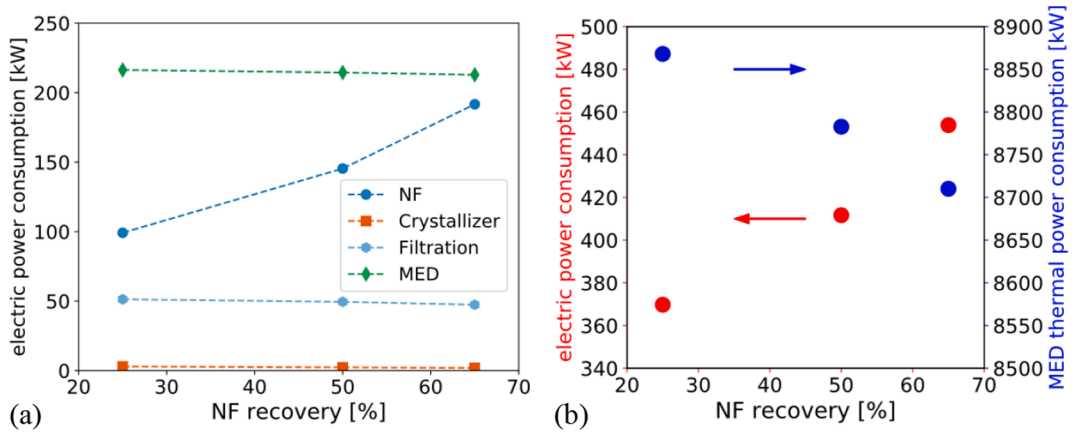

Fig. 10. Electric power consumption of the treatment chain for the three NF recovery values (a) and overall thermal (due to MED only) and electric power consumption vs the recovery (b).

minimum calculated LBC. It is remarkable that the LBC variation is around 30%, even for a variation of the total capital cost of 50%. The trend of the LBC with the NF recovery remains the same and the maximum calculated LBC is still lower than 8 $/m^3.

Moreover, it is interesting to evaluate the impact of the variation of the price of the materials on the overall costs, in order to identify the key components of the system. This analysis is performed for the scenario with a recovery of 25% and the results are shown in Fig. 13. In this figure the effect of NaOH cost and of $Mg(OH)_2$, $Ca(OH)_2$ and water selling prices is reported. The red line indicates a LBC variation leading to a LBC equal to the current cost of the regenerant solution. It is evident that the cost of NaOH is the prominent term in the definition of the LBC: a NaOH cost increase of 50% corresponds to a LBC increase of around 180%. This strong dependency is somehow expected on the basis of the data shown in Fig. 8. Moreover, the effect of the variation of $Mg(OH)_2$ and $Ca(OH)_2$ selling price is comparable, although the specific prices are very different (the price of $Ca(OH)_2$ is varied from 150 to 450 $/ton, while the price of $Mg(OH)_2$ from 600 to 1800 $/ton): this is due to the fact that they have very different concentrations in the NF retentate. Finally, the impact of the water selling price is much lower compared to the other terms and its variation of 50% gives a variation of the LBC of around 25%.

4.2.2.2. Sensitivity analysis on the feed flow rate M_{feed}. The sensitivity analysis on the feed flow rate aims at investigating how much economies of scale may affect the overall cost of the treatment chain and the relevant LBC. In all data shown so far, the feed flow rate is equal to 130 m^3/h, in line with the brine volumes produced by the

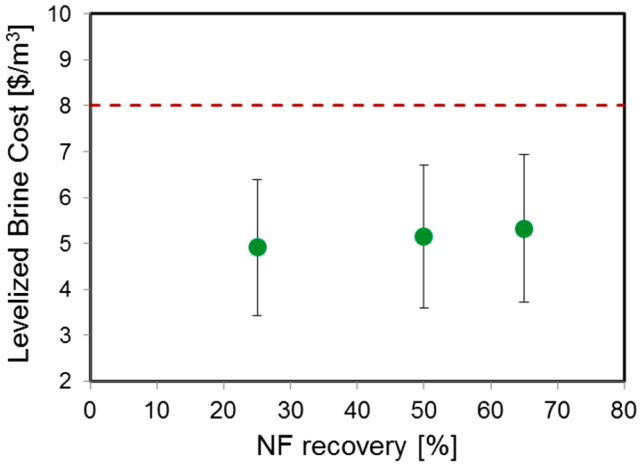

Fig. 12. Sensitivity of the Levelized Brine Cost [$/m^3] on the capital costs estimation. Bars are related to a ± 50% of total CAPEX.

regeneration of the IEX resins in a real water softening plant. However, the flow rates of waste effluents may be lower. It is well known that the specific cost of a generic plant increases when its size decreases because of economies of scale. For this reason, it is important to recognize a range of feed flow rates in which the treatment chain is still more economically advantageous than supplying the fresh regenerant solution. Fig. 14 shows the LBC as a function of M_{feed} for the case of

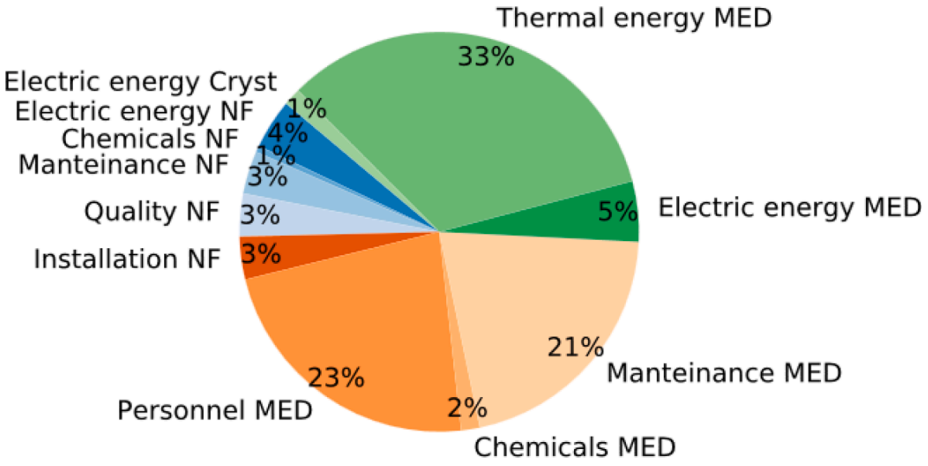

Fig. 11. Main operating costs of the treatment chain, excluding the cost of the NaOH solution.

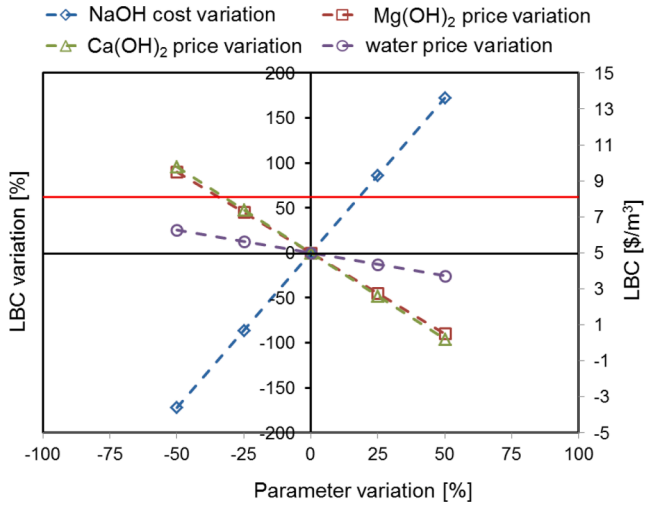

Fig. 13. Sensitivity analysis on the cost of the reactant NaOH and on the selling price of $Mg(OH)_2$, $Ca(OH)_2$ and water for the case of recovery equal to 25%.

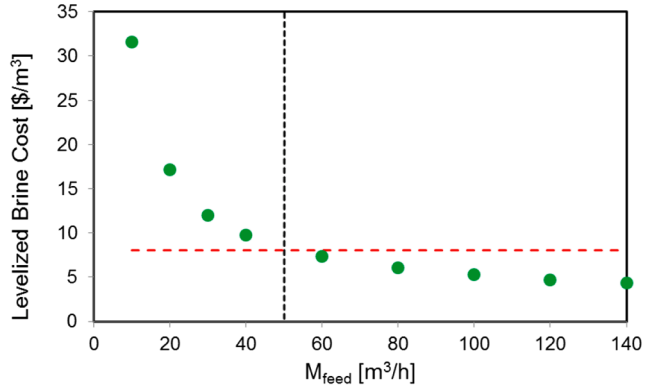

Fig. 14. Variation of the Levelized Brine Cost [$/m^3] with M_{feed}.

a recovery of 25%. The LBC relevant to the whole treatment chain decreases as M_{feed} increases, in agreement with economy of scale, and it shows very high values at very low M_{feed}, a sharp decrease until a flow rate of around 40 m^3/h and a flatter trend at the largest M_{feed}. It is remarkable that all industrial cases with a M_{feed} higher than 50 m^3/h would exhibit LBC values lower than the current value of the regenerant solution (i.e. 8 $/m^3), thus the proposed treatment chain results very competitive with the state of the art even in a wide range of operating conditions.

5. Conclusions

Within the wide framework of the water-energy nexus, this work presents an 'energy for water' system in which a treatment chain is devised for the industrial wastewater produced by the regeneration of ion exchange resins in a water softening plant. A comprehensive techno-economic assessment of the treatment chain, given by the combination of membrane and thermal desalination processes, and an evaluation of the energy requirements are presented for the first time. The chain aims at recovering the minerals in the form of hydroxides, and at producing the NaCl-water solution re-usable as a reactant in the following regeneration cycle. The treatment chain includes nanofiltration, double-stage crystallization for the production of $Mg(OH)_2$ and $Ca(OH)_2$ and multi-effect distillation. A techno-economic model was set up for each unit and these models were interconnected via mass balances to simulate the integrated system. A global economic parameter, called Levelized Brine Cost (LBC) is used to assess the economic feasibility. Among the energy requirements of the system, the thermal energy required by the multi-effect distillation is the most relevant term (around 60 kWh_{th}/m^3_{dist}), while the electric demand of the other units are between 1 and 3 kWh_{el}/m^3_{dist}.

Regarding the economic analysis, the multi-effect distillation covers the highest fraction of the capital costs, nevertheless the operating costs, and in particular the cost of the alkaline solution employed in the crystallizers, play the most important role. Notably, the revenues coming from the hydroxides production are almost able to counterbalance the expense due to the NaOH solution, especially at low nanofiltration recovery. Moreover, the analysis of the other operating cost terms, with the exclusion of the alkaline solution cost, showed that the total energy demand of the multi-effect distillation unit covers almost 40% of the OPEX. Therefore, the energy cost, and in particular the thermal energy cost, may be of crucial importance and the availability of waste heat at low cost allows a net reduction of the total cost of the treatment chain.

When the nanofiltration recovery increases, on the one hand, the membrane rejection worsens and since both revenues and expenditure decrease, the trend of the annualized total cost showed only a slight variation. On the other hand, the flow rate of the produced brine decreases: the combination of the variations of total cost and brine production leads to an increasing trend of the Levelized Brine Cost. However, for all scenarios investigated, the Levelized Brine Cost was found much lower than the current cost of the regenerant solution, thus proving the economic feasibility of the proposed treatment chain. The most feasible configuration presented a Levelized Brine Cost of 4.9 $/m^3 with a nanofiltration recovery of 25%.

Finally, varying the feed flow rate M_{feed}, we found that, although economies of scale are responsible for higher Levelized Brine Cost at low flow rates, the proposed treatment solution remains economically advantageous for all processes with M_{feed} higher than 50 m^3/h, which are typical sizes of industrial wastewater treatment plants.

Overall, this study presents an innovative system for the treatment and recycling of industrial wastewater, which was developed and parameterized for a practical application: the treatment of the spent regenerant solution of ion exchange resins employed for water softening. The analysis of the costs and energy demands of the single units in the treatment chain allows for identifying the most expensive (in terms of investment cost as well as operating cost) and the most energy-intensive units. The presented results give comprehensive indications concerning the economic feasibility of the investigated system and clearly indicate which aspects may be improved in the future.

Acknowledgements

This work was funded by the ZERO BRINE project (ZERO BRINE – Industrial Desalination – Resource Recovery – Circular Economy) - Horizon 2020 programme, Project Number: 730390: www.zerobrine.eu.

Appendix A

A.1. Low-scale: Membrane model, discretization along the thickness (y axis)

The mechanisms within the membranes are described via the Donnan Steric Pore Model with Dielectric Exclusion (DSPM-DE). The DSPME-DE model derives from the resolution of the extended Nernst-Plank equation along the thickness of the membrane: it takes into account the three

different mechanisms of ion transport, i.e. convection, diffusion and electro-migration (Eq. (1) in Table A1). Along the y axis, which corresponds to the thickness of the membrane, the membrane is discretized in a certain number of elements, taken equal to 50 in the present work on the basis of a preliminary sensitivity analysis (as shown in paragraph A.4). The index employed for the elements along the y axis is 'j', while the index 'i' represents the different ionic species, as typically used in literature.

The main equations are reported in Table A1, where $C^m_{i,j}$, C^{bm}_i, C^b_i and C^p_i represent the concentration of the species *i* in the j-th interval within the membrane, at the bulk-membrane interface just before entering in the pore, in the bulk solution and in the permeate, respectively. J_i and J_v are the overall flux of the species *i* and the solvent (water) convective flux across the membrane, respectively. In addition, ψ represents the electric potential across the membrane, ξ the electric potential gradient at the bulk-membrane interface, outside the electric double layer, and $\Delta\psi_{D,bm}$ and $\Delta\psi_{D,pm}$ represent the Donnan potential difference at the bulk-membrane interface and at the permeate-membrane interface, respectively. $K_{i,c}$ and $k_{i,d}$ are the hindered convective and diffusive mass transfer coefficients of the ions within the pore, depending on λ_i, i.e. the ratio between the solute radius (r_i) and the pore radius (r_{pore}), defined in Eqs. (2) and (3). $D_{i,p}$ (Eq. (4)) is the diffusivity of the species *i* within the pore, which is corrected with respect to the diffusivity in the bulk via $k_{i,d}$. Solving the system of equations reported in Table A1 provides the ion partitioning at the two membrane interfaces (Eq. (5) for the bulk-membrane interface and Eq. (6) for the permeate-membrane interface), which is determined by the Donnan equilibrium, the steric effect (evaluated via the coefficient Φ_i, calculated via Eq. (11)) and the dielectric exclusion (estimated through the coefficient $\Phi_{B,i}$, i.e. the Born solvation contribution for partitioning, see Eqs. (9) and (10)). This last effect was widely investigated in literature, since it has a prominent role in the definition of the ion rejection [51,61]. In the interface equilibrium, the concentrations are multiplied by the activity coefficient γ, to take into account the non-ideality of the solutions, estimated via the Davies equations (see Eqs. (7) and (8)). Other conditions which have to be fulfilled are the electro-neutrality on the bulk, on the permeate side and inside the membrane, where a fixed charge density X_d is present (Eqs. (12)–(14) respectively). Moreover, the mass transfer resistance on the bulk side is taken into account to calculate the concentration of the ions on the bulk-membrane interface (just before entering into the pore). Therefore, the balance in Eq. (15) represents the solute flux from the bulk to the membrane and it is used to estimate the role of the concentration polarization. The mass transfer coefficient in the bulk, $k^{bulk}_{c,i}$ depends on the flow regime and is estimated via the correlation developed for spiral wound membranes [62], reported in Eq. (17). According to Eq. (16), $k'^{bulk}_{c,i}$ is obtained multiplying the mass transfer coefficient $k^{bulk}_{c,i}$ by a factor depending on the permeation flux through the membrane [63]. The concentration polarization effect is neglected on the permeate side. The solvent flux J_v through the membrane, defined in Eq. (18), is estimated via Hagen-Poiseuille relation. It depends on the membrane geometric parameters and on the net driving pressure, ΔP, which is given by the pressure difference between bulk and permeate channel minus the osmotic pressure $\Delta\Pi$, given by Eq. (19). Finally, η_{mix} is the mixing efficiency of the net of the spacer [62], h_f is

Table A1
Equations of the implemented DSPM-DE model.

$$j_i = J_v C_{i,p} = -D_{i,p}\frac{C^m_{i,j+1} - C^m_{i,j}}{\delta y_j} - \frac{1}{2}z_i(C^m_{i,j+1} + C^m_{i,j})D_{i,p}\frac{F}{RT}\frac{\psi_{j+1} - \psi_j}{\delta y_j} + \frac{1}{2}k_{i,c}(C^m_{i,j+1} + C^m_{i,j})J_v \quad (1)$$

$$k_{i,d} = \frac{1 + 9/8\lambda_i ln(\lambda_i) - 1.56034\lambda_i + 0.528155\lambda_i^2 + 1.91521\lambda_i^3 - 2.81903\lambda_i^4 + 0.270788\lambda_i^5 + 1.10115\lambda_i^6 - 0.435933\lambda_i^7}{\phi_i} \quad (2)$$

$$k_{i,c} = \frac{1 + 3.867\lambda_i - 1.907\lambda_i^2 - 0.834\lambda_i^3}{1 + 1.867\lambda_i - 0.741\lambda_i^2} \quad (3)$$

$$D_{i,p} = k_{i,d}D_{i,\infty} \quad (4)$$

$$\frac{\gamma^m_{i,1}C^m_{i,1}}{\gamma^{bm}_i C^{bm}_i} = \phi_i\phi_{Bi}\exp\left(-\frac{z_iF}{RT}\Delta\psi_{D,bm}\right) \quad (5)$$

$$\frac{\gamma^m_{i,N}C^m_{i,N}}{\gamma^p_i C^p_1} = \phi_i\phi_{Bi}\exp\left(-\frac{z_iF}{RT}\Delta\psi_{D,pm}\right) \quad (6)$$

$$\log\gamma_i = -Az_i^2\left(\frac{\sqrt{I}}{1+\sqrt{I}} - 0.3I\right) \quad (7)$$

$$A = \frac{e_0^3 N_A^{1/2}}{\ln(10)4\pi\sqrt{2}(\varepsilon k_B T)^{3/2}} \quad (8)$$

$$\phi_{Bi} = \exp\left(-\frac{\Delta W_i}{k_B T}\right) \quad (9)$$

$$\Delta W_i = \frac{z_i^2 e_0^2}{8\pi\varepsilon_0 r_i}\left(\frac{1}{\varepsilon_{pore}} - \frac{1}{\varepsilon_{bulk}}\right) \quad (10)$$

$$\phi_i = (1-\lambda_i)^2 \quad (11)$$

$$\sum_i z_i C^{bm}_i = 0 \quad (12)$$

$$\sum_i z_i C^p_i = 0 \quad (13)$$

$$\sum_i z_i C^m_{i,j} + X_d = 0 \quad (14)$$

$$j_i = -k'^{bulk}_{c,i}(C^{bm}_i - C^b_i) + J_v C^{bm}_i - z_i C^{bm}_i D_{i,\infty}\frac{F}{RT}\xi \quad (15)$$

$$k'^{bulk}_{c,i} = k^{bulk}_{c,i}\Xi = k^{bulk}_{c,i}\left[\frac{J_v}{k^{bulk}_{c,i}} + \left(1 + 0.26\left(\frac{J_v}{k^{bulk}_{c,i}}\right)^{1.4}\right)^{-1.7}\right] \quad (16)$$

$$k^{bulk}_{c,i} = 0.753\left(\frac{\eta_{mix}}{2-\eta_{mix}}\right)^{1/2}\left(\frac{D_{i,\infty}}{h_f}\right)Sc^{-1/6}\left(\frac{Pe_i h_f}{L_{mix}}\right)^{1/2} \quad (17)$$

$$J_v = \frac{\Delta P r_{pore}^2}{8\eta\delta_m} \quad (18)$$

$$\Delta\Pi = RT\sum_i (C^{bm}_i - C^p_i) \quad (19)$$

$$Pe = \frac{2h_f u_f}{D_{i,\infty}} \quad (20)$$

$$Sc = \frac{\eta_f}{\rho_f D_{i,\infty}} \quad (21)$$

the height of the feed channel, L_{mix} is the mixing length of the spacer, Pe and Sc are the Peclet and the Schmidt adimensional numbers respectively, defined in Eqs. (20) and (21), and u_f, ρ_f and η_f are the feed solution velocity, density and viscosity respectively.

The system of equations composing the DSPM-DE model is linearized according to [36] and solved in Python via the *LAPACK routine_gesv*. The problem is then solved via iterations, updating the coefficients of the linearized equations and solving the linear system, until the residuals relevant to the imposed conditions are low enough ($< 1\,0^{-4}$).

A.2. Middle-scale: Element model, discretization along the length (x axis)

At the middle scale, the low scale model is integrated for the resolution of a whole NF element. In the present middle-scale model, an iterative calculation is set up, where the average values of the concentration, flow rates and pressure are firstly guessed in each discretization interval (x-th interval) for the calculation of the osmotic pressure and the bulk mass transfer coefficient, thus the low-scale model is applied to calculate the ions rejection and the water flux. Finally, the outlet concentrations and flow rates for each discretization interval are calculated via mass balances, as reported in Table A2. The pressure losses along the element are defined according to [37].

In Table A2, M_p and C_i^p are the mass flow rate and the concentrations in the permeate channel, M_{ret} and C_i^{ret} are the flow rate and the concentrations in the retentate channel, which are equal to the feed flow rate and the concentration of the feed in the next interval (M_b and C_i^b). $A_{membr,elem}$ and $n_{discr,L}$ are the total membrane area of a NF element and the number of discretization intervals along the main feed flow direction. Regarding the pressure losses definition, f is the friction factor, l is the length of the discretization interval and D_H is the hydraulic diameter relevant to the feed channel, employed also in the calculation of the Reynolds number Re, defined in Eq. (30).

Table A2
Equations to model a nanofiltration element.

$M_{p_x} = M_{p_{x-1}} + J_{v_x}\frac{A_{membr,elem}}{n_{discr,L}}$	(22)
$M_{ret\,x} = M_{b_x} - J_{v_x}\frac{A_{membr,elem}}{n_{discr,L}}$	(23)
$C^p{}_{i_x} = \frac{C^p{}_{i_{x-1}} M_{p_{x-1}} + j_{i_x}\frac{A_{membr,elem}}{n_{discr,L}}}{M_{p_x}}$	(24)
$C^{ret}{}_{i_x} = \frac{C^b{}_{i_x} M_{b_x} - j_{i_x}\frac{A_{membr,elem}}{n_{discr,L}}}{M_{ret\,x}}$	(25)
$M_{b_x} = M_{ret\,x-1}$	(26)
$C^b{}_{i_x} = C^{ret}{}_{i_{x-1}}$	(27)
$P_x = P_{x-1} - \Delta P_{losses} = P_{x-1} - \frac{f}{2}\frac{l}{D_H}\varrho_f u_f{}^2$	(28)
$f = \frac{6.23}{Re^{0.3}}$	(29)
$Re = \frac{\rho_f u_f D_H}{\eta_f}$	(30)

A.3. High-scale: Plant model, vessels arrangement

The high scale model is devoted to calculating the total number of vessels required for the achievement of a certain recovery. In the model, an iterative calculation is performed to estimate the total membrane area required to achieve a certain recovery rate. Firstly, a guess number of vessels in parallel (i.e. a guess total membrane area) is given through the ratio between the required permeate flow rate and a guessed average water flow rate through the membrane (J_v). On the basis of the number of vessels in parallel, the feed flow rate for each vessel is calculated and the series of elements within the single vessel is solved. Then, the average solvent flux in the vessel is recalculated in relation to the net driving pressure along the elements, and the total recovery rate is calculated. At this point, the number of pressure vessels in parallel is updated assuming a linear correlation between the number of vessels and the recovery and another iteration starts. The iterative calculation stops as soon as the overall recovery ratio is higher than or equal to the required one. This last iterative procedure is of crucial importance, since the solvent flux through the membrane changes significantly within one element and along the vessel. As a matter of fact, assuming an average flux equal to the one at the first element entrance may lead to a strong underestimation of the required number of vessels, which would have important economic consequences.

A.4. Membrane-scale model validation and sensitivity analysis

As mentioned in paragraph A.1, the membrane thickness has been discretized in 50 elements. The discretization has been selected as the result of a sensitivity analysis, where the number of steps was varied from 10 to 100. Fig. A1 shows the trends of the concentration of Ca^{2+} and Mg^{2+} throughout the membrane thickness at different numbers of discretization steps. Notably, the trends are overlapped for N higher than or equal to 50. Therefore, it is possible to conclude that a 50-steps discretization is able to predict accurately the behaviour of the NF membrane.

Finally, the implemented DSPM-DE model was validated via the comparison with some experimental results reported in literature for two different salt solutions in presence of NF270 membranes [51]. For this case, we adopted the same membrane parameters reported in the reference work. As shown in Fig. A2, there is a very good agreement between the experimental and the model results for both cases.

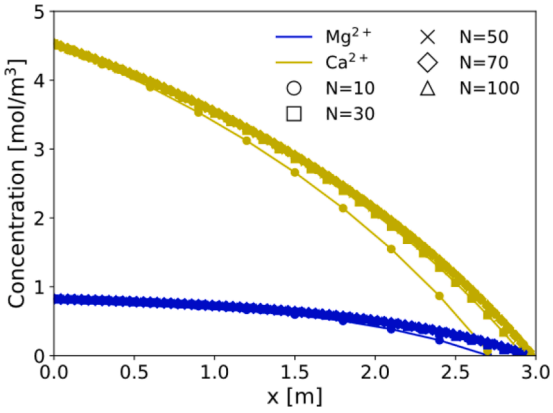

Fig. A1. Sensitivity analysis results: trend of the concentration of Mg^{2+} and Ca^{2+} throughout the membrane thickness varying the number of discretization steps.

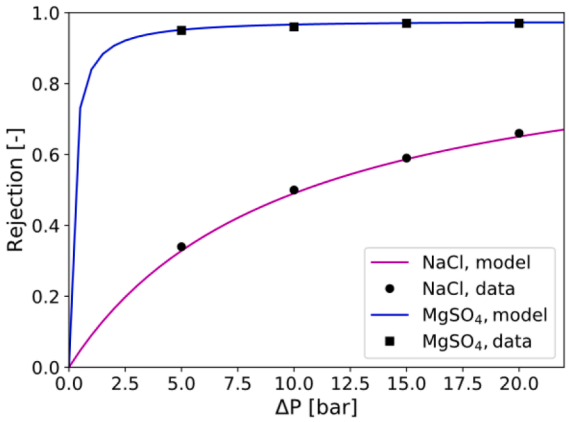

Fig. A2. Experimental values of rejection of ions and trends simulated by the model in presence of NaCl or $MgSO_4$ solutions with NF270 membranes.

References

[1] Dai J, Wu S, Han G, Winberg J, Xie X, Wu X, et al. Water-energy nexus: A review of methods and tools for macro-assessment. Appl Energy 2018;210:393–408.
[2] Gilron J. Water-energy nexus: matching sources and uses. Clean Technol Environ Policy 2014;16:1471–9.
[3] Tsolas SD, Karim MN, Hasa MMF. Optimization of water-energy nexus: A network representation-based graphical approach. Appl Energy 2018;224:230–50.
[4] Owen A, Scott K, Barrett J. Identifying critical supply chains and final products: An input-output approach to exploring the energy-water-food nexus. Appl Energy 2018;210:632–42.
[5] Dubreuil A, Assoumou E, Bouckaert S, Selosse S, Maizi N. Water modeling in an energy optimization framework – The water-scarce middle east context. Appl Energy 2013;101:268–79.
[6] Gjorgiev B, Sansavini G. Electrical power generation under policy constrained water-energy nexus. Appl Energy 2018;210:568–79.
[7] Lee U, Han J, Elgowainy A, Wang M. Regional water consumption for hydro and thermal electricity generation in the United States. Appl Energy 2018;210:661–72.
[8] Gjorgiev B, Sansavini G. Water-energy nexus: Impact on electrical energy conversion and mitigation by smart water resources management. Energy Convers Manage 2017;148:1114–26.
[9] Lee M, Keller AA, Chiang PC, Den W, Wang H, Hou CH, et al. Water-energy nexus for urban water systems: A comparative review on energy intensity and environmental impacts in relation to global water risks. Appl Energy 2017;205:589–601.
[10] Warsinger DM, Chakraborty S, Tow EW, Plumlee MH, Bellona C, Loutatidou S, et al. A review of polymeric membranes and processes for potable water reuse. Prog Polym Sci 2018;81:209–37.
[11] Panepinto D, Fiore S, Zappone M, Genon G, Meucci L. Evaluation of the energy efficiency of a large wastewater treatment plant in Italy. Appl Energy 2016;161:404–11.
[12] Kirchem D, Lynch M, Bertsch V, Casey E. Market effects of industrial demand response and flexibility potential from wastewater treatment facilities. 15th International Conference on the European Energy Market (EEM). 2018. p. 1–6.
[13] Longo S, d Antoni BM, Bongards M, Chaparro A, Cronrath A, Fatone F, Lema JM, Mauricio-Iglesias M, Soares A, Hospido A. Monitoring and diagnosis of energy consumption in wastewater treatment plants. A state of the art and proposals for improvement. Appl Energy 2016;179:1251–68.
[14] Torregrossa D, Hansen J, Hernandez-Sancho F, Cornelissen A, Schutz G, Leopold U. A data-driven methodology to support pump performance analysis and energy efficiency optimization in Waste Water Treatment Plants. Appl Energy 2017;208:1430–40.
[15] Gu Y, Li Y, Li X, Amd Wang Luo HP, Robinson ZP, Wang X, Wu J, Li F. The feasibility and challenges of energy self-sufficient wastewater treatment plants. Appl Energy 2017;204:1463–75.
[16] Ahmetovic E, Ibric N, Kravanja Z. Optimal design for heat-integrated water-using and wastewater treatment networks. Appl Energy 2014;135:791–808.
[17] Yang L, Grossmann IE. Water targeting models for simultaneous flowsheet optimization. Ind Eng Chem Res 2013;52:3209–24.
[18] Molinos-Senante M, Sala-Garrido R. Evaluation of energy performance of drinking water treatment plants: use of energy intensity and energy efficiency metrics. Appl Energy 2018;229:1095–102.
[19] Roberts DA, Johnston EL, Knott NA. Impacts of desalination plant discharges on the marine environment: a critical review of published studies. Water Res 2010;44(18):5117–28.
[20] Giwa A, Dufour V, Marzooqi FA, Kaabi MA, Hasan SW. Brine management methods: Recent innovations and current status. Desalination 2017;407:1–23.
[21] Casas S, Aladjem C, Larrotcha E, Gibert O, Valderrama C, Cortina JL. Valorisation of Ca and Mg by-products from mining and seawater desalination brines for water treatment applications. J Chem Technol Biotechnol 2014;89:872–83.
[22] Gozálvez-Zafrilla JM, Sanz-Escribano D, Lora-García J, Hidalgo MCL. Nanofiltration of secondary effluent for wastewater reuse in the textile industry. Desalination 2008;222(1):272–9.
[23] Bilińska L, Gmurek M, Ledakowicz S. Textile wastewater treatment by AOPs for brine reuse. Process Saf Environ Prot 2017;109:420–8.
[24] Choe JK, Bergquist AM, Jeong S, Guest JS, Werth CJ, Strathmann TJ. Performance and life cycle environmental benefits of recycling spent ion exchange brines by catalytic treatment of nitrate. Water Res 2015;80:267–80.
[25] Flodman HR, Dvorak BI. Brine reuse in ion-exchange softening: salt discharge, hardness leakage, and capacity tradeoffs. Water Environ Res 2012;84(6):535–43.
[26] Hu J, Chen Y, Guo L, Chen X. Chemical-free ion exchange and its application for desalination. Desalination 2015;365:144–50.
[27] Chandrasekara NPGN, Pashley RM. Study of a new process for the efficient regeneration of ion exchange resins. Desalination 2015;357:131–9.
[28] Li J, Koner S, German M, SenGupta AK. Aluminum-cycle ion exchange process for hardness removal: a new approach for sustainable softening. Environ Sci Technol 2016;50:11943–50.
[29] Birnhack L, Keller O, Tang SCN, Fridman-Bishop N, Lahav O. A membrane-based

recycling process for minimizing environmental effects inflicted by ion-exchange softening applications. Sep Purif Technol 2019;223:24–30.
[30] Chen Y, Davis JR, Nguyen CH, Baygents JC, Farrell J. Electrochemical ion-exchange regeneration and fluidized bed crystallization for zero-liquid-discharge water softening. Environ Sci Technol 2016;50:5900–7.
[31] www.zerobrine.eu, "Zero Brine.".
[32] Micari M, Moser M, Cipollina A, Fuchs B, Ortega-Delgado B, Tamburini A, et al. Techno-economic assessment of multi-effect distillation process for the treatment and recycling of ion exchange resin spent brines. Desalination 2019;456:38–52.
[33] Bowen WR, Mohammad AW, Hilal N. Characterisation of nanofiltration membranes for predictive purposes — use of salts, uncharged solutes and atomic force microscopy. J Membr Sci 1997;126(1):91–105.
[34] Bowen WR, Welfoot JS. Modelling the performance of membrane nanofiltration—critical assessment and model development. Chem Eng Sci 2002;57(7):1121–37.
[35] Schaep J, Vandecasteele C, Mohammad AW, Bowen WR. Modelling the retention of ionic components for different nanofiltration membranes. Sep Purif Technol 2001;22–23:169–79.
[36] Geraldes V, Alves AMB. Computer program for simulation of mass transport in nanofiltration membranes. J Membr Sci 2008;321(2):172–82.
[37] Roy Y, Sharqawy MH, Lienhard JH. Modeling of flat-sheet and spiral-wound nanofiltration configurations and its application in seawater nanofiltration. J Membr Sci 2015;493:360–72.
[38] Filmtec Reverse Osmosis Membranes Technical Manual.
[39] Van der Bruggen B, Everaert K, Wilms D, Vandecasteele C. Application of nanofiltration for removal of pesticides, nitrate and hardness from ground water: rejection properties and economic evaluation. J Membr Sci 2001;193(2):239–48.
[40] Mohammad AW, Ali N, Ahmad AL, Hilal N. Optimized nanofiltration membranes: relevance to economic assessment and process performance. Desalination 2004;165:243–50.
[41] Mohammad AW, Hilal N, Al-Zoubib H, Darwish NA, Ali N. Modelling the effects of nanofiltration membrane properties on system cost assessment for desalination applications. Desalination 2007;206(1):215–25.
[42] Kesieme UK, Milne N, Aral H, Cheng CY, Duke M. Economic analysis of desalination technologies in the context of carbon pricing, and opportunities for membrane distillation. Desalination 2013;323:66–74.
[43] Papapetrou M, Micale G, Zaragoza G, Kosmadakis G. Assessment of methodologies and data used to calculate desalination costs. Desalination 2017;419:8–19.
[44] Turton R, Bailie RC, Whiting WB, Shaeiwitz JA, Bhattacharyya D. Analysis synthesis and design of chemical processes. Prentice Hall; 2012.
[45] El-Dessouki HT, Ettouney HM. Fundamentals of salt water desalination. Elsevier; 2002.
[46] Sayyadi H, Saffari A. Thermoeconomic optimization of multi effect distillation desalination systems. Appl Energy 2010;87:1122–33.
[47] El-Dessouky H, Alatiqi I, Bingulac S, Ettouney H. Steady-state analysis of the multiple effect evaporation desalination process. Chem Eng Technol 1998;21(5):437–51.
[48] Laukemann T, Baten R, Fichter T. MENA Regional Water Outlook, Phase II, Desalination using Renewable Energy. Fichtner and DLR, 2012.
[49] Labban O, Chong TH, Lienhard JH. Design and modeling of novel low-pressure nanofiltration hollow fiber modules for water softening and desalination pretreatment. Desalination 2018;439:58–72.
[50] Roy Y, Warsinger DM, Lienhard JH. Effect of temperature on ion transport in nanofiltration membranes: diffusion, convection and electromigration. Desalination 2017;420:241–57.
[51] Oatley DL, Llenas L, Pérez R, Williams PM, Martínez-Lladó X, Rovira M. Review of the dielectric properties of nanofiltration membranes and verification of the single oriented layer approximation. Adv Colloid Interface Sci 2012;173:1–11.
[52] Schaep J, Vandecasteele C, Mohammad AW, Bowen WR. Analysis of the salt retention of nanofiltration membranes using the donnan-steric partitioning pore model. Sep Sci Technol 1999;34(15):3009–30.
[53] Oatley DL, Llenas L, Aljohani NHM, Williams PM, Martínez-Lladó X, Rovira M, et al. Investigation of the dielectric properties of nanofiltration membranes. Desalination 2013;315:100–6.
[54] Ernst M, Bismarck A, Springer J, Jekel M. Zeta-potential and rejection rates of a polyethersulfone nanofiltration membrane in single salt solutions. J Membr Sci 2000;165:251–9.
[55] Bandini S. Modelling the mechanism of charge formation in NF membranes: Theory and application. J Membr Sci 2005;264:75–86.
[56] Mazzoni Carolina, Bruni Luigi, Bandini S. Nanofiltration: role of the electrolyte and pH on Desal DK performances. Ind. Eng. Chem. Res. 2007;46:2254–62.
[57] Teixera MR, Rosa MJ, Nyström M. The role of membrane charge on nanofiltration performance. J Membr Sci 2005;265:160–6.
[58] Zhou D, Zhu L, Fu Y, Zhu M, Xue L. Development of lower cost seawater desalination processes using nanofiltration technologies — A review. Desalination 2015;376:109–16.
[59] Al-Hajouri AA, Al-Amoudi AS, Farooque AM. Long term experience in the operation of nanofiltration pretreatment unit for seawater desalination at SWCC SWRO plant. Desalin Water Treat 2013;51(7–9):1861–73.
[60] Llenas L, Martinez-Lladó X, Yaroshchuk A, Rovira M, Pablo J. Nanofiltration as pretreatment for scale prevention in seawater reverse osmosis desalination. Desalin Water Treat 2011;36:310–8.
[61] Vezzani D, Bandini S. Donnan equilibrium and dielectric exclusion for characterization of nanofiltration membranes. Desalination 2002;149:477–83.
[62] Senthilmurugan S, Ahluwalia A, Gupta SK. Modeling of a spiral-wound module and estimation of model parameters using numerical techniques. Desalination 2005;173:269–86.
[63] Geraldes V, Afonso MD. Generalized Mass-Transfer Correction Factor for Nanofiltration and Reverse Osmosis. AIChE J 2006;52:3353–62.

Journal of Cleaner Production 255 (2020) 120291

Contents lists available at ScienceDirect

Journal of Cleaner Production

journal homepage: www.elsevier.com/locate/jclepro

Towards the implementation of circular economy in the water softening industry: A technical, economic and environmental analysis

M. Micari [a, **], M. Moser [a], A. Cipollina [b], A. Tamburini [b, *], G. Micale [b], V. Bertsch [a, c]

[a] German Aerospace Center (DLR), Institute of Engineering Thermodynamics, Pfaffenwaldring 38-40, 70569, Stuttgart, Germany
[b] Dipartimento di Ingegneria, Università Degli Studi di Palermo (UNIPA), Viale Delle Scienze Ed. 6, 90128, Palermo, Italy
[c] Ruhr-Universität Bochum, Chair of Energy Systems and Energy Economics, Universitätsstr. 150, 44801, Bochum, Germany

ARTICLE INFO

Article history:
Received 10 July 2019
Received in revised form
22 January 2020
Accepted 26 January 2020
Available online 28 January 2020

Handling editor: Kathleen Aviso

Keywords:
Industrial wastewater
Circular economy
Treatment chain
CO_2 emissions
Recycling
Membrane processes

ABSTRACT

To reduce the environmental impact of the industrial sectors, circular strategies should be implemented to purify the effluents and recover raw materials. In this context, a novel integrated methodological approach is proposed to identify the most suitable strategy to improve the sustainability of the water softening industry via the treatment and recycling of the produced wastewater. Different concentration technologies and energy supply systems are compared to find economically feasible and environmentally friendly treatment systems. The investigated chains present the same pre-treatment step (nanofiltration and crystallization) and different concentration technologies: Multi-Effect Distillation (MED), Membrane Distillation (MD) and the coupling of Reverse Osmosis and Membrane Distillation (RO-MD). In the case of electricity supplied by the grid, the MED and the RO-MD chain are economically competitive with the state of the art (Levelized Brine Cost (LBC) between 4 and 6$/m^3, lower than the regenerant solution cost, equal to 8$/m^3). Moreover, the specific CO_2 emissions due to the energy required by the treatment processes (10.8 $kg_{CO2}/m^3_{regenerant}$ for the MED chain and 16.7$kg_{CO2}/m^3_{regenerant}$ for the RO-MD chain) are lower than those produced by the current system (19.7$kg_{CO2}/m^3_{regenerant}$). Varying the feed flow rate, the MED-chain is more feasible at larger plant sizes for its lower energy demand, while the chain including RO-MD shows lower costs at smaller plant sizes for its lower investment costs. When a photovoltaic-battery system is coupled, both the MED-chain and RO-MD-chain show a CO_2 emission reduction of more than 75% with respect to the state of the art. Furthermore, their LBC values are very competitive, especially if the plant is located in a region with high solar potential.

1. Introduction

Sustainable development (SD) is considered the only feasible answer to the simultaneous growth of energy and water demand and the increase in environmental pollution. According to the definition given by the Brundtland commission in 1987, SD is able to "*meet the needs of the present without compromising the ability of future generations to meet their own needs*" (World Commission on Environment and Development, 1987). SD is typically presented as a three-dimensional concept, which accounts for environmental, social and economic aspects. Therefore, different criteria may be employed to assess the sustainability of a process, such as CO_2 emissions, water and energy requirements, costs, labour conditions and economic growth (Janeiro and Patel, 2015). One of the most acknowledged ways to achieve the SD consists in the application of the circular economy (CE) concept (Geissdoerfer et al., 2017). The concept was originally introduced by Boulding in 1966 and suggests that economy should be a circular system to ensure the sustainability of human life on Earth (Boulding and Jarrett, 1966). According to the definition given by the Ellen MacArthur Foundation, CE is "*an industrial economy that is restorative and regenerative by intention and design*" (Ellen MacArthur Foundation, 2013). The main objective of CE is the promotion of a more appropriate and environmentally friendly management of resources, to achieve a *cleaner industrial production* (Ghisellini et al., 2016). To this aim, new business models (Gusmerotti et al., 2019) and, eventually, a redesign of the industrial processes (Zhijun and Nailing, 2007) are required to decouple the economic growth and the consumption of resources (Suárez-Eiroa et al., 2019). Different methodologies and

* Corresponding author.
** Corresponding author.
E-mail addresses: marina.micari@dlr.de (M. Micari), alessandro.tamburini@unipa.it (A. Tamburini).

https://doi.org/10.1016/j.jclepro.2020.120291
0959-6526/

Nomenclature

C	Concentration
$C_{battery}$	Capacity of the battery [h]
CAPEX	Capital Expenditure [$/y]
CE	Circular Economy
$Cost_{El}$	Electricity cost [$/kWh]
$Cost_{Heat}$	Thermal energy cost [$/kWh]
Cryst	Crystallizer
DCMD	Direct Contact Membrane Distillation
$f_{CO2,emission}$	CO_2 emission factor [kg_{CO2}/kWh]
IEX	Ion Exchange resins
LBC	Levelized Brine Cost
LBC_{CAP}	Capital Levelized Brine Cost
LBC_{OP}	Operating Levelized Brine Cost
LCOE	Levelized Cost of Electricity
MD	Membrane distillation
MED	Multi-effect distillation
NF	Nanofiltration
OPEX	Operating Expenditure [$/y]
P	Power [kW]
PV	Photovoltaic
Q	Flow rate [m^3/h]
RCE	Remote Component Environment
RO	Reverse osmosis
SD	Sustainable Development

Subscripts

Prim	primary energy
PV,inst	installed PV power

indicators are used to assess the CE performances: most methods concern Life Cycle Assessment analyses and process design to enable the circularity (Sassanelli et al., 2019). The indicators, which were proposed in 2018 by the European Commission within a CE monitoring framework, mostly concern circularity degree, waste generation and production of secondary raw materials (Eurostat, 2018). These can be categorized according to the levels of application: *micro* (single processes or consumers), *meso* (industrial parks) and *macro* (cities, regions or nations) (Saidani et al., 2019).

Several works in literature focused on the implementation of CE at the micro-level, investigating new strategies to treat the industrial effluents and to produce (i) sellable raw materials and/or (ii) material streams to be reused in the industrial process. Significant attention has been devoted to the food industry (Mirabella et al., 2014). Depending on the specific food, different types of waste are produced and consequently different substances may be extracted (Cardinali et al., 2012; Abdelkader et al., 2019). The sugar industry produces a significant amount of waste and the investigated waste valorisation strategies mostly regard the utilization of sugarcane biomass for energy (Gopinath et al., 2018) and biofuels production (Cardona et al., 2010). Also in textile industry, the production of wastewater streams represents a severe issue, because of the high content of colour, organic compounds and salt in the discharged dyeing solution (Holkar et al., 2016). Different strategies have been developed to treat and recycle the effluent as fresh dyeing solution: these include combinations of membrane processes, as ultrafiltration and nanofiltration (Nadeem et al., 2019), advanced oxidation processes (Bilińska et al., 2017) and biological treatments (Sarayu and Sandhya, 2012). Finally, other industrial sectors are characterized by high water consumption and, consequently, by the production of significant volumes of wastewaters, such as paper, laundering and coal mine industry. To achieve a sustainable production, the wastewater may be treated to reduce the organics content (Man et al., 2017) and to recover valuable materials, as water and detergent in the laundering industry (Giagnorio et al., 2017) and salts (Turek et al., 2008) as well as rare earth elements in the coal mine industry (Lopez et al., 2019).

Another industrial process producing significant volumes of wastewater is the water softening industry. Water softening is a purification process aimed at removing the hardness from water, via the employment of Ion Exchange resins (IEX). Periodically, the resins are regenerated supplying a NaCl-water solution and the regeneration produces a wastewater stream, containing sodium, chloride and bivalent ions (magnesium, calcium and sulphate ions). Currently, this effluent is disposed into the environment, since there are no organic pollutants or harmful components. However, the frequent release of concentrated brine from Na-charged softeners is becoming a crucial concern as it is detrimental to agriculture and downstream water quality (Li et al., 2016). A few works in the literature focused on the design of alternative ion exchange resins (Li et al., 2016; Birnhack et al., 2019) or alternative thermal (Chandrasekara and Pashley, 2015) and electrochemical regeneration processes (Chen et al., 2016) to avoid the release of a high amount of Na^+. However, in most cases, the technical investigation is not coupled with an economic and environmental analysis of the proposed systems.

This work proposes and demonstrates a novel methodological approach for the identification of the most suitable treatment chains to achieve a *cleaner* production in the industrial water softening. This approach is based on the integration of technical, economic and environmental analyses. The proposed treatment chains are devised to reduce the demand of raw materials in the industrial process and to limit the environmental pollution due to the effluent disposal. In fact, in the proposed configurations, the Na-rich effluent is not disposed into the environment, as it is treated and then recycled to the industrial process. The chains present a pre-treatment and a concentration step, as shown in Fig. 1. The pre-treatment processes (nanofiltration (NF) and crystallization) aim at separating the bivalent ions, while in the concentration steps the remaining NaCl-water solution is concentrated up to the concentration of the fresh regenerant solution to be recycled. Three alternative concentration technologies are considered: (i) multi-effect distillation (MED), (ii) membrane distillation (MD) and (iii) reverse osmosis (RO) coupled with membrane distillation (RO-MD).

Firstly, the chains with different concentration technologies are compared, by assessing the economic feasibility, the energy requirements and the environmental impact due to the CO_2 emissions. Secondly, the impact of different drivers on the selected technologies is investigated, with a focus on the self-generation of electricity via a Photovoltaic (PV)-battery system and on the solar radiation conditions of the region selected for the plant location.

Overall, for the first time, this work aims at establishing a methodological approach that allows for identifying the most economically feasible and environmentally friendly strategy to move towards a CE approach in the water softening industry, comparing different concentration technologies and energy supply systems.

2. Methodological approach

The methodological approach followed in this work is sketched

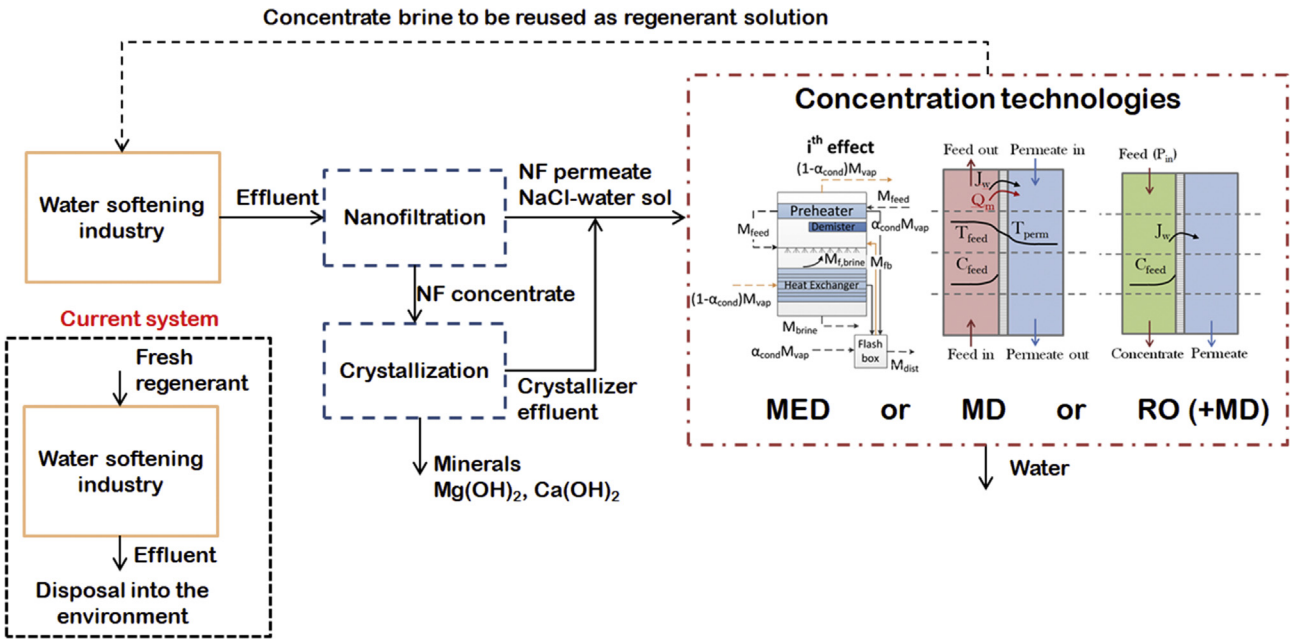

Fig. 1. Scheme of the treatment chains for the presented case study. The industrial process is represented by the box framed in yellow (solid line), the pre-treatment steps by the ones in blue (dashed line) and the concentration step alternatives in red (dash-dotted line). The box on the left (black dotted line) represents the current industrial process. (For interpretation of the references to colour in this figure legend, the reader is referred to the Web version of this article.)

in the block diagram of Fig. 2. This novel multi-step approach provides various levels of investigation. Firstly, techno-economic models are developed and implemented for each process on the basis of literature equations, experimental data and data given by the vendors. Secondly, the most significant technical and economic inputs and outputs of the models are defined and, accordingly, the models are interconnected. Different systems can be devised depending on how the models are interconnected and, correspondingly, different treatment chains can be simulated. Finally, for a given set of operating conditions and input data, the performance of each chain is estimated via the definition of global outputs, accounting for technical, economic and environmental aspects.

2.1. Development of technical and economic models

In the following, a short description of the techno-economic models is reported. The models of NF and MED were described in previous works (Micari et al. 2019a, 2019b) and RO and MD models are presented in the Supplementary Materials.

2.1.1. Nanofiltration

Nanofiltration is a pressure-driven membrane process that is suitable to remove bivalent and multivalent ions thanks to the high membrane rejection.

A multi-scale model including three different scales was implemented. The *low-hierarchy model* assesses the membrane behaviour and is based on the Donnan Steric Pore Model with Dielectric Exclusion (Geraldes and Brites Alves, 2008). The model solves the extended Nernst-Planck equation within the thickness of the membrane and takes into account the boundary conditions given by the exclusion mechanisms (Labban et al., 2017). The main results of the low-hierarchy model are the ionic rejections and the water flux. These are some of the inputs of the *medium-hierarchy model*, which describes the NF unit along the feed main flow direction. Thus, mass balances are applied to define the concentration and flow-rate of permeate and feed for each discretization step (Roy et al., 2015). Finally, the *high-hierarchy model* estimates the required size of the NF plant, given by NF units arranged in series and in parallel, to achieve a certain total recovery (ratio between permeate and feed flow-rates). Regarding the energy demand, the

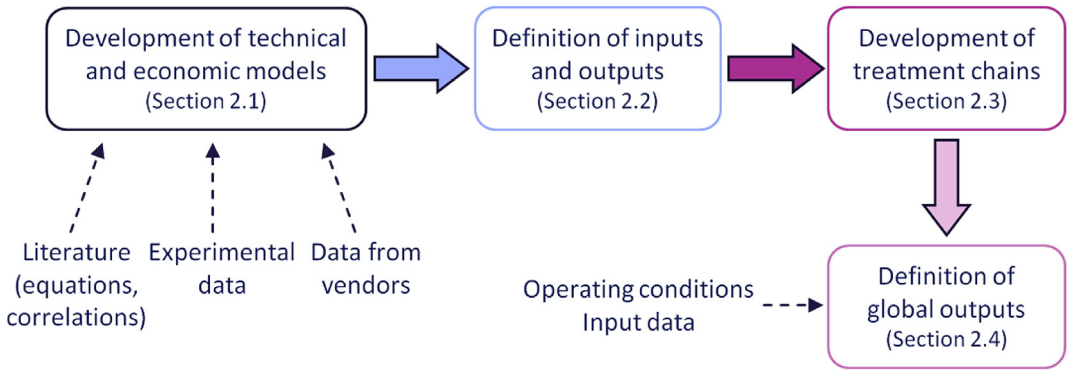

Fig. 2. Block diagram showing the methodological approach followed in this work.

NF process requires electricity to pump the feed up to the defined pressure. The economic model follows the Verberne cost model (Van der Bruggen et al., 2001).

2.1.2. Crystallization

Two crystallization units are included in the chains to produce $Mg(OH)_2$ and $Ca(OH)_2$, using a NaOH-water solution as alkaline reactant. Each crystallizer is followed by a filter, where the crystals are obtained from the magma produced in the crystallizer. For this process, a simplified model was implemented, based on mass balances under the assumption of a 100% conversion of the dissolved Mg^{2+} and Ca^{2+} into $Mg(OH)_2$ and $Ca(OH)_2$ respectively (Cipollina et al., 2014). Concerning the energy demand, two terms are estimated: (i) the pumping energy to pump the solutions to the crystallizers and (ii) the electric energy required by the filters. Finally, regarding the economic model, the Module Costing Technique is applied for the estimation of the capital costs, with suitable parameters for crystallizers and filters found in literature (Turton et al., 2012). The operating costs are due to the reactant and the energy supply, while the revenues are given by the minerals, which are supposed to be sold at the current market price.

2.1.3. Multi-effect distillation

The MED process has been widely investigated in literature, mostly for seawater desalination purposes (El-Dessouky and Ettouney, 1999; Kamali et al., 2008). The MED plant modelled for this work presents a forward-feed arrangement, since this is more suitable to the high temperatures and concentrations expected in the investigated cases (Ortega-Delgado et al., 2017). The plant is composed of a certain number of stages in series, each one presenting a heat exchanger, where the feed partially evaporates, and a preheater, where the feed is heated up before entering inside the stage. The model includes an iterative procedure, which runs until three conditions are simultaneously achieved: (i) the areas of the heat exchangers of each stage are equal, (ii) the areas of the preheaters are equal and (iii) the outlet distillate flow-rate fulfils the overall mass balances, depending on the required brine concentration. The distillate is supposed to be pure water, which can be sold at the current market selling price.

Concerning the energy requirements, the thermal energy is the prominent term, given by the steam flow-rate multiplied by the latent heat at the given pressure. The electricity demand is fixed and equal to 1.5 kWh/m^3_{dist} (Gebel and Yuce, 2008). The details of the economic model are reported in a previous work (Micari et al., 2019b).

2.1.4. Reverse osmosis

Reverse Osmosis is a desalination process based on a membrane separation under an applied pressure. The model has a hierarchical structure, as shown in detail in the Supplementary Materials: it goes from the investigation of the membrane properties and the estimation of the fluxes to the design of a whole plant. The RO plant typically presents many vessels arranged in parallel to reach a certain total recovery, similarly to the NF plant (Dow Water and Process Solutions). Each vessel contains a number of RO units in series with spiral-wound geometry. Concerning the energy demand, RO requires only electricity to pump the feed up to the inlet pressure. Finally, the economic model includes the calculation of the capital costs, composed of the costs of membrane elements, pressure vessels, high pressure pumps, piping and intake costs (Malek et al., 1996; Wilf and Bartels, 2005). The operating costs account for electricity demand, maintenance (3%/y of the investment plus 20% of the annual labour cost), labour, chemicals and membrane replacement (Vince et al., 2008).

2.1.5. Membrane distillation

MD is a separation process that presents a microporous hydrophobic membrane, permeable only to water vapour. A temperature gradient between the two membrane interfaces leads to a vapour pressure difference, which generates a vapour flux through the membrane. The present model describes a Direct Contact MD (DCMD) configuration, which was selected for its simplicity and the high vapour fluxes (Winter et al., 2011). The details of the implemented model are reported in Supplementary Materials. In the *DCMD membrane model*, the trans-membrane vapour flux is calculated combining heat and mass transfer equations (Qtaishat et al., 2008). In the *DCMD unit model*, mass and energy balances are set up to investigate flow-rate, concentration and temperature profiles along the feed stream-wise direction (Hitsov et al., 2017). Finally, the *DCMD plant model* simulates a high-scale plant, where the MD units are arranged in series and in parallel to reach a high recovery (Ali et al., 2018). Regarding the energy consumption, heat is required to increase the temperature of the feed from the intake to the inlet temperature and in each intermediate heater. Electricity is required to pump the feed and the permeate entering each module in series. The economic model estimates the capital costs, given by the costs of modules, membrane, pumps and heat exchangers, together with the cost for intake and pre-treatment (Hitsov et al., 2018). Conversely, the operating costs comprise the electricity and heat demand, maintenance (2.5%/y of the investment cost without the cost of membranes and modules), labour, chemicals and membrane replacement cost (Al-Obaidani et al., 2008).

2.2. Definition of inputs and outputs

Every treatment process presents inlet and outlet material and energy flows, which correspond to inputs and outputs of the technical models. Most of the outputs generated by the technical models are fundamental for cost estimations. The most important inputs and outputs for each model are reported in Table 1, where the outputs constitute the inputs for the relevant economic model.

2.3. Development of the treatment chains

The techno-economic models are integrated and interconnected in a simulation platform called Remote Component Environment (RCE) (Deutsches Zentrum für Luft- und Raumfahrt e.V., 2019). Fig. 3 shows the workflow generated to simulate the chain with RO-MD (NF-cryst-RO-MD). The blocks corresponding to the processes call the relevant models and exchange data (e.g. the NF retentate concentration and flow-rate constitute the concentration and flow-rate of the crystallizer feed). Analogous workflows are built for the other two chains, with MED (NF-cryst-MED) and with MD (NF-cryst-MD).

2.4. Definition of global outputs

For a proper comparison of the treatment chains, some representative output parameters were defined to inform about the technical, economic and environmental performances of the whole system. Concerning the technical aspects, the heat and electricity demands [kW] were adopted as reference outputs. Regarding the economic analysis, the total annualized capital costs (CAPEX [$/y]) and the total operating costs (OPEX [$/y]) are the most significant parameters for each unit. For each treatment chain, a levelized cost is used, which represents the price at which the main product of the chain should be sold to break-even and which includes all the capital and operating expenses of the units

Table 1
Main inputs and outputs of the technical models.

MODEL	INPUTS	OUTPUTS
Nanofiltration (NF)	- Feed flow-rate and composition - Feed pressure - Total recovery - N° of elements (vessel) - Membrane rejection	- Permeate flow-rate and composition - Retentate flow-rate and composition - N° of vessels in parallel - Electricity demand
Crystallization (cryst)	- Feed flow-rate - Feed concentration (Mg^{2+} and Ca^{2+}) - Alkaline solution concentration	- Produced flow-rate of hydroxides - Flow-rate of alkaline solution - Effluent flow-rate and composition - Electricity demand
Reverse Osmosis (RO)	- Feed flow-rate and concentration - Retentate outlet concentration - N° of stages and of elements (vessel)	- Permeate flow-rate and composition - Retentate flow-rate - N° of vessels in parallel - Electricity demand
Membrane Distillation (MD)	- Feed flow-rate and concentration - Retentate outlet concentration - Inlet feed and permeate temperatures - Intake temperature	- Distillate and retentate flow-rate - N° of elements (series and parallel) - Heat and electricity demand
Multi-Effect Distillation (MED)	- Feed flow-rate and concentration - Retentate outlet concentration - N° of effects - Steam temperature	- Area of heat exchangers - Steam flow-rate - Heat and electricity demand

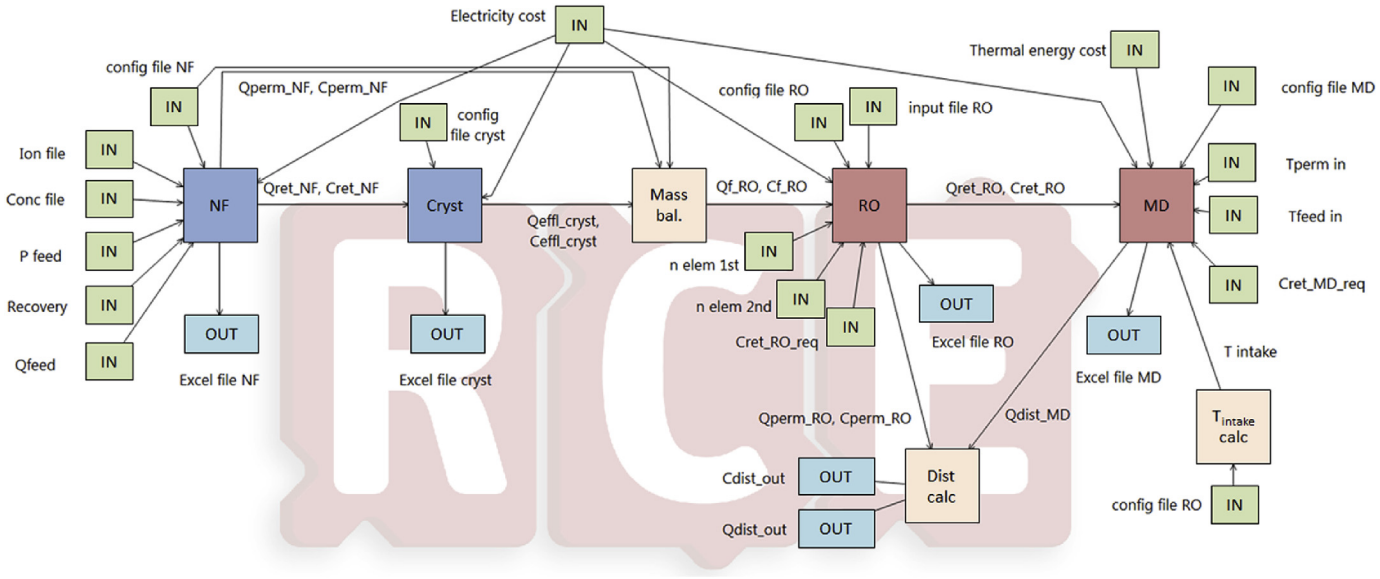

Fig. 3. Workflow of the NF-cryst-RO-MD chain as implemented in RCE. The dark-blue blocks represent the units in the pre-treatment step and the red blocks the units in the concentration step; the green units the input values or files; the light blue blocks the outputs; the light orange blocks the intermediate tools (mixing units). (Q: flow-rate; C: concentration; P: pressure; T: temperature). (For interpretation of the references to colour in this figure legend, the reader is referred to the Web version of this article.)

and the revenues coming from the by-products. In the present case, the main product is the concentrate brine (Q_{brine}) that can be reused as a reactant in the industrial process and a global parameter called Levelized Brine Cost (LBC_{tot} [$/m$^3_{brine}$]) is taken as the reference economic output (Micari et al., 2019b). The LBC_{tot} is given by the combination of the terms relevant to the capital costs (LBC_{cap}) and to the operating costs and the revenues (LBC_{op}).

$$LBC_{tot} = LBC_{cap} + LBC_{op} = \frac{\sum_{units} CAPEX}{Q_{brine}} + \frac{\sum_{units} OPEX - Revenue_{Mg(OH)_2} - Revenue_{Ca(OH)_2} - Revenue_{water}}{Q_{brine}} \quad (1)$$

Finally, regarding the environmental aspects, all chains allow to minimize the direct discharge of effluent into the environment, which, instead, occurs in the current system. Another important aspect consists in the CO_2 emissions due to the heat and electricity supply. The present work includes only the operational CO_2 emissions, as these resulted to be much higher than the ones due to the construction of desalination plants (Liu et al., 2015). The

CO_2 emissions per m^3 of produced brine [kg_{CO2}/m^3_{brine}] are used to compare the different chains and to compare each chain with the current system.

3. Description of case study and scenarios

The general methodological approach described in Section 2 has been developed to be flexible and applicable to different case studies. In the present work, this approach was followed to identify the most suitable treatment chain for the effluent produced by the regeneration of ion exchange resins employed for water softening. In this section, the case study and the scenarios are presented.

3.1. Description of the case study

The regeneration process producing the effluent is sketched in Fig. 4. The effluent is given by the sum of the regenerant and the rinse solutions, which contribute to the outlet flow-rate with an approximate ratio of 1:9. Under the assumption of a continuous operation, a plant producing around 130 m^3/h of effluent firstly receives the regenerant solution with a flow-rate of 13 m^3/h and secondly receives pure water, as the rinse solution, with a flow-rate of 117 m^3/h.

The effluent contains sodium, chloride and bivalent ions removed from the spent resins during the regeneration process. The composition of the wastewater produced by a real water softening plant located in Rotterdam, The Netherlands, is reported in Table 2.

The treatment chains are devised to produce a concentrate solution (brine) with a NaCl concentration equal to the one of the fresh reactant required by the regeneration process. Therefore, for any chain, the main constraint consists in the concentration of the produced brine (MED concentrate or MD retentate solution), which has to be equal to 90,000 ppm. In the case of the RO-MD chain, firstly, the solution is concentrated up to 70,000 ppm in the RO unit (this is the maximum achievable concentration in RO (Kesieme et al., 2013)) and then up to 90,000 ppm in the MD unit.

Concerning the operating conditions, the NF plant operates with a feed pressure of 20 bar and a recovery of 25% (Micari et al., 2019a). The membrane rejections are equal to 94.8% for Mg^{2+}, 83% for Ca^{2+}, 93.6% for SO_4^{2-}, −50.6% for Na^+ and 49.9% for Cl^-, which are in line with values reported in literature (Zhou et al., 2015). The MED plant includes 13 stages, on the basis of a previous MED cost minimization analysis (Micari et al., 2019b) and the thermal energy is supplied in the form of vapour at a pressure of 1 bar. The RO plant includes two stages (presenting 8 and 6 elements per vessel), since the recovery is between 50 and 70%. Finally, regarding the MD plant, the inlet feed and permeate temperatures are equal to 80 °C and 20 °C and each MD module presents 6 units wounded in parallel.

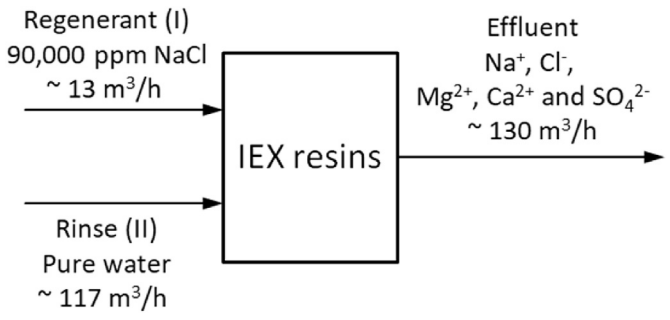

Fig. 4. Schematic description of the IEX resins regeneration phase assuming a continuous operation.

Table 2
Composition of the effluent produced by the water softening process.

	Na^+	Cl^-	Mg^{2+}	Ca^{2+}	SO_4^{2-}
C [mol/m^3]	173.9	662.2	55.6	191.7	3.1
C [ppm]	3892	22,556	1298	7462	292

For the economic analysis, the capital costs are annualized by defining depreciation period and discount rate, while the operating costs depend on several factors, such as plant capacity and pumps' efficiency. These parameters, the specific costs of the utilities and the selling price of the products are reported in Table 3.

3.2. Definition of the scenarios

To assess the role of the electricity supply on the costs and the environmental impact, *two scenarios* were defined:

1. In the first, electricity is completely taken from the grid;
2. In the second, electricity is mostly supplied by a PV power system, with Li-Ion battery storage units operating in conjunction, while the remaining fraction of required electricity is taken from the grid. The PV technology has been chosen rather than the wind technology, because it is more modular and its power production is less uncertain compared to wind. The natural irregularity of wind requires implementation of oversized batteries, which lead to much higher Levelized Cost of Electricity (LCOE) values.

Regarding the *first scenario*, the current mix of electricity carriers of the grid in The Netherlands is used (since the reference real water softening plant is located in Rotterdam), with the corresponding efficiencies and CO_2 emission factors reported in Table 4. The combination of the emission factors of the single carriers, their

Table 3
Parameters used for the economic analyses.

Parameter	Value	Units
Discount rate	6	%
Units' life time (Straight line depreciation)	• NF, structure: 30 (Van der Bruggen et al., 2001) • NF, electrical and mechanical: 15 • Crystallizer: 20 • RO: 25 (Vince et al., 2008) • MED: 25 (Papapetrou et al., 2017) • MD: 10 (Hitsov et al., 2018) • PV and battery: 25	y
Capacity factor	0.94	–
Pumps' efficiency	0.8	–
Cost of electricity (grid)	0.103	$/kWh
Cost of thermal energy	0.01	$/kWh
Replacement rate of membranes	RO, MD: 15 (Al-Obaidani et al., 2008) NF: 20 (Van der Bruggen et al., 2001)	%/y
Price of $Mg(OH)_2$	1200 (U.S. Department of the Interior, 2017)	$/ton
Price of $Ca(OH)_2$	300 (U.S. Department of the Interior, 2017)	$/ton
Price/cost of water	1 (Mezher et al., 2011)	$/m3
Cost of NaCl for the regenerant solution (current technology)	80 (Micari et al., 2019b)	$/ton
Cost of PV modules	1000 (Fraunhofer ISE, 2015)	€/kW
Cost of battery	400 (Breyer et al., 2017)	€/kWh
Cost of converter	200 (Breyer et al., 2017)	€/kWh

Table 4
Electricity carriers' mix in the grid in The Netherlands in 2016: electricity output, efficiency and CO2 emission factor for each carrier (IPCC 2006; International Energy Agency 2018).

Electricity Carriers The Netherlands (2016)	Electricity output [%]	Efficiency (total output) [-]	CO_2 emission factor [kg/kWh_{prim}]
Hard Coal, coal products	37.69	0.42	0.335
Natural Gas	44.87	0.54	0.201
Biomass	4.45	0.34	–
Mineral oil product	1.27	1	0.27
Nuclear	3.72	0.33	–
Hydro	0.09	1	–
PV	1.00	1	–
Wind	6.90	1	–
Total	100		

Table 5
Summary of the analyses reported in the present work.

	Scenario	Variable input	Fixed inputs
Wastewater: spent IEX regenerant solution	Scenario 1. Electricity supply: grid only (Section 4.1)	Q_{feed} (10–150 m^3/h) (Section 4.1.1)	$Cost_{El}$ = 0.103 $/kWh $Cost_{Heat}$ = 0.01$/kWh
		Q_{feed} and $Cost_{Heat}$ (different heat sources) (Section 4.1.2)	$Cost_{El}$ = 0.103 $/kWh
	Scenario 2. Electricity supply: PV-battery-grid (Section 4.2)	$Cost_{El}$ and $f_{CO2,emission}$ (different PV-battery system configurations) (Sections 4.2.1 and 4.2.2)	Q_{feed} = 130 m^3/h $Cost_{Heat}$ = 0.01$/kWh

efficiency and share of the electricity output gives rise to a global CO_2 grid intensity equal to 0.471kg_{CO2}/kWh.

Concerning the *second scenario*, the share of energy demand covered by the PV-battery system is estimated running an integrated model implemented in INSEL (Moser et al., 2014). More details are given in the Supplementary Materials. The produced power corresponds to a certain share of the total load, given by the electricity demand of the treatment chain in one year [MWh/y]. The plant is supposed to work in stationary operation conditions, therefore the total electricity demand is considered always constant. The remaining demand is supplied by the grid, with the electricity carriers' mix used in the previous scenario (Table 2). In this case, the CO_2 emissions are only due to the fraction of electricity supplied by the grid. Finally, the PV-battery system located in The Netherlands is compared with an analogous system located in one of the European regions with the highest solar potential, i.e. Valencia in Spain.

Concerning the costs, in the *first scenario* the current cost of electricity for non-household consumers is considered (Eurostat, 2019). In the *second scenario* the cost is calculated as the combination of the LCOE due to the PV-battery system and the cost of electricity from the grid. Within the first term, the capital costs are given by the cost of the PV modules and the battery. The operating cost of the PV and the battery are calculated as 1.5%/y and 2.5%/y of the investment cost, respectively. Finally, within this scenario, in one case no taxation was supposed to be imposed on the CO_2 emissions, while in the other case an average CO_2 price of 80 €/ton_{CO2} was given (International Energy Agency, 2018).

3.3. Overview of the performed analyses

Once the operating conditions and the scenarios were defined, simulations were carried out by varying technical (Q_{feed}), economic ($Cost_{El}$ and $Cost_{Heat}$) and environmental ($f_{CO2,emission}$) inputs. The overview of the analyses performed within the two scenarios is reported in Table 5.

4. Results and discussion

All analyses are performed applying the same circularity concept: the brine produced by the concentration step is recycled to the IEX resins as the fresh regenerant. Therefore, the target concentration of the brine is fixed for all cases and, consequently, on the basis of the global mass balances, its flow-rate is always around 40% of the effluent flow-rate. In other words, the chains are able to produce around 4 times the volume of solution required for regeneration, thus they ensure the self-sufficiency for raw materials (i.e. the regenerant solution), which is one of the CE indicators provided by the European Commission. Moreover, the three chains present the same pre-treatment unit, which is able to recover more than 95% of dissolved Mg^{2+} and Ca^{2+} as $Mg(OH)_2$ and $Ca(OH)_2$. Finally, all chains are devised to allow the complete recycling of the effluent and to minimize the waste generation. Overall, the CE approach is analogous in the three chains, while the costs and the energy demands for its implementation depend on the processes and will be compared in the following sections.

4.1. Scenario 1. Electricity supply from the grid

In Scenario 1, electricity is supplied from the grid at a constant cost, which is the current cost of electricity for non-household consumers in The Netherlands, equal to 0.086€/kWh (0.103$/kWh, by using the currency conversion factor EUR/USD of 1.2 valid in 2018 (FXTOP, 2020)).

4.1.1. Feed flow-rate variation

Firstly, the three chains are compared by varying the inlet effluent flow-rate: this variation causes a variation of both capital and operating costs, since the required size of the plant and the energy consumption depend on the flow-rate. The trends of LBC_{cap} and LBC_{op} vs. the feed flow-rate are reported in Fig. 5.

In agreement with economy of scale, for each system, the highest levelized cost is found at the lowest flow-rates, while much lower and slowly decreasing values are observable at high flow-rates (Fig. 5A). At small scales, the plants with RO and MD show lower capital costs with respect to the one with MED, since RO and MD are modular technologies, typically suitable to small scales. Conversely, at higher flow-rates, the gap between the LBC_{cap} of the RO-MD and the MED chain significantly decreases and the MD chain reports the highest LBC_{cap} because of the high number of required modules. The design flow-rate of each commercial MD module is fixed and defines the number of branches in parallel. Moreover, since the recovery of the single MD unit is thermodynamically low, it is necessary to arrange more modules in series and in particular, each branch in parallel presents 15 modules in series in the first stage and 8 in the second.

Regarding the operating costs (Fig. 5B), at low flow-rates, the trends present an evident diminution, due to the variation of the maintenance costs, which depend directly on the investment costs. Conversely, at higher flow-rates, the profiles are almost constant, since most of the operating costs are due to the energy demand, which is linearly proportional to the feed flow-rate. Notably, the MD-chain operating costs are much higher than the others in the whole range of Q_{feed} because of the high MD thermal demand. The combination of LBC_{cap} and LBC_{op} (which includes the revenues coming from minerals and water production) gives rise to LBC_{tot}, reported in Fig. 6

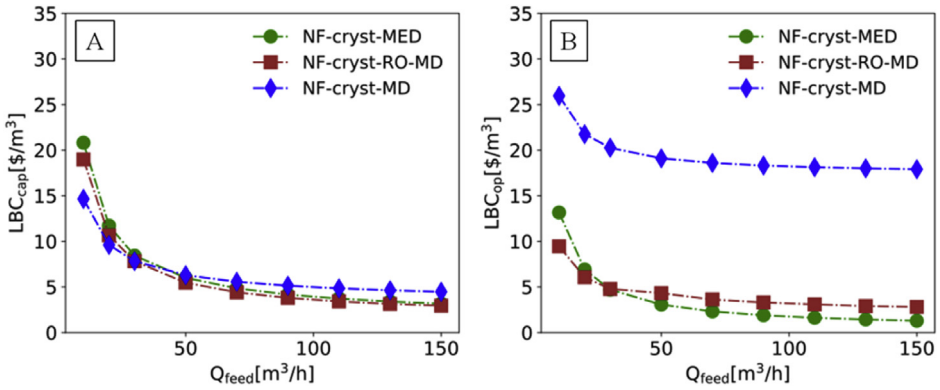

Fig. 5. LBC_{cap} (A) and LBC_{op} (B) of the three chains (NF-cryst-MED, NF-cryst-RO-MD, NF-cryst-MD) as a function of Q_{feed} [m^3/h]. Grid supply, $Cost_{El}$ = 0.103$/kWh; waste heat, $Cost_{Heat}$ = 0.01$/kWh.

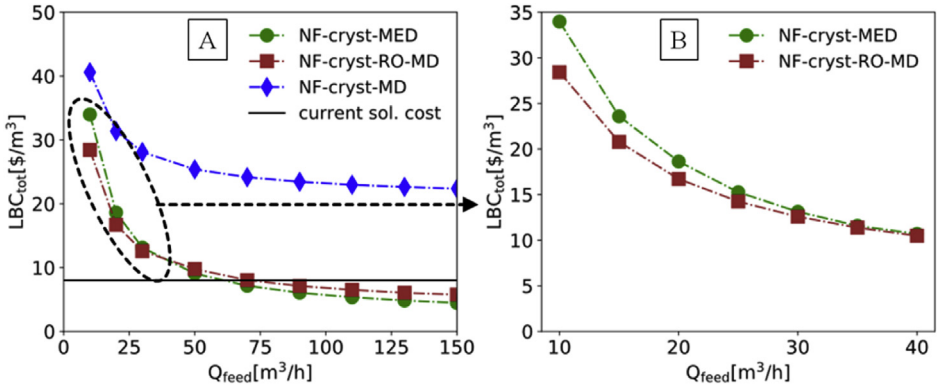

Fig. 6. (A) LBC_{tot} of the three chains (NF-cryst-MED, NF-cryst-RO-MD, NF-cryst-MD) as a function of Q_{feed} [m^3/h] and (B) a zoom in the low flow rates region to compare NF-cryst-MED and NF-cryst-RO-MD chains. Grid supply, $Cost_{El}$ = 0.103$/kWh; waste heat, $Cost_{Heat}$ = 0.01$/kWh.

The comparison of the LBC_{tot} of the three systems highlights that the chains with MED and with RO-MD behave similarly, while the chain with MD shows much higher LBC_{tot} in the whole range of Q_{feed}, because of the crucial operating costs of MD. Interestingly, the curves of LBC_{tot} of the two most performing plants intersect at a feed flow-rate of around 40 m^3/h (see the zoom in Fig. 6B): at lower flow-rates the RO-MD plant is more convenient because of its modularity which leads to lower investment costs, while at higher flow-rates the MED chain is more feasible thanks to the lower energy requirements. Finally, it is remarkable that in a very wide range of Q_{feed} (higher than 60 m^3/h for the MED chain and higher than 70 m^3/h for the RO-MD chain) the LBC_{tot} falls below the current cost of the fresh regenerant solution (Fig. 6A). This implies that both chains are more economically convenient than the state of the art which provides a continuous supply of fresh reactant at a cost of 8$/$m^3$.

Furthermore, the total electricity and heat requirements of the three chains varying the feed flow-rate are reported in Fig. 7.

Firstly, in all cases, both electricity and heat demand show a linear trend, as expected. The RO-MD chain shows the highest electricity demand, since the RO unit is a pressure-driven process. Conversely, the MD-chain exhibits a significantly higher heat demand, because of the high MD specific thermal consumption (around 900kWh_{th}/m^3_{dist}). Moreover, in the RO-MD chain, MD leads to an increase of the thermal demand of the chain beyond that of the MED one, even if it is supposed to cover only a fraction of the concentration change (from 70,000 ppm to 90,000 ppm).

To compare these results with previous works, the system costs and the energy consumption per equivalent of hardness removed during regeneration are estimated (the removed hardness was calculated from the concentration of Mg^{2+} and Ca^{2+} in the effluent, shown in Table 2). For the case of a plant producing 130 m^3/h of effluent, the cost calculated in this work was 0.022$/$eq_{hardness}$ without the revenues coming from the by-products. For an alternative treatment system providing also the recycle of the NaCl regenerant solution, a previous work reported a cost of 0.172$/$eq_{hardness}$ (Birnhack et al., 2019). Concerning the energy consumption, they presented a solely electricity-driven treatment process with a consumption of around 0.132$kWh_{el}/eq_{hardness}$. The chain with MED proposed in this work shows lower values of electricity demand (~0.0062$kWh_{el}/eq_{hardness}$) but it requires also thermal energy (~0.138$kWh_{th}/eq_{hardness}$). However, it is difficult to perform an exact comparison, since the involved processes and the scale of the systems are different.

Finally, the environmental impact of the three chains is assessed looking at the CO_2 emissions due to the energy production. Since the thermal energy is supposed to be industrial waste heat, additional electricity is considered for pumping and compressing the heat. The guidelines report a default value of 0.09 GJ of electricity required per GJ of heat recovered (Harmelink and Bosselaar, 2013). Thus, this electricity demand is also accounted for the calculation of the CO_2 emissions. Fig. 8 shows the CO_2 emissions due to the total energy demand of the three chains.

Also from an environmental point of view, the MD-chain is the worst performing, because of its large energy demand. Conversely, the other two chains show lower emissions. To compare the CO_2

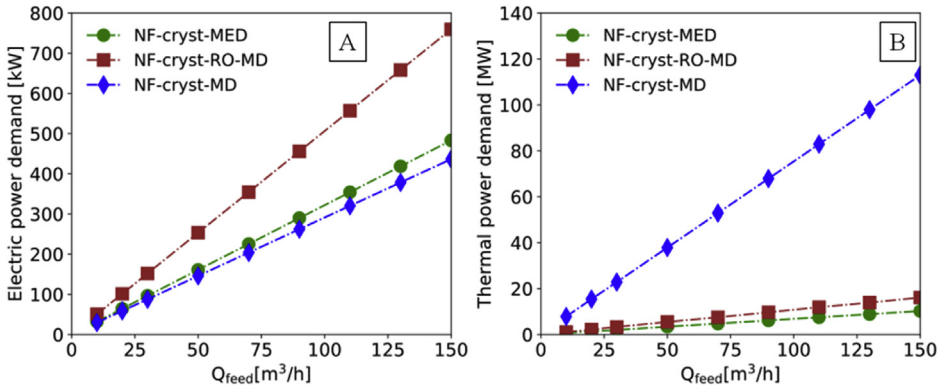

Fig. 7. Electric (A) and thermal (B) power demand for the three chains varying Q_{feed}.

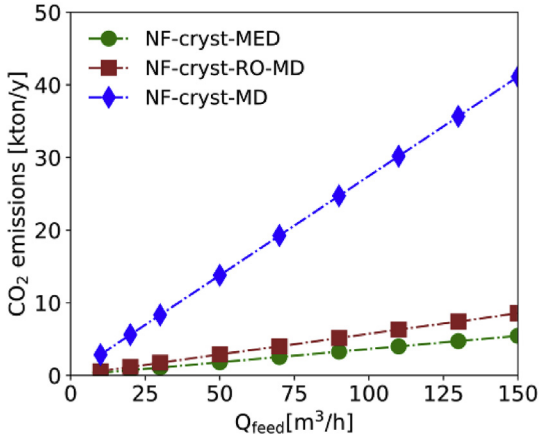

Fig. 8. CO_2 emissions of the three chains, considering the current power generation mix from the grid and assuming a demand of $0.09GJ_{el}$ for each GJ of waste heat recovered.

emissions of the chains with the current industrial process, it has to be considered that around 10,000ton/year of NaCl are required for the preparation of the regenerant solution with the flow-rates reported in Section 3.1. The NaCl production is very energy intensive: the electricity demand for salt crystallization by mechanical vapour recompression is 450 kWh/ton_{salt} (Sedivy, 2006). The energy demand of the salt production process, considering the yearly requirement of salt in the plant, leads to around 2.1kton/y of CO_2 emissions. On top of this, the emissions due to the production of the demineralized water used for the preparation of IEX regenerant solution and the salt transportation should be accounted. However, these terms are too site-specific and, conservatively, have not been considered in this study. For comparison, the CO_2 emissions were divided by the fresh regenerant (brine) flow-rate and the ratio was equal to $19.7kg_{CO2}/m^3_{brine}$ for the current system. In the proposed treatment schemes, the MED and the RO-MD chains treat the same flow rate of effluent (130 m^3/h) and produce around 53 m^3/h of brine solution, reusable as regenerant. The chains show global values of CO_2 emissions equal to 4.7 and 7.3kton/y respectively, which correspond to a ratio between the CO_2 emissions and the produced brine of 10.8 and $16.7kg_{CO2}/m^3_{brine}$. Thus, the CO_2 emissions can be reduced, with both chains, even considering the current energy mix of the grid.

4.1.2. Simultaneous variation of feed flow-rate and energy cost

To investigate also the role of the heat cost, feed flow-rate and thermal energy cost were simultaneously varied. Three heat sources are considered: industrial waste heat available in the site, gas turbine co-generation cycle and boiler burning natural gas. The relevant heat costs define a range, which goes from 0 up to about $0.07\$/kWh_{th}$, in the case of the boiler where natural gas at a cost of 0.065$/kWh is burnt with an efficiency of 90% (EIA, 2019).

Fig. 9 reports the contour-maps of LBCtot for the NF-cryst-MED and the NF-cryst-RO-MD chains varying feed flow-rate and heat cost. The NF-cryst-MD chain was not further analysed since it reported the worst results in all cases. The line in black collects all the points where LBC_{tot} is equal to $8\$/m^3$, which is the value used as a threshold, since it is the current cost of the regenerant solution. In both cases, the feasibility area, i.e. the region above the line, enlarges as Q_{feed} increases, since the levelized capital costs are lower and a higher expense for the thermal energy can be met within the feasibility region. Comparing the two technologies, the NF-cryst-RO-MD chain shows a smaller feasibility area and this is explicable considering its higher energy requirement. However, the minimum flow rate found in its feasibility region is lower (around 38 m^3/h) and this demonstrates that the RO-MD system is more economically convenient in the case of smaller plant size. Overall, both systems show a significantly wide range of operating conditions where they result more competitive than the state of the art.

4.2. Scenario 2. Electricity supply from a PV-battery system

In Scenario 2, electricity is supplied by a dedicated PV-battery system. On the basis of the meteorological characteristics of the location, the electricity self-sufficiency (i.e. the share of the demand covered by the PV-battery system) is derived; the rest is taken from the grid, assuming the cost used in Scenario 1.

4.2.1. PV-battery system configurations: global LCOE and emission factors

Parametric analyses performed by varying the installed PV power and the capacity of the battery give rise to a scatter of LCOE values as a function of the CO_2 emission factor. The configurations found in correspondence to the lower envelope of the scatter plots, shown in Fig. 10, are used to define the LCOE values and the corresponding emission factors in Scenario 2. In chart A, the emissions are not subjected to taxation, while in chart B the CO_2 emissions are taxed with a price of 80€/ton. More details about the PV-battery system simulations are given in the Supplementary Materials.

4.2.2. Treatment chains results

Fig. 11A shows the trends of LBC_{tot} of the NF-cryst-MED and NF-cryst-RO-MD chains varying the LCOE within the ranges reported in Fig. 10A and B. Notably, for each chain, the LBC_{tot} trends with or

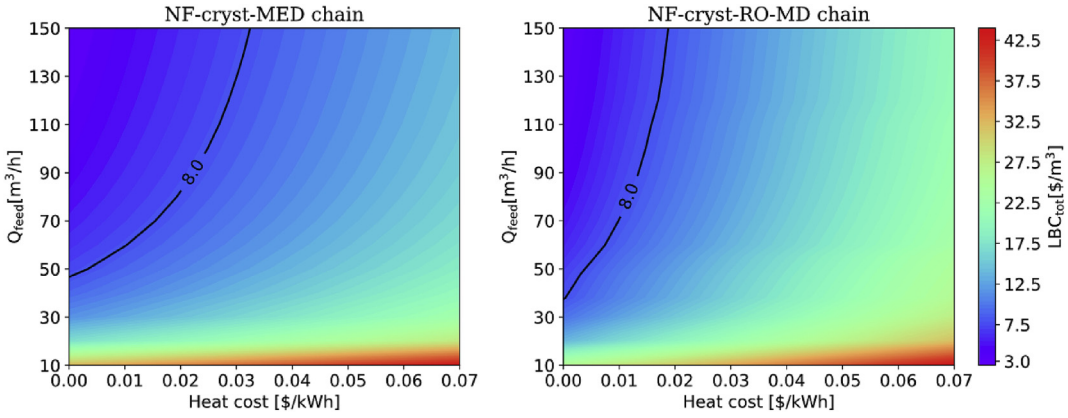

Fig. 9. Heat maps of the LBC_{tot} of the NF-cryst-MED chain (left) and of the NF-cryst-RO-MD chain (right) varying Q_{feed}[m^3/h] and $Cost_{Heat}$[$/kWh]. Grid supply, $Cost_{El}$ = 0.103$/kWh. Black line: LBC_{tot} equal to 8$/$m^3$ (current cost of the fresh regenerant solution).

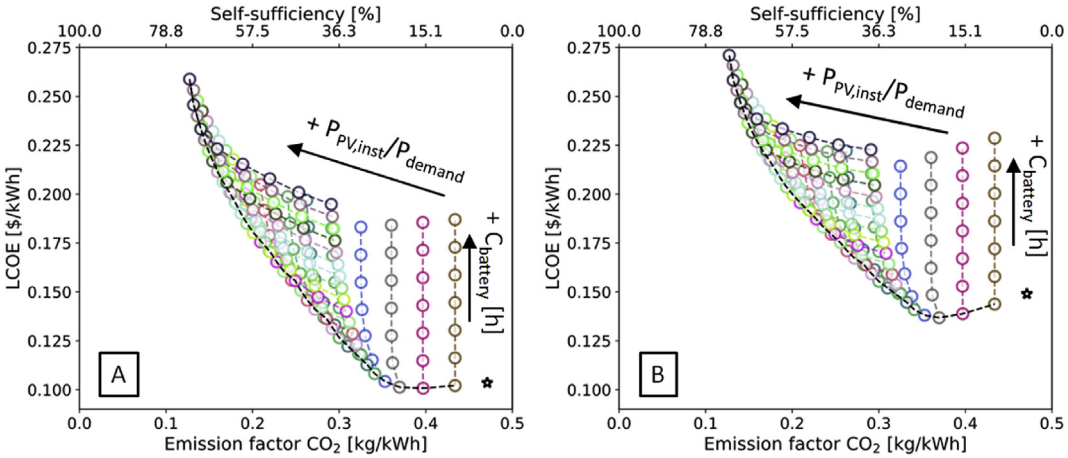

Fig. 10. LCOE [$/kWh] of the PV-battery-grid supply as function of the CO_2 emission factor from the grid [kg/kWh] varying the P_{inst}/P_{demand} ratio from 0.5 to 10 (step of 0.5) and the full load hours of the battery from 0 to 17.5 h (step of 2.5 h). For Figure A no taxation on the CO_2 emissions is considered, while in Figure B the CO_2 emissions have a cost of 80€/ton_{CO2}. The asterisk symbol (*) indicates the grid supply point.

without the taxation on the CO_2 emissions are partially overlapped, since part of the estimated LCOE range is the same, even if in correspondence to different CO_2 emission factors (see Fig. 10A and B). The two chains exhibit a linear trend of LBC_{tot} vs. LCOE, since the operating cost due to the electricity demand is the only varying term and it linearly depends on the given LCOE. Remarkably, even if the LCOE becomes more than two times the value of the electricity cost from the grid, the competitiveness of both chains is ensured almost in all cases: the MED chain presents values of LBC_{tot} much lower than the threshold in the full range of LCOE, whereas the RO-MD chain presents values of LBC_{tot} slightly higher than the threshold only for LCOE higher than 0.25$/kWh. Fig. 11B shows how much the LBC_{tot} increases when the CO_2 emissions decrease, in correspondence to higher shares of renewables in the energy supply system. As expected, the difference between the cases with or without taxation becomes more evident when higher shares of electricity are taken from the grid. Finally, it is remarkable the difference in the CO_2 emissions between Scenario 1, represented by the star marker and the cases analysed in Scenario 2. Therefore, with a PV-battery system, it is possible to reduce dramatically the emissions and, at the same time, ensure the economic feasibility of both chains. In the case with CO_2 taxation, the most environmentally friendly and feasible systems are the MED chain with LBC_{tot} of 6.1$/$m^3_{brine}$ and CO_2 emissions of 2.9kg_{CO2}/m^3_{brine} and the RO-MD chain with LBC_{tot} of 7.9$/$m^3_{brine}$ and CO_2 emissions of 5.1kg_{CO2}/m^3_{brine}. Therefore, the MED chain ensures a CO_2 emissions reduction with respect to the current system of 85% and the RO-MD chain of 75%.

4.2.3. Impact of the meteorological characteristics: comparison with a plant in Valencia, Spain

The analysis discussed above is performed also considering a different plant location: Valencia in Spain, which was selected since it is one of the European areas with the highest solar potential. Fig. 12 shows the lower envelopes of the scatter plots of LCOE vs. CO_2 emission factor for the case of a PV-battery system located in Rotterdam (shown in Fig. 10) and in Valencia, with or without CO_2 taxation. Notably, the LCOE values found are much lower than the ones found for Rotterdam and the difference between the corresponding curves increases moving to the region of lower CO_2 emissions. This is because the installed PV power necessary to reach high electricity self-sufficiency decreases dramatically for the plant located in Valencia. Moreover, it is evident that the LCOE trend is flatter in this last case, especially in the scenario with the tax on the CO_2 emissions.

The LCOE values calculated for the system in Valencia are employed as inputs for the two selected chains and the LBC_{tot} values (only the ones including the taxation on the CO_2 emissions)

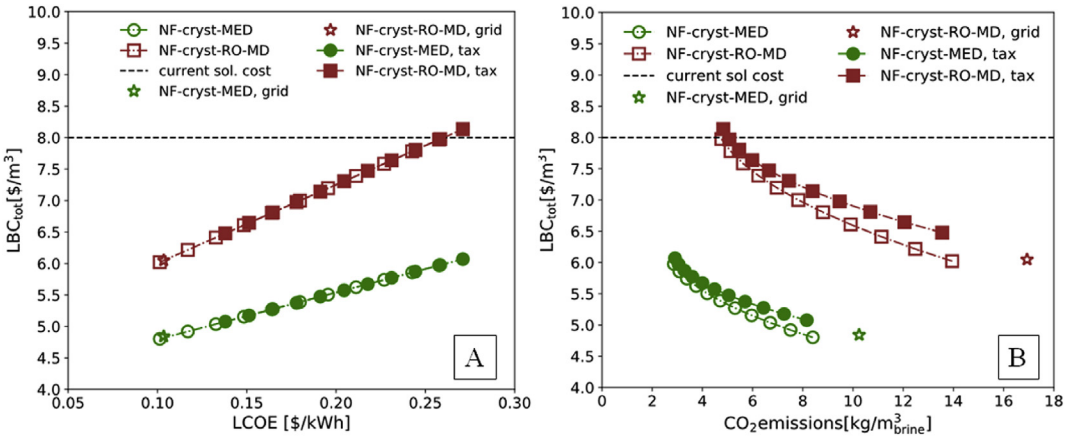

Fig. 11. LBC_{tot} vs. LCOE (A) and LBC_{tot} vs. the CO_2 emissions (B) for the NF-cryst-MED and the NF-cryst-RO-MD chains, with and without taxation on the CO_2 emissions. The asterisk symbol (*) represents the cases of grid supply (Scenario 1).

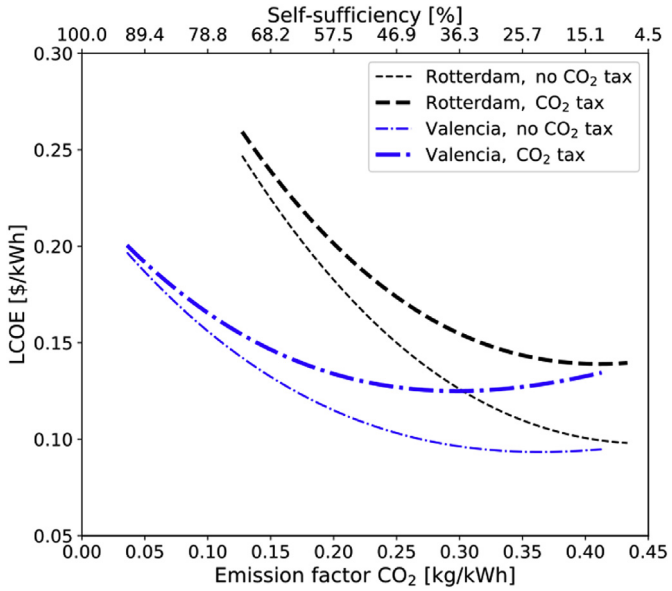

Fig. 12. Lower envelopes of the scatter plots of LCOE [$/kWh] vs. the CO_2 emission factor [kg/kWh], varying $P_{PV,inst}/P_{demand}$ between 0.5 and 10 (step of 0.5) and $C_{battery}$ between 0 and 17.5 h (step of 2.5 h), for the case of a plant located in Rotterdam and in Valencia. Thinner lines: no taxation on the CO_2 emissions, thicker lines: taxation of 80€/ton_{CO2}.

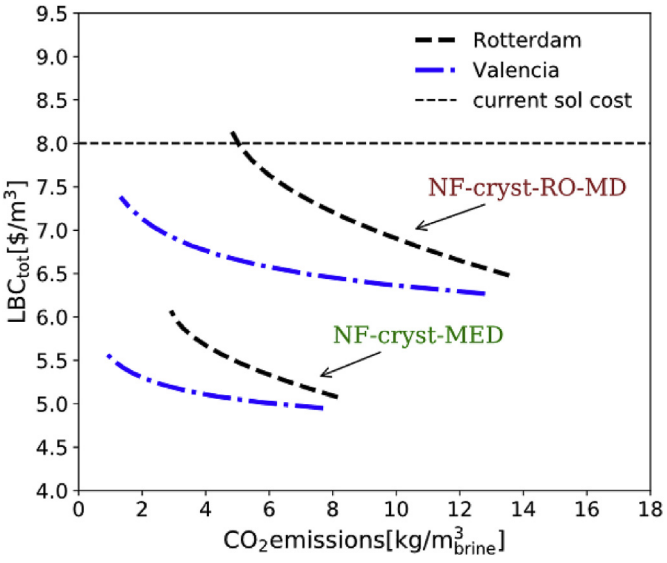

Fig. 13. Comparison of the LBC_{tot} trends [$/$m^3_{brine}$] of the two chains (NF-cryst-MED and NF-cryst-RO-MD) vs. the CO_2 emission [kg/m^3_{brine}], assuming CO_2 taxation of 80€/ton_{CO2}, for the case of a plant located in Rotterdam (case study, in black) and in Valencia, Spain (in blue). (For interpretation of the references to colour in this figure legend, the reader is referred to the Web version of this article.)

are reported vs. the CO_2 emissions in Fig. 13. Both chains show a much flatter trend of LBC_{tot} vs. the specific CO_2 emissions, because of the flatter LCOE trend in the case of Valencia. Remarkably, both curves shift towards lower CO_2 emissions, since the self-sufficiency (fraction of self-generated electricity) reaches 92%, while in the Rotterdam case the maximum self-sufficiency was around 73%. Moreover, in this case, both chains result economically feasible in the whole range of LCOE, since LBC_{tot} is always lower than the threshold cost. This analysis shows the high potential of the proposed systems, which result economically competitive and able to guarantee a significant reduction of the CO_2 emissions. In fact, the CO_2 emissions go down to 0.77kg_{CO2}/m^3_{brine} in the case of the MED chain and to 1.26kg_{CO2}/m^3_{brine} in the case of the RO-MD chain. Thus, in both cases, an emission reduction higher than 90% compared to the current system is achieved.

4.3. Implications

The global outputs obtained in the two scenarios were compared to highlight the implications of the proposed strategies in terms of economic feasibility and environmental impact. Fig. 14 reports the LBC_{tot} and the CO_2 emissions per m^3 of brine. In particular, the current CO_2 emissions due to the fresh NaCl salt production are compared with the ones due to the chains' energy demand (i) when the electricity is taken from the grid and (ii) when the electricity is partially supplied by a PV-battery system, in the two different locations and with the maximum share of renewables at which the LBC_{tot} resulted below the threshold. The corresponding values of LBC_{tot} are compared with the current cost of the fresh regenerant solution. Notably, all systems ensure a reduction of the CO_2 emissions and a more competitive LBC_{tot} in comparison with the current system. The employment of renewable energy sources allows a net reduction of the CO_2 emissions, but the LBC_{tot} are higher than in scenario 1; conversely, the relatively low cost of

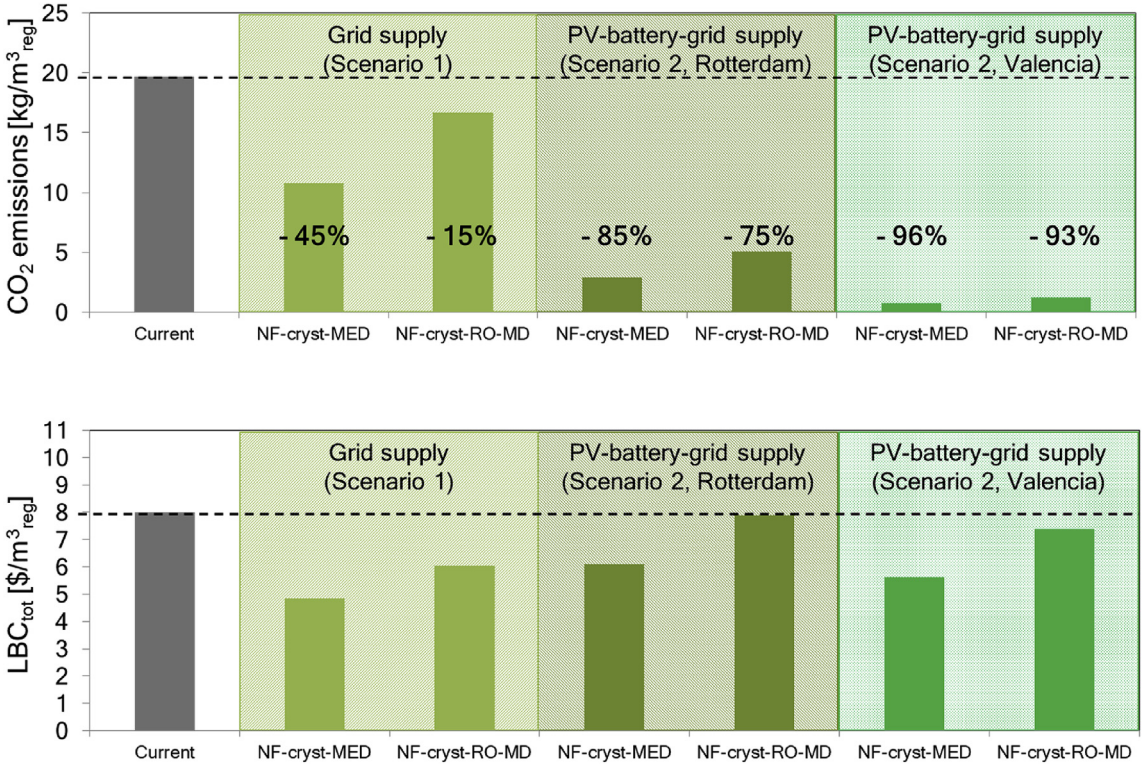

Fig. 14. Values of CO_2 emissions per $m^3_{regenerant}$ (figure above) and the corresponding LBC_{tot} (figure below) for the current system and for the analysed scenarios. For scenario 2, LBC_{tot} refer to the cases with carbon tax and minimum emissions (maximum self-sufficiency). Q_{feed} = 130 m^3/h; waste heat, $Cost_{heat}$ = 0.01$/kWh$_{th}$.

the electricity from the grid leads to lower LBC_{tot} but the reduction of CO_2 emissions is less significant than in scenario 2.

5. Conclusions

This work presents an integrated methodological approach used to conduct a comprehensive analysis of different strategies to move towards Circular Economy in the water softening industry. These strategies aim (i) at recycling the effluent as reactant in the regeneration of IEX resins and (ii) at recovering valuable raw materials. Using the developed approach, for the first time, different concentration technologies and energy supply systems are proposed to identify the most economically convenient and environmentally friendly system to treat the wastewater. The proposed treatment chains include a pre-treatment step, composed of nanofiltration and crystallization, and a concentration step. Three alternative concentration steps are evaluated: MED, MD and the combination of RO and MD. For these, a common target concentration of the treated solution was set, to recycle the solution to the industrial process. Therefore, the systems present the same circularity degree, which in turn corresponds to different costs and energy demand depending on the processes involved. The chains with RO-MD and with MED showed a wide range of feasible flow-rates and heat costs. In particular, the RO-MD chain resulted more convenient at small scales for its lower investment costs, while the MED chain resulted more feasible at larger scales, for its lower energy requirements. Concerning the environmental impact of the two chains, the CO_2 emissions per m^3 of brine reusable as regenerant were lower than those due to the production of the fresh regenerant, when electricity is taken from the grid. In particular, for a feed flow-rate of 130 m^3/h, the two chains are economically feasible since the LBC_{tot} is equal to 4.6 and 6.4$/$m^3$ for the MED and the RO-MD chain respectively (both lower that the current cost of the regenerant, i.e. 8$/$m^3$). Also, they have lower carbon footprints, since the respective operational CO_2 emissions amount to 10.8 and 16.7kg_{CO2}/m^3_{brine}, while the currently produced ones to 19.7kg_{CO2}/m^3_{brine}. The chain with MD only reported the worst results in terms of costs and CO_2 emissions, for the high MD thermal demand.

The other main focus of this work concerned the possibility to couple the chains with a PV-battery system placed in two locations: Rotterdam (The Netherlands, location of the real softening plant) and Valencia (Spain, for its high solar potential). A large decrease of the emissions was found: in Rotterdam, the CO_2 emission per m^3_{brine} resulted 75% and 85% lower than the current ones with the RO-MD and the MED chain, respectively and in Valencia, the reduction was higher than 90% for both chains. Moreover, the plants resulted economically feasible, even when the LCOE was more than two times the electricity cost from the grid.

Overall, the MED chain resulted more economically convenient and showed lower emissions in most cases, because of the lower energy requirements. However, the chain with RO-MD proved to be more feasible at lower scales and, in general, this system should be taken into account for its higher modularity and flexibility. Concluding, the NF-cryst-MED and NF-cryst-RO-MD chains should be regarded as valuable options for the implementation of a CE approach in the water softening industry.

Future works will investigate the other terms having an environmental impact, beyond the energy requirements of the treatment systems. The analysis will include the assessment of the CO_2 footprints due to the construction of the treatment units. Other future developments will consist in the application of the presented methodological approach to other case studies with different industrial effluents, to evaluate the most feasible and environmentally friendly strategy to treat and recycle the wastewater.

Declaration of competing interest

The authors declare that they have no known competing financial interests or personal relationships that could have appeared to influence the work reported in this paper.

CRediT authorship contribution statement

M. Micari: Conceptualization, Methodology, Software, Writing - original draft. **M. Moser:** Methodology, Software, Funding acquisition. **A. Cipollina:** Conceptualization, Supervision. **A. Tamburini:** Supervision, Writing - review & editing. **G. Micale:** Supervision, Funding acquisition. **V. Bertsch:** Supervision, Writing - review & editing.

Acknowledgements

This work was funded by the ZERO BRINE project (ZERO BRINE—Industrial Desalination—Resource Recovery—Circular Economy)-Horizon 2020 programme, Project Number: 730390. www.zerobrine.eu.

Appendix A. Supplementary data

Supplementary data to this article can be found online at https://doi.org/10.1016/j.jclepro.2020.120291.

References

Abdelkader, S., Gross, F., Winter, D., Went, J., Koschikowski, J., Geissen, S.U., Bousselmi, L., 2019. Application of direct contact membrane distillation for saline dairy effluent treatment: performance and fouling analysis. Environ. Sci. Pollut. Control Ser. 26, 18979–18992.

Al-Obaidani, S., Curcio, E., Macedonio, F., Diprofio, G., Alhinai, H., Drioli, E., 2008. Potential of membrane distillation in seawater desalination: thermal efficiency, sensitivity study and cost estimation. J. Membr. Sci. 323, 85–98.

Ali, A., Tsai, J.-H., Tung, K.-L., Drioli, E., Macedonio, F., 2018. Designing and optimization of continuous direct contact membrane distillation process. Desalination 426, 97–107.

Bilińska, L., Gmurek, M., Ledakowicz, S., 2017. Textile wastewater treatment by AOPs for brine reuse. Process Saf. Environ. Protect. 109, 420–428.

Birnhack, L., Keller, O., Tang, S.C.N., Fridman-Bishop, N., Lahav, O., 2019. A membrane-based recycling process for minimizing environmental effects inflicted by ion-exchange softening applications. Separ. Purif. Technol. 223, 24–30.

Boulding, K.E., Jarrett, H., 1966. Essays from the Sixth Resources for the Future Forum on Environmental Quality in a Growing Economy.

Breyer, C., Afanasyeva, S., Brakemeier, D., Engelhard, M., Giuliano, S., Puppe, M., Schenk, H., Hirsch, T., Moser, M., 2017. Assessment of Mid-term Growth Assumptions and Learning Rates for Comparative Studies of CSP and Hybrid PV-Battery Power Plants.

Cardinali, A., Pati, S., Minervini, F., D'Antuono, I., Linsalata, V., Lattanzio, V., 2012. Verbascoside, isoverbascoside, and their derivatives recovered from olive mill wastewater as possible food antioxidants. J. Agric. Food Chem. 60, 1822–1829.

Cardona, C.A., Quintero, J.A., Paz, I.C., 2010. Production of bioethanol from sugarcane bagasse: status and perspectives. Bioresour. Technol. 101, 4754–4766.

Chandrasekara, N.P.G.N., Pashley, R.M., 2015. Study of a new process for the efficient regeneration of ion exchange resins. Desalination 357, 131–139.

Chen, Y., Davis, J.R., Nguyen, C.H., Baygents, J.C., Farrell, J., 2016. Electrochemical ion-exchange regeneration and fluidized bed crystallization for zero-liquid-discharge water softening. Environ. Sci. Technol. 50, 5900–5907.

Cipollina, A., Bevacqua, M., Dolcimascolo, P., Tamburini, A., Brucato, A., Glade, H., Buether, L., Micale, G., 2014. Reactive crystallisation process for magnesium recovery from concentrated brines. Desalin. Water Treat. 55, 2377–2388.

Deutsches Zentrum für Luft- und Raumfahrt e.V., 2019. https://rcenvironment.de/.

Dow Water and Process Solutions. Filmtec Reverse Osmosis Membrane. Technical Manual.

EIA, 2019. Monthly Report of Natural Gas Purchases and Deliveries to Consumers.

El-Dessouky, H., Ettouney, H., 1999. Multiple-effect evaporation desalination systems: thermal analysis. Desalination 125, 259–276.

Ellen MacArthur Foundation, 2013. Towards the Circular Economy-Economic and Business Rationale for an Accelerated Transition (part 1).

Eurostat, 2018. Which Indicators Are Used to Monitor the Progress towards a Circular Economy?.

Eurostat, 2019. Electricity Prices for Non-household Consumers - Bi-annual Data (from 2007 onwards).

Fraunhofer, I.S.E., 2015. Current and Future Cost of Photovoltaics. Long-Term Scenarios for Market Development, System Prices and LCOE of Utility-Scale PV Systems. Agora Energiewende.

FXTOP, 2020. https://fxtop.com/en/historical-currency-converter.php.

Gebel, J., Yuce, S., 2008. An Engineer's Guide to Desalination. VBG PowerTech.

Geissdoerfer, M., Savaget, P., Bocken, N.M.P., Hultink, E.J., 2017. The Circular Economy – a new sustainability paradigm? J. Clean. Prod. 143, 757–768.

Geraldes, V., Brites Alves, A.M., 2008. Computer program for simulation of mass transport in nanofiltration membranes. J. Membr. Sci. 321, 172–182.

Ghisellini, P., Cialani, C., Ulgiati, S., 2016. A review on circular economy: the expected transition to a balanced interplay of environmental and economic systems. J. Clean. Prod. 114, 11–32.

Giagnorio, M., Amelio, A., Grüttner, H., Tiraferri, A., 2017. Environmental impacts of detergents and benefits of their recovery in the laundering industry. J. Clean. Prod. 154, 593–601.

Gopinath, A., Bahurudeen, A., Appari, S., Nanthagopalan, P., 2018. A circular framework for the valorisation of sugar industry wastes: review on the industrial symbiosis between sugar, construction and energy industries. J. Clean. Prod. 203, 89–108.

Gusmerotti, N.M., Testa, F., Corsini, F., Pretner, G., Iraldo, F., 2019. Drivers and approaches to the circular economy in manufacturing firms. J. Clean. Prod. 230, 314–327.

Harmelink, M., Bosselaar, L., 2013. Allocating CO2 Emissions to Heat and Electricity. Harmelink consulting.

Hitsov, I., Eykens, L., Schepper, W.D., Sitter, K.D., Dotremont, C., Nopens, I., 2017. Full-scale direct contact membrane distillation (DCMD) model including membrane compaction effects. J. Membr. Sci. 524, 245–256.

Hitsov, I., Sitter, K.D., Dotremont, C., Nopens, I., 2018. Economic modelling and model-based process optimization of membrane distillation. Desalination 436, 125–143.

Holkar, C.R., Jadhav, A.J., Pinjari, D.V., Mahamuni, N.M., Pandit, A.B., 2016. A critical review on textile wastewater treatments: possible approaches. J. Environ. Manag. 182, 351–366.

International Energy Agency, 2018. World Energy Outlook 2018.

IPCC, 2006. 2006 IPCC Guidelines for National Greenhouse Gas Inventories. National Greenhouse Gas Inventories Programme, IGES, Japan.

Janeiro, L., Patel, M.K., 2015. Choosing sustainable technologies. Implications of the underlying sustainability paradigm in the decision-making process. J. Clean. Prod. 105, 438–446.

Kamali, R.K., Abbassi, A., Sadough Vanini, S.A., Saffar Avval, M., 2008. Thermodynamic design and parametric study of MED-TVC. Desalination 222, 596–604.

Kesieme, U.K., Milne, N., Aral, H., Cheng, C.Y., Duke, M., 2013. Economic analysis of desalination technologies in the context of carbon pricing, and opportunities for membrane distillation. Desalination 323, 66–74.

Labban, O., Liu, C., Chong, T.H., Lienhard V, J.H., 2017. Fundamentals of low-pressure nanofiltration: membrane characterization, modeling, and understanding the multi-ionic interactions in water softening. J. Membr. Sci. 521, 18–32.

Li, J., Koner, S., German, M., SenGupta, A.K., 2016. Aluminum-cycle ion exchange process for hardness removal: a new approach for sustainable softening. Environ. Sci. Technol. 50, 11943–11950.

Liu, J., Chen, S., Wang, H., Chen, X., 2015. Calculation of carbon footprints for water diversion and desalination projects. Energy Procedia 75, 2483–2494.

Lopez, J., Reig, M., Gibert, O., Cortina, J.L., 2019. Integration of nanofiltration membranes in recovery options of rare earth elements from acidic mine waters. J. Clean. Prod. 210, 1249ß1260.

Malek, A., Hawlader, M.N.A., Ho, J.C., 1996. Design and economics of RO seawater desalination. Desalination 105, 245–261.

Man, Y., Shen, W., Chen, X., Long, Z., Pons, M.-N., 2017. Modeling and simulation of the industrial sequencing batch reactor wastewater treatment process for cleaner production in pulp and paper mills. J. Clean. Prod. 167, 643–652.

Mezher, T., Fath, H., Abbas, Z., Khaled, A., 2011. Techno-economic assessment and environmental impacts of desalination technologies. Desalination 266, 263–273.

Micari, M., Cipollina, A., Tamburini, A., Moser, M., Bertsch, V., Micale, G., 2019a. Combined membrane and thermal desalination processes for the treatment of ion exchange resins spent brine. Appl. Energy 254.

Micari, M., Moser, M., Cipollina, A., Fuchs, B., Ortega-Delgado, B., Tamburini, A., Micale, G., 2019b. Techno-economic assessment of multi-effect distillation process for the treatment and recycling of ion exchange resin spent brines. Desalination 456, 38–52.

Mirabella, N., Castellani, V., Sala, S., 2014. Current options for the valorization of food manufacturing waste: a review. J. Clean. Prod. 65, 28–41.

Moser, M., Trieb, F., Fichter, T., Kern, J., Hess, D., 2014. A flexible techno-economic model for the assessment of desalination plants driven by renewable energies. Desalin. Water Treat. 1–15.

Nadeem, K., Guyer, G.T., Keskinler, B., Dizge, N., 2019. Investigation of segregated wastewater streams reusability with membrane process for textile industry. J. Clean. Prod. 228, 1437–1445.

Ortega-Delgado, B., García-Rodríguez, L., Alarcón-Padilla, D.-C., 2017. Opportunities of improvement of the MED seawater desalination process by pretreatments allowing high-temperature operation. Desalin. Water Treat. 97, 94–108.

Papapetrou, M., Cipollina, A., La Commare, U., Micale, G., Zaragoza, G., Kosmadakis, G., 2017. Assessment of methodologies and data used to calculate desalination costs. Desalination 419, 8–19.

Qtaishat, M., Matsuura, T., Kruczek, B., Khayet, M., 2008. Heat and mass transfer

analysis in direct contact membrane distillation. Desalination 219, 272–292.
Roy, Y., Sharqawy, M.H., Lienhard, J.H., 2015. Modeling of flat-sheet and spiral-wound nanofiltration configurations and its application in seawater nanofiltration. J. Membr. Sci. 493, 360–372.
Saidani, M., Yannou, B., Leroy, Y., Cluzel, F., Kendall, A., 2019. A taxonomy of circular economy indicators. J. Clean. Prod. 207, 542–559.
Sarayu, K., Sandhya, S., 2012. Current technologies for biological treatment of textile wastewater–a review. Appl. Biochem. Biotechnol. 167, 645–661.
Sassanelli, C., Rosa, P., Rocca, R., Terzi, S., 2019. Circular economy performance assessment methods: a systematic literature review. J. Clean. Prod. 229, 440–453.
Sedivy, V.M., 2006. Environmental balance of salt production speaks in favour of solar saltworks. In: 1st International Conference on the Ecological Importance of Solar Saltworks (Santorini).
Suárez-Eiroa, B., Fernández, E., Méndez-Martínez, G., Soto-Oñate, D., 2019. Operational principles of circular economy for sustainable development: linking theory and practice. J. Clean. Prod. 214, 952–961.
Turek, M., Dydo, P., Klimek, R., 2008. Salt production from coal-mine brine in NF — evaporation — crystallization system. Desalination 221, 238–243.
Turton, R., Bailie, R.C., Whiting, W.B., Shaeiwity, J.A., Bhattacharzza, D., 2012. Analysis, Synthesis and Design of Chemical Processes. Prentice Hall.
U.S. Department of the Interior, 2017. Mineral Commodity Summaries - U.S. Geological Survey.
Van der Bruggen, B., Everaert, K., Wilms, D., Vandecasteele, C., 2001. Application of nanofiltration for removal of pesticides, nitrate and hardness from ground water: rejection properties and economic evaluation. J. Membr. Sci. 193, 239–248.
Vince, F., Marechal, F., Aoustin, E., Bréant, P., 2008. Multi-objective optimization of RO desalination plants. Desalination 222, 96–118.
Wilf, M., Bartels, C., 2005. Optimization of seawater RO systems design. Desalination 173, 1–12.
Winter, D., Koschikowski, J., Wieghaus, M., 2011. Desalination using membrane distillation: experimental studies on full scale spiral wound modules. J. Membr. Sci. 375, 104–112.
World Commission on Environment and Development, 1987. Our Common Future.
Zhijun, F., Nailing, Y., 2007. Putting a circular economy into practice in China. Sustain. Sci. 2, 95–101.
Zhou, D., Zhu, L., Fu, Y., Zhu, M., Xue, L., 2015. Development of lower cost seawater desalination processes using nanofiltration technologies — a review. Desalination 376, 109–116.

Journal of Cleaner Production 270 (2020) 122472

Contents lists available at ScienceDirect

Journal of Cleaner Production

journal homepage: www.elsevier.com/locate/jclepro

Techno-economic analysis of integrated processes for the treatment and valorisation of neutral coal mine effluents

M. Micari [a, *], A. Cipollina [b], A. Tamburini [b, **], M. Moser [a], V. Bertsch [a, c], G. Micale [b]

[a] German Aerospace Center (DLR), Institute of Engineering Thermodynamics, Pfaffenwaldring 38-40, 70569, Stuttgart, Germany
[b] Dipartimento di Ingegneria (DI), Università Degli Studi di Palermo (UNIPA), Viale Delle Scienze Ed. 6, 90128, Palermo, Italy
[c] Ruhr-Universität Bochum, Chair of Energy Systems and Energy Economics, Universitätsstr. 150, 44801, Bochum, Germany

ARTICLE INFO

Article history:
Received 21 January 2020
Received in revised form
22 May 2020
Accepted 23 May 2020
Available online 1 June 2020

Handling editor: Prof. Jiri Jaromir Klemeš

Keywords:
Coal mine effluent
Wastewater treatment
Techno-economic analysis
Economic feasibility
Resource recovery
Energy demand

ABSTRACT

The disposal of highly-concentrated neutral coal mine effluents into the environment constitutes a severe threat to the natural ecosystem. This work proposes and compares five novel treatment chains to purify the effluent and recover raw materials. The chains present different combinations of pre-treatment and concentration technologies. In all cases, the solution sent to the concentration step is concentrated up to saturation to recover water and sodium chloride.

Concerning the technical performances, the treatment chains are compared in terms of total energy demand and salt recovery. Furthermore, the economic feasibility assessment is performed via a novel global parameter, i.e. the levelized cost of the produced NaCl crystals (Levelized Salt Cost, LSC).

The energetic and economic analysis of the chains highlighted that the thermal energy demand of the concentration technology covers the highest share of the total demand and the relevant costs are among the highest expenditures. Also, the revenues given by $Mg(OH)_2$ production were found to play a key role in offsetting the treatment costs. Among the treatment chains analysed, the one composed by two nanofiltration units and two crystallizers in the pre-treatment step and a multi-effect distillation unit in the concentration step showed the highest recovery of NaCl and turned out to be the most economically feasible. The relevant LSC (~100 $/ton$_{NaCl}$) was the lowest and it was comparable with the lower bound of the current range of price of high-purity NaCl crystals.

In conclusion, the findings of this work contribute to improving the sustainability of the coal mine industrial sector, by proposing economically feasible solutions for the treatment and valorisation of its neutral effluent.

1. Introduction

Coal extraction is realized through opencast or underground methods and both strongly affect the environment for the discharge of significant wastewater volumes (Tiwary, 2001). Coal mine wastewater may assume a wide range of physicochemical properties and pH, depending on the hydrogeology of the mine responsible for its discharge (Masindi et al., 2018). In particular, coal mine operations may lead to the production of acid effluents, called *Acid Mine Drainage* (AMD), and of *Neutral Effluents* with high concentration of salt and hardness. Both effluents would cause severe problems to human health and environment, if discharged.

Concerning *AMD*, the acidity of the solutions depends on the content of pyrite (FeS_2) in the coal and their release into the environment would deteriorate the quality of the receiving water and would damage natural ecosystems (Baruah and Khare, 2010). AMD typically presents metal ions, such as iron, copper, aluminium, nickel, whose solubility increases at low pH up to toxic levels (Akcil and Koldas, 2006). Several studies focused on the development of processes to neutralize the discharged solution: among these, active mine treatment is one of the most common methods (Qin et al., 2019). This process consists in mixing the effluent with alkaline solutions to increase the pH and to let the metal ions precipitate as hydroxides (Kalin et al., 2006). Alternative methods include the employment of wetlands where neutralization occurs via microbial communities (Tarutis et al., 1999) and in-situ bioremediation by adding sulphate-reducing bacteria, whose

* Corresponding author.
** Corresponding author.
E-mail addresses: Marina.Micari@dlr.de (M. Micari), alessandro.tamburini@unipa.it (A. Tamburini).

https://doi.org/10.1016/j.jclepro.2020.122472
0959-6526/

Nomenclature

AMD	Acid mine drainage
C	Concentration [mol/m^3 or g/L]
CAPEX	Capital Expenditures [$/y]
Cryst	Crystallizer
LSC	Levelized Salt Cost [$/ton$_{NaCl}$]
LSC$_{cap}$	Capital Levelized Salt Cost [$/ton$_{NaCl}$]
LSC$_{op}$	Operating Levelized Salt Cost [$/ton$_{NaCl}$]
LWC	Levelized Water Cost [$/m^3]
MD	Membrane distillation
MED	Multi-effect Distillation
NF	Nanofiltration
OPEX	Operating Expenditures [$/y]
RCE	Remote Component Environment
RO	Reverse Osmosis
TBT	Top Brine Temperature [°C]
TDS	Total dissolved solids

performances were tested from the bench (Christensen et al., 1996) to the full-scale (Gibert et al., 2002). In this context, bioremediation systems were employed to produce water reusable for irrigation. Some of the analysed systems were found to be effective in sulphate removal and economically advantageous (Martins et al., 2010). Other possible methods to treat AMD include precipitation of heavy metals and ion-exchange (Feng et al., 2000), adsorption (Motsi et al., 2009) and the employment of magnetic nanoparticles of magnetite and cobalt ferrite (Kefeni et al., 2017a). The selection of the treatment method is often made by considering only technical and economic factors. However, recent studies focused on the environmental impact of the remediation systems by performing Life Cycle Assessment analyses (Martínez et al., 2019). In this regard, the environmental impact of the metal-rich sludge generated by the active treatment of AMD was assessed and valorisation strategies were proposed to recover metals and to reduce the waste production (Macías et al., 2017). In addition, other valuable materials may be recovered from the effluents via suitable valorisation strategies, such as ferrite, ferric hydroxide, gypsum, sulphuric acid and rare earth elements (Kefeni et al., 2017b). Various treatment strategies have been proposed: neutralization coupled with reaction steps to produce gypsum ($CaSO_4$) and limestone ($CaCO_3$) (Masindi et al., 2018) or nanofiltration to recover rare earth elements (López et al., 2019). Moreover, Nleya et al. assessed the technical and economic feasibility of applying wastewater treatment technologies to recover sulphuric acid (Nleya et al., 2016).

Concerning the highly concentrated *Neutral Effluents*, these are characterised by high hardness and high Total Dissolved Solids (TDS). In Poland, significant amounts of chlorides and sulphates were daily discharged into the rivers because of the release of coal mine effluents (Ericsson and Hallmans, 1996). This caused severe ecological problems, thus novel treatment strategies were proposed to reduce the waste and recover valuable materials, in particular gypsum and NaCl crystals (Turek et al., 2005a). The first treatment plant proposed by Ericsson et al. for the effluents of two coal mines in Poland was constituted by a pre-treatment step, two concentration steps (reverse osmosis and thermal desalination) and crystallization of NaCl (Ericsson and Hallmans, 1996). Then, Turek et al. proposed a treatment process to achieve a zero liquid discharge utilization of the effluent discharged by another polish coal mine (Turek et al., 2005a). In this case, two treatment trains with different pre-treatment and pre-concentration steps were devised for highly-concentrated and poorly-concentrated water: they proposed nanofiltration and evaporation for the first and electrodialysis for the second. Then, the two permeates were further concentrated and sent to the NaCl crystallizer. Moreover, the same authors demonstrated that using nanofiltration as pre-treatment step allowed for increasing the energetic efficiency of the treatment plant, by reducing the energy consumption of the NaCl crystallizer (Turek et al., 2008). Another work suggested using Vacuum Membrane Distillation to treat a coal mine effluent with high TDS, containing iron and aluminium together with calcium and magnesium (Sivakumar et al., 2013). The obtained permeate met the quality standards for potable water, since most of the ions (>95%) was removed during the treatment.

Overall, the rising concerns about the release of coal mine effluents into the environment lead to the need to develop new strategies for minimising this problem. Among these, the circular approach to reduce the waste production and to recover valuable materials looks as the most promising and feasible on the techno-economic level (Dharmappa et al., 2000). However, so far, only a very few works concerned novel combinations of treatment processes and strategies for materials recovery applicable to neutral coal mine effluents and in particular, none of these works presented a comprehensive comparison of different strategies in terms of energy demand, material recovery and costs.

This work presents for the first time various integrated treatment schemes for the purification and valorisation of neutral coal mine effluents. Each of the proposed treatment schemes derives from the combination of different technologies and is here simulated via the integration of the corresponding validated techno-economic models, available in literature. The results of these modelling activities will be used as the basis for the optimized design of a pilot plant within the EU project Zero Brine (European Union's Horizon, 2020).

The chains, given by the combination of pre-treatment and concentration processes, have been compared via novel assessment criteria, such as the levelized cost of the produced salt, to identify the most suitable and cost-effective treatment chain for the specific application. Such application refers to real coal mine effluents produced in Poland, which present high concentration of chloride and sulphate ions and a neutral pH (between 7.6 and 7.8). It is worth mentioning that these chains are devised considering the composition of the investigated real effluents and would not be suitable to acid mine effluents, which require specific treatment processes for the removal of pollutants.

The proposed chains make reference to the general treatment scheme reported in Fig. 1. This includes a pre-treatment step, composed by Nanofiltration (NF) and crystallization units, for recovering bivalent ions as Mg^{2+} and Ca^{2+}. The pre-treatment phase is followed by a concentration step, which can be completely thermal or given by the combination of thermal and electric membrane processes. In particular, two configurations were investigated: the concentration step was either based on Multi-Effect Distillation (MED) or given by the combination of Reverse Osmosis (RO) and direct contact Membrane Distillation (MD). Finally, an end-crystallization step is adopted in all chains to produce NaCl crystals.

Five chains are proposed and analysed in details from the energetic and the economic point of view, looking at the energy demands of the single processes, the relevant annualized capital and operating costs and the revenues coming from the by-products. For each system, the economic feasibility is assessed via the calculation of a novel parameter: the levelized cost of the main product of the chain, i.e. the NaCl crystals (here defined as *Levelized Salt Cost*, LSC [$/ton]). Then, the chains are compared in terms of the total energy requirements, the LSC and the salt recovery.

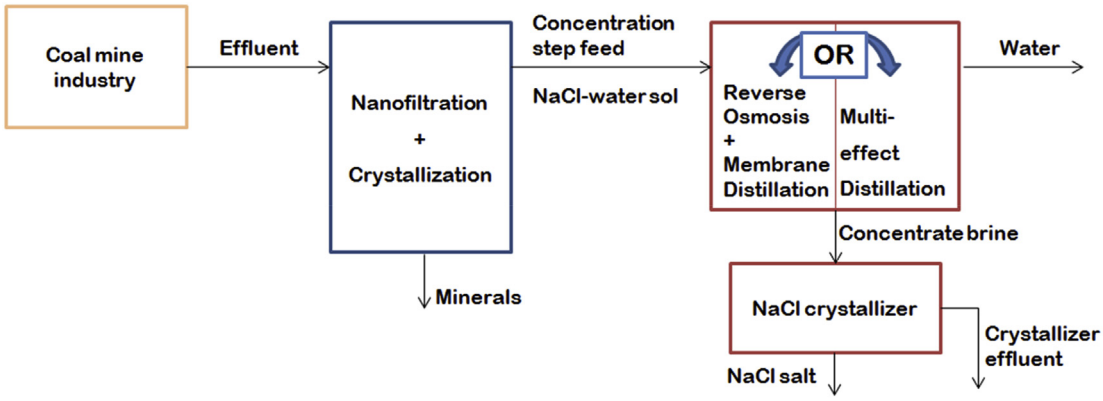

Fig. 1. Schematic representation of the treatment process proposed for coal mine effluents.

Overall, this work aims at the identification of the most feasible and less energy-intensive process to treat neutral coal mine effluents and to recover valuable materials.

2. Materials and methods

This section includes three paragraphs. The first presents the methodological approach employed in this work. The second describes the five treatment chains devised to purify the coal mine effluent and to recover minerals, water and salt. Finally, the third paragraph reports the definitions of the global outputs used to compare the chains.

2.1. Methodological approach

The methodological approach employed to develop, analyse and compare treatment chains for coal mine effluents has been extensively described in a previous work (Micari et al., 2020). This method is flexible and applicable to different case studies, when a number of integrated systems have to be developed and compared.

The methodology consists of four inter-related steps:

(a) implementation of techno-economic models of treatment technologies;
(b) definition of inputs and outputs of the models;
(c) development of treatment chains (i.e. how the technologies are interconnected);
(d) comparison through global outputs.

The technologies accounted in this work are NF and crystallization in the pre-treatment step and MED or RO plus MD, coupled with NaCl crystallization, in the concentration step. The relevant techno-economic models have been implemented in Python and integrated in a common simulation platform (*Remote Component Environment, RCE*) to simulate the entire chains.

As regards the step (a) of the methodology, previous works described extensively the techno-economic models of MED (Micari et al., 2019b) and NF units (Micari et al., 2019a). The main equations describing RO and MD are reported in the supplementary materials of (Micari et al., 2020). For the reactive crystallizers employed to produce $Mg(OH)_2$ and $CaCO_3$, we set up a simplified model based on mass balances, under the assumptions of a 100% conversion of the dissolved cations and a purity of the produced minerals higher than 99.5%. The assumptions of purity and conversion (i) are based on experimental data available within the Zero Brine project consortium and (ii) have been verified via the chemical equilibrium diagrams obtained for each crystallizer with the software Spana (Puigdomènech et al., 2014). Also, we implemented a simplified model for the end-crystallizer, used to produce NaCl. We employed mass and energy balances to define the amount of crystals produced, the thermal energy required and the outlet flow-rates. The fundamental equations used for the three crystallizers, together with the chemical equilibrium diagrams for the reactive crystallizers, are reported in the supplementary materials.

All models have been validated by comparing the trends with experimental results and/or results of other models in the literature. Our previous works report the results of the validation campaigns concerning MED (Micari et al., 2019b), NF (Micari et al., 2019a), RO and MD (Micari et al., 2020). The validation of the models makes this method particularly useful to simulate reliably full-scale plants and to compare them to identify the most performing one.

Concerning the step (b), the main inputs relevant to composition and flow-rate of the feed solution are reported in section 3, together with the parameters representing the operating conditions of the different technologies.

Paragraph 2.2 deals with the step (c) as it extensively describes the five treatment chains developed and analysed in this work. The details about the integration on RCE are given in (Micari et al., 2020).

Finally, the definitions of the global outputs (step (d)) used for the comparison of the chains are reported in paragraph 2.3.

2.2. Description of the treatment chains (step (c))

This paragraph describes the five treatment chains analysed in this work. The first chain, represented in Fig. 2, is taken as a reference and the others are presented in terms of their differences with respect to the first.

The pre-treatment part of the first chain includes two NF units in series: the permeate of the first NF unit is fed to the second to remove the bivalent ions almost completely. The retentates produced by the two NF units are mixed and sent to a two-step crystallization train. In the first crystallization unit, $Mg(OH)_2$ is produced by adding an alkaline solution; whereas, in the second, limestone ($CaCO_3$) is produced by adding a solution of Na_2CO_3.

The crystallization train aims at removing the bivalent ions contained in the two retentate solutions and at producing valuable materials. More in detail, the first crystallizer employs a water solution of dolime as alkaline reactant. Dolime is given by the calcination of dolomite that is a mixture of calcium and magnesium carbonates. The calcination process consists in heating the dolomite up to high temperatures, at which the dolomite decomposes into MgO and CaO and CO_2 gas is released. The purity of the

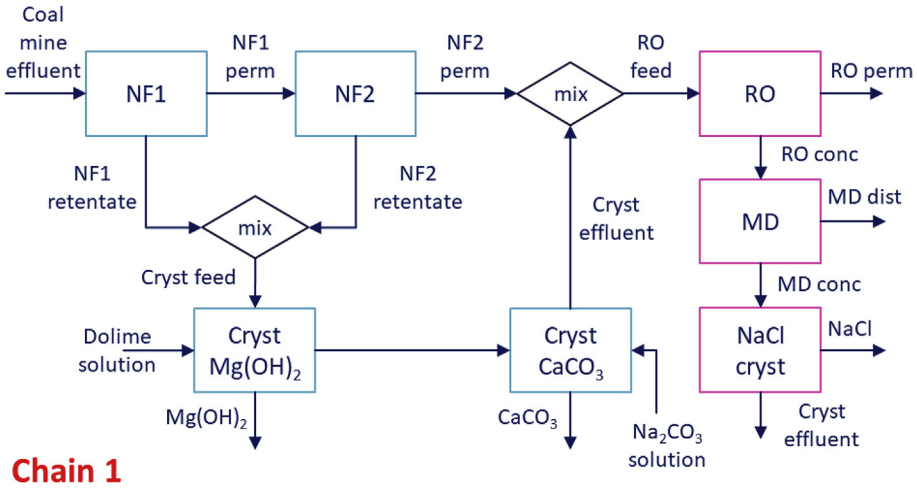

Fig. 2. Schematic representation of the first treatment chain (2NF-2cryst-RO-MD-cryst chain). Blue boxes: pre-treatment; purple boxes: concentration. (For interpretation of the references to colour in this figure legend, the reader is referred to the Web version of this article.)

$Mg(OH)_2$ crystals produced in the crystallizer depends on the calcination process. The complete calcination leads to the complete breakdown of the carbonates, whereas, if the calcination is not completed, the carbonates would pollute the produced crystals (Jakić, 2016). The suspension of dolime (obtained after the complete calcination of the dolomite) contains Mg^{2+} and Ca^{2+} ions in equal molar concentration, as in the dolime, and OH^- ions, given by the reaction of the oxides with water. Since the alkaline solution itself contains Mg^{2+} ions, the yield in $Mg(OH)_2$ is doubled and the effluent solution is enriched in Ca^{2+} ions.

Therefore, the 1st crystallizer outlet solution is rich of Ca^{2+} ions, which are supposed to be completely removed when the solution is mixed with a solution of Na_2CO_3 to produce $CaCO_3$ in the last crystallization step. The 2nd crystallizer effluent, rich in NaCl, is firstly neutralized with a very small amount of hydrochloric acid solution (negligible in terms of cost), to bring the pH back to a neutral value and then, is mixed with the 2nd NF permeate and the mixture is sent to the concentration step.

In the first chain, the concentration step presents two technologies in series: RO and MD. In this step, the concentrations of the bivalent ions are much lower than the saturation points of the species which are typically responsible of fouling, such as $CaSO_4$ or $MgSO_4$. Even in the recovery heat exchangers of MD, the calculated concentration of $CaSO_4$ is lower than the saturation point at the highest temperature (80°C), thus the risk of scaling can be neglected.

The MD retentate is sent to the end-crystallizer to produce NaCl crystals. To estimate the maximum amount of producible NaCl crystals, we considered two conditions to be fulfilled: (i) the amount of Ca^{2+} and Mg^{2+} should not exceed a certain concentration to ensure the effectiveness of the end-crystallizer (Turek et al., 2008) and (ii) the moles of SO_4^{2-} should be limited by the saturation concentration of Na_2SO_4, since Na^+ is so more abundant than Ca^{2+}, that the saturation point might be reached before the gypsum one. In this 1st chain, since the sulphate ions are not removed in the crystallization step and the 2nd crystallizer effluent is mixed with the NF permeate and sent to the RO unit, the second condition on the sulphate concentration is stricter and defines the amount of produced crystals.

The difference between the first and the second treatment chain stays in the pre-treatment part: the second chain, depicted in Fig. 3, presents only one crystallization step to produce $Mg(OH)_2$. Also, the effluent of the crystallization step, after being neutralized with a small amount of hydrochloric acid, is disposed as a waste (at a certain cost, reported in Table 2) and not mixed with the NF permeate. Thus, the feed solution sent to the concentration step has lower flow-rate and lower concentration of NaCl and bivalent ions. Therefore, also in this case, the risk of scaling in the concentration units can be neglected.

Concerning the amount of NaCl crystals produced in the end-crystallizer, the first condition on the maximum amount of bivalent cations is stricter since the SO_4^{2-} ions are more rejected than Ca^{2+} and Mg^{2+} in the two NF units.

The other three chains present a concentration step based only on MED.

The difference between the first and the third chain is in the concentration step, since in the third chain (Fig. 4) a MED plant is responsible for the whole concentration rise. In this chain, even if the concentration of components possibly responsible of scaling is always lower than their saturation point, the problem of scaling is more likely to occur and it may be more damaging since the feed evaporation takes place on the external surface of the tube bundle (Al-Rawajfeh et al., 2005). Therefore, suitable Top Brine Temperatures (TBT) and number of effects of the MED plant (reported in section 3) have been given to minimize the risk for scaling. Concerning the end-crystallizer, as in the 1st chain, the condition on the maximum sulphate concentration in the crystallizer effluent is stricter.

In the 4th chain (Fig. 5), both pre-treatment and concentration steps are different than those of the 1st chain. The pre-treatment is composed of two NF units and one crystallizer to produce $Mg(OH)_2$ and the crystallizer effluent is disposed as a waste, analogously to the 2nd chain. For the brine disposal, a certain cost per unit of disposed solution is assumed, as reported in Table 2. The concentration step presents the MED plant, coupled with an end-crystallizer to produce NaCl crystals. In this case, the amount of bivalent ions present in the NF permeate fed to the MED can be neglected and a higher TBT is allowed. In the calculation of the produced NaCl crystals, the maximum amount is limited by the concentration of bivalent cations.

Finally, the 5th chain, sketched in Fig. 6, presents a third NF stage in the pre-treatment step. This is included to further treat the mixture of the NF permeate and the crystallizer effluent, before being fed to the concentration step. The 3rd NF retentate constitutes a waste to be disposed with a certain cost (reported in Table 2). Analogously to the 4th chain, the content of bivalent ions in the

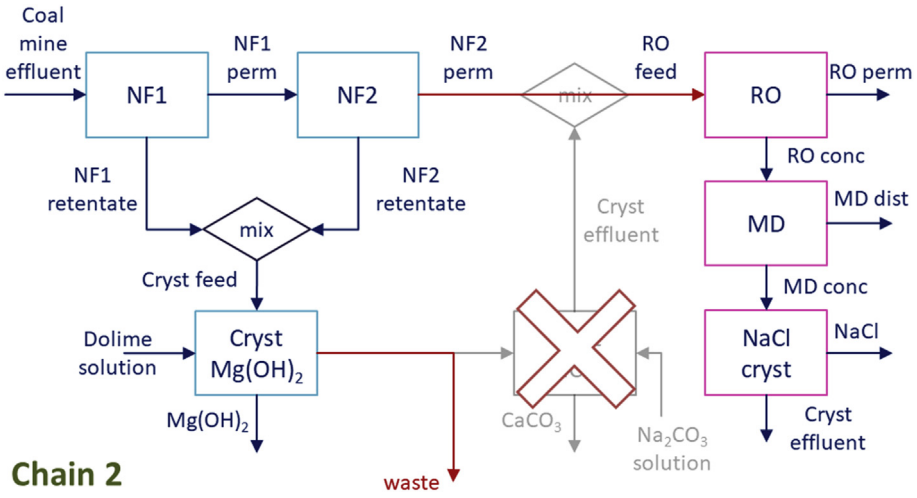

Fig. 3. Schematic representation of the second treatment chain (2NF-cryst-RO-MD-cryst chain). Blue boxes: pre-treatment; purple boxes: concentration. Differences with the 1st chain in red. (For interpretation of the references to colour in this figure legend, the reader is referred to the Web version of this article.)

Table 1
Main components of the five treatment chains.

Chain	Pre-treatment: NF	Pre-treatment: cryst	Concentration step
1	2 units, permeate-staging	2 units: $Mg(OH)_2$ and $CaCO_3$	RO-MD + end-crystallizer
2	2 units, permeate-staging	1 unit: $Mg(OH)_2$	RO-MD + end-crystallizer
3	2 units, permeate-staging	2 units: $Mg(OH)_2$ and $CaCO_3$	MED + end-crystallizer
4	2 units, permeate-staging	1 unit: $Mg(OH)_2$	MED + end-crystallizer
5	2 units, permeate-staging + 1 unit before MED	2 units: $Mg(OH)_2$ and $CaCO_3$	MED + end-crystallizer

MED feed is negligible since it is abated in the NF. Therefore, higher TBT can be used also in this case. Moreover, analogously to the 3rd chain, the condition on the sulphate concentration is the strictest condition to estimate the maximum amount of producible NaCl crystals.

The main features of the five proposed treatment chains are summarized in Table 1.

2.3. Main economic parameters and global output values

This paragraph presents the methods used to estimate the capital and operating costs of the single units, reports the most important parameters used for the economic analysis and defines the global outputs used as assessment criteria for the chains. The economic analysis is based on the calculation of the capital and operating expenditures (CAPEX and OPEX) of every unit. The annualized capital costs are calculated by assuming different depreciation periods, depending on the technology, and a common discount rate of 6% (Papapetrou et al., 2017). The economic models employed for NF (Micari et al., 2019a) and MED (Micari et al., 2019b) are described elsewhere. Concerning the RO unit, the CAPEX includes the cost for membrane elements and pressure vessels, high-pressure pump, piping and intake. These are annualized by assuming a depreciation period of 25 years (Vince et al., 2008). The OPEX takes into account electricity, labor, maintenance (3%/y of the investment plus 20% of the labor cost), chemicals and membrane replacement cost (replacement rate of 15%/y) (Wilf, 2007).

Regarding the MD unit, the investment costs of modules, pumps and heat exchangers are calculated, together with the costs for intake and pretreatment (Al-Obaidani et al., 2008). The total investment cost is annualized assuming a depreciation period of 10 years (Hitsov et al., 2018). The OPEX accounts for electric and thermal energy costs, maintenance cost (2.5%/y of the investment

Table 2
Main specific terms of cost and revenues used for the economic analysis. The costs of chemicals (reactants or products) are from (U.S. Department of the Interior, 2017).

Main specific terms of cost and revenues			
Terms of cost	NF membrane (Drioli et al., 2006)	30	$/m^3
	Dolime (Humphries et al., 2019)	60	$/ton
	Na_2CO_3	275	$/ton
	Brine disposal (Kesieme et al., 2013)*	0.04	$/m^3
	RO element (Wilf, 2007)	450	$/element
	MD module (Hitsov et al., 2018)	1000	$/module
	MD membrane (Hitsov et al., 2018)	60	$/m^2
	Thermal energy cost	0.01	$/kWh$_{th}$
	Electricity cost	0.103	$/kWh$_{el}$
Terms of revenue	$Mg(OH)_2$	1200	$/ton
	$CaCO_3$	300	$/ton
	Pure water (Mezher et al., 2011)	1	$/m^3

*Disposal of the 2nd crystallizer effluent in chains 2 and 4 and of the 3rd NF unit in chain 5.

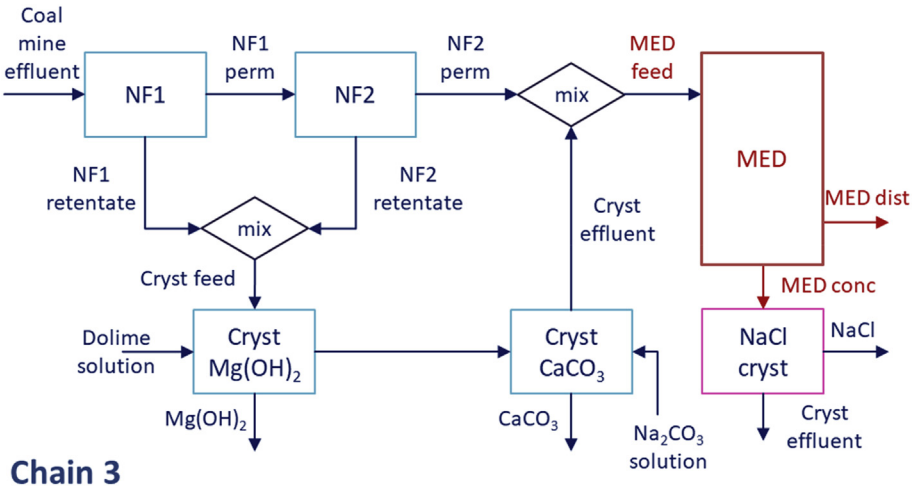

Fig. 4. Schematic representation of the third treatment chain (2NF-2cryst-MED-cryst chain). Blue boxes: pre-treatment; purple boxes: concentration. Differences with the 1st chain in red. (For interpretation of the references to colour in this figure legend, the reader is referred to the Web version of this article.)

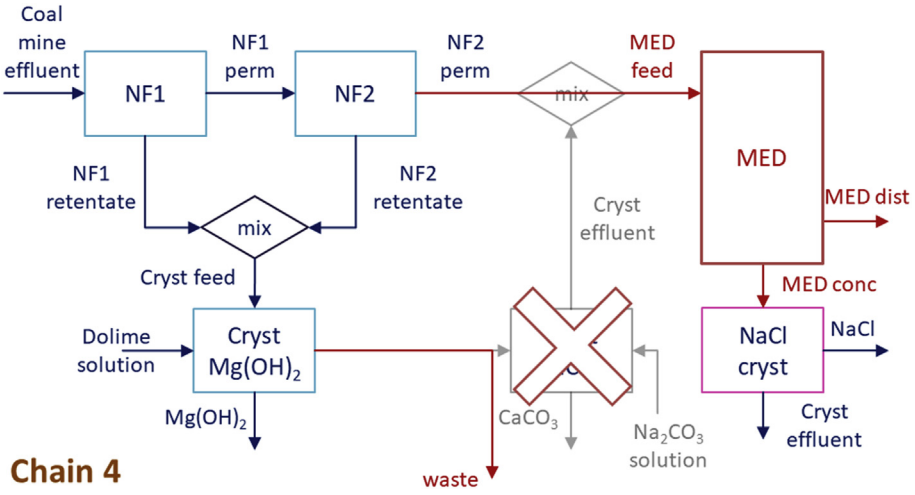

Fig. 5. Schematic representation of the fourth treatment chain (2NF-cryst-MED-cryst chain). Blue boxes: pre-treatment; purple boxes: concentration. Differences with the 1st chain in red. (For interpretation of the references to colour in this figure legend, the reader is referred to the Web version of this article.)

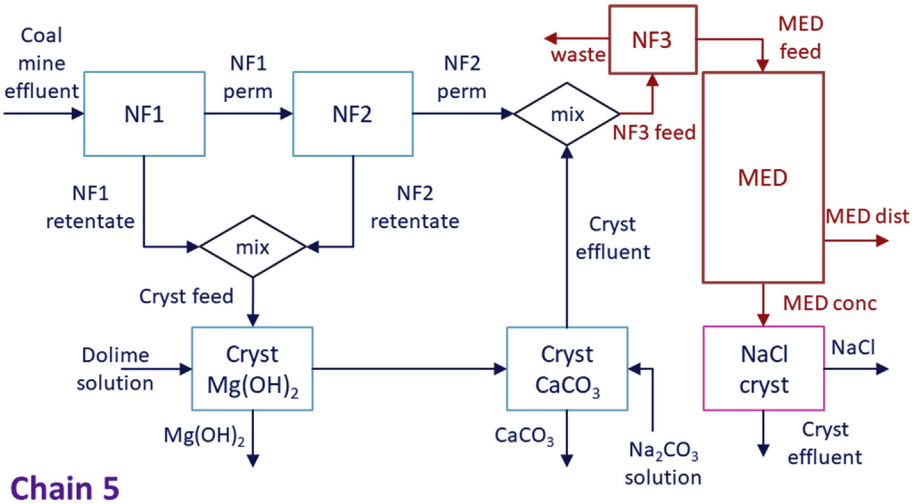

Fig. 6. Schematic representation of the fifth treatment chain (3NF-2cryst-MED-cryst chain). Blue boxes: pre-treatment; purple boxes: concentration. Differences with the 1st chain in red. (For interpretation of the references to colour in this figure legend, the reader is referred to the Web version of this article.)

cost minus the cost of membranes and modules), labor, chemicals and membrane replacement cost (replacement rate of 15%/y (Al-Obaidani et al., 2008)) (Hitsov et al., 2017).

The CAPEX of each crystallization stage includes the cost of the crystallizer and of a disc and drum filter, calculated via the Module Costing Technique as function of their volume and area, respectively (Turton et al., 2012). The capital costs are annualized assuming a depreciation period of 20 years. The OPEX accounts for the pumping costs and the cost of the reactant, in the case of the crystallization of $Mg(OH)_2$ and $CaCO_3$, or of the thermal energy, in the case of the NaCl crystallizer.

For all equipment, we used the index CEPCI (Chemical Engineering Plant Cost Index) to update the costs from the year of the available data to the current time.

Conservatively, we assumed that the salvage value of the technologies at the end of the project lifetime was equal to zero.

The most relevant terms of cost are reported in Table 2. The electricity cost is the cost for non-household consumers in Poland ([dataset] Eurostat, 2019), while the thermal energy cost is estimated for the case of low-temperature waste heat available in the industrial site (Micari et al., 2019b). The selling prices of the minerals are based on the assumption that they have a purity of 99.5%. This assumption is supported by experimental results on the reactive crystallizers, by previous works in the literature on reactive crystallizers (Cipollina et al., 2014; Jakić, 2016) and on the end-crystallizer (Ericsson and Hallmans, 1996), and by the chemical equilibrium diagrams reported in the supplementary materials.

Finally, in order to compare the systems, a global output value is introduced under the name of Levelized Cost of Salt (LSC) in [$/ton$_{NaCl}$]. The LSC is the cost that the produced NaCl crystals would have to allow the project to break-even at the end of its lifetime. This is defined in analogy with the Levelized Water Cost (LWC) used as a reference parameter for desalination plants (Papapetrou et al., 2017). The LSC is defined in equation (1):

$$LSC\left[\frac{\$}{ton}\right] = LSC_{cap} + LSC_{op} = \frac{CAPEX_{chain}\left[\frac{\$}{y}\right]}{NaCl\ crystals\ produced\left[\frac{ton}{y}\right]} + \frac{OPEX_{chain} - Revenue_{water} - Revenue_{minerals}\left[\frac{\$}{y}\right]}{NaCl\ crystals\ produced\left[\frac{ton}{y}\right]} \quad (1)$$

3. Description of the case study

This section presents the case study investigated in this work: firstly, the data relevant to the specific effluent treated in the proposed chains are reported and, secondly, the operating conditions and fundamental geometric features of the treatment units are described.

The analyses have been performed considering a fixed flow-rate and composition of the coal mine effluent to be treated. In particular, the inlet feed flow-rate is always equal to 100 m^3/h, in line with the produced volumes of highly-concentrated coal mine effluents mentioned in the literature (Turek et al., 2005b). The inlet composition is reported in Table 3. This composition refers to a real coal mine effluent produced in Poland and investigated within the EU-funded project Zero Brine (European Union's Horizon, 2020). Analyses of various samples of the effluent showed that the major components are sodium, chloride, magnesium, calcium and sulphate ions, with the concentrations reported in Table 3 (the variation of ionic concentrations among the samples was in the range ±2% of the values reported) and that the solution is neutral, being the pH comprised between 7.6 and 7.8. Notably, no iron and aluminium were found in the effluent. The same major components were reported by other authors, also working on the treatment of neutral coal mine effluents produced in Poland (Turek et al., 2008).

The operating conditions of the units in the treatment chains have been given through suitable sets of parameters. These are taken from literature (e.g. the rejection of NF membranes) or from novel sensitivity analyses carried out with the single models (e.g. the number of effects of the MED plant).

Regarding the pre-treatment step, all chains include at least two NF units to reduce as much as possible the content of bivalent ions in the permeate. Typical NF membrane rejections taken from literature are employed (Turek et al., 2018), as reported in Table 4. These values are in line with experimental rejections found at the lab-scale with the neutral coal mine effluent. In all simulations, the feed pressure and recovery are 30 bar and 80% in the first stage and 50 bar and 80% in the second stage. In the 5th chain, the third NF unit is supposed to have the same membrane rejections, feed pressure and recovery of the second NF unit.

Concerning the concentration steps, the inlet NaCl concentration of the end-crystallizer (i.e. the outlet concentration of either MD or MED) is fixed to 250,000 ppm. This value was obtained via a preliminary minimization of the sum of capital and operating costs of the chain. In the first two chains, the RO unit is responsible for the concentration growth up to the maximum achievable concentration, i.e. 70,000 ppm. The limit on the maximum concentration depends on the maximum applicable pressure (Kesieme et al., 2013). Therefore, the total RO recovery is equal to 70% and a double-stage RO plant is employed: in the first stage, the vessels in parallel contain 8 modules in series and in the second, they contain 6 modules. The operating feed pressure in the first stage is equal to 65 bar.

The RO retentate is sent to the MD unit that has to concentrate it up to 250,000 ppm. The MD plant is composed by two stages, each one with modules arranged in parallel and in series. Each module presents six MD membranes wounded together in a parallel configuration. The inlet temperatures of the feed and the permeate solutions in the direct contact MD are fixed at 80°C and 20°C, respectively (Hitsov et al., 2018).

Table 3
Concentration of the major components of the coal mine effluent investigated in the present case study.

Ion	C [mol/m^3]	C [g/L]
Na^+	358	8.23
Cl^-	383	13.58
Mg^{2+}	11.7	0.28
Ca^{2+}	8.51	0.34
SO_4^{2-}	7.71	0.747

Table 4
Rejection of NF membranes in the 1st and in the 2nd stage. The rejections of NF membranes in the 3rd stage (in the 5th chain only) are equal to those of the 2nd stage.

Ion	Rejection 1st stage [-]	Rejection 2nd stage [-]
Na^+	0.06	0.3
Cl^-	0.2	0.45
Mg^{2+}	0.8	0.98
Ca^{2+}	0.7	0.97
SO_4^{2-}	0.98	0.98

Conversely, in the other three chains, MED is responsible for the whole concentration increase, up to 250,000 ppm. The temperature of the inlet steam in the MED plant depends on the composition of the feed solution and the risk of scaling due to the presence of bivalent ions. Since the MED feed of the 3rd chain presents a higher amount of bivalent ions, the temperature of the steam is fixed at 70°C, to have a TBT lower than 70°C. Conversely, in the other two chains, the risk of scaling is negligible and the temperature of the steam is fixed at 100°C. The TBT determines the number of effects that minimizes the total MED costs. The techno-economic model of the MED plant was run to find the number of effects corresponding to the minimum total cost (Micari et al., 2019b). In particular, the optimum number of effects resulted to be 7 for the 3rd and the 4th chains and 9 for the 5th chain.

4. Results and discussion

In this section, firstly, the results of the energetic and economic analysis of the single units are reported. Secondly, the chains are compared in terms of total electric and thermal energy demand, LSC and NaCl salt recovery. Finally, the results of sensitivity analyses are shown to investigate how much the LSCs of the five systems are affected by the market value of the by-products, the specific costs of energy and the chloride concentration.

4.1. Energetic and economic analysis of each chain

In this paragraph, each chain is analysed in detail, by assessing and comparing the energy demand and the costs of the single units involved. The energy requirements of the five chains are reported in Fig. 7. In all cases, the heat required by the main concentration stage (i.e. MD in the first two chains and MED in the other three) is prominent. In fact, MD and MED are responsible for a very significant concentration change and the distillate to be produced is more than 70% of the inlet feed.

The thermal energy requirement of the main concentration stage depends on its feed flow-rate and concentration. Concerning the chains with MD (pie chart on the left in Fig. 7), the MD feed concentration is always the same and the feed flow-rate is lower in the 2nd chain. Thus, the fraction of MD thermal energy is lower in the 2nd than in the 1st chain. Conversely, in the chains with MED and two NF units (pie chart on the right in Fig. 7), two effects have to be accounted: on the one hand, the MED feed flow-rate in the 4th chain is lower, but on the other hand, the inlet concentration of MED feed is lower and the total concentration factor is higher. Therefore, the fraction of MED thermal energy is slightly lower in the 3rd than in the 4th chain. Also, in the chains where the effluent of the crystallizer is sent to the concentration stage (1st and 3rd), the second term per relevance is the heat required by the end-crystallizer. Conversely, in the chains with only one crystallization step (2nd and 4th), the second term per relevance is the total electric demand of the NF units. In these cases, the thermal demand of the NaCl crystallizer is lower, because of its lower feed flow-rate.

It is worth noting that, whereas the specific electric consumption of RO is higher than that of NF because of the higher operating pressures, the share of electricity demand of NF in Fig. 7 (left) is higher because we incorporated the terms relevant to the two NF units in one term.

Concerning the 5th chain, although MED thermal energy represents again the main term, the fraction covered by the other units, in particular by the three NF units and the NaCl crystallizer, is much higher than in the other chains. In this regard, the third NF unit plays a key role, because it operates at higher pressure with a higher flow-rate in comparison with the other two NF units.

Furthermore, we carried out a detailed economic analysis of the five treatment chains and we reported CAPEX, OPEX and revenues in the bar charts in Fig. 8.

The OPEX of the main concentration stage is always the most significant term, except for the 5th chain where the total OPEX of the NF units turns out to be higher than the OPEX of MED. In the first two chains, the most significant expenditure is the OPEX of MD, especially in the 1st chain, where the MD feed flow-rate is higher. In the 3rd and the 4th chain, the OPEX of MED is the highest term, even if in the 4th chain it is comparable with the costs of NF. Moreover, the chains with one crystallization step (2nd and 4th) present lower CAPEX and OPEX of the concentration stage because of the lower flow-rates. These chains have also reduced crystallization costs, since they present only one crystallization step. Concerning the 5th chain, the presence of an additional NF unit operating at a higher pressure and flow-rate makes the total CAPEX and OPEX of the NF units the highest expenditures. Also, it is worth noting that the costs of MED and of the NaCl crystallizer are intermediate between those of the 3rd and the 4th chain. This is because the flow-rate fed to the MED is given by the permeate of NF3, which is higher than the flow-rate fed to MED in the 4th chain but lower than the one in the 3rd chain (since the recovery of NF3 is 80%, the MED feed flow-rate is 80% of the MED feed flow-rate of the 3rd chain).

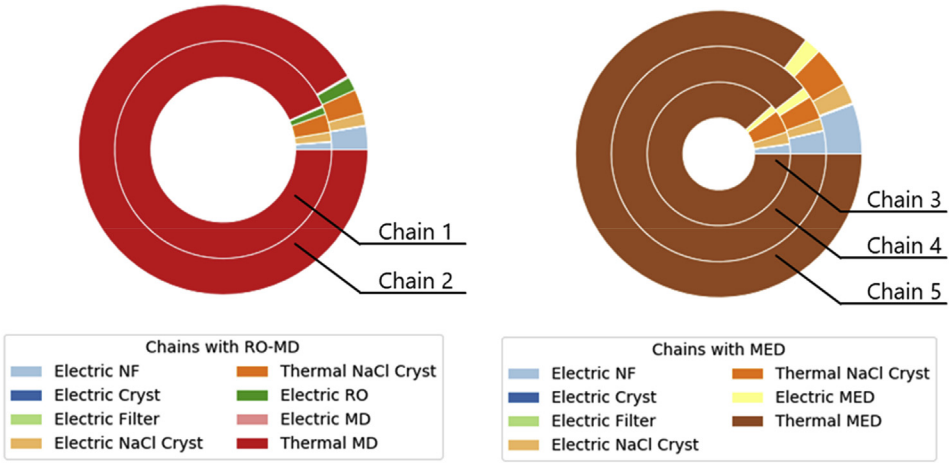

Fig. 7. Nested pie charts representing the energy requirements of the five treatment chains.

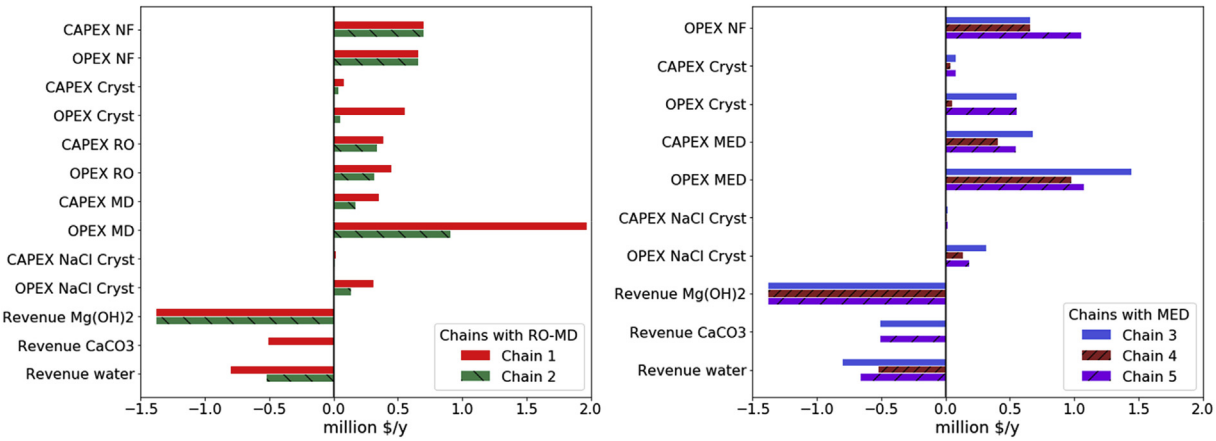

Fig. 8. Bar charts with the CAPEX, OPEX and revenues (negative) of the five treatment chains.

Concerning the revenues, the main term is always due to the production of $Mg(OH)_2$ in the crystallizer and it is followed by the revenue due to the water production. With this regard, a significant amount of water is produced to concentrate the solution up to the saturation point and the relevant revenues have an important role. In the chains with two NF units and two crystallization steps (1st and 3rd chain), the OPEX of the concentration stage is higher than the revenues given by $Mg(OH)_2$ production. Conversely, in the others, the $Mg(OH)_2$ revenues offset the OPEX of the concentration step. However, the global revenues of the chains with one crystallization step are lower, because $CaCO_3$ production is missing and less water is produced in the concentration step.

Overall, for all chains, the OPEX is mostly given by the energy costs. However, MED has always lower thermal consumptions than MD and consequently lower costs, although it is responsible for a larger concentration rise.

4.2. Comparison of the representative output values of the five systems

The aim of this paragraph is to compare the chains via global outputs, used to represent their technical and economic performances. Firstly, the outlet flow-rates of minerals and water, the NaCl productivity and the total electric and thermal energy demand of the five chains are compared. Secondly, the values of LSC are estimated and compared with the market value of NaCl crystals.

The comparison of the produced flow-rates of minerals and water is depicted in Fig. 9. In the case of MED, the produced water is pure water, whereas, with RO and MD, the water has a maximum salt concentration of 150 ppm. The chart shows that the highest production of water occurs in the chains with two NF units and two crystallization steps (1st and 3rd chain), because a higher flow-rate is sent to the concentration step. Conversely, in the chains with two NF units and one crystallization step (2nd and 4th chain), part of the water is lost with the effluent of the crystallizer, which is disposed as a waste. The 5th chain, with three NF units and two crystallization steps, presents an intermediate water production, because the retentate of the 3rd NF unit is disposed as a waste. Remarkably, the production of $Mg(OH)_2$ is the same in all systems since the composition of the feed is constant and the relevant crystallization step is present in every system and behaves in the same way. On the contrary, crystals of $CaCO_3$ are produced only in the 1st, 3rd and 5th chain because the other two chains have only one crystallizer.

Furthermore, we compared the amount of NaCl crystals produced in the chains by defining the NaCl recovery, which is reported for the five chains in Fig. 10. The 1st and the 3rd chains ensure an almost total recovery of NaCl (~94%), since these are devised to minimize the losses of NaCl. In both cases, the limit on the maximum amount of NaCl crystals is defined on the basis of the maximum concentration of SO_4^{2-} to avoid the precipitation of Na_2SO_4. Chains 2 and 4 have a lower NaCl recovery, around 42%, since most of the salt is lost with the crystallizer effluent that is not fed to the concentration step. In the 5th chain, the NaCl recovery is around 58%, because a certain amount of Na^+ and Cl^- ions is lost

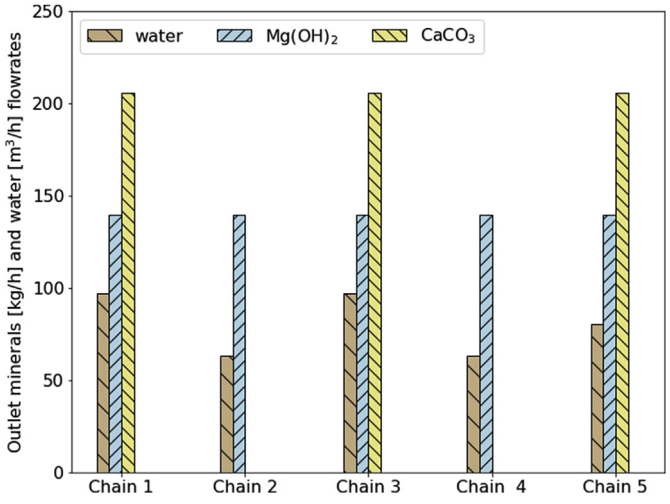

Fig. 9. Outlet flow-rates of the minerals ($Mg(OH)_2$ and $CaCO_3$) [kg/h] and of water [m^3/h] for the five chains.

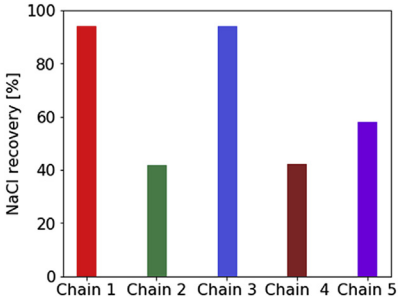

Fig. 10. Values of NaCl recovery [%] for the five chains.

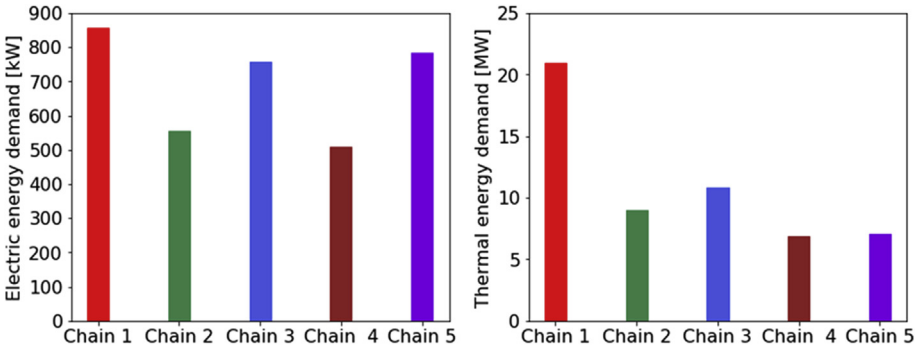

Fig. 11. Total electric (left) and thermal (right) energy demand of the five chains. The total capacity in terms of feed flow-rate to be treated is equal to 100 m^3/h.

with the retentate of the third NF step, whose membranes have a rejection toward Na^+ and Cl^- of around 30%. Thus, the 3rd NF allows for operating the MED at higher TBT without risks of scaling but the disposal of its retentate leads to a certain loss of NaCl.

Fig. 11 presents the total electric and thermal energy demand of the five chains. The electricity demands of the chains with two NF units and one crystallizer (chains 2 and 4) are significantly lower than those with two crystallizers (chains 1 and 3). This is due to the lower feed flow-rate in the concentration step, which is the most energy-intensive phase. Moreover, the chains with the RO-MD coupling (1st and 2nd) have higher electricity consumption than the chains with MED (3rd and 4th), because RO is the most electricity-intensive unit with a specific demand between 3 and 4 kWh_{el}/m^3_{dist}. In addition, MD has a specific electric demand of around 1.8 kWh_{el}/m^3_{dist}. Conversely, MED has a specific electricity demand of 1.5 kWh_{el}/m^3_{dist}. The 5th chain presents a total electricity demand comparable with the one of the 3rd chain and this is mostly due to the additional electricity requirement of the third NF step.

Concerning the thermal demand, the 1st chain has the highest demand, because of the high thermal consumption of MD. Notably, the difference between the chains with RO-MD is more enhanced than that between the chains with MED. In the first two chains, the MD feed has the same inlet concentration (i.e. 70,000 ppm) and different flow-rate: since the flow-rate is almost three times higher in the 1st chain, the corresponding total thermal demand increases proportionally. Conversely, the MED feed in the 3rd chain has higher flow-rate, but also higher concentration with respect to the MED feed in the 4th chain. The smaller concentration growth to be performed in the MED in the 3rd chain partially counterbalances the higher flow-rate and this leads to a slighter difference between the two MED chains.

The heat demand of chain 5 is comparable to that of chain 4. In this case, the MED feed concentration and flow-rate are intermediate between those of the 3rd and the 4th chains. However, the employed number of effects is higher (equal to 9) than the one used for the other two chains (equal to 7), so the specific as well as the total heat demand are lower. The number of effects is selected to minimize the total MED costs: in the last chain, the optimum number of effects is higher because, at the same steam temperature, the concentration factor is lower, so the capital costs are significantly lower.

From the economic point of view, the systems are compared through the LSC, which is reported for the five chains in Fig. 12. Firstly, it is evident that the chains where the 2nd crystallizer effluent is sent to the concentration step (Chains 1 and 3) are more economically feasible than those presenting only one crystallizer (Chains 2 and 4). Secondly, the RO-MD chains (1st and 2nd) have higher LSCs with respect to the corresponding MED ones (3rd and 4th). Therefore, it is possible to conclude that the MED technology, less heat-intensive than the MD, allows for devising cheaper solutions.

Finally, in the 5th chain, the inclusion of an energy-intensive third NF step and a significant loss of NaCl in the disposed NF retentate make the chain the least economically feasible.

The obtained values of LSC are compared with the typical market values of high purity (99.5%) NaCl salt, which can vary between 80 and 150$/$ton_{NaCl}$ (U.S. Department of the Interior, 2017). This area is highlighted in grey in Fig. 12.

The LSC found for the chains with MED and two NF units (Chain 3 and 4) result to fall within this area and this finding confirms the feasibility of these treatment processes. In particular, the 3rd chain is the most economically feasible with a LSC of around 100$/$ton_{NaCl}$. Notably, the LSC of the 1st chain is slightly higher than 150$/$ton_{NaCl}$, thus further technological improvements can easily make this chain competitive with the market value of NaCl crystals.

4.3. Sensitivity analyses

This paragraph presents the results of sensitivity analyses performed by varying economic parameters (i.e. selling price of $Mg(OH)_2$, water and $CaCO_3$ and cost of thermal and electric energy) and input relevant to the feed solution (i.e. inlet chloride concentration). Concerning the first analysis, the variation of the selling price of the products may be connected to a variation of their purity, which would make such products sellable in a market sector rather than another requiring higher purity. The variation range goes from −50% to +50% of the reference prices and costs reported in Table 2. Simulations are performed for every chain by varying one parameter per time, while the others are kept equal to the

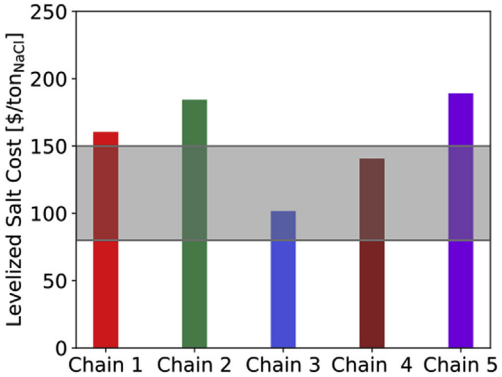

Fig. 12. Levelized Salt Cost (LSC) calculated for the five chains. The grey area corresponds to the range of market values of NaCl crystals with high purity (99.5%).

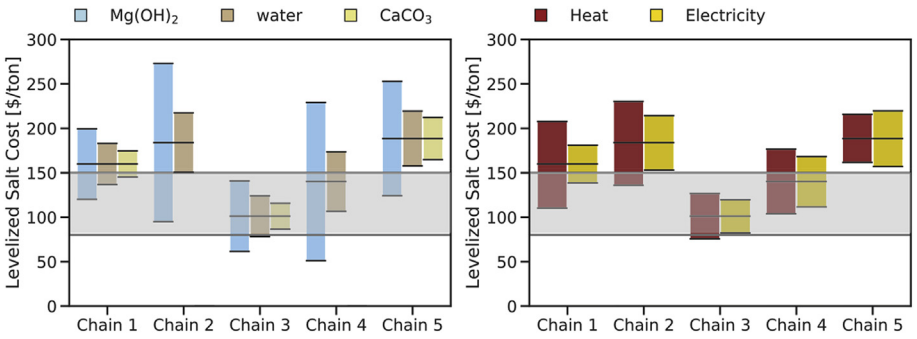

Fig. 13. LSC variation with the price of $Mg(OH)_2$, $CaCO_3$ and water (left) and with the costs of electricity and heat (right). The upper and lower values of each bar correspond to a variation of the price/cost of ±50%. The value in the middle is the LSC found in the reference case.

reference ones (Table 2). Fig. 13 (left) shows the LSC variation for the five investigated chains when the price of $Mg(OH)_2$ is varied between 600 and 1800$/ton, the price of $CaCO_3$ is varied between 150 and 450$/ton (only for the 1st, 3rd and 5th chains) and the price of water is varied between 0.5 and 1.5$/m^3. The results are depicted in bar plots, showing the LSC range of variation with respect to the reference, highlighted in the middle.

In all cases, the most significant LSC variation occurs when the price of $Mg(OH)_2$ is varied. This is because the revenues due to the $Mg(OH)_2$ production constitute one of the most significant term in the costs breakdown of each chain.

With this regard, the range of variation of the LSC in the 2nd and 4th chain is much wider than that found for the 1st and the 3rd chain. Moreover, the lowest LSCs obtained at the highest $Mg(OH)_2$ price in chains 2 and 4 are even lower than the corresponding ones of chains 1 and 3, respectively. As shown in the costs breakdown of the 2nd and 4th chains in Fig. 8, $Mg(OH)_2$ revenues have an absolute value significantly higher than all the other terms, also because the concentration processes are fed by a lower flow-rate. Thus, the variation of $Mg(OH)_2$ price has a major impact on the total costs in these cases. However, the amount of $Mg(OH)_2$ produced is the same in all chains, thus it is expected that the systems with a higher production of NaCl salt (chains 1 and 3) show a slighter variation of the LSC with respect to the chains with a lower NaCl production, when a certain annual term of cost or revenue is changed of the same amount.

On the contrary, the amount of water produced by the chains is different, thus these variously respond to water price variations. In particular, the water production is higher in the chains with two crystallization steps (chain 1 and 3). At the same time, the global expenses of these chains are higher and the relative weight of the water revenue in the general cost breakdown is smaller than in the 2nd and the 4th chain. Overall, the LSC variation due to the water cost change is still bigger in the chains where the crystallizer effluent is disposed (2nd and 4th) but comparable with the one found for the other chains (1st and 3rd).

Concerning the impact of $CaCO_3$ price variation, this is bigger in the 5th chain than in the 1st and the 3rd. As mentioned for the $Mg(OH)_2$ price variation, the $CaCO_3$ productivity is the same in the three chains but the variation of LSC is bigger when the NaCl productivity is lower.

Fig. 13 (right) reports the LSC obtained for each chain by varying the cost of heat and electricity. The higher thermal consumption of MD leads to a stronger impact of the heat cost on the RO-MD chains (1st and 2nd). Also, the variation range is larger in the 1st chain than in the 2nd, because of the higher total thermal demand. Conversely, the variation range of the 3rd chain is smaller than that of the 4th chain, because the higher salt production makes the LSC more stable. Finally, it was found that the range of LSC variation with the cost of electricity is always slightly smaller than that with the heat cost, except for the 5th chain. Although thermal energy covers the highest share of the energy demand in all chains, the additional energy requirement due to the 3rd NF unit in the 5th chain makes it slightly more sensitive to electricity cost variations.

The second analysis regards the effect of inlet chloride concentration on the LSC. In fact, whereas multiple samples of the investigated effluent showed a ±2% variation in the composition, effluents produced by different mines may present different compositions. In particular, we compared the composition of various effluents produced by polish coal mines and chloride concentration showed the widest range of variation. While sulphate concentration was always between 600 and 800 ppm, the chloride one was found to vary from 3,500 ppm (around 100 mol/m^3) to more than 20,000 ppm (around 600 mol/m^3). Previous works reported values of chloride concentrations up to 35,000 ppm (Turek et al., 2005b). Therefore, we assessed the impact of inlet chloride concentration on the LSC_{cap} and LSC_{op} (showed in Fig. 14 on the left) and on the global LSC (showed in Fig. 14 on the right) for the three most feasible chains (Chain 1, 3 and 4). The concentration of sodium was varied accordingly, while the concentrations of the other ions were kept equal to the reference case.

Firstly, LSC_{cap} and LSC_{op} (including revenues) have opposite trends for all chains, but the increase of LSC_{op} with concentration for the RO-MD chain is much stronger than that for the MED chains. On the one hand, in Chain 1, the variation of chloride concentration affects the concentration of the RO feed. Since the outlet concentration of RO brine is fixed, the RO retentate flow-rate, that is the feed of the MD unit, changes accordingly. Therefore, the MD thermal consumption and OPEX increase significantly with the concentration of Cl^- ions and this leads to an increase of LSC_{op} that almost offsets the decrease of LSC_{cap}. On the other hand, in the chains with MED, the MED feed is always the same and the total thermal consumption and the LSC_{op} present a slighter increase with concentration. Therefore, the global LSC of the MED chains is more affected by the decreasing trend of LSC_{cap} and presents higher slope than the one of the RO-MD chain. This leads to the fact that Chain 1 (with RO-MD) shows a much flatter behaviour than the other two chains (with MED).

Secondly, it is worth noting that the LSCs of the three chains mostly fall within the feasibility range (grey area in Fig. 14-right) and, at high chloride concentration, the LSCs of the MED chains are even lower than the lower bound. This shows that the chains are promising treatment solutions for various neutral coal mine effluents with high chloride concentration.

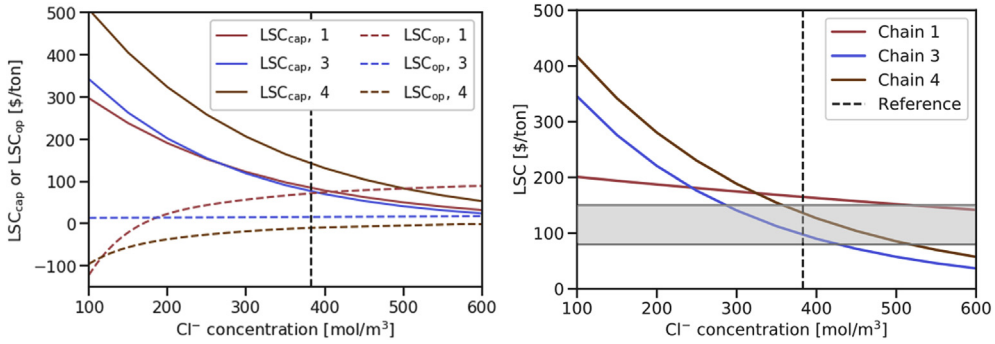

Fig. 14. Variation of LSC_{cap} and LSC_{op} (left) and of the global LSC (right) with the inlet chloride concentration for the three most performing chains (Chain 1, 3 and 4). The black dotted line represents the chloride concentration in the reference case (Table 3).

5. Conclusions

The neutral effluent produced by coal mines is a severe threat to the environment if directly disposed into the rivers, because of its high concentration of chloride and sulphate. In this work, we devised and analysed five treatment chains to purify the effluent and to recover valuable materials. The chains are composed by a pre-treatment step, given by nanofiltration and crystallization units, and a concentration step, including multi-effect distillation and NaCl crystallizer or reverse osmosis, membrane distillation and NaCl crystallizer.

The analysis of the energy demands and the costs of the chains showed that the heat demand constitutes in all cases the highest fraction of the total demand, especially in the chains with MD. Consequently, the OPEX of the concentration technologies was always among the most crucial expenses. However, in most cases, it was found that the revenues due to $Mg(OH)_2$ production are able to offset the highest expenditures.

The comparison of the chains was focused on the total energy demands, the NaCl recovery and the levelized cost of the salt (LSC). This last parameter allowed for assessing the feasibility of the chain, by comparing it with the current market values of high-purity NaCl crystals. The results showed that the chains devised to maximize the NaCl recovery have higher thermal and electric energy demand but also lower LSC, thus being more economically feasible. Moreover, the MED technology allowed for strongly reducing the global LSC, for its lower thermal demand: the treatment chain with two NF units, two crystallizers and MED has a LSC of 100$/$ton_{NaCl}$ that falls within the range of typical high-purity NaCl price. Therefore, this chain was found to be economically competitive with the market value.

Overall, different solutions have been proposed to treat a coal mine effluent and to recover valuable products: water, minerals and NaCl crystals. The findings of this study can have important consequences on the industrial sector of the coal mines, since they can heavily contribute to improve the sustainability of the process, while proposing economically feasible treatment configurations for neutral effluents. The proposed chains allow for a strong reduction of the environmental impact of the industrial process by avoiding the disposal of a highly-concentrated solution into the environment. Future studies will focus on a detailed assessment of the environmental impact of the proposed configurations, in terms of CO_2 emissions due to construction and operation of the treatment processes.

CRediT authorship contribution statement

M. Micari: Conceptualization, Methodology, Software, Writing - original draft. **A. Cipollina:** Conceptualization, Supervision. **A. Tamburini:** Supervision, Writing - review & editing. **M. Moser:** Methodology, Software, Funding acquisition. **V. Bertsch:** Supervision, Writing - review & editing. **G. Micale:** Supervision, Funding acquisition.

Declaration of competing interest

The authors declare that they have no known competing financial interests or personal relationships that could have appeared to influence the work reported in this paper.

Acknowledgements

This work was funded by the ZERO BRINE project (ZERO BRINE – Industrial Desalination – Resource Recovery – Circular Economy) - Horizon (2020) programme, Project Number: 730390: www.zerobrine.eu.

Appendix A. Supplementary data

Supplementary data to this article can be found online at https://doi.org/10.1016/j.jclepro.2020.122472.

References

Akcil, A., Koldas, S., 2006. Acid Mine Drainage (AMD): causes, treatment and case studies. J. Clean. Prod. 14, 1139–1145.
Al-Obaidani, S., Curcio, E., Macedonio, F., Diprofio, G., Alhinai, H., Drioli, E., 2008. Potential of membrane distillation in seawater desalination: thermal efficiency, sensitivity study and cost estimation. J. Membr. Sci. 323, 85–98.
Al-Rawajfeh, A.E., Glade, H., Ulrich, J., 2005. Scaling in multiple-effect distillers: the role of CO2 release. Desalination 182, 209–219.
Baruah, B.P., Khare, P., 2010. Mobility of trace and potentially harmful elements in the environment from high sulfur Indian coal mines. Appl. Geochem. 25, 1621–1631.
Christensen, B., Laake, M., Lien, T., 1996. Treatment of acid mine water by sulphate reducing bacteria; results from a bench scale experiment. Water Res. 30, 1617–1624.
Cipollina, A., Bevacqua, M., Dolcimascolo, P., Tamburini, A., Brucato, A., Glade, H., Buether, L., Micale, G., 2014. Reactive crystallisation process for magnesium recovery from concentrated brines. Desalin. Water Treat. 55, 2377–2388.
Dharmappa, H.B., Wingrove, K., Sivakumar, M., Singh, R., 2000. Wastewater and stormwater minimisation in a coal mine. J. Clean. Prod. 8, 23–34.
Drioli, E., Curcio, E., Di Profio, G., Macedonio, F., Criscuoli, A., 2006. Integrating membrane contactors technology and pressure-driven membrane operations for seawater desalination. Chem. Eng. Res. Des. 84, 209–220.
Ericsson, B., Hallmans, B., 1996. Treatment of saline wastewater for zero discharge at the Debiensko coal mines in Poland. Desalination 105, 115–123.
European Union's Horizon, 2020. Research and innovation programme, 2020. https://zerobrine.eu/.
Eurostat, 2019. Electricity Prices for Non-household Consumers - Bi-annual Data (From 2007 Onwards).
Feng, D., Aldrich, C., Tan, H., 2000. Treatment of acid mine water by use of heavy metal precipitation and ion exchange. Miner. Eng. 13, 623–642.
Gibert, O., de Pablo, J., Cortina, J.L., Ayora, C., 2002. Treatment of acid mine drainage by sulphate-reducing bacteria using permeable reactive barriers: a review from

laboratory to full-scale experiments. Rev. Environ. Sci. Biotechnol. 1, 327–333.
Hitsov, I., Eykens, L., Schepper, W.D., Sitter, K.D., Dotremont, C., Nopens, I., 2017. Full-scale direct contact membrane distillation (DCMD) model including membrane compaction effects. J. Membr. Sci. 524, 245–256.
Hitsov, I., Sitter, K.D., Dotremont, C., Nopens, I., 2018. Economic modelling and model-based process optimization of membrane distillation. Desalination 436, 125–143.
Humphries, T.D., Møller, K.T., Rickard, W.D.A., Sofianos, M.V., Liu, S., Buckley, C.E., Paskevicius, M., 2019. Dolomite: a low cost thermochemical energy storage material. J. Mater. Chem. 7, 1206–1215.
Jakić, J., 2016. Characterization of dolomitic lime as the base reagent for precipitation of Mg(OH)2 from seawater. Chem. Biochem. Eng. Q. 30, 373–379.
Kalin, M., Fyson, A., Wheeler, W.N., 2006. The chemistry of conventional and alternative treatment systems for the neutralization of acid mine drainage. Sci. Total Environ. 366, 395–408.
Kefeni, K., Mamba, B.B., Msagati, T.A.M., 2017a. Magnetite and cobalt ferrite nanoparticles used as seeds for acid mine drainage treatment. J. Hazard Mater. 333, 308–318.
Kefeni, K., Msagati, T.A.M., Mamba, B.B., 2017b. Acid mine drainage: prevention, treatment options, and resource recovery: a review. J. Clean. Prod. 151, 475–493.
Kesieme, U.K., Milne, N., Aral, H., Cheng, C.Y., Duke, M., 2013. Economic analysis of desalination technologies in the context of carbon pricing, and opportunities for membrane distillation. Desalination 323, 66–74.
López, J., Reig, M., Gibert, O., Cortina, J.L., 2019. Integration of nanofiltration membranes in recovery options of rare earth elements from acidic mine waters. J. Clean. Prod. 210, 1249–1260.
Macías, F., Pérez-López, R., Caraballo, M.A., Cánovas, C.R., Nieto, J.M., 2017. Management strategies and valorization for waste sludge from active treatment of extremely metal-polluted acid mine drainage: a contribution for sustainable mining. J. Clean. Prod. 141, 1057–1066.
Martínez, N.M., Basallote, M.D., Meyer, A., Cánovas, C.R., Macías, F., Schneider, P., 2019. Life cycle assessment of a passive remediation system for acid mine drainage: towards more sustainable mining activity. J. Clean. Prod. 211, 1100–1111.
Martins, M., Santos, E.S., Pires, C., Barros, R.J., Costa, M.C., 2010. Production of irrigation water from bioremediation of acid mine drainage: comparing the performance of two representative systems. J. Clean. Prod. 18, 248–253.
Masindi, V., Madzivire, G., Tekere, M., 2018. Reclamation of water and the synthesis of gypsum and limestone from acid mine drainage treatment process using a combination of pre-treated magnesite nanosheets, lime, and CO2 bubbling. Water Resour. Ind. 20, 1–14.
Mezher, T., Fath, H., Abbas, Z., Khaled, A., 2011. Techno-economic assessment and environmental impacts of desalination technologies. Desalination 266, 263–273.
Micari, M., Cipollina, A., Tamburini, A., Moser, M., Bertsch, V., Micale, G., 2019a. Combined membrane and thermal desalination processes for the treatment of ion exchange resins spent brine. Appl. Energy 254, 113699.
Micari, M., Moser, M., Cipollina, A., Fuchs, B., Ortega-Delgado, B., Tamburini, A., Micale, G., 2019b. Techno-economic assessment of multi-effect distillation process for the treatment and recycling of ion exchange resin spent brines. Desalination 456, 38–52.
Micari, M., Moser, M., Cipollina, A., Tamburini, A., Micale, G., Bertsch, V., 2020. Towards the implementation of circular economy in the water softening industry: a technical, economic and environmental analysis. J. Clean. Prod. 255, 120291.
Motsi, T., Rowson, N.A., Simmons, M.J.H., 2009. Adsorption of heavy metals from acid mine drainage by natural zeolite. Int. J. Miner. Process. 92, 42–48.
Nleya, Y., Simate, G.S., Ndlovu, S., 2016. Sustainability assessment of the recovery and utilisation of acid from acid mine drainage. J. Clean. Prod. 113, 17–27.
Papapetrou, M., Cipollina, A., La Commare, U., Micale, G., Zaragoza, G., Kosmadakis, G., 2017. Assessment of methodologies and data used to calculate desalination costs. Desalination 419, 8–19.
Puigdomènech, I., Colàs, E., Grivé, M., Campos, I., García, D., 2014. A tool to draw chemical equilibrium diagrams using SIT: applications to geochemical systems and radionuclide solubility. MRS Proc. 1665, 111–116.
Qin, J., Cui, X., Yan, H., Lu, W., Lin, C., 2019. Active treatment of acidic mine water to minimize environmental impacts in a densely populated downstream area. J. Clean. Prod. 210, 309–316.
Sivakumar, M., Ramezanianpour, M., O'Halloran, G., 2013. Mine water treatment using a Vacuum membrane distillation system. APCBEE Procedia 5, 157–162.
Tarutis, W.J.J., Stark, L.R., Williams, F.M., 1999. Sizing and performance estimation of coal mine drainage wetlands. Ecol. Eng. 12, 353–372.
Tiwary, R.K., 2001. Environmental impact of coal mining on water regime and its management. Water Air Soil Pollut. 132, 185–199.
Turek, M., Dydo, P., Klimek, R., 2005a. Salt production from coal-mine brine in ED–evaporation–crystallization system. Desalination 184, 439–446.
Turek, M., Dydo, P., Surma, A., 2005b. Zero discharge utilization of saline waters from "Wesola" coal-mine. Desalination 185, 275–280.
Turek, M., Dydo, P., Klimek, R., 2008. Salt production from coal-mine brine in NF — evaporation — crystallization system. Desalination 221, 238–243.
Turek, M., Mitko, K., Laskowska, E., Chorążewska, M., Piotrowski, K., Jakóbik-Kolon, A., Dydo, P., 2018. Energy consumption and gypsum scaling assessment in a hybrid nanofiltration-reverse osmosis-electrodialysis system. Chem. Eng. Technol. 41, 392–400.
Turton, R., Bailie, R.C., Whiting, W.B., Shaeiwity, J.A., Bhattacharzza, D., 2012. Analysis, Synthesis and Design of Chemical Processes. Prentice Hall.
U.S. Department of the Interior, 2017. Mineral Commodity Summaries - U.S. Geological Survey.
Vince, F., Marechal, F., Aoustin, E., Bréant, P., 2008. Multi-objective optimization of RO desalination plants. Desalination 222, 96–118.
Wilf, M., 2007. The Guidebook to Membrane Desalination Technology. Balaban Desalination Publications.